Surface Modification Of Titanium Implants By Grit-blasting With Novel Bioactive Glasses

By

Farah Nabeel Mohammed Tahir Al-Khayyat

BDS, MSc

A thesis submitted in fulfilment of the requirement for the Degree of Doctor of Philosophy in The Institute of Dentistry, Barts and The London School of Medicine and Dentistry, Queen Mary University of London

September 2017

Statement of originality

I, Farah Nabeel Mohammed Tahir Al-Khayyat, confirm that the research included within this thesis is my own work or that where it has been carried out in collaboration with, or supported by others, that this is duly acknowledged below and my contribution indicated. Previously published material is also acknowledged below.

I attest that I have exercised reasonable care to ensure that the work is original, and does not to the best of my knowledge break any UK law, infringe any third party's copyright or other Intellectual Property Right, or contain any confidential material.

I accept that the College has the right to use plagiarism detection software to check the electronic version of the thesis.

I confirm that this thesis has not been previously submitted for the award of a degree by this or any other university.

Signature: Farah Al-Khayyat

Date: 15 /09/2017

Abstract

Introduction: The survival of dental implants depends on osseointegration. Modifications to the implant surface are attractive for promoting the success of the implant. Abrading the surface of the implant with bioactive glass is an attractive option for improving the speed of osseointegration.

Aims: To develop a bioactive glass that has the ability to enhance the surface roughness of the implant by embedding particles into the surface and to investigate the effect of grit blast parameters on the removal of the titanium from the surface.

Methods: Three glasses based on SiO_2-CaO-Na_2O-P_2O_5-CaF_2 were synthesized by a melt quench technique. The glasses were characterised and investigated for their bioactivity. Titanium discs were abraded with coarse glass particles by using a grit blast technique with different parameters, such as, distance, air pressure and speed. The depth, width of the abraded line and surface roughness (R_a) were measured by light profilometer. The distribution of the glasses on the titanium surface was measured by SEM-EDX. The biocompatibility of the abraded discs was tested *in vitro* using MC3T3-E1 cell line.

Results: All glasses exhibited an amorphous structure with varied bioactivity. Changing the abrasion parameters influenced the amount of titanium removed and the surface coverage. The harder the glass the lower the amount of titanium removed and the wider the width of the abraded area. The R_a was significantly increased from 0.1µm to 1.6µm. The SEM-EDX analysis confirmed that the glasses were widely distributed and a higher coverage was seen with the harder glass. The abraded discs showed good biocompatibility *in vitro*.

Conclusions: The designed compositions were successfully modifying the surface of the titanium. They are abrasive enough to significantly embed into the titanium surface by using the grit blast technique and increase their surface roughness. The glass abraded discs show both good bioactivity and biocompatibility *in vitro*.

Table of Contents

List of Figures

List of Tables

List of Abbreviations

HAP	Hydroxyapatite
T_g	Glass transition temperature
T_m	Melting temperature
BO	Bridging oxygen bond
NBO	Non-Bridging oxygen bond
NC	Network connectivity
NC’	Modified network connectivity
SBF	Simulated body fluid
HCA	Hydroxycarbonate apatite
FAP	Fluoroapatite
MAS-NMR	Magic Angle Spinning-Nuclear Magnetic Resonance
T_c	Crystallisation temperature
Ca-P	Calcium-phosphate layer
α-MEM	Alpha Eagle’s Minimum Essential Medium
SEM-EDX	Scanning Electron Microscopy with Energy Dispersive X-Ray analysis
SFα-MEM	Serum free α-MEM
Sα-MEM	Serum containing α-MEM
XRD	X-Ray diffraction
FTIR	Fourier Transform Infra-Red Spectroscopy
DSC	Differential Scanning Calorimetry
ICP-OES	Inductively Coupled Plasma-Optical Emission Spectroscopy

F^--ISE	Fluoride ion-selective electrodes
PFR	Powder flow rate
WLP	White light profilometry
ALP	Alkaline phosphatase activity
OCP	Octacalcium phosphate
ACP	Amorphous calcium phosphate
PBS	Phosphate buffer solution
SE	Secondary electron mode
BSE	Backscattered mode

Acknowledgements

First, I would like to express my sincere gratitude to my first supervisor **Professor Robert Hill** for his excellent supervision, immense knowledge, continuous guidance and encouragement throughout my research study.

My sincere thanks also go to my second supervisor **Dr Simon Rawlinson**, for his motivation, patience, advice and guidance in the biological studies.

Besides my supervisors, I would like to thank **Dr Natalia Karpukhina**, for her valuable advices throughout my project, her guidance all the time in the MAS-NMR data analysis and her skills in spreading happiness on the scientifically hard days.

I gratefully acknowledge the funding received towards my PhD from the **Ministry Of Higher Education and Scientific Research** in **Iraq (MOHER)**.

I am also hugely appreciative to **Dr Harold Toms**, for his excellent training on how to run the MAS-NMR experiment, to **Mr Jeff Brown** from Kemet Company, for his kind help and expertise in polishing the titanium discs, to **Dr Rory Wilson** for running the XRD experiment, to **Mr Russell Bailey** and **Mr Thomas Baumard** for their training in how to use the SEM and the hardness machine and to **Mr Peter Tomlins** for his advices regarding the statistical analysis.

Special mention goes to my friends **Jamila Al-Mohammadi, Alessia D'Onofrio, Sherif Elsharkawy, Alexander Cresswell-Boyes, Agron Hoxha, Xiaojing Chen, Natheer Aleesa, Mohammed Hassan, Kseniya Shuturminska** and **Tomas Duminis** for providing a comfortable work environment besides their helpful discussions and advices during the lab work.

Millions of thanks go to **Heba Aldehlawi** for her help and training in the cell biology work, to **Amel Kadhum** for her prayers and spiritual support during my study and to

the new PhD students **Saja Mannaa, Abdullah Holldar, Thaer Al-Khaffaji, Wei-Te Huang** and **Bajram Ferizolli** for surrounding me with their love and support.

Finally, I warmly appreciate **my family**, for their prayers, endless love and support all the time. Thank you for encouraging me to follow my dreams and to reach a higher level in education. Thanks my beloved **Mustafa** and **Joshua** for the happy period that we spent together which really gave me the power to carry on with my study and passing the hard moments.

1 Introduction

1.1 Introduction

The routine treatment for a missing tooth or teeth in partially and completely edentulous patients is the construction of either fixed or removable prosthesis. These prostheses usually depend on the adjacent natural teeth, as well as the soft tissue for their support and retention. However in the late 1960s, there was the invention of endosseous implants. These implants were demonstrated to be used as an alternative method of treatment for various cases of congenital and/or acquired missing teeth, as they provide the required retention, support and stability for the superstructure prosthesis (Buser et al., 1991, Zarb et al., 2013).

A wide range of materials have been used for the fabrication of oral and orthopaedic implants, such as, cobalt-chromium-molybdenum, stainless steel and other alloys. However, commercially pure titanium and its alloys are the most commonly used materials in medical and dental applications. This is due to their excellent corrosion resistance, physical properties and high biocompatibility (Pourbaix, 1984, Saiz et al., 2002, Zarb et al., 2013). The clinical success and the highest survival rate of the implants depend on their anchorage and stability within the surrounding bone during the loading period and this is known as osseointegration (Buser et al., 1991, Zhang, 2011). Osseointegration is defined as a process of direct bone formation and deposition on to the surface of the implant without the presence of fibrous tissue at the bone-implant interface (Albrektsson and Johansson, 2001, Berglundh et al., 2003). It is characterised by the structure of the bone-implant interface, in which the components, such as, cells, collagen fibres and minerals have a fundamental role in the bone formation process (Zhang, 2011). Therefore, many studies have focused on the importance of providing a direct bone-implant interface and enhancing the

bone remodelling around the implants in order to provide long lasting integrated implants. This can be performed either by changing the chemical structure of the implant surface or altering their surface topography (Berglundh et al., 2003, Ehrenfest et al., 2010). Regarding the first method, the metal implant surface can be modified by coating them with bioactive materials, such as, hydroxyapatite or bioactive glasses (Albrektsson and Johansson, 2001). Bioactive glasses, in general, have the ability to dissolve in the body fluid and form a chemical bond with bone. This bond will provide a typical site for bone apposition around the implant, which in turn will lead to an enhancement in the anabolic bone metabolism process and rapid fixation of the implant to bone tissue (Romanos et al., 2003, Coelho et al., 2009, Ehrenfest et al., 2010). On the other hand, many clinical studies have emphasised the importance of the surface quality of the implant and demonstrated that there is a direct relation between surface topography and bone remodelling around the implant. Therefore, osseointegration could be subsequently enhanced by increasing the surface roughness of the implant and thus exposing more surface area to the bone (Albrektsson and Wennerberg, 2004). There are various techniques which have been utilised for altering the surface topography of the implant and these include acid etching, plasma spraying, enamelling and grit blasting (Sykaras et al., 2000, Brunette et al., 2012). The latter technique was used in this study, as it has several advantages over the other techniques. First, the simplicity of the technique, in which the substrate material surface is bombarded by abrasive particles leading to, marked physical changes in the substrate surface. Second, it eliminates the need for acid-etching step from the processing, as in the case with alumina. Finally, matching the coefficient of thermal expansion of the substrate material is not crucial in this technique. Despite these strong advantages compared to the more sophisticated processes, grit blasting with bioactive glass has not been investigated thoroughly, and therefore this study was carried out.

1.2 Aims and Objectives of the study

The aim of this study is to modify the surface of the titanium implant with high fluoride/phosphate containing bioactive glasses of variable sodium concentration by using a grit blast technique. This is to improve the surface properties of the titanium implant and to enhance the bone formation process around the implant. Moreover, the glass abraded titanium discs were investigated for their biocompatibility *in vitro*.

Objectives:

1. To design three compositions of bioactive glasses differing in their sodium concentration giving different hardness values.
2. To investigate the ability of the designed bioactive glasses to form apatite when immersed in solutions of different ion contents.
3. To evaluate the ability of the designed glasses to embed physically into the titanium implant surface, and assess the effect of their hardness on the amount of area coverage, as well as the amount of titanium removal.
4. To optimise the grit blast parameters, such as, the pressure output, the velocity of the moving stage and the distance from the hand piece nozzle on the amount of substrate removal and the surface roughness.
5. To determine the *in vitro* biocompatibility of the bioactive glasses and the glass-abraded titanium discs with osteoblast cells.

1.3 Structure of the thesis

The thesis is divided into 9 chapters. The first chapter includes a brief introduction to the study with the aims and objectives of the study. The second chapter presents the literature review, which is divided into three parts. The first part focuses on the biomaterials of the dental implants, the biology of the osseointegration process and the failure of dental implants. In the second part, there is a review of the structure of the bioactive glasses, the role of different components in the glasses and the mechanism of the glass interaction with bone tissue. The last part of the review discusses and criticises the modification methods used for implant surfaces. The third chapter of the thesis contains the materials and methods, which were used during the study and this is divided into four major sections. The first section is focusing on the synthesis of the bioactive glass and its characterisation. Additionally, some properties are also investigated, such as, hardness and density. The second part involves investigating the bioactivity of the designed glasses in four testing solutions and detecting the apatite formation by both solid and solution characterisation. The third part focuses on the preparation of titanium discs and coating them with the designed bioactive glasses using grit blast/air abrasion technique. The effect of different operating parameters on the coating properties is also investigated. Finally, a cell culture study is carried out to examine the biocompatibility of the glasses and the coated samples.

Chapters 4, 5, 6 and 7 demonstrate the results and discussion of the whole research. Chapter 8 comprises the conclusions of the research and the recommended future work. Chapter 9 present the references used in the thesis.

2 Literature review

2.1 Dental implants

2.1.1 Overview

A dental implant is a device inserted into the maxilla or the mandible, in partially or completely edentulous patients, underneath the mucosa and the periosteum in order to act as an anchor for a fixed and removable prosthesis (Stellingsma et al., 2004). There are different kinds of dental implants depending on the material of their fabrication, dimension, location, surface morphology and properties. Therefore, dentists have to select the appropriate type of implant for each specific case (Jokstad et al., 2003).

Regarding the location of the implant, the dental implant can be classified into subperiosteal, transosteal and endosteal implants. The former is used mainly in case of edentulous mandible with insufficient height. It is composed of a cast metal frame which is located on the bone underneath the mucoperiosteum Figure (2.1). The failure rate of this implant is high due to the epithelial ingrowth, the possibility of infection and paraesthesia of the mental nerve. Therefore, it is rarely used nowadays due to their many drawbacks (Garefis, 1978, Bodine et al., 1996).

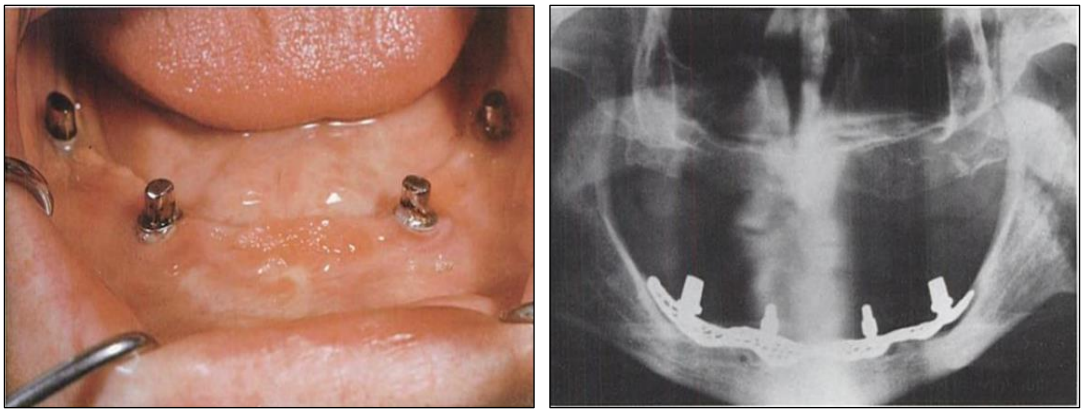

Figure 2.1: Sub-periosteal implant (Schroeder et al, 1996).

Transosteal implants are mostly used in the mandible specifically in the frontal region with limited alveolar ridge height of around 8-9 mm. They are inserted through the lower border of the mandible crossing the whole thickness of the alveolar bone and their posts emerge in the oral cavity to support the dental prosthesis. This type is also not commonly used, because it is surgically invasive and the occurrence of bone saucerization is possible (Albrektsson et al., 1986). Endosteal implants are the most widely used type of dental implants due to their convenient application. It is inserted into the alveolar bone by either one-stage surgery or two-stage surgery techniques. In the first technique, the implant directly emerges in the oral cavity while, in the second technique the implant is covered by the oral mucosa and after few months it will be exposed in the oral cavity to support the prosthesis. This type can come in different designs, such as, cylinder, screw and blade Figure (2.2) (of Prosthodontics et al., 1999, Stellingsma et al., 2004).

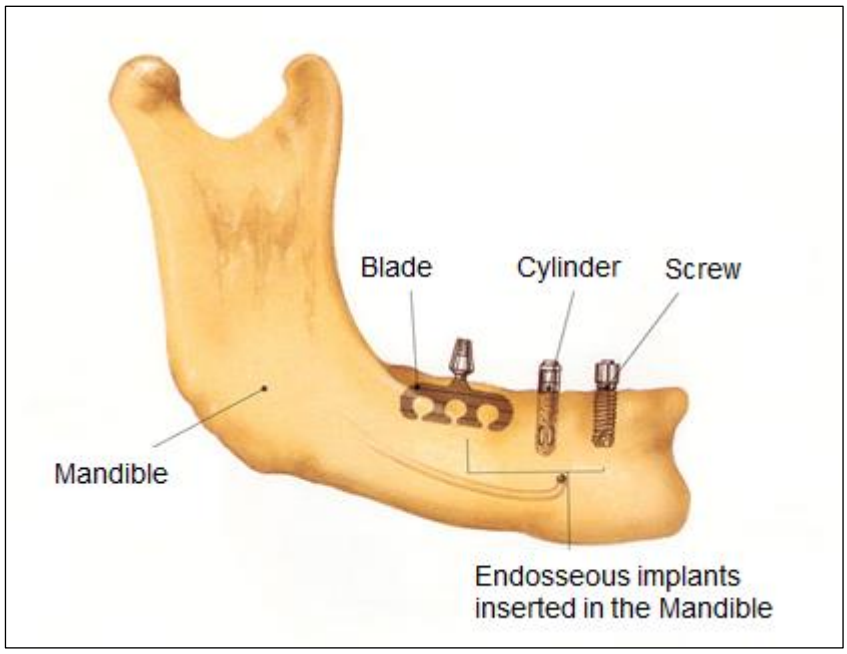

Figure 2.2: Endosseous implant designs.

Taken from (http://dentalimplants.uchc.edu/about/types.html).

According to the time of implantation, dental implants can be divided into: first, ‘immediate implant’, which can be placed immediately after the extraction of the tooth and before the healing of the surgical site. Second, ‘early implant’ means the insertion of the implant after 4-8 weeks from the time of tooth extraction and finally, ‘late implants’ which means the placement of the implant after the complete bone healing (Pivodova et al., 2011). There is a controversy about the time of implant loading with the dental prosthesis. The time required for the implant immobilisation is around 6 months for implants inserted in the maxilla and 3 months in the mandible.

2.1.2 Biomaterials of dental implants

There is a wide variety of materials which are used for the fabrication of dental implants. These are either metals, such as, pure titanium, Ti-6Al-4V alloy and cobalt-chromium molybdenum alloy or ceramics, such as, zirconia, aluminium oxide and hydroxyapatite (HAP) (Jung et al., 2001). The high ductility and fracture toughness are the main advantages of metal implants, while low corrosion resistance is their main drawback (Von Recum, 1998). In addition to that, their abilities to bond with bone are markedly less significant when compared with the ceramics (Habibovic et al., 2005). Many studies have shown that commercially pure titanium and titanium alloys are the most biocompatible materials among the metal implants (Alla et al., 2011, Brunette et al., 2012).

Biocompatibility is a dynamic process and it can be defined as the ability of the material to adapt to the surrounding tissue without eliciting any harmful effect to the recipient tissue (Williams, 2008). It is important that the material has high biocompatibility, because biocompatibility will enhance the process of osseointegration and the attachment of soft tissue around the collar portion of the implant (Mustafa et al., 1998).

Strunz 1985 classified the implant material according to their compatibility in the bone into (Schroeder et al., 1996):

Distant osteogenesis (biotolerated materials): this includes materials, such as, stainless steel, cobalt-chromium-molybdenum alloys and polymethylmethacrylate. These materials have the ability to form a more or less thick connective tissue capsule at the bone-implant interface. However, this implant should not be subjected to loading during the healing process.

Contact osteogenesis: this type is also known as bioinert material and it includes titanium and aluminium oxide ceramic. There is a bone formation at the area adjacent to the implant surface however; there is no real bond at the bone-implant interface.

True bond osteogenesis: this group includes bioglasses, bioceramics and calcium phosphate apatite and also known as bioactive materials. These materials are installed in bone and able to form a chemical bond to bone. Thus, this type of material can withstand the physiologic loading.

Bond osteogenesis: this group includes titanium with coating material. These materials when implanted in the bone will show both physical and chemical bonding to bone.

Titanium (Ti) is a light weight, high-strength, low corrosion structural metal. Its density is about 4.5 g/cm^3 and its alloys were used as surgical implant materials from the 1960s (Gonzalez and Mirza-Rosca, 1999). Commercially pure titanium is the material of choice for dental implant manufacturing, due to its excellent mechanical properties and its ability to react with the bone (Albrektsson et al., 1981). However, this reaction is not chemical because the material is chemically inert (Manero et al., 2002). The inert material is highly tolerated by the body tissue producing no adverse effect on the surrounding structures (Oldani et al., 2012).

Pure titanium metal comes in four grades according to a number of impurities that are found in the material which are oxygen, carbon, nitrogen and iron. Grade 4 pure titanium is the most commonly used between the four grades because, it shows high oxygen and iron contents which are responsible for the enhancement of the mechanical properties. However, the low elastic modulus, poor abrasion resistance and the greater difficulty in fabrication than stainless steel are the drawbacks of the material (Hill, 1998).

Regarding biocompatibility, this metal has the ability to form a strong and stable titanium oxide (TiO_2) layer on the surface when it is exposed to air or aqueous medium. This oxide layer is responsible for decreasing the rate of its corrosion and enhancing its ability to interact with bone (Moritz et al., 2004, Olmedo et al., 2009). Many proteins, such as, proteoglycans, collagenase and fibronectin are adsorbed readily from the surrounding body fluids on the surface of the metal. However, there is no clear conclusion about the significance of the proteins in the biological reaction (Brunette et al., 2012). (Linder and Hansson, 1983) showed that titanium implants are separated from bone by a 20-40 nm layer of proteoglycan which contains a calcium deposit. The formation of this layer is related to the stability of the TiO_2 layer on the titanium metal surface. Cell growth and differentiation are enhanced on the titanium surface as the osteoprogenitor cells migrate to the site of implantation and differentiate into osteoblast cells.

Titanium alloys, such as, Ti-6Al-4V and Ti-6Al-7Nb are the most suitable implant materials for orthopaedic applications. Ti-6Al-4V is the first and the most widely employed material because it possesses good mechanical properties and little or no adverse effects on the surrounding tissue (Sittig et al., 1999). The mechanical properties are improved when compared with pure titanium and this is achieved by the addition of aluminium (Al). Vanadium (V) is added for the purpose of maintaining the corrosion resistance of the alloy (Khan et al., 1999). However, vanadium is a

toxic element to the human body because Ti-6Al-4V forms a passive vanadium oxide layer on the surface and this layer is thermodynamically unstable. Therefore, vanadium is released in the human body and it may accumulate in specific organs, such as, kidneys, liver and bone. As a result of this**,** vanadium free alloys and Ti-6Al-7Nb have been developed (Akahori et al., 2002). Ti-6Al-7Nb is used for hip and elbow joints replacements.

Titanium and its alloys have certain limitations. There is a wide controversy about the osteogenesis of Ti-6Al-4V alloy (Blumenthal and Cosma, 1989, Maurer et al., 1994). The release of vanadium and aluminium ions from these alloys is thought to inhibit osseointegration (Okazaki and Gotoh, 2005, YORUC et al., 2007), leading to failure of implant prosthesis (Bedi et al., 2009). Although, titanium has high survival rate the dark greyish colour can shine through the thin mucosa causing aesthetic problems, especially in the anterior region. Therefore, zirconia has been used clinically. This material has natural tooth-like colour, good mechanical properties and dimensional stability, as well as comparable biocompatibility to titanium (Aydın et al., 2013). Moreover, (Kohal et al., 2002) demonstrated that zirconia can withstand long-term loading and the stress distribution along the bone-implant interface is similar to commercially pure titanium. In 2004, (Kohal et al., 2004) compared the histological finding of loaded titanium and zirconia implants in monkeys. The study showed that the reaction of the soft tissue in both materials is the same and there is a direct bone attachment on to both surfaces without the formation of fibrous tissue at the bone-implant interface.

2.1.3 Osseointegration

The successful insertion of implants in bone with no signs of infection or rejection by the living tissues leads to a lot of developments in the field of medicine and dentistry. The success and prognosis of implant supported prostheses depend on the physical and biological integration at the bone-implant interface, *i.e.* osseointegration, which

is an important factor in the stability of the implant. Any disruption in this process will cause implant mobility and subsequent failure (Ashley et al., 2003, Matusovits, 2009).

Osseointegration reveals an active process during its formation and maintenance. The formation stage of this process represents a slight direct interaction between the implant and the living bone while, the maintenance stage represents the continuous bone remodelling around the implant and its adaptation to function (Berglundh et al., 2003). The process of osseointegration was first discovered by Swedish orthopaedic surgeon Brånemark in 1969 when he inserted a piece of titanium in the femur of a rabbit and observed that this material fused with the surrounding bone and the soft tissues. From that time, the term “osseointegration” was recognised. However, there are many factors which affect this process like the material and surface properties of the implant, bone quality and time of functional loading (Alla et al., 2011).

2.1.4 Definition of Osseointegration

Osseointegration can be defined histologically as the direct attachment of the implant with bone by the formation of bony tissue at the bone-implant interface without any interposition of fibrous tissue. While, clinically it is the ankylosis of the implant in the bone during functional loading (Albrektsson and Zarb, 1993, Albrektsson and Johansson, 2001, Ehrenfest et al., 2010).

However, there are other terms which are related to osseointegration, such as, osteoinduction and osteoconduction; they are different from osseointegration. The former is defined as the stimulation of the undifferentiated cells, preosteoblast cells to induce bone formation, and this process is elicited in bone healing and after the insertion of an implant in the bone. While, osteoconduction refers to the ability of the implant surface to allow the bone formation on the top of it and this process is affected by the implant material that used and its reaction with bone (Albrektsson and Johansson, 2001).

2.1.5 Biology of Osseointegration

Bone is a specialised highly active form of connective tissue, which is composed of cells and extracellular matrix. The matrix consists of organic and inorganic components. The former composed of 90% collagen type I and 10 % non-collagenous proteins, these components are responsible for the properties, such as, toughness *i.e.* (resistance to crack propagation). The latter components, on the other hand, are responsible for the compressive strength and stiffness and are composed mainly of HAP crystals. Therefore, bone can be described as a hard, dense and composite like structure (Miller and Parker, 1984, Martin et al., 1988, Doblaré et al., 2004). There are two major types of bones, cortical or compact bone, which forms the outer surface of the bones and constitutes 80% from the total bones of the body. While trabecular or cancellous bone is found in the inner portions of the cortical bone and form about 20% of the bones Figure (2.3).

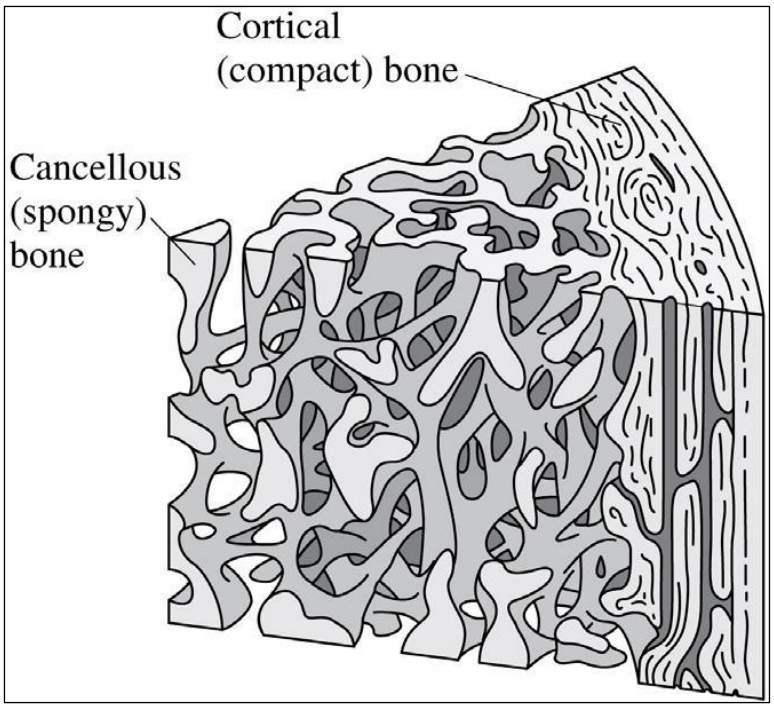

Figure 2.3: Types of bones in human body (Knight et al., 2015).

However, there is a third type of bone which is known as woven bone. This type of bone is an immature bone that can be formed during the process of bone remodelling, where four types of cells are present Figure (2.4). The first type of cells are known as osteoblast cells, these cells are fully differentiated cells found on the surface of the bone and responsible for the production of growth factors and the formation of new bone or matrix, such as, osteoid. They can be differentiated into bone lining cells and osteocytes. Bone lining cells are elongated cells found on the surface of the bone and considered as metabolically inactive, however, they can be stimulated by chemical or mechanical stimuli. Osteocytes, on the other hand, are stellate-shaped mature osteoblast cells found within the mineralised bone matrix in the lacunae. These cells are attached to other bone cells by processes, which give them the ability to transfer the information of the mechanical loading to the adjacent cells. The fourth type is the osteoclasts, which are large multinucleated cells found on the bone surface whose function is to resorb the bone (Weiner et al., 1991, Cowin, 1999, Loveridge, 1999, Lindhe et al., 2003, Doblaré et al., 2004).

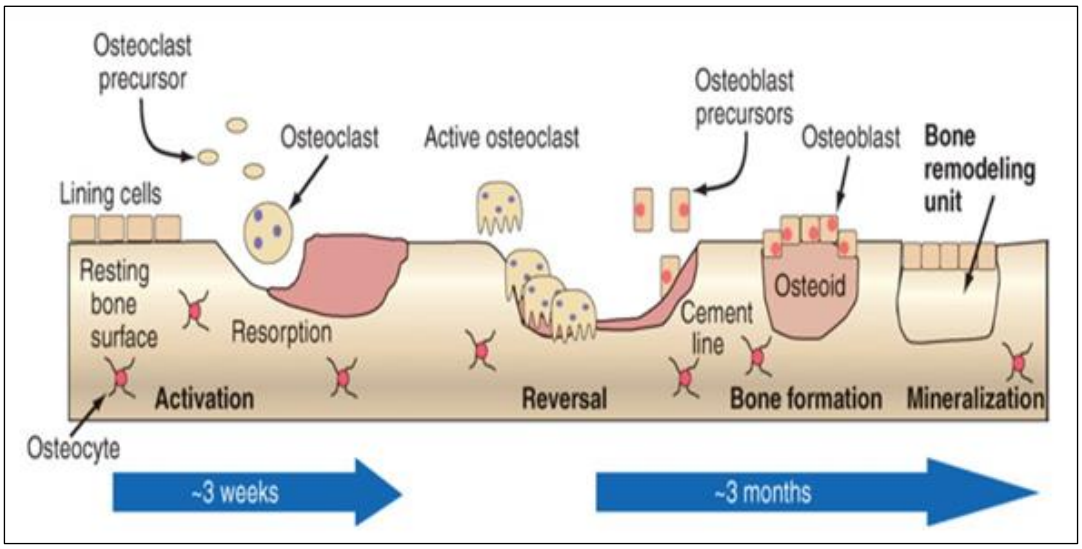

Figure 2.4: Bone remodelling cycle (Bray et al., 1998).

Bone tissue has the ability to heal after injury or fracture without the formation of scar tissue. The mechanism of implant osseointegration process is similar to that in the bone healing process and this includes four stages: inflammatory, vascularisation, bone formation and bone remodelling stage. Different factors contribute through the stages of osseointegration, such as, the type of cells, growth factors and cytokines (Søballe, 1993).

After the surgical trauma and insertion of the implants in bone, there is a formation and accumulation of a blood clot at the bone-implant interface accompanied with the migration of inflammatory cells, vasodilation and resorption of traumatised bone by the action of osteoclast cells (Davies, 1996, Park and Davies, 2000). The next step is the adsorption of proteins from the blood and body fluid. However, the structure of the protein layer can be affected by the type and the surface morphology of the implant (Dee et al., 2003). After 5 days, the implant surface is lined with flattened cells and small blood vessels, then one week later; the clot is replaced with highly vascularized granulation tissue (Franchi et al., 2004, Berglundh et al., 2003). (Meyer et al., 2004) showed that from the first day of implantation osteoblast cells successfully attached to the implant surface and after few days they start to deposit collagen matrix, either directly at the implant interface or on a layer that resembles a cement line. This line is rich in non-collagenous proteins (Puleo and Nanci, 1999). Woven bone is formed after the deposition of the new calcified matrix and it is replaced by lamellar bone after remodelling, thus finalising the process of biological fixation of the implant (Chappard et al., 1999).

Generally, the process of implant osseointegration is a slow process and may take several months (Hofmann et al., 1997). However, to optimise this process a better knowledge is required about the cellular and molecular mechanisms of cells at the bone implant interface (Dimitriou and Babis, 2007).

2.1.6 Failure of dental implants

The high success rate and good prognosis of dental implants are related to the osseointegration process, which is responsible for the primary and secondary stability of the implant through mechanical and biological processes respectively. Many studies report that there is a high success rate of dental implants, which is about 95-97% (Pye et al., 2009); however, failures still occur and the rate is around 7.7% for Branemark dental implants after 5 years as stated by (Esposito et al., 1998a). Moreover, the Meta-analysis study, which was conducted by (Esposito et al., 1998a) confirmed that the implant loss and the rate of failure in edentulous cases were double that of partially edentulous cases and the rate in the maxilla was three times more than in the mandible, except in partially edentulous cases where the rate of failure was nearly the same.

Failure of dental implants can be classified into early and late failures. The former is defined as the failure in the accomplishment of the osseointegration process around the implant surface. While late failure, is defined as the breakdown of the osseointegration after the prosthetic rehabilitation. The failure of dental implants is related to a complex and multifactorial process. Therefore, there are many factors associated with failures some of them related to the early failures and others related to the late failures (Alvim-Pereira et al., 2008).

2.1.6.1 Factors associated with early failures

This can be classified into surgical technique, implant design and patient-related factors.

The skill of the surgeon is one of the factors that affect the process of osseointegration. The excessively traumatic surgical technique may lead to the formation of a fibrous tissue capsule around the implant surface. This capsule will cause improper attachment of the implant with bone. Inadequate cooling or using

excessive speed during the drilling procedure may cause excessive heating of the bone. This will lead to injury of the bone cells and will end up to necrosis and implant loss (Eriksson and Albrektsson, 1984, Ashley et al., 2003, Cavalcante Gomes de Souza Carvalho et al., 2011). Therefore, one of the possible reasons behind dental implant failure within the first few months after insertion is the tissue overheating during a surgical procedure. Moreover, the drilling speed plays an important role in the primary stability of the implant, as it affects osteotomy and heat generation (Iyer et al., 1997, Hadi et al., 2011).

Failure in controlling the heat during the surgical drilling to less than 47 °C or 50 °C for 1 min can cause a reduction in the bone formation around the implant. While heating to 44 °C for 1 min had no effect on the bone regeneration process. Thus, the 47 ^{o}C temperature is considered as a critical temperature for bone necrosis (Eriksson and Albrektsson, 1984).

The conventional drilling method is used with most of the implant systems. This method depends on the drilling protocol with 800 to 1500 rpm, with sufficient amount of water irrigation to prevent overheating. (Anitua et al., 2007) suggested a new method for drilling using low speed 50 rpm without cooling. This procedure gives the operator more precision in the path of drilling and enhances bone healing after the operation. This is due to less friction and trauma to the bone structure (Kim et al., 2010). Despite this advantage, this procedure was considered as a time-consuming procedure. The excessive slow or high-speed drilling may cause a rise in heat generation and lead to high friction with an increase in the amount bone necrosis. Thus, using high drilling speed at 1000 rpm yielded the best biological responses (Yeniyol et al., 2013). (Gaspar et al., 2013) stated that using both low-speed drilling technique without cooling and the conventional method with cooling has no effect on the vitality of the bone cells.

Implant design is also one of the factors that influence the implant stability and ability to withstand the functional forces during and after osseointegration (Abuhussein et al., 2010).

Regarding the shape of the implant, (Carlsson et al., 1986) reported that the screw implant has better stability than cylindrical and T- Plates implants and can withstand both compressive and tensile stresses. The implant shape also plays a fundamental role in determining the type of generated force at the bone-implant interface. The ideal implant design should reduce the amount of shear force which is generated and obtain a good equilibrium between the compressive and tensile forces. Shear forces are responsible for reducing the bone density and the formation of weak bone. Therefore, some authors state that the high failure rates are mostly seen with cylindrical implants rather than tapered implants. This is because of the generation of more shear forces with the cylindrical design than the other types (Misch, 2007). However, (Holmgren et al., 1998) compared the stress distribution around the stepped cylindrical and the straight implants by using finite element analysis and concluded that the stresses are more evenly distributed and dissipated in the former design than with tapered implants.

The diameter of the implant has also an effect on the amount of bone engagement at the bone-implant interface and on the success rate of dental implants. (Ivanoff et al., 1997) investigated the effect of various implant diameters on the osseointegration in rabbit tibia. They found that using a larger diameter implant may recommend higher torque removal. Large diameter implants can be used clinically to enhance implant stability, as they form more supportive cortical bone. Increasing the number and the diameter of the implants in conjunction with the proper positioning of them in high-quality bone all can cause improvement in the biomechanical behaviour of implants and the treatment outcome (Şahin et al., 2002).

(Winkler et al., 2000) focused on the relationship between the failure rate and the diameter of the implants and concluded that 4 mm diameter implants have a lower failure rate when compared to 3 mm diameter implants. Although, narrow diameter implants are the most reliable type to be used in case of narrow residual ridges and edentulous areas with limited interdental width. These implants cannot withstand high occlusal loading and they are susceptible to fracture. This criterion was considered as one of their drawbacks (Kanie et al., 2004, Himmlova et al., 2004).

Regarding implant length, there is limited information about the relationship between the implant length and the survival rate. Some authors stated that long implants have low failure rates compared to short implants, while others reported that there is no effect of the implant length on the survival rate (Testori et al., 2001, Naert et al., 2002, Herrmann et al., 2005). A study of single fixed unit restorations demonstrated that there is no relation between the implant length of more than 13 mm and the implant survival rate (Eckert et al., 2001).

(Herrmann et al., 2005) reported that implant with 7 mm length had the highest rate of failure and the 10 mm lengths had a higher failure than 13 mm length or more. Another study by (Olate et al., 2010) demonstrated that short implants have high failure rates of around 9.9% while, medium implants showed the least rate of 3.0% and the long implants were in between 3.4%. However, (Ali, 2014) stated that short implants had a high success rate when compared with the conventional implants specifically in the case of atrophic alveolar bone. Short implants showed limited usage clinically. This is because of their small surface area which cannot distribute the force evenly over the entire surface. This will generate excessive stresses at the bone-implant interface.

Patient-related factors can be classified into ‘local factors’ which include bone quality and quantity, immune response and radiation therapy and ‘systemic factors’ which include age, smoking and general health (Esposito et al., 1998b, Pye et al., 2009, Baqain et al., 2012).

Bone quality played an important role in the success of dental implant, as it provides a proper site for the implant to integrate with the bone. This integration will lead to better stability and prognosis (Turkyilmaz and McGlumphy, 2008). The mechanical properties of the bone-implant interface can be improved by higher bone density. The higher the density, the lower the implant micro-movement and stress concentration. Therefore, the survival rate of the implant is proportional to bone quality. Some authors stated that the success rate of the implants inserted in the mandible is around 90% over 5 years while; in the maxilla it is around 80% over 10 years (Jaffin and Berman, 1991, Şahin et al., 2002). Moreover, the presence of poor bone quality in the maxilla can lead to a high failure rate of the implants (Herrmann et al., 2005). The high failure of the maxillary implants is related to the variation in the bone densities between both arches (Snauwaert et al., 2000). The densest bone can be seen in the anterior mandible followed by the posterior mandible, the anterior maxilla and the lowest density is in the posterior maxilla (Truhlar et al., 1997, Şahin et al., 2002).

Regarding the immune response, studies have shown that there are no allergic or adverse reactions against the commercially pure titanium and coated titanium implants. However, theoretically, it can be possible that hypersensitivity might be one of the reasons for implant failures (Esposito et al., 1998b). A patient with radiation therapy is susceptible to osteoradionecrosis, infections, less bond strength of bone to implant connection and delayed bone healing around the implant surfaces. This is due to the effect of radiation on bone cells, which causes a reduction in the proliferation of bone marrow cells and damage to the osteoclast

cells (Ihde et al., 2009). (öhrnel et al., 1997) demonstrated that bone thickness and contact to the implant surfaces is remarkably decreased in irradiated rat tibias when compared to the healthy control tibias. Moreover, (Johnsson et al., 2000) studied the effect of implant placement time in irradiated bone on the bone healing around the titanium implants. This study concluded that bone healing is improved as the time interval between the radiation therapy and the implant insertion is prolonged. There is an enhancement in the osseointegration process around the titanium implants. In addition, greater forces are needed to unscrew these implants from the irradiated bones as the time is prolonged.

Systemic factors, such as, age; gender and smoking are also contributed to the failure of dental implants. Dental implants may cause disruption in growth and development of jawbones in young patients. This is due to the implant ankylosis which interferes with the normal eruption process of the natural dentition (Heij et al., 2003). However, the advanced age can also lead to implant failure. This is due to health problems and osteoporosis, which are usually associated with increased patient age (Salonen et al., 1993). Moreover, there is a change in the mineral composition of the bone, as well as the bone proteins and collagen in older patients, which enables the bones to heal over a long period of time. Gender, on the other hand, showed no clear effect on the failure of implants (Porter and Von Fraunhofer, 2004, Moy et al., 2005).

Smoking has a clear effect on implant treatment and many studies reported that there is a high percentage of implant failure in smoker patients in comparison to non-smokers (Lambert et al., 2000). It is evident that smoking is a risk factor that can cause progressive marginal bone loss and periodontal disease, which is also known as peri-implantitis. All these causes correspond to the low success rate of dental implants (Esposito et al., 1998b).

2.1.6.2 Factors associated with late failures

Peri-implantitis and occlusal overloading are the major aetiological factors which are responsible for the late failures of dental implants (Esposito et al., 1998b). Plaque accumulation on the surface of the implant will induce the colonisation of bacteria on the surface which will cause inflammation of the implant mucosa known as peri-implant mucositis. The bacterial infection, on the other hand, may invade the supporting bone and cause peri-implantitis which is responsible for the failure of the implant in case of its progression (Zitzmann and Berglundh, 2008).

(Serino and Ström, 2009) stated that there is a relation between plaque control and peri-implantitis. In patients with proper plaque control and good oral hygiene, the occurrence of pre-implant bone loss is less frequently detected. The same finding was also seen with non-smoker patients because smoking has a direct effect on the oral hygiene. However, the occlusal load may also be responsible for the pathogenesis of peri-implantitis particularly, when the implants are inserted in a loose trabecular bone, this will cause an adverse effect on the osseointegration. This process has three stages when the implant inserted in the bone. The first stage showed an apposition of woven bone on the site of implant placement, then deposition of fibrous tissue and in the final stage there is an adaptation of bone structure to occlusal load. This is performed by replacing the woven bone with mature lamellar bone (Heitz-Mayfield et al., 2004). Many studies showed that excessive loading on dental implants will cause marginal bone loss for newly inserted implants or will cause loss of previously integrated implants (Isidor, 1997). This is due to the absence of periodontal ligaments around the dental implants, unlike the natural teeth which can act as a shock absorber for the excessive occlusal load. Also, during the occlusal loading of the implant the greater amount of stresses will be directed to the coronal portion of the bone. This is related to the type of contact between the two materials, when one of them is subjected to a specific load

the stress will be greater at the first contact area between the two materials (Isidor, 2006).

2.2 Glass and bioactive glass

2.2.1 Glass definition

A glass is defined as “an inorganic product of fusion that has been cooled into a rigid condition without crystallisation”. It is a translucent material that has specific characteristics, such as, rigidity, brittleness and hardness (McMillan, 1979). Pure silica glasses are mainly composed of a network of silicon atoms bonded to each other by covalent bonds with oxygen atoms.

Glass is similar to liquid because both of them possess a random arrangement of atoms and exhibit no crystalline lattice (Paul, 1989). Therefore, glass is different from a crystalline material, as the latter has regular or long periodic order of atoms. While, glass has no long-range periodicity, it may have short and intermediate structural order of scales (Chrissanthopoulos et al., 2008).

Moreover, glasses exhibit no diffraction peaks when examined by X-ray diffraction Figure (2.5) and they do not have a specific melting temperature. When heating the glass up to a high temperature, it will soften and ease into a viscous liquid. This is known as the glass transition temperature (T_g), which is a unique property for the glass, and it can be defined as the temperature where the solid glass will transform into a viscous liquid state. Consequently, the glass will behave as an elastic solid below this temperature and as a viscous liquid above it. In contrast, crystalline solids which exist as a single phase show the occurrence of a specific melting temperature. However, multiple crystallite phases exhibit multiple melting temperatures (Höland, 2012).

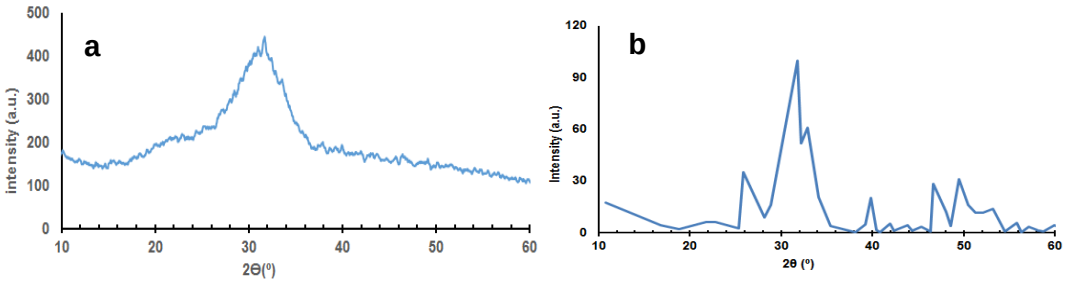

Figure 2.5: X-Ray Diffraction pattern of a) amorphous glass b) crystalline solid.

Regarding the process of glass formation, glasses can be formed when a liquid is cooled below its melting temperature (T_m) and transformed into a rigid solid. This process can be described according to the volume-temperature diagram Figure (2.6). When a liquid is cooled with a slow rate below its T_m, the fluidity of the liquid will decrease in addition to the appearance of a sharp reduction in the material volume. Therefore, the material will have a high possibility to crystallise unlike when a liquid is cooled at a fast rate. In the latter case the liquid can show a gradual decrease in the volume, as well as in the fluidity. This will give no opportunity for the material to crystallise (Paul, 1989).

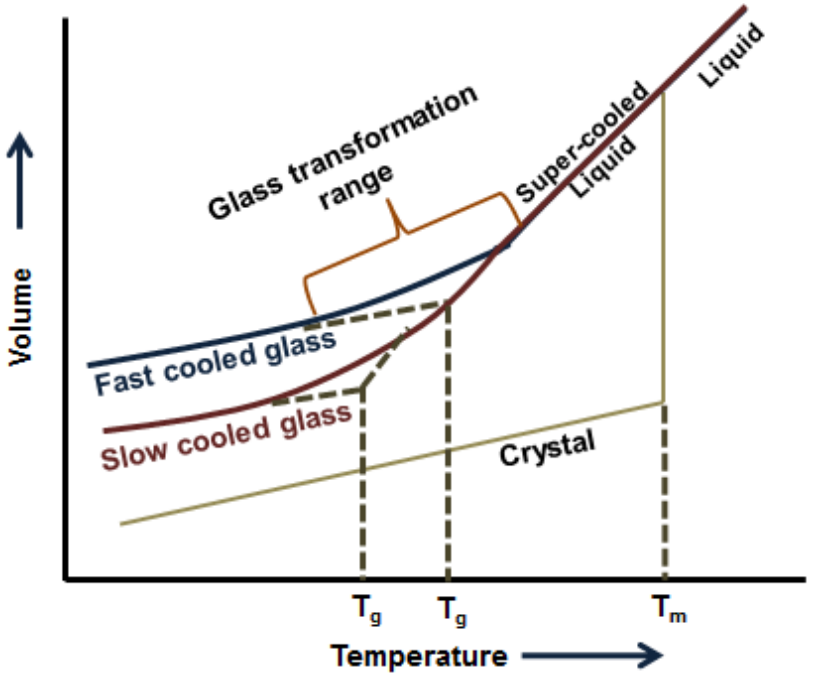

Figure 2.6: The effect of temperature on glass formation (Shelby, 2005).

2.2.2 Glass structure

Glasses and crystals, as hypothesised by Zachariasen theory, are formed from the same basic unit, which is known as polyhedral network or tetrahedron. Although the interatomic distances in this network are similar in both structures, the orientation of these distances in the glass three-dimensional network is not symmetrical and periodic as in the crystalline network (Paul, 1989).

The silicate glass tetrahedral network structure is composed of a silicon atom which is located in the middle part of the unit and it is connected with four oxygen atoms by covalent bonds as shown in Figure (2.7).

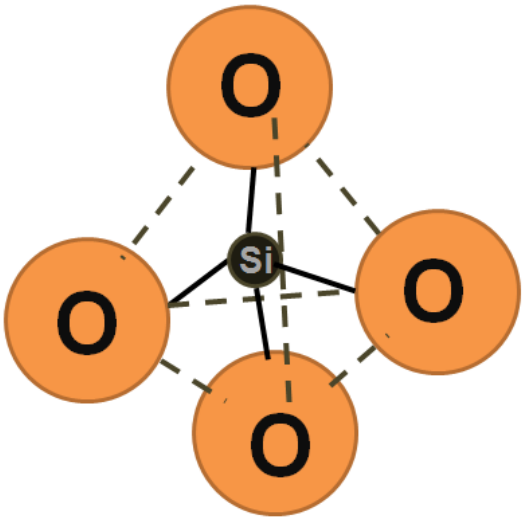

Figure 2.7: Schematic diagram shows the basic composition of silica glass (Höland, 2012).

In the amorphous glass, each tetrahedron is connected through their oxygen atoms to four adjacent tetrahedrons in a random order forming a three-dimensional network. This random structure is related to the variances in the bonding length between the adjacent tetrahedral units and the bonds length within these units. This feature differentiates glass from crystalline structure, where the latter is composed of ordered tetrahedral units as shown in Figure (2.8).

Zachriasen stated rules for glass formation and the ability of oxides to form a short range ordered 3-dimensional network glasses. These rules illustrated that oxygen atom should be bonded to two glass forming atoms. Moreover, the oxygen atoms should share the corners of the polyhedral and not the edges or the faces (Paul, 1989, Shelby, 2005, Höland, 2012).

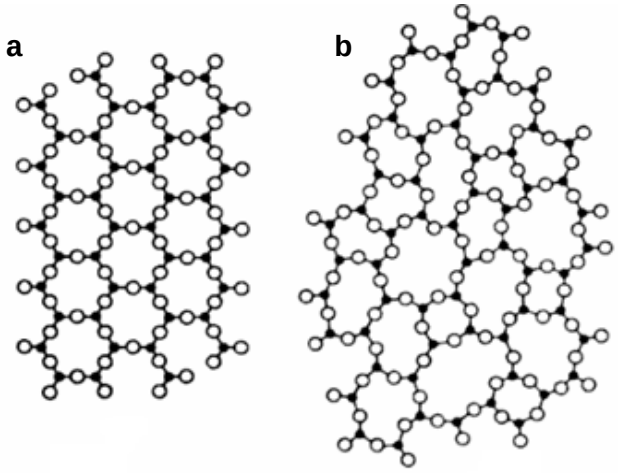

Figure 2.8: Schematic diagram illustrates the differences between a) crystalline structure b) glass structure (Paul, 1989).

There are three types of oxides which take a part in the glass formation and these can be classified as follows (Shelby, 2005, Al-Noaman, 2012):

Glass formers: these are oxides with small cations that have the ability to form the 3-dimensional network of the glass with random order, example: silicon dioxide (SiO_2), boric oxide (B_2O_3) and phosphorus pentoxide (P_2O_5). The largely covalent bond between the glass former and the oxygen is called bridging oxygen bond (BO)

Glass modifiers: these are oxides of large cations, which do not have the ability to form a 3-dimentional glass network. However, they disturb and weaken the network structure by forming non-bridging oxygen bonds (NBO). These bonds can be defined as the ionic bonds between the oxygen and the modifiers. Examples: calcium oxide (CaO) and sodium oxide (Na_2O).

Glass intermediates: these oxides are also known as conditional glass formers. They have the ability to form a glass network only when they are mixed with glass formers *i.e*. they cannot form a glass by their own. Example: aluminium oxide (Al_2O_3) and zinc oxide (ZnO) Figure (2.9).

The glasses' biological behaviour can be affected by the ratio of the BO to NBO that are present in the glass composition (Hench and Wilson, 1993). The presence of large ratio in the glass network will lead to the reduction of the degradation of the glass in the body and turn it into non-bioactive material (Höland, 2012).

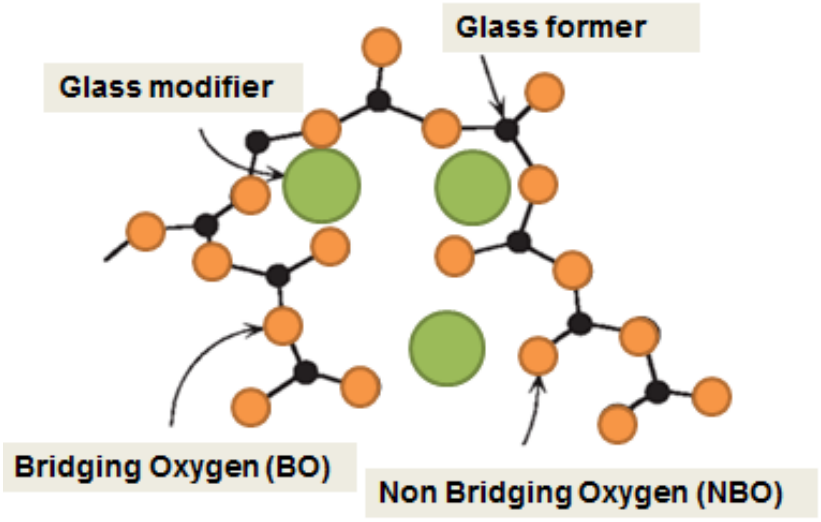

Figure 2.9: Schematic diagram showing glass network structure (Hench and Wilson, 1993).

2.2.3 Glass Network Connectivity (NC):

Silicate glasses resemble inorganic polymers as the silicon atoms are cross-linked with oxygen. This cross-link density or the network connectivity (NC) of the glass network plays an important role in the prediction of some glass properties, such as, solubility, reactivity, T_g and thermal expansion coefficient.

The network connectivity is defined as, the average number of bridging oxygen bonds per unit tetrahedron or silicon atom in the glass (Hill, 1996).

The dissolution rate of the glass in the body fluid and the ability of the bioactive glass to form apatite on the surface can be predicted by the NC. The presence of glass modifiers in the glass network structure can affect the connectivity by disturbing the structure of the tetrahedron and forming NBO bonds. This lowers the connectivity and rendering the bioactive glass to be more degradable or bioactive (Höland, 2012). Therefore, there is a direct relationship between network connectivity and Q structure of glass (Q is short for quaternary), which both depend on the BO content in the glass structure. For example, pure silica or quartz glasses have a Q^4 structure, which is equivalent to NC of 4.0. This means that the silicon atom is connected by four BO bonds. In a 3-dimensional glass structure, the NC is equal to 3.0, which is related to the presence of three BO per silicon atom and is corresponded to Q^3 structure. In linear glass network, the Q structure is 2.0 which is equivalent to NC of 2 and the presence of two BO per silicon atom.

The NC can be calculated depending on the composition of the glasses. (O'Donnell et al., 2008) calculated the NC of the glass by using two equations. In the first equation (2.1), P_2O_5 was supposed to form a part of the glass network and exist as a mixed sodium-calcium orthophosphate. This assumption is no longer used because of the development of the second equation (2.2), which is a modification of the former one. This is known as "modified network connectivity" (NC') which assumed that the phosphate is forming a separate phase (orthophosphate units) and its requiring charge balance from the other cations in the glass network as Na^+ and Ca^{2+}. This will lead to an increase in the NC of the silicate glasses.

Equation 2.1

$$NC = 2 + \frac{[(2 \times SiO_2) + (2 \times P_2O_5)] - [(2 \times CaO) + (2 \times Na_2O)]}{SiO_2 + (2 \times P_2O_5)}$$

Equation 2.2

$$NC' = 2 + \frac{(2 \times SiO_2) - [(2 \times CaO) + (2 \times Na_2O) + (6 \times P_2O_5)]}{SiO_2}$$

(Hill and Brauer, 2011) demonstrated that the bioactivity of the glass is dependent on its NC. Therefore, when the glass NC decreases, the bioactivity or the dissolution rate will increase. This is due to the changes of the glass structure from cross-linked network to linear chains of low molar mass. The glasses with NC~ 2.0 are the most bioactive due to the presence of largely Q^2 species in the glass structure whereby, glasses with NC values above 2.4 shows low bioactivity or are non-bioactive materials (Elgayar et al., 2005). (Fujibayashi et al., 2003) compared the ability of the glass granules with different NC or silica content to form an apatite layer both *in vivo* and *in vitro* using simulated body fluid (SBF) solution. The study showed that there is an inverse correlation between apatite formation and NC as the amount of bone formation decreased when the NC value increased. Moreover, (O'Donnell and Hill, 2010) stated that glasses of NC lower than 2.0 are known as invert glasses. These glasses have the ability to dissolve rapidly and increase the amount of alkali ions in the surrounding biological environment, which might cause a rise in the pH level, cytotoxicity and formation of fibrous tissues capsule around the material surface.

There are limitations in the use of the NC and the NC' models in designing new glass compositions and predicting bioactivity. A significant decrease is shown in the predictive nature of the both models for the glass bioactivity as more chemical compounds included in the glass composition (Hill, 1996). This is due to the dependence of the network connectivity on the glass compositions, which in turn should indicate the presence of homogenous structure and regular co-ordination numbers of the network-forming ions in the glass composition. Therefore, the role of the components in the glasses should be known to ensure the successful use of these models. In addition, these models emphasise the biological response of glasses and neglected the nature of modifying cations. The field strength or the

charge to size ratio of modifier cations has an influence on the glass network by expanding the network or providing more ions for apatite formation. Although, the NC' will remain constant and does not reflect this behaviour.

2.2.4 Bioactive glass:

Bioactive materials were defined by (Williams, 1999) as materials that have the ability to stimulate biological responses and form a direct bond with living tissues.

In the 1960s, Hench and co-workers discovered the first bioactive glass, which is known as bioglass 45S5. This glass is composed of the following oxides 45 % SiO_2, 24.4 % CaO, 24.5 % Na_2O and 6 % P_2O_5 (all in weight percent) and it shows high bioactivity and ability to form a true bond to hard and soft tissues both *in vitro* and *in vivo* environments through the formation of hydroxycarbonate apatite (HCA) on the material's surfaces (De Aza et al., 2007, Ylänen, 2011).

To design a bioactive glass, there are many factors that should be taken into consideration; one of them is the chemical reactivity of the glass and its ability to form apatite in body fluid and aqueous solutions. This is highly dependent on the glass composition. However, the strength is another important property for the bioactive glass; this depends on the surface properties of the glass rather than the chemical composition.

The reason behind the importance of glass strength is that glass possesses a high strength but, it cannot withstand heavy forces. This is due to their brittle nature and susceptibility to flaws. Therefore, this material is not used in the loading bearing areas, however it can be used as a coating for other materials (Ylänen, 2011).

The bioactive glass has the ability to form a strong glass-bone contact when implanted in the bone. This strong bond renders the removal of the implant from its location very difficult and this may lead to a fracturing of the implant itself or the bone and not the contact area in between (Rawlings, 1993).

Regarding the bioactive glass processing, this material can be formed by two main processing routes: the first one is known as the melt derived route. This method is similar to the conventional method which is used to form the soda-lime glasses and it requires the melting of the metal oxides at high-temperature 1350 ºC -1450 ºC. While, the second method requires lower temperatures 600 ºC -700 ºC and this is known as the sol-gel method (Li et al., 1991). The glasses produced by the latter method showed higher bioactivity than the glasses made by the melt quench technique. This is due to the high porosity of the sol-gel glasses revealed by the high ratio of the surface area to the volume.

2.2.5 Role of Fluoride in bioactive glass:

The incorporation of fluoride into the bioactive glasses has several advantages in both dental and orthopaedic applications. For the dental applications, fluoride plays an important role in preventing dental caries by inhibiting enamel and dentine demineralisation process, as well as bacterial enzymes. Also, it enhances the dental remineralisation process. This is because; fluoride ion has the ability to substitute for OH^- group in HAP and form fluoroapatite (FAP) which is more acid stable than HAP (Grynpas, 1990, Thuy et al., 2008, Brauer et al., 2009). While for orthopaedic applications, fluoride can stimulate osteoblast cells, bone mineralisation and increase bone density. Thus it is used in the treatment of osteoporosis (Aaseth et al., 2004, Vestergaard et al., 2008).

The nature of fluoride incorporation in the structure of bioactive glasses has been studied in many papers, but still, its role in the structure is controversial. Solid-state magic angle spinning nuclear magnetic resonance (MAS-NMR) is a useful technique in providing information about the structures of various materials including glasses (Miller, 1996).

Several studies have been performed to determine the role of F^- in different glasses. Some of them concluded that the addition of CaF_2 in the glass will cause disruption in the glass network, leading to the formation of Si-F bonds. While, others reported that F^- is coordinated with Ca^{2+} and form complexes without the breakage of Si–O–Si bonds (Hayashi et al., 2002).

(Lusvardi et al., 2008) incorporated fluoride into glass compositions by substituting the network modifying oxide, such as, CaO or Na_2O with a metal fluoride. This method resulted in a reduction in the modifier content and in the number of the NBO bonds in the silicate glass network. This led to an increase in the compactness of the network connectivity and the formation of a high percentage of Q^3 and Q^4 species and formation of (Si-F bonds) as the amount of fluorine increased. Thus, this will lead to a more cross-linked or less degradable glass. In addition, there is the occurrence of a slow release of ions in the solution during the bioactivity process. (Brauer et al., 2009) and (Mneimne et al., 2011) added CaF_2 to the glass composition without substituting it for the modifying oxides, therefore, they kept the ratio of the other components constant, as well as the value of the NC, which was around 2.13. In this method, they assumed that the fluorine is forming a complex with sodium and/ or calcium and reducing their possibilities to form non-bridging fluorine bonds. Also, ^{29}Si MAS-NMR results demonstrated that Q^2 is the main species with the availability of small amount of Q^3 and there is no detectable level of Si-F bonds. Therefore, the addition of CaF_2 will not cause an alteration in the silicate structure. Furthermore, (Hill et al., 2005) stated that the formation of Si-F bonds is unlikely in glasses with a large number of NBOs and network connectivity around 2.0 due to the high affinity of Si^{4+} to the oxygen in comparison with F^- ions. Therefore, the NBOs are attached to Si and there is no formation of Si-F bonds.

Some authors stated that fluoride prefers to form a complex with calcium over sodium (Stebbins and Zeng, 2000) while, recent studies showed that there is no

preference for the fluoride to bond with either Ca^{+2} or Na^{+} ions, but it is embedded in the mixed species (Christie et al., 2011, Pedone et al., 2012). As a result of the fluoride binding with the glass modifiers, there will be an increase in the polymerisation of the silica network for charge balancing NBO (Cocchi et al., 2012). However, the degree of network polymerisation can be kept constant by adding F^{-} to the glass structure and keeping the network former to modifier ratio constant (Brauer et al., 2010).

Furthermore, increasing CaF_2 content in glasses has demonstrated a significant effect on the glass thermal properties, such as, T_g and crystallisation temperature (T_c). The studies showed that increasing the fluoride content will cause a decrease in both temperatures. This is due to the role of fluoride in reducing the compactness of the silicate network and forming complexes with the calcium. In fluorine-free glass, calcium ions are divalent and they will bind with the silicate anions by electrostatic forces, as well as forming ionic bridges between two NBO. When CaF_2 is added, CaF^{+} species will cause a reduction in the electrostatic forces between NBO and decrease the compactness of the network Figure (2.10), thus the T_g will decrease (Brauer et al., 2009, Al-Noaman et al., 2012a).

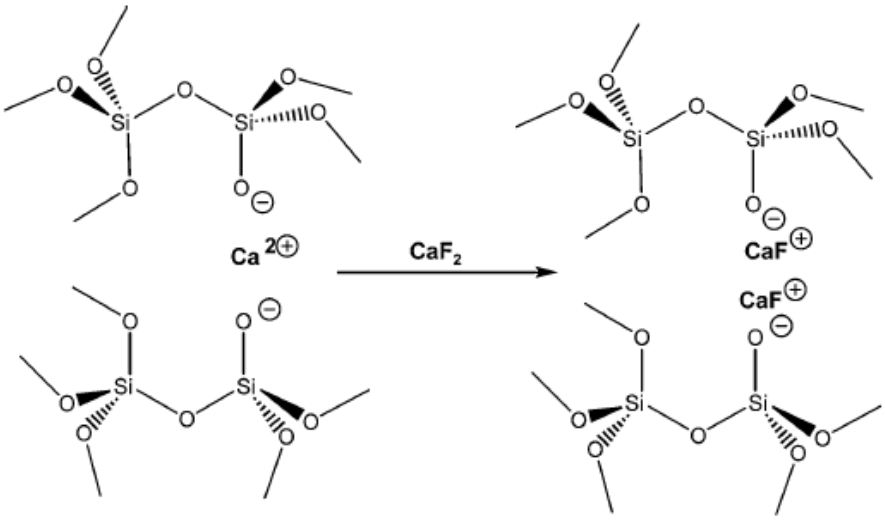

Figure 2.10: The effect of adding CaF_2 to silicate network (Brauer et al., 2009).

The effect of CaF_2 on the pH and the formation of apatite were investigated by (Brauer et al., 2010, Al-Noaman et al., 2012a). The studies showed that the increase in the pH of the solutions, such as, Tris buffer and SBF is less pronounced when increasing the fluoride content in the glass composition. This is related to the buffering effect of the fluoride ions which exchange with the OH^- from the solution reducing the alkalinity of the previous solutions. The alkalinity was caused by the ions exchange with the H^+ of the solution, therefore; the production of high pHs should be avoided because of the harmful effect on the living cells *in vivo* (Aina et al., 2009). Apatite formation, on the other hand, is highly dependent on the pH level of the solution where the glass immersed and as the amount of pH increase is low, the deposition of the apatite in the solutions decreases with the increase in the amount of fluoride. However, the increase in fluoride caused the formation of fluorite, which inhibits fluoroapatite formation and this is due to the low phosphate concentration as explained by (Brauer et al., 2010). (Mneimne et al., 2011) showed that the addition of fluoride to the glass composition in combination with increasing phosphate content will significantly increase the rate of apatite formation. Higher phosphate would suppress the fluorite formation and enhance the formation of FAP; therefore, phosphate has a critical effect on the apatite formation rate.

Biologically, fluoride has an effect on the bone cells, as well as on the mineral composition of the bone because it can be incorporated into the mineral component of bone during the process of bone formation (Grynpas, 1990). The effect of fluoride on bones is dose dependent. Studies showed that the fluoride concentration of 25-500 ng mL^{-1} stimulates the osteoblast cells and forms a favourable condition for bone formation or promotes bone mineralisation. While, a high concentration of fluoride, greater than 500 ng mL^{-1}, leads to the suppression of osteoblasts and may cause the abnormal bone condition known as fluorosis (Grynpas et al., 2000, Hoppe et al., 2011). However, the effect of fluoride on osteoclast cells activity is poorly

understood; (Sakae et al., 2001, Oguro et al., 2003) stated that the usage of an appropriate concentration of fluoride will inhibit the bone marrow progenitor cell development into osteoclast cells and suppress the phagocytic cell activity.

Regarding dental implants, some authors have demonstrated that the incorporation of fluoride into the titanium surfaces can enhance bone formation around the implant. This depends on the fact that the incorporation of ions in the superficial layer of the material can modify the biological responses toward the implant material due to the biological role of the added ion. Low concentration of fluoride can be incorporated in the structure of surface titanium dioxide layer of the implant to modify it physically and chemically. This modified surface has the affinity to attract the calcium and phosphate ions and precipitate them on the surface. Also, it stimulates the differentiation of osteoprogenitor cells and increases the trabecular bone density in addition to the mineralisation at the bone-implant interface (Ellingsen et al., 2006). Therefore, fluoride-modified titanium implants showed superior osseointegration behaviour in comparison with non-modified implants. Fluoride-modified titanium implants showed faster osseointegration due to more bone formation at the bone-implant interface. This attributed to the enhancement of osteoblasts differentiation. Therefore, high anchorage is shown with these modified implants (Ellingsen et al., 2004, Cooper et al., 2006) .

2.2.6 Role of sodium in bioactive glass:

The basic components of most bioactive glasses are SiO_2, CaO, Na_2O and P_2O_5. The reactivity of this system is varying from surface dissolution material, which showed the formation of a bond with bone, to bulk scaffold degradable material, which resorbed within a specific period of time in the living tissues. Sodium is known as a critical component of this system and its inclusion cause improvements in the mechanical strength of these materials without affecting the material biodegradability (Chen et al., 2012). Bioactive glass scaffolds generally have low mechanical

strength and are therefore not used in areas where high forces are applied. Therefore, extensive densification is required to increase the strength of the bioglass foam-like scaffolds. This can be achieved by sintering the foam material at high temperature to increase the compactness of its particles and to form a strong crystalline phase, which in turn can affect the bioactivity of the material. As crystallisation will have taken place the bioactive material may be transformed into a bioinert material (Chen et al., 2006). Thus, the addition of Na_2O is advantageous in the densification and crystallisation treatment of bioceramic, which is attributed to the formation of $Na_2Ca_2Si_3O_9$ crystal phase on the surface of the material. This phase can slow the process of apatite formation *in vitro* rather than suppressing it, as stated by (Peitl Filho et al., 1996, Clupper et al., 2002).

Furthermore, the addition of Na_2O to silicate-based glasses will decrease the T_g and the T_c of these glasses as these two temperatures are critical for the glass sintering. This is attributed to the role of Na_2O in increasing the processing window between the two temperatures which in turn enhances the sintering of the glasses without crystallisation. This is performed by decreasing the degree of the glass network packing which will cause expansion of the glass network and a decrease of the glass density while keeping the network connectivity of the glasses unchanged. Therefore, increasing the sodium content in the glasses will act as a disruptor to the network causing a reduction in the T_g and T_c, as well as decreasing the thermal expansion coefficient of the glasses. The latter thermal property is important for the coating of metal implants because bioactive glasses possess thermal expansion coefficient higher than the titanium and titanium alloys implants, which may cause chipping or interfacial separation of the glass from the metal surface (Wallace et al., 1999).

(Farooq et al., 2013) suggested that there is a relationship between T_g and hardness. The latter is an important property for the grit blast application. As the T_g is dependent on the sodium content, therefore, the hardness of the glass can be

altered by modifying the concentration of sodium in the glass network. Thus, increasing the sodium content in the glass network will decrease the T_g, as well as decreasing the hardness of the material. This is related to the lower field strength of Na^+ which forms a weak ionic linkage between the NBO bonds in the glass structure in addition to the effect of sodium on the glass density by decreasing the packing density of the glass as shown in Figure (2.11) (Wallace et al., 1999).

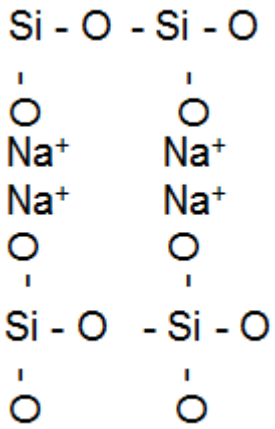

Figure 2.11: Role of sodium in the glass structure (Wallace et al., 1999).

Regarding biocompatibility, (Wallace et al., 1999) showed that the high concentration sodium containing glasses produce low *in vitro* biocompatibility when compared to the low concentration sodium containing glasses. This is related to the high ion exchange between the sodium of the glass and the proton of the medium which causes a high elevation in the pH level of the medium. This alkalinity will elicit a cytotoxic response to the living cells. However, (Hench, 1991) demonstrated that sodium is an important factor in glass bioactivity and apatite formation whilst (Farooq et al., 2013) showed that sodium free glasses can form apatite in Tris buffer within 6 h. This indicates that calcium ions and orthophosphate are released into the surrounding solution causing precipitation of apatite on the surface of the glasses. Therefore, increasing the sodium content in the glass structure should not necessarily increase the bioactivity.

2.2.7 Role of phosphate in bioactive glass:

The glass structure and the role of ions in the structure have been investigated by many authors, however; the role of phosphate in the glass structure is still controversial. Previous studies assumed that P_2O_5 is a network former and it enters the glass network. Therefore, phosphate should form six bridging oxygen bonds Figure (2.12 a). However, recent studies showed that P_2O_5 exist as an orthophosphate–like species Figure (2.12 b) and this indicates the removal of sodium and calcium ions from their role in the silicate network to charge balance. This will lead to an increase in the Q^n structure of the silicate network, which corresponds to the crosslinking of the silicate network (Elgayar et al., 2005).

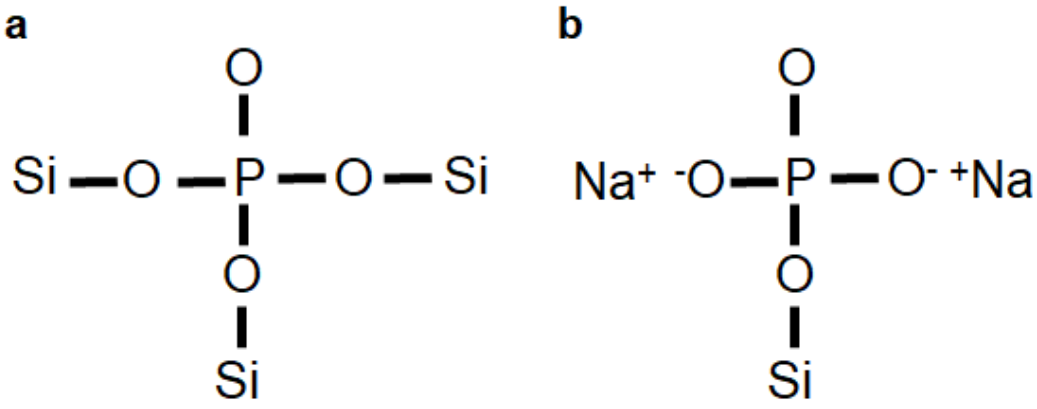

Figure 2.12: Phosphate role a) as a network former in glass network b) as orthophosphate structure (Elgayar et al., 2005).

The existence of higher P_2O_5 percentage in the glass network will cause an increase in the polymerisation of the silicate glass or the formation of a higher proportion of Q^3, which is less bioactive (Lockyer et al., 1995) . This is due to the removal of more network modifying ions from the silicate network and decreasing the number of the BO bonds that are attached to the Si atoms in addition to the formation of P-O-Si linkages (Tilocca and Cormack, 2007). Thus, there is a preference for network modifiers as sodium and calcium to associate with phosphate instead of silicon

species. The glasses of this study were prepared by an annealing technique, and the use of slow cooling. This increases the possibility of having phase separation and the occurrence of orthophosphate species. However, this orthophosphate species clearly appears in the glass structure when the glass is rapidly quenched in cold water, as this technique reduces the possibility of producing phase separation in the glass (Elgayar et al., 2005, O'Donnell et al., 2008). This indicates the presence of phosphate as a separate species and not included in the glass network as a network former.

Regarding glass bioactivity, (Hench, 1991) proved that phosphate takes part in the bioactivity mechanism, and it is responsible for the formation of the calcium-phosphate layer (Ca-P), which is responsible for the precipitation of HCA. However, phosphate-free glasses can also show the formation of HAP on their surfaces and form a bond with bone structure. This is due to the presence of phosphate in the surrounding physiological fluid which can take part in the mechanism of apatite formation. Therefore, P_2O_5 is not essential in the development of HAP layer (Izquierdo-Barba et al., 1999). The addition of small percentages of P_2O_5 in the glasses can enhance the crystallisation of HAP, as the phosphate dissolves in the body fluid causing increase in the amount of saturation of the fluid which in turn hastens the crystallisation process of HAP layer (Ebisawa et al., 1990). Therefore, P-containing glasses demonstrate higher bond strength to the bone when compared with P-free glasses. This is because of the uneven thickness of the Ca-P layer which is formed on the P-free glass surface.

(O'Donnell et al., 2009) studied the effect of phosphate concentration on the bioactivity of the glasses in SBF using two glass series. In the first series, phosphate is assumed to have entered the silicate network, and its addition had achieved by replacing the SiO_2 and keeping the glass modifiers ratio constant.

While in the second series, the phosphate was added to the glass by increasing the amount of Na^{+} and Ca^{2+} to have charge balance with the PO_4^{3-} complex. In this series, phosphate is supposed to form separate species. They concluded that increasing the phosphate content in both glass series had a significant effect on the bioactivity even in the case of increasing the network connectivity for the first series. So, phosphate content is more important than the network connectivity of the glass. This is because phosphate occurred as Q^0 species in the glass which gives it the opportunity to produce more apatite and speed up the process of apatite formation. Also, the presence of high phosphate content in the glass showed an obvious effect on the pH rise of the tested solution. Phosphate will act as a buffer to reduce the alkalinity of the solution due to the release of network modifiers from the glass. This reduction of the pH will be optimum for the apatite deposition. Furthermore, (Mneimne et al., 2011) studied the effect of phosphate content on the apatite formation in Tris buffer by increasing the CaF_2 concentration in the glasses and keeping the other components ratio constant. The conclusion of this study was coincident with the previous study by (O'Donnell et al., 2008) in addition to the feature of increasing the ability of the high-phosphate glass to form fluoroapatite rather than fluorite which is more important in dental and orthopaedic applications. Therefore, the usage of high-phosphate containing glass coatings on dental implants could have a significant enhancement in the formation of apatite around the implant within a short period of time. This can promote the process of osseointegration and improve the stability of the implant. Moreover, combining these advantages with the advantages of having fluoride containing glass may give significant results when using these glasses as a coating material for implants.

2.2.8 Mechanism of bioactive glass interaction with bone:

When bioactive glass material comes in contact with a physiological medium, its surface will undergo structural and chemical changes to form HCA layer. This layer has the same mineral composition as the bone and it bind chemically with bone. Therefore, HCA facilitates the biological interaction and fixation of the bone with the surface of the material. Many *in vitro* studies have demonstrated that the degree of reactivity and the thickness of the bonding layer differ according to many factors, such as, the chemical composition of the bioactive glass, surface area to the solution ratio, and the test solution (Sepulveda et al., 2002). Recent studies have shown that the bioactivity of the glass is increased when the Q structure of the glass moves from the 3-dimensional network to linear chains, the latter corresponding to a disrupted glass structure. This feature was neglected in the Hench model of bioactivity (O'Donnell et al., 2008).

The mechanism of bonding can be illustrated as follows (Hench, 1991, De Aza et al., 2007, Rahaman et al., 2011):

1. Exchange of cations between the network modifiers of the bioactive glass as Na^+, K^+ and Ca^{2+} with the H^+ or H_3O^+ ions of the physiological media. The existence of weak bonds between the network modifiers and the glass network render the cations of the glass to detach easily from the network and exchange with the ions in the surrounding fluids. This exchange process will lead to an increase in the pH level at the glass-solution interface. The level of the pH rise can be affected by powder particle size. The finer the particles size, the more surface area exposed to the solution and the higher the pH level.

$$Si\text{-}O\text{-}Na^+ + H^+ \longrightarrow Si\text{-}OH + Na^+ \text{ (solution)}$$

2. As a result of the rise in pH or of OH^- concentration, breakage of the silicon network bond (Si-O-Si) and dissolution of the silica will take place. This is due to the

hydrolysis of the (Si-O-Si) bond by the OH^- ion, which will lead to the release of the silica in the surrounding fluid in the form of silicic acid $Si(OH)_4$. Also, there is a continuous formation of silanols (Si-OH) at the glass-solution interface.

However, the solubility of the silicic acid is low but, there is evidence of high concentration of silicate-ions in the surrounding fluid as a result of the dissolution process of the bioactive glass in physiological fluids. This indicates that the mechanism of silica dissolution is a significant factor in process of apatite deposition (Rahaman et al., 2011).

3. Then the amorphous SiO_2-rich layer at the interface area becomes condensed and re-polymerized, leading to the formation of silica gel layer on the glass surface which lacks Na^+ and Ca^{2+} ions. Therefore, the combination of a high level of hydroxyl groups and the negative charges of the silica gel layer were important in the induction of the HCA layer (Mami et al., 2008).

4. Migration of Ca^{2+} and PO_4^{3-} ions to the surface of the glass from the solution, leading to the formation of an amorphous layer known as Ca-P rich layer on the top of the SiO_2-rich layer.

5. This amorphous layer will crystallise as a result of the incorporation of OH^- and CO_3^{2-} or F^- from the solution to form a HCA layer and/or FAP layer.

6. After that, the biological steps or the bonding process with living tissues start by the adsorption of the growth factors toward the HCA layer. This layer is responsible for the activation of the stem cells differentiation.

7. Stem cells will attach to the glass surface and start to form osteoblast cells. The osteoblasts will secrete Ca-P extracellular matrix around themselves, which will crystallise after a period of time to enclose the living cells.

In 1980, Hench et al. studied the surface bioactivity of the 45S5 using Tris buffer. This study showed that the bioglass has the ability to form a SiO_2-rich layer and the

$CaO\text{-}P_2O_5$ layer on its surface after the immersion in Tris solution at pH 7.4 (Kokubo and Takadama, 2006). On the other hand, Kokubo and co-workers in 1990 introduced a solution known as SBF, which contains a combination of ions similar to that found in the human blood. They tested the bioactivity of the bioactive glass in this fluid and demonstrated that the calcium and phosphorus ions in the SBF accelerated the formation of the Ca-P layer and the crystallisation of the HCA layer. Thus, this fluid represents a condition that resembles the *in vivo* condition. (Sepulveda et al., 2002) studied the effect of cell culture medium Alpha Eagle's Minimum Essential Medium (α-MEM) and SBF solutions on the dissolution rate of melt quench and sol-gel glasses. The results showed that the dissolution rate for both glasses is slower in the culture media than SBF. Also, the rate of HCA layer formation together with the dissolution rate for the both glasses were investigated by (Jones et al., 2001) using a different concentration of glass powder immersed in SBF solution. The study showed that the rate of dissolution was increased as the concentration of the powder increased in the solution. However, the intensity of the HCA formation showed a significant decrease with the increase of the powder concentration. This is due to the rise in calcium/phosphate ratio, which leads to the formation of calcium carbonate layer instead of HCA and this reduced the bioactivity.

2.3 Surface roughness

The long term success of dental implant depends on the mechanical and biological stability of the implant in the bone tissue, and this can be affected by many factors like the design, chemistry, wettability and the surface topography of the implant (Stanford, 2008). The nature and texture of the implant surface are fundamental factors in the tissue response around the implants. A textured implant surface exhibits more tissue growth and osseointegration than the smooth surface implant. This is due to the large surface area which is produced by different modification methods, such as, grit blasting, plasma spraying and acid etching.

This large surface area of the implant will cause enhancement in the attachment of more collagen fibres and increase the cellular activity towards the implant. This is responsible for improving the osseointegration process, increasing the bone apposition around the implant and the production of good bone-implant interlock. As a result of these reasons, an implant with a rough surface is the preferable choice for treatment in patients with poor bone quality (Lacefield, 1999, Alla et al., 2011). A rough implant surface can form a direct contact with the blood clot in the implant bed and stimulate the migration of the mesenchymal stem cells to the bone-implant interface. Also, this surface improves the attachment of fibrin and promotes the migration process, which is known as osteoconduction. The mesenchymal stem cells will differentiate into osteoblast cells and the latter start to form bone tissue in direct contact with the implant surface (Park and Davies, 2000, Davies, 2003). In contrast to the smooth surface implants, where the blood clot shows a considerable shrinkage from the surface and leads to the formation of a gap in the bone-implant interface. This gap will prevent the osteoblast cells from reaching the interface area, therefore, there will be a fibrous tissue capsule surrounding the dental implant (Sennerby et al., 2008). The osseointegration process can be performed more rapidly in implants with rough surfaces than with smooth surfaces. This integration leads to a highly stable and successful implant in addition to the ability of the implant to withstand functional forces particularly after the healing period (Zechner et al., 2003).

Regarding the parameters for the surface roughness, in general the parameters are scale dependent and the roughness value may depend on the analytical techniques used for their determination. The comparison of roughness data can be done when the data is obtained in the same spatial frequency domain. Complementary techniques are usually required to determine the implant surface topography like stylus profilometry, optical profilometry and scanning electron microscopy in order to

obtain at least three parameters (amplitude, spatial, and hybrid) for the purpose of surface characterisation (Ellingsen et al., 2006). The R_a value is the most widely used parameter for the measurement of surface roughness and it can be defined as "the arithmetic mean value of the surface departures from the mean plane" (Cooper, 2000). Some studies showed that dental implants with different surface morphologies may share the same R_a value Figure (2.13). (Hansson, 2000) demonstrates that there is a relation between the surface morphology of the implant and the shear strength of the bone-implant interface despite having similar R_a values. Although the surface morphology Figure (2.13 a and b) having the same R_a value, the amount of the shear bond strength for the first one is higher than the second one. This is due to the greater amount of bone interlocking at the bone-implant interface in (a) than in (b). Therefore, this study suggested that the shear strength of the interface area can be estimated by examining the shape, size and density of the rough surface.

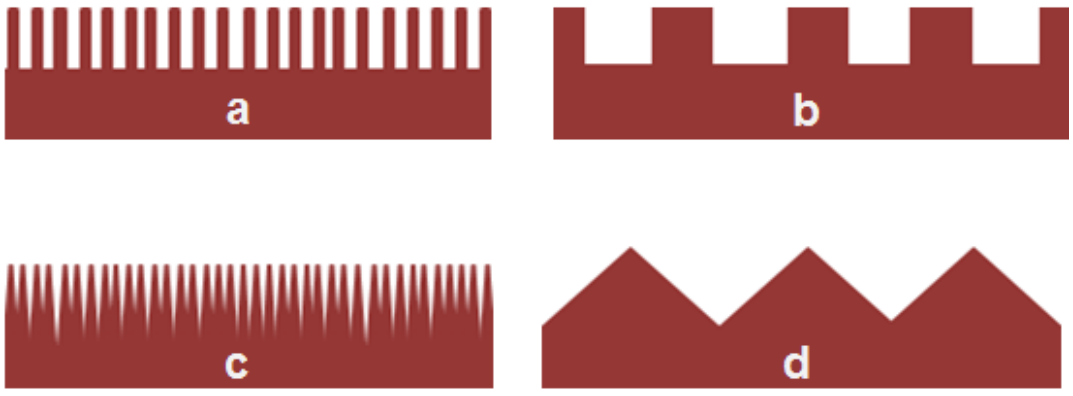

Figure 2.13: Shows four types of surface morphologies all of them having the same R_a value (Hansson, 2000).

Surface roughness can be classified into three categories macro, micro and nano-sized topologies depending on the technique which is used for modifying the surface topography and chemistry. Macro-sized topography is attributed to the implant design which includes threaded screw and macroporous implant surface. The

amount of surface roughness for both of them ranges from millimetres to around 10 µm. However, this range of roughness can increase the amount of bone growth around the implant by providing volumetric spaces and enhance the bone-implant interface; there is a risk of producing peri-implantitis and having leakage at the interface. Thus, moderate roughness or the micro-scale surface implants, which is around 1-10 µm, may be effective in reducing the possibility of these drawbacks and enhancing the osteoinduction and osteoconduction processes (Lacefield, 1999, Stanford, 2008). Although the optimum range for the nanometre-sized implant surfaces is still controversial and there is difficulty in its production by chemical treatments, this surface showed an effective role in protein adsorption and osteoblast cell adhesion. On the other hand, (Albrektsson and Wennerberg, 2004) classified the surface roughness of the commercially available implants into four categories smooth, minimum rough, moderately rough and rough surfaces according to the roughness value (S_a), which can be defined as "the mean height of peaks and pits of the surface. The (S_a) value for the four groups was less than 0.5 µm, 0.5-1.0 µm, 1.0-2.0 µm and greater than 2.0 µm respectively.

2.3.1 Methods of modification for dental implant surfaces:

To provide successful and mechanically stable implants, there are various methods used for the modification of their surfaces. These can be divided into two major methods, subtraction method and addition method. The former method includes: grit-blasting and acid etching. Both are attributed to the process of removing material from the surface of the implant leading to the formation of pits and pores on the surface of the bulk material. While, addition method means the deposition of a material on the bulk implant surface and this includes plasma spraying and enamelling techniques (Çehreli et al., 2004, Wennerberg and Albrektsson, 2009).

2.3.1.1 Subtraction methods

2.3.1.1.1 Grit-blasting method

The grit blasting technique is the most widely used method in the modification of dental implant surfaces. This technique results in a significant increase in the amount of surface roughness of titanium implants by creating depressions and elevations on the surface. Furthermore, it reduces the implant surface contamination and improves its reactivity (Wennerberg et al., 1996). This is carried out by bombarding the surface of the implant with high speed, hard and dry abrasive materials which have the ability to remove particles from the implant surface. Sometimes there is the persistence of these blasting materials in the abraded surfaces (Ellingsen et al., 2006). However, the magnitude of the implant roughness performed by this technique can be controlled by many factors, such as, the type of the blasting material, the size, the shape and the density of the blasting particles and finally the speed or velocity of the particles when bombarding the bulk implant material (Ballo et al., 2011). (Wennerberg et al., 1998) stated that the modification of the titanium implant surface by grit blasting using alumina particles with sizes of 25-75 μm produces higher surface roughness than the machined surface implant. The R_a value for the blasting surface is around 1.22-1.5 μm while, for the machined surface it is less than 1 μm. As a result of this, the bone-implant interface in the blasted surface is stronger than the machined surface and with a higher torque required for removal. (Aparicio et al., 2003) compared the surface roughness of the commercially pure titanium implant after blasting with alumina and silica carbide (SiC). The study concluded that alumina produces more surface roughness than the SiC material, despite possessing the same particle sizes. This is attributed to the size distribution of the particles, fracture toughness and the density of the alumina material which is higher in comparison to SiC. These factors result in higher impact forces to the bombarded surface and lead to an increase in the surface roughness.

Regarding the blasting material properties, these materials should be chemically stable and biocompatible. Also, they should not demonstrate an interference with the osseointegration process or elicit an adverse reaction to the biological structures. The most commonly used materials for the blasting process are alumina (Al_2O_3), titanium oxide (TiO_2), silica and calcium phosphate.

Blasting the titanium implant surface with alumina is controversial and some studies showed that the alumina residues might remain on the implant surface even after acid treatment and ultrasonic cleaning. The aluminium ions will release into the surrounding structures and will cause inhibition of bone mineralisation and decrease the corrosion resistance of the titanium; therefore TiO_2 is used as an alternative to Al_2O_3 (Le Guéhennec et al., 2007). However, (Wennerberg et al., 1996) suggested that there is no significant difference in the surface roughness of the blasted implant with TiO_2 and Al_2O_3 of the same particle sizes and there is no difference in their biological outcomes, due to the low concentration of the aluminium that is used in this technique.

Many studies showed that the stability and anchorage of the implants modified with the TiO_2 blasting method are higher than the machined implant surface. However, (Gotfredsen and Karlsson, 2001) stated that there is no significant difference between the two implant surfaces in the survival rate and the marginal bone loss within 5 years observation. (Rasmusson et al., 2005) investigated the survival rate and the marginal bone loss of the TiO_2 modified implants after 10 years function in both maxilla and mandible. This study concluded that the TiO_2 blasted implant showed a longer-term success rate with lower marginal bone loss. This is attributed to the surface roughness of the implant, which results in an improvement in bone formation and healing process of the soft tissues around the implant.

Calcium phosphate is another material used in this technique, (Piattelli et al., 2002) suggested that these materials have the ability to improve the osteoconduction

process and form a firm bone-implant interface. (Müeller et al., 2003) demonstrated that hydroxyapatite material can elicit modifications in the topography and composition of the implant surfaces which form a higher bond with bone in comparison to that for the Al_2O_3.

2.3.1.1.2 Acid etching method

This method is used to remove the oxide layer from the implant surface and sometimes remove parts of the bulk material. This is done by dipping the implant material in strong acids in order to increase the implant roughness by the formation of micro pits in the surface and provide a clean surface (Lausmaa, 2001). The magnitude of the removed material from the surface depends on many factors, such as, the concentration, the temperature of the acids in addition to the treatment time; the latter is usually between 1-60 min. Several studies stated that the degree of surface roughness which is obtained by this method ranges from 0.5 µm to 2 µm and the most widely used acids for the modification are either a mixture of nitric acid (HNO_3) and hydrofluoric acid (HF) or a mixture of hydrochloric acid (HCl) and sulfuric acid (H_2SO_4) (Alla et al., 2011). (Cho and Park, 2003) stated that the usage of dual-acid etch technique in roughening the titanium implant surface can produce implants with micro roughness and stronger osseointegration than the machined surface implants. This is done by the immersion of the titanium implant for several minutes in HF and a mixture of concentrated HCl and H_2SO_4 at high temperature around 80°C. This surface showed an improvement in the osteoconduction process by enhancing the attachment of fibrin and stimulating the adhesion and colonisation of the osteoblast cells to the titanium surface. Thus, the implant with this treatment method demonstrated a higher removal torque than the machined surface due to the direct apposition of the bone on the implant surface and the formation of a stronger bone-implant interface.

2.3.1.2 Addition methods

2.3.1.2.1 Plasma spraying method

This method is one of the methods which have been used for the modification of titanium implant surfaces. It is performed by coating the implant surface with either titanium or HAP particles. The powder particles are inserted in a plasma torch at high temperature and projected to the surface of the implant, where they combine with the bulk material and forming a coating (Le Guéhennec et al., 2007). The thickness of the coating material varies due to many factors, such as, the size of the powder particles, the time of the impact, the temperature of the molten particles and the implant-nozzle distance. The range of the coating thickness is about 10-40 μm and 50-70 μm for Ti and HAP respectively (Sykaras et al., 2000). However, this technique showed many drawbacks particularly when using it with the HAP material. The drawbacks include the formation of an uneven thickness of the coating material, porosity and heterogenecity. The latter is elicited due to the formation of the amorphous calcium phosphate (ACP) phase besides the crystalline phase. This will cause uneven degradation of the coating with higher resorption of the amorphous phase and may lead to the delamination of the coating and failure at the coating-implant interface (Cheang and Khor, 1996, Junker et al., 2009).

2.3.2 Surface modification of dental implants using bioactive materials

Metallic implants are commonly used in load bearing areas in both medical and dental applications due to their excellent mechanical properties. However, it is often stated that these implants are bioinert in nature and they are not able to produce a chemical bond with bone. Thus, this may cause inadequate fixation with the surrounding host tissues and limit their survival rate. Therefore, there are attempts to coat these metallic implants with bioactive materials in order to overcome this

problem and to increase the integrity of the bone-implant interface or enhancing the osseointegration process (Bharati et al., 2009).

The first successful bioactive material, which has been used for coating of an implant, is known as HAP material. This synthetic material has the same chemical composition and structure to the bone mineral phase. Therefore, it has the ability to promote the bone formation around the implant surface and produces a good chemical bond with bone and a highly stable implant interface (Pazo et al., 1998, Park and Bronzino, 2002). However, this material has several drawbacks, such as, low bonding strength to the titanium implant surface in addition to the uneven degradation rate. This is due to the presence of both amorphous and crystalline Ca-P phases in the material (Sun et al., 2001). The second drawback is the possibility of micro-cracks occurrence in the material itself or along the material-substrate interface. This is due to the high differences in the thermal expansion coefficient of HAP and the titanium implant material. These drawbacks are clearly seen when the plasma spraying technique is used for the coating of titanium implant with HAP material (Chern Lin et al., 1994). Moreover, there is a slight change in the chemical composition of the final HAP material after the spraying procedures, which will in turn affect the bond strength of this coating material to the metal implant (Pazo et al., 1998).

Therefore, these drawbacks demand the researcher to find other successful materials that have the ability to stimulate the osteoblasts, in addition, to increase the apposition of bone around the implant and enhance the bone-implant interface. One of these potential materials is a bioactive glass.

Bioactive glasses have shown several advantages over HAP, such as, the ability of the material to form a chemical bond with bone and the soft tissue. This is due to the attachment of collagen fibres to the silica rich layer and the migration of the osteogenic cells to the material surface (Hench and Wilson, 1993, Höland, 2012).

Also, bioactive glass has a fast degradation rate in comparison to the pure HAP material, particularly when the silica content in the bioactive glass is less than 60 wt%. This is due to the rapid surface reactivity of the bioactive glass when it comes in contact with the physiological body fluid which leads to the fast bonding with the adjacent tissues. Furthermore, bioactive glasses have the ability to release several ions, such as, sodium and calcium to the body fluid during their reaction with the adjacent structures. This ionic exchange will elevate the pH of the surrounding solution which in turn forms an alkaline environment that is preferable for the enhancement of apatite formation and decreasing the susceptibility of bacterial infection (Stoor et al., 1998). Furthermore, there are possibilities in modifying the chemical composition of the glass by the addition of fluoride and strontium in the glass structure to gain the benefits from the release of these ions in the body fluid. (Gentleman et al., 2010) stated that substituting strontium for calcium in the glass composition showed enhancement in osteoblast cell proliferation and an increase in the alkaline phosphatase activity in addition to the inhibition of the osteoclast cell activity. Therefore, the addition of strontium to the glass improves the process of bone formation and decrease bone resorption. Moreover, the addition of fluoride in the structure of the glass showed enhancement in the osteoblast differentiation and proliferation which leads to improving the bone formation rates (Gentleman et al., 2013). Besides, bioactive glasses have shown an ability to form a good bone-implant interface via enhancing the osteoinduction and osteoconduction processes.

The main drawback for the bioactive glass is a low strength and fracture toughness. This is attributed to the structure of the bioactive glass which is composed of 2-dimensional networks. Therefore, this material is either used in non-loading bearing areas or as a coating material for metal implants (Hench and Wilson, 1993).

2.3.3 Coating techniques for titanium implant with bioactive glasses

The technical trials for implant coating with the bioactive glasses have shown limited success due to the poor bond that has been developed between this material and the bulk implant material during the coating procedure. Generally, there are two main techniques used for coating of dental implants with bioactive glasses, these are enamelling and plasma spraying techniques (Hench and Wilson, 1993).

The enamelling technique is an inexpensive and simple technique for coating of the implant surface with bioactive glasses and it can provide a variable coating layer thicknesses. This technique is carried out by dipping the implant in a suspension of glass powder and then the formed coating layer is dried and glazed by subjecting the material to a high temperature. The temperature should be controlled in order not to cause an adverse effect on the glass coating material and on the implant material (Sola et al., 2011). However, there is a clear problem with this technique, which is the mismatching of the coefficient of thermal expansion of the bioactive glass with that of the implant material. This mismatching causes chipping and delamination of the glass coating material from the implant surface during the fabrication process. This is because of the thermal stresses which are applied from the coating material to the substrate, which possesses a lower coefficient of thermal expansion than the glass material (Lopez-Esteban et al., 2003, Ylänen, 2011). Therefore, there have been many attempts to overcome this problem. One of them is increasing the SiO_2 content in the glass composition as suggested by (Hench and Wilson, 1993). However, this method demonstrated a significant reduction in the bioactivity of the glass. This is due to the considerable increases in the crosslinking of the glass network by the formation of a more Q^3 structure, which reduces the ability of the glass to dissolve in the solution. The second attempt is performed by the substitution of CaO by MgO and Na_2O by K_2O (Lopez-Esteban et al., 2003) and the substitution of CaO by MgO depending on the molar percent (Al-Noaman et al.,

2012b). Although both studies showed a thermal expansion coefficient matching between the glass and the titanium, however a clear retardation is detected in the process of apatite formation. This is attributed to the presence of the Mg^{2+} ion in the glass composition which causes retardation in the deposition of the calcium and phosphate ions in the test solutions. The third method is achieved by the use of an intermediate coating layer, which possesses a thermal expansion coefficient similar to that of the implant substrate, but between the bioactive glass coating and the titanium implant. This layer is advantageous in reducing the mismatching between the two materials and in the same time not eliciting an adverse effect on the bioactivity of the top bioactive coating layer (Gomez-Vega et al., 2000, Kim and Lee, 2005). However, this technique is complicated and time-consuming. The second technique, which is used for coating of the implant with bioactive glasses, is known as plasma spraying. This technique showed a good deposition rate of the glass particles to the metal substrate and a controlled coating thickness in comparison to the previous technique (Sola et al., 2011). Moreover, it does not cause any changes in the composition of the bioactive glass and does not influence its bioactivity, because it will not elicit any crystallisation in the coating material (Bolelli et al., 2009). However, this method is expensive and it may produce a residual micro or macro-porosity in the coating material (Hench and Wilson, 1993, Höland, 2012). Also, there is a poor mechanical adhesion between the glass coating material and the titanium surface (Sola et al., 2011).

Due to the limitations of the two previous techniques in providing a successful coating for the implants with bioactive glasses, grit blast technique was introduced. (Koller et al., 2007) used the 45S5 glass as an abrasive material in modifying the surface of the titanium and increasing its roughness. Their idea was originated from previous studies, which showed that the abrasive alumina particles embedded into the implant surface after blasting, despite treating the surface with acids. Therefore,

(Koller et al., 2007) used the Bioglass® with this technique in order to produce a biological active surface. The investigation was done by using the light interferometry and scanning electron microscopy (SEM) to test the surface roughness and the topography respectively. This study showed successful results, however the preparation parameters were not defined. Another study was also used the same method in the surface modification, but with Sylc® and silica-modified alumina oxide (Vasankari, 2011). They found that there is a low percentage of glass particles embedded in the titanium surface when analysed by scanning electron microscopy coupled to energy dispersive X-ray (SEM-EDX). This study was performed under static conditions using a fixed distance and time; therefore, it is not mimicking potential manufacturing conditions.

In this study, glasses with different hardness values will be used in conjunction with different grit blasting parameters. This is to optimise the conditions for the surface modification. Additionally, the effectiveness of the surface in enhancing the apatite formation and cell responses *in vitro* will also be investigated.

3 Materials and Methods

3.1 Diagram of the experimental work

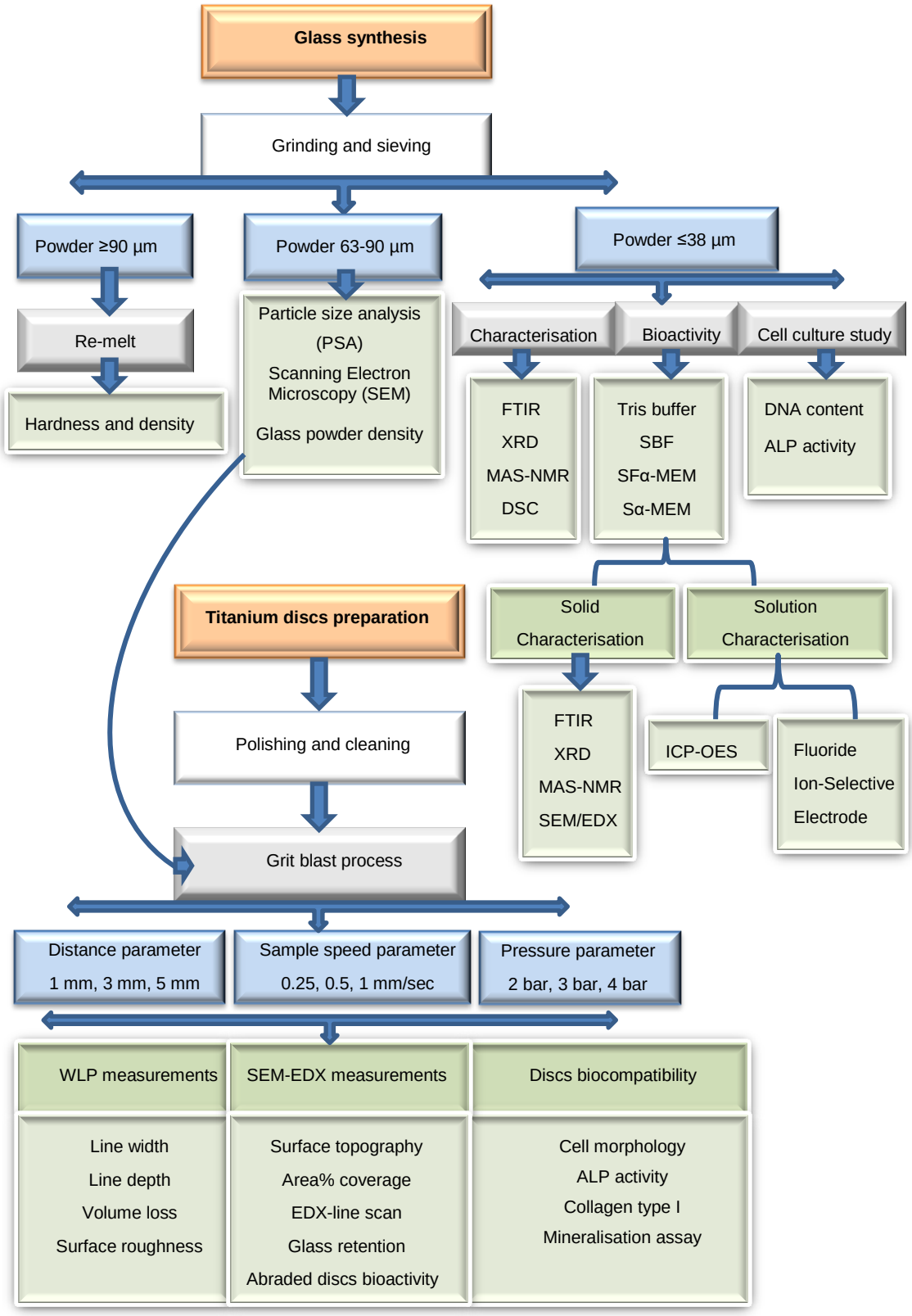

3.2 Glass synthesis

Three bioactive glasses in the SiO_2-P_2O_5-CaO-Na_2O-CaF_2 system were designed based on the QMMM1 glass (B2 glass, as named in (Mneimne et al., 2011) with decreasing sodium oxide and increasing calcium oxide mole percentages. All the glasses have constant network connectivity. The glass compositions and their NC are shown in Table (3.1).

Table 3.1: Chemical composition of the bioactive glasses in (mole %) with decreasing Na_2O content and increasing CaO content, glasses network connectivity and the temperature of glasses preparation.

Glass (Code)	SiO_2	P_2O_5	CaO	Na_2O	CaF_2	NC	Temperature of preparation
QMMM1	36.41	6.04	24.74	28.28	4.53	2.08	1350 ºC
QMFA1	36.41	6.04	31.81	21.21	4.53	2.08	1390 ºC
QMFA2	36.41	6.04	38.88	14.14	4.53	2.08	1450 ºC
QMFA3	36.41	6.04	45.95	7.07	4.53	2.08	1490 ºC

The reagents SiO_2 (Prince Minerals Ltd., Stoke-on-Trent, UK), P_2O_5, $CaCO_3$, Na_2CO_3 and CaF_2 (all Sigma-Aldrich, Gillingham, UK) were weighed by using a balance accurate to ±0.01 g and mixed vigorously in a sealed glass container to prepare 200 g batch for each glass composition. Each batch was placed in a clean platinum-rhodium crucible and inserted into an electric furnace (Hope Valley, Lenton Thermal Designs, UK) at temperatures between 1390 ºC and 1490 ºC for 1 h. The melted glass was rapidly quenched into deionised water to prevent crystallisation and dried at a temperature of 80 ºC for 12 h. The preparation procedure was repeated 8 times for each glass composition in order to produce a big batch of glass frits of around 800 g.

After drying, the glass frits (100 g each) were ground in a gyro-mill (Gyro mill, Glen Creston, London, UK) Figure (3.1) for 45 s in order to produce glass powder with coarse particles.

Figure 3.1: Gyro-mill.

Then, every 100 g of ground powder was sieved through three different mesh size sieves (Endecotts Ltd., London, UK) 90 µm, 63 µm and 38 µm for 45 min by using a shaking machine (Retsch vs 1000). The powders with particle size 63-90 µm and ≤ 38 µm were collected, kept separately in re-sealable plastic bags and stored in a desiccator to prevent them absorbing water from the atmosphere. The sieving procedure was repeated till all the 800 g powder finished. The amount of the collected glass powder of particle size range 63-90 µm was around 250 g and this was used for the grit blast coating process. While, the finer particle size powder was used for the glass characterisation, bioactivity study and cell culture studies.

For the hardness measurements, glass monoliths were used and they were prepared by re-melting 100 g from each glass powder composition of particle size ≥ 90 μm for 30 min at a temperature range between 1390 ºC and 1490 ºC. The melted glass was poured into a preheated cylindrical graphite mould with 15 mm diameter and 20 mm length, which was then immediately placed in a furnace (ELF 11/6B, Carbolite, Hope Valley, U.K) set to a temperature 30 ºC below the glass transition temperature. After 15 min, the furnace was switched off allowing the mould to cool slowly to room temperature overnight.

3.2.1 Glass characterisation

3.2.1.1 X-Ray Diffraction (XRD)

XRD is a non-destructive technique used to study the structure of the amorphous materials and to determine the crystalline phase and the orientation of the crystals of solid materials (Fultz and Howe, 2012). This technique was conducted on the prepared glass powders to check that they are all in an amorphous state. In addition, treated glass powders after bioactivity study were also examined by this technique. This is to confirm the formation of the apatite layer on their surfaces.

A glass powder with particle size ≤ 38 μm from each composition was run in X Pert Pro X-ray diffractometer (Panalytical, Netherlands) using Ni-filtered Cu-Kα radiation at 40 kV/40 mA and with scan range 2θ of 5° to 70° and a step size of 0.334°.

3.2.1.2 Fourier Transform Infrared Spectroscopy (FTIR)

FTIR is a technique used to measure the vibrations of the active groups in the molecular structure of the material which is responsible for the chemical reaction (Doyle, 1992). The material molecules have the ability to absorb the energy from the infrared beams and this absorbance will cause either stretching or vibration to the molecules. The remaining energy from the incident beam will be detected and plotted against the radiation wavelength. This will lead to the detection and the

categorisation of the vibrational and the stretched band that absorb the radiation energy (Siesler and Holland-Moritz, 1980).

In this study, FTIR was used to detect the activities of the Si-O groups and the NBO bands in the glasses. In addition, it can determine the formation of apatite on the glass surface by detecting the P-O vibration bands after the bioactivity study. Therefore, this technique was applied to both untreated and treated glass powders. This is to compare the changes in the chemical structure of the glasses before and after the bioactivity study.

A background measurement was conducted before the actual measurements in order to avoid any artefacts from the instrument. About 10-20 mg of glass powder from each formulation was examined by Perkin–Elmer Spectrum GX IR spectrometer Figure (3.2). The powder was pressed against the lens of the machine and then, approximately 10 scans for each tested sample were taken. The absorbance spectra were collected in the range of 500-1800 cm^{-1} at a resolution of 4 cm^{-1}.

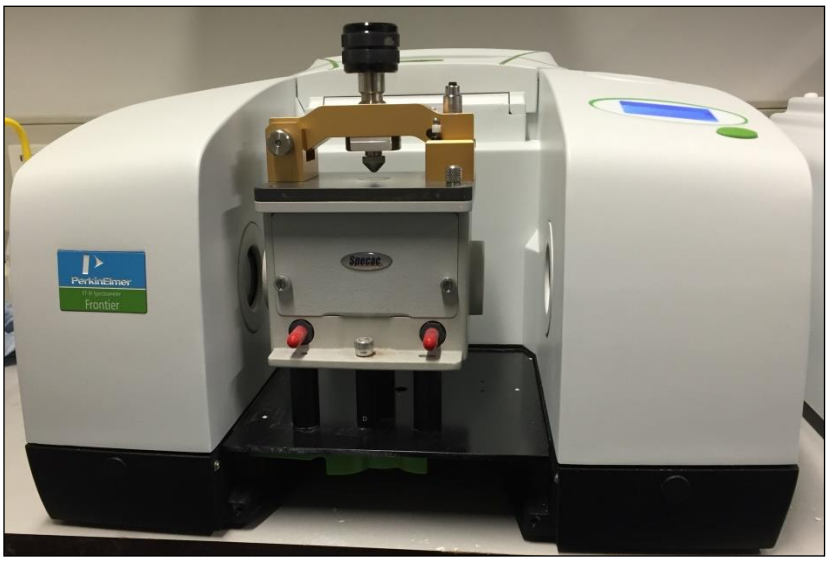

Figure 3.2: FTIR spectrometer.

3.2.1.3 ^{19}F and ^{31}P Magic Angle Spinning-Nuclear Magnetic Resonance Spectroscopy (MAS-NMR)

MAS-NMR is a sensitive technique used to describe and study the atomic and molecular structure of the glasses in addition to the dynamics of the oxide in the glasses (Massiot et al., 2008).^{19}F and ^{31}P MAS-NMR were both used to investigate the interactions of both fluoride and phosphorus ions respectively in the solutions treated glass powders and compare them with the original glasses.

This technique was done by using a 14.1 Tesla spectrometer (600 MHz Bruker, Coventry, UK) Figure (3.3). The untreated and treated glass powders were packed in zirconia rotors of 2.5 mm diameter, spun at MAS frequency 22 kHz and the spectra were collected with 60 seconds recycle time with the accumulation of 32 scans. The ^{19}F and ^{31}P chemical shift were referenced to the -120 ppm peak and the 0 ppm peak of a 1 M NaF solution and H_3PO_4 solution respectively.

Figure 3.3: MAS-NMR spectrometer.

3.2.1.4 Differential Scanning Calorimetry (DSC)

DSC is an analytical technique used to evaluate the thermal behaviour of the materials by measuring the heat flow difference between the reference material and the tested material. The glass is usually subjected to physical and chemical changes which may develop exothermic or endothermic reactions and this can be investigated by calorimetry techniques. There are two essential temperatures in bioactive glasses and these are glass transition temperature (T_g) and crystallisation temperature (T_c) Figure (3.4). T_g is considered as an important factor in optimising the composition of the glass and understanding its physical properties (Rajendran et al., 2002).

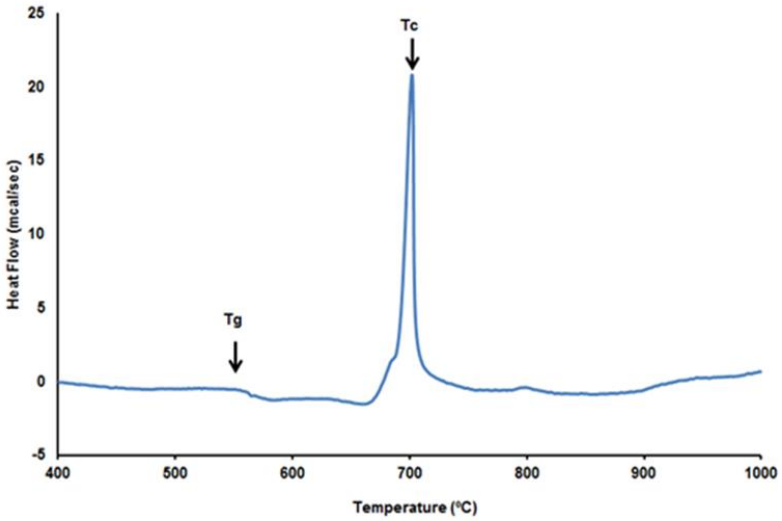

Figure 3.4: DSC Plot of a bioactive glass showing the glass transition temperature and crystallisation temperature.

A Stanton–Redcroft DSC 1500 (Rheometric Scientific, Epsom, UK) was used for the thermal analysis of the bioactive glasses. 50 mg of glass powder with particle size ≤38 μm was placed in a platinum crucible and then transferred to the stage of the machine beside a reference alumina material of the same weight. The experiment was conducted from room temperature to 1000 ºC, with a heating rate 10 ºC /min and conducted in an air atmosphere.

3.2.1.5 Particle size analysis

Particle size analysis was used to measure the distribution of the particle size of the material. This technique depends on measuring the intensity of the scattered light from the suspension when it is exposed to the laser beam. The angle of the scattered light increases relatively when the size of the particles decreases. It is simple and reproducible technique and it can cover a wide range of particle sizes (Beuselinck et al., 1998).

The coarse glass powder, which was collected for the grit blast technique, was tested by using Mastersizer 2000 (Mastersizer/E, Malvern Instruments Ltd, UK). The procedure was performed by taking a background measurement as a control reading prior to the sample measurements. Then, around 5-6 mL of the tested glass powder suspension in water was added gradually into the tank of the machine until achieving the optimum obscuration level which is around 15%. Five measurements were taken for each sample and the results were expressed in numerical values as percentiles D (10), D (50) and D (90). The final results were presented as mean ± standard deviation (SD) besides a graph showing the particle size distribution profile.

3.2.1.6 Scanning Electron Microscopy (SEM)

The surface morphologies and the elemental compositions of the coarse glass powder, as well as the solutions treated glass powder were examined by SEM-EDX (FEI Inspect F Oxford Instruments, UK) Figure (3.5). Each glass powder was fixed on a stub by double sided adhesive tape and sputter coated with carbon (Balzers CED030, UK) in order to avoid the sample charging and facilitate the conduction of the electron beam current. The samples were examined by using an accelerating voltage of 10 kV and a working distance of 10 mm. EDX was utilised to show the elemental composition of the surface of the treated glass powders after their immersion in different solutions and confirm the formation of apatite layer.

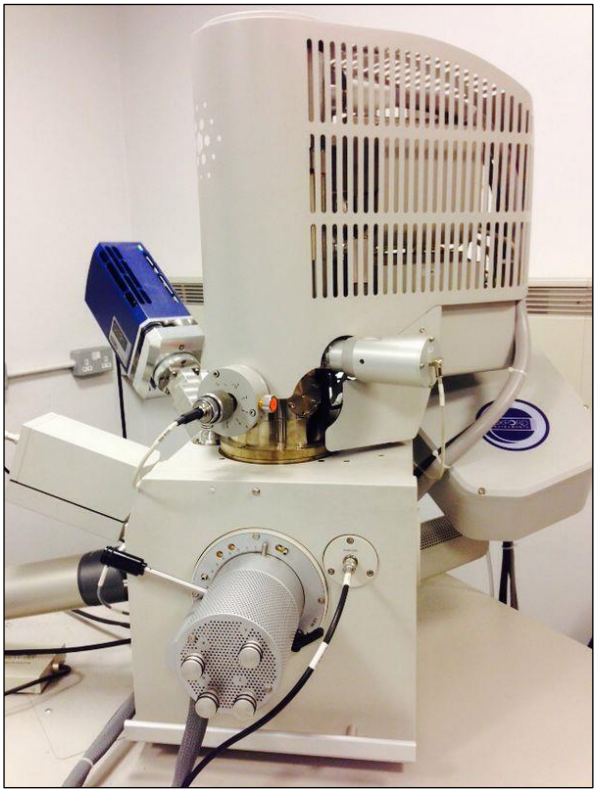

Figure 3.5: A scanning electron microscope.

3.2.1.7 Glass Hardness and Density

3.2.1.7.1 Hardness

Glass monoliths were cut by a diamond cutting machine Accutom-5 diamond saw (Streurs, Willich, Germany) to produce 7 mm length cylindrical blocks. Each glass block was embedded in an epoxy resin; finished with (p 320, p 600, p 800, p 1000, p 2500 and p 4000) carbide papers (Kemet International Ltd, Kent, UK) and polished to 0.25 µm using alumina micro polishes (Buehler, USA). The hardness measurement was performed for the glass monoliths and for the polished titanium discs.

A Vickers hardness (HV) test was carried out at room temperature by using a Zwick/Roell hardness test machine (Zwick/ZHU- universal hardness tester, Germany). A pyramid diamond indenter with an angle of 136° and a static load of 30 N was applied on the glass sample for 10 s. The diagonal lengths of each

indentation were recorded, as shown in Figure (3.6). The readings were calculated automatically by the testing machine, and then the values were converted to GPa by multiplying the HV readings by 0.009807. Ten indents were taken for each glass composition and the results were analysed by one-way analysis of variance (ANOVA) followed by Tukey post-hoc test with a statistical significance at *(p≤0.05)* using IBM-SPSS version 24 software program.

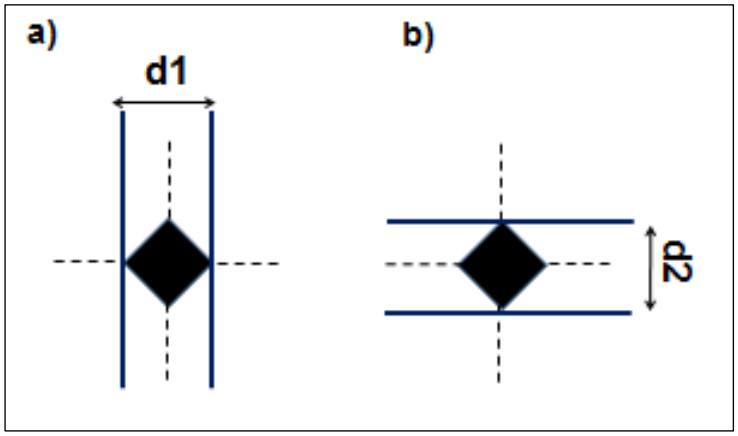

Figure 3.6: Measuring the diagonal indentation a) d1 first diagonal measurement b) d2 second diagonal measurement.

3.2.1.7.2 Glass density and oxygen density

The glass density was measured depending on Archimede's principle by using an analytical balance accurate to ± 0.001 g (Denver Instrument, SI-403, UK) fitted with a density determination kit (Mettler ME-33360, Mettler instruments Ltd, UK). The glass density measurements were taken for each composition at a temperature of 20 ºC by weighing bubble-free sample blocks in air and in distilled water, as the latter has a known density of 0.998 g/cm^3. The density (ρ) of the glass sample was then calculated using the equation (3.1) below (Rajendran et al., 2002):

Equation 3.1

$$\rho = A/(A - B) * \rho°$$

Where A is the weight of the glass block sample in air, B is the weight of the block in distilled water, and ρ_o is the water density at a given temperature.

The oxygen density, on the other hand, was calculated by the following equation (3.2):

Equation 3.2

$$Oxygen\ Density = glass\ density * \frac{molecular\ weight\ of\ oxygen}{molecular\ weight\ of\ glass}$$

The oxygen density value can provide information about the compactness of glass network and the crosslinking structure of the glass after ions substitution.

Moreover, the density of the abrasive glass powder of particle size 63-90 µm was also measured. This is to determine the degree of compactness of the glass powder and its effect on the powder flow rate when using the grit blast machine. The procedure was carried out by weighing a 10 mL glass cylindrical tube before and after the addition of 5 mL of glass powder using a balance accurate to ±0.01 g. Five measurements were taken for each glass powder composition and the density of the powder was calculated by the equation (3.3). The compactness of the powder and amount of air included between the glass particles was then calculated by dividing the density of the glass powder on the density of the glass block. The glass powder density data were analysed for significant difference *($p \leq 0.05$)* by using one way ANOVA followed by Tukey post-hoc test.

Equation 3.3

$$Density = \frac{Mass\ (g)}{Volume\ (cm^3)}$$

3.2.2 Bioactivity Study

This study was used to assess the ability of the glasses to dissolve and form an apatite layer on their surfaces when immersed in four different solutions. These solutions varied in their ion concentrations and these include Tris buffer, SBF, serum free cell culture medium (SFα-MEM) and serum containing cell culture medium (Sα-MEM). The glass powders were immersed in the previously mentioned solutions for a specific time period reaching up to 7 days in Tris and SBF, while for both cell culture media the immersion time reached to two months.

3.2.2.1 Preparation of testing solutions

3.2.2.1.1 Tris buffer

This solution is ions free and it is used for the purpose of detecting the dissolution behaviour of the glass and its ability to release ions (Aina et al., 2009).

Tris solution was prepared in two steps. The first step includes the addition of 15.090 g Tris (hydroxymethyl aminomethane) (Sigma-Aldrich, Gillingham, UK) to 800 mL of deionised water in a 2 L polyethylene bottle. Then, 44.2 mL of 1 M HCl (Sigma-Aldrich, Gillingham, UK) was added slowly to the mixture and the prepared solution was kept in a shaking incubator for 12 h at a constant temperature 37 ºC. In the second step, the pH of the prepared solution was adjusted by adding 1 M HCl slowly until the pH of the solution reaches about 7.35-7.36. Finally, the prepared solution was transferred to a glass flask, filled up to 2 L, then poured again in the polyethylene bottle and placed in a shaking incubator at 37 ºC for two hours.

3.2.2.1.2 SBF

SBF was used to investigate the bioactivity of the glass powder *in vitro*. This solution consists of ions, whose concentrations are similar to that of the human body plasma. In addition, it is free of proteins, hormones and other organic components.

Therefore, SBF only mimics the inorganic composition of the body fluid (Müller and Müller, 2006).

According to the Kokubo method (Kokubo et al., 1990), this solution was prepared in two stages. In the first stage, the chemical reagents which are listed in Table (3.2) (all Sigma-Aldrich, Gillingham, UK) were sequentially added to 1500 mL of deionised water. The mixture was stored in a 2 L polyethylene bottle for 12 h in a shaking incubator at a temperature 37 ºC. On the second day, the pH was adjusted to 7.35 by adding a small amount of 1 M HCl to the mixture. Then, a specific amount of deionised water was added to prepare 2 L of SBF.

Table 3.2: Chemical composition of (SBF).

Chemical reagents	Tris aminomethane	NaCl	$NaHCO_3$	KCl	$K_2HPO_4.3H_2O$	$MgCl_2$	$CaCl_2.2H_2O$	Na_2SO_4	1N HCl Aqueous Solution
Concentration	12.114g	15.992g	0.700g	0.448g	0.456g	0.610g	0.736g	0.142g	70mL

3.2.2.1.3 Cell culture media

The *in vitro* bioactivity of the glasses was further studied in Alpha Eagle's Minimum Essential Medium (α-MEM) cell culture medium. This is due to the limitations of the SBF, such as, the absence of proteins and other organic components. In addition, SBF contained uncontrolled carbonate content and this showed an influence on the pH buffering of the solution (Bohner and Lemaitre, 2009). Therefore, α-MEM was used in the bioactivity study, as this medium simulated the human body environment by containing amino acids, organic components and inorganic components.

Serum free α-MEM (SFα-MEM) and serum containing α-MEM (Sα-MEM) were both used to test the ability of the glasses to form apatite. The Sα-MEM medium was also used for culturing and for the nutrition of the cell line MC3T3-E1, as it will be

discussed later in this Chapter. The Sα-MEM medium was prepared by the supplementation of the α-MEM medium (Lonza, London, UK) with 10% foetal calf serum (FCS, First Link Ltd, UK), 1% penicillin streptomycin antibiotic and 1% L-glutamine (all Invitrogen, UK). The proteins supplementation was carried out for the purpose of enriching the organic parts of the α-MEM, while the addition of the antibiotics was done for preventing the degradation of the medium during the experiment (Rohanová et al., 2014).

3.2.2.2 Glass dissolution process

This procedure was carried out by weighing 75 mg of QMFA1, QMFA2 and QMFA3 glass powders with particle size ≤38 μm and placing them in plastic containers. 50 mL of each testing solution (Tris buffer, SBF, 10% Sα-MEM and SFα-MEM) was added to each container after measuring its pH by a pH meter (Oakton Instruments, Nijkerk, Netherlands). Then, all the containers were kept in a shaking incubator at a constant temperature 37 ºC with a rotation rate 60 rpm for a specific time period ranging from 3 h to 7 days for Tris and SBF samples, whereas for all the α-MEM samples the immersion time was lasted for two months.

After each time point, the glass powders were filtered through (5-13 μm particle retention, VWR International) filter paper and the solution's pH were measured. The collected powders were kept in Petri dishes and stored in an incubator at 37 ºC for 12 h to dry. While, the collected solutions were kept in Falcon tubes and stored in a fridge at 4 ºC.

3.2.2.3 Characterisation of solutions treated glass powder

After complete drying, the collected glass powders were analysed by using FTIR, XRD and ^{19}F, ^{31}P MAS-NMR. This is to evaluate the formation of apatite like phase on their surfaces. Furthermore, the treated glass powders were examined by SEM-EDX in order to identify the morphological and chemical changes that occurred on their surfaces after the immersion process.

3.2.2.4 Characterisation of filtered Solutions:

To measure the chemical composition of the filtered solutions, as well as the ions exchange between the glass powders and the solutions, two techniques were used.

3.2.2.4.1 Inductively Coupled Plasma-Optical Emission Spectroscopy (ICP-OES)

The changes in the concentrations of silicon, calcium and phosphorus in the filtered solutions were quantitatively analysed by ICP-OES (Varian Vista-PRO, Varian Ltd., Oxford, UK). ICP-OES is a sensitive technique used to provide qualitative and quantitative information about the tested material. It can determine the elemental compositions of the material and their concentrations by measuring the amount of emitted and/or absorbed wavelength radiation and electromagnetic radiation respectively. The tested material is subjected to high heat and this can cause decomposition of the material into atoms and ionisation of the atoms. Both of which will produce emission of electromagnetic radiation of specific wavelength. The emitted radiation will be detected by a photo-electric detector and the data will be processed by a computer to provide the analytic results. The intensity of the emitted radiation represents the concentration of the element, while the specific wavelength refers to the element of interest (Boss and Fredeen, 1999, Moore, 2012).

In this study, three replicates from each sample were measured and the mean values ± standard deviations were determined. The process was carried out by diluting the filtered Tris buffer and SBF samples (1:5) with de ionised water, while α-MEM samples were diluted (1:10). This is because of the difference in the ions concentration that exists in the original solutions. For all samples, 2% of 96% Nitric acid (VWR International Ltd) was added to facilitate the detection of the ions by the machine and to prevent the precipitation of ions during the experiment.

3.2.2.4.2 Fluoride Ion-Selective Electrode (F^--ISE)

Fluoride concentration in the filtered solutions was measured by F^--ISE (NICO2000 Ltd, Middlesex, UK). F^--ISE is a membrane electrode, which responds selectively to F^-ion in the presence of other ions in the tested solution. This membrane electrode will measure the potential of F^-ion in solution against a constant reference electrode of persistent potential. The activity of the F^- in the solution will produce a potential difference between the two electrodes. This will lead to a net charge, the strength of which is related to the concentration of the fluoride ion in the testing solution.

Standard solutions were prepared first for calibrating the ion strength by diluting 10,000 ppm F^- solution in deionised water to form four standard solutions 5, 20, 30 and 50 ppm. The potentials of these solutions were measured in (mV) and plotted against the F^- concentration to obtain a standard calibration curve. Then, 5 mL of each sample solution was measured and the amount of F^- released from the glasses was calculated by using the calibrating curve and presented in ppm.

3.3 Titanium discs preparation and coating procedure

3.3.1 Discs preparation

400 discs of 10 mm diameter and 1 mm thickness were cut from grade II commercially pure titanium sheet (Advent Research Materials, Oxford, UK) using a laser cut machine (Doncaster laser services, Carcroft, UK). This cutting technique was recommended in this study, as the pilot study results showed that the manually punched discs demonstrated uneven surfaces when scanned by the white light profilometer (WLP). The curved surface of the punched disc resulted in an uneven abrasion across the sample as shown in Figure (3.7 a). The abrasion was more deeply detected on the edges of the sample than the middle part and this resulted in false measurements. Thus for more accurate measurements, the manual punching technique was replaced by the laser cut technique. Laser cutting produced samples

with flat and even surfaces, as seen in Figure (3.7 b). The flat surface resulted into a standardised sample-nozzle distance and a homogenised abrasion across the sample surface. Furthermore, this cutting method can give more accurate and objective analysis when using the WLP.

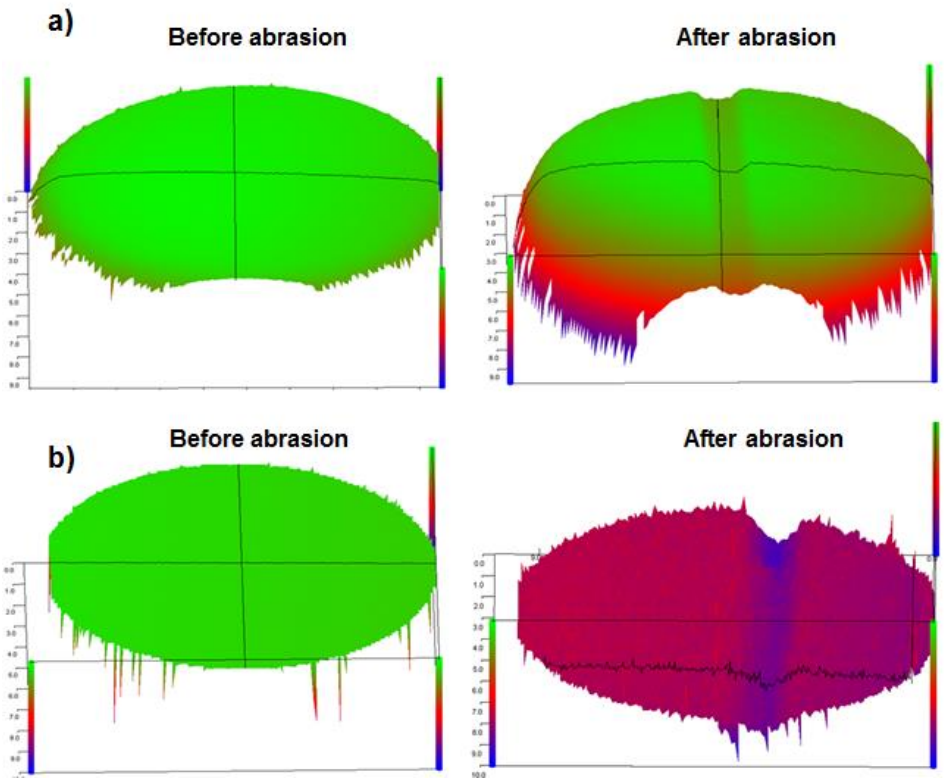

Figure 3.7: Proscan 3-D profile showing the surface configuration of the Ti disc prepared by two cutting techniques a) manual punching method, where the disc surface appears convex and the abrasion line is deep at the edges of the disc b) Laser cutting technique, where the surface is flat and the abrasion line is even across the entire surface.

After the cutting procedure, the discs were subjected to sequential polishing and cleaning processes. This is to produce a smooth surface of low surface roughness value. The prepared discs were polished by an automatic lapping and polishing unit (Kemet 300 LVAC, Kemet International Ltd, Kent, UK) to a surface finish of 0.1 µm. The process started with silicon carbide paper of decreasing grain sizes P 600-P 4000 for disc's levelling and finished with Micro cloth and diamond suspension of 1 µm and 0.25 µm respectively (Kemet International Ltd, Kent, UK) for shiny mirror

surface Figure (3.8). All samples were cleaned ultrasonically in ethanol and deionised water for 10 min in total.

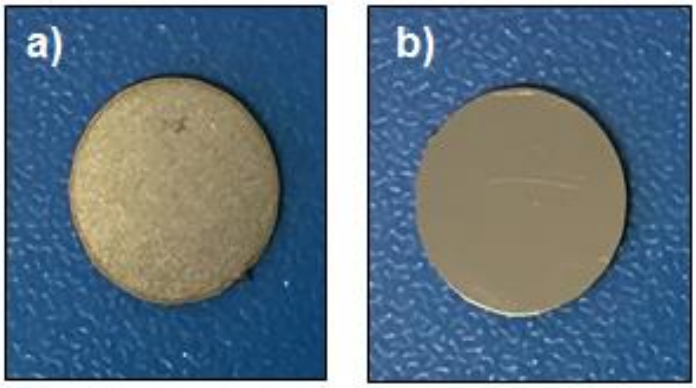

Figure 3.8: Prepared Titanium disc of 10 mm diameter and 1 mm thickness a) before polishing b) after polishing and cleaning.

3.3.2 Powder flow rate (PFR) calibration

Prior to the grit blast coating procedure, the glass powders flow rate was calibrated. This is to investigate the effect of the propellant air pressure on the PFR and to ensure the consistency of the powder flow during the experiment. A constant flow rate is important in controlling the abrasion characteristics of the stream and the loss of material (Banerjee et al., 2008, Milly et al., 2014).

The calibration procedure was carried out by using AquaCare-Dental air abrasion and polishing unit (Velopex, Harlesden, UK) in which the powder feed rate dial was fixed at the middle setting and the pressure was adjusted to 2, 3 and 4 bars.

The powder reservoir was kept constant during the experiment as its level affects the PFR of the glass (Banerjee et al., 2008) and it was refilled after three measurements. The nozzle of the grit blast hand piece was inserted into the top of a collecting container and the weight of the container was measured by a balance accurate to ±0.01 g before and after 1 min of the active air abrasion method. Eight measurements were conducted for each composition at each propellant pressure

parameter. The results were statistically analysed by IBM SPSS version 24 statistical software using one-way (ANOVA) followed by Tukey post-hoc test for a statistical significance (*P≤0.05)*.

The collecting container was designed, as described by (Banerjee et al., 2008), by inserting a thick sponge layer in the middle part of the container and a thick dry facial mask in the bottom Figure (3.9). The sponge layer will act as a pre-filter for the glass powder, during the running of the experiment and it will prevent the build-up of the internal pressure inside the container. The facial mask was placed to prevent the leakage of the powders from the bottom of the container. Moreover, the collecting container was held above a black paper during the experiment. This was to ensure that there is no leakage of the powder from the facial mask.

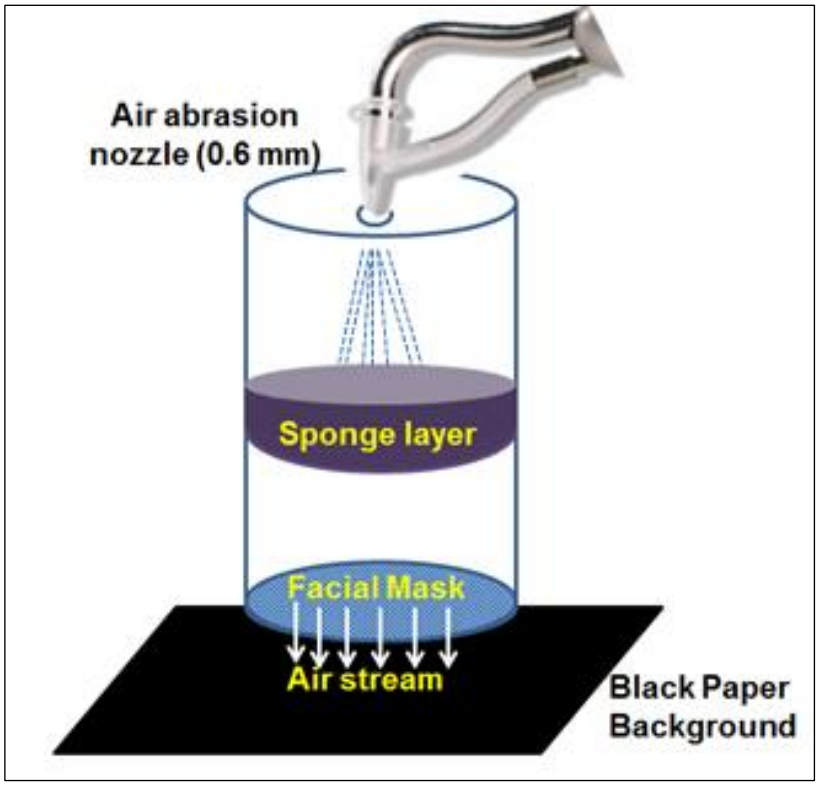

Figure 3.9: Schematic diagram of the powder flow rate calibration as described by (Banerjee et al., 2008).

3.3.3 Coating of Ti discs by grit blast technique (dynamic air abrasion technique)

Grit blast is a technique used for abrading the surface of the implant and increasing its roughness by using Al_3O_2 or TiO_2 abrasive particles (Rønold and Ellingsen, 2002, Koller et al., 2007). In this study, grit blast was used for abrading and coating the titanium surface by bioactive glass particles. These particles were introduced to the target surface by applying a stream of compressed air. The efficiency of the abrading process could be affected by many variables.

For the dynamic abrading procedure AquaCare-Dental air abrasion and polishing unit with a nozzle of 0.6 mm internal diameter was used Figure (3.10). The reason of using the dynamic air abrasion instead of the static procedure is to mimic the practical procedure that will be used in the coating process of the implants.

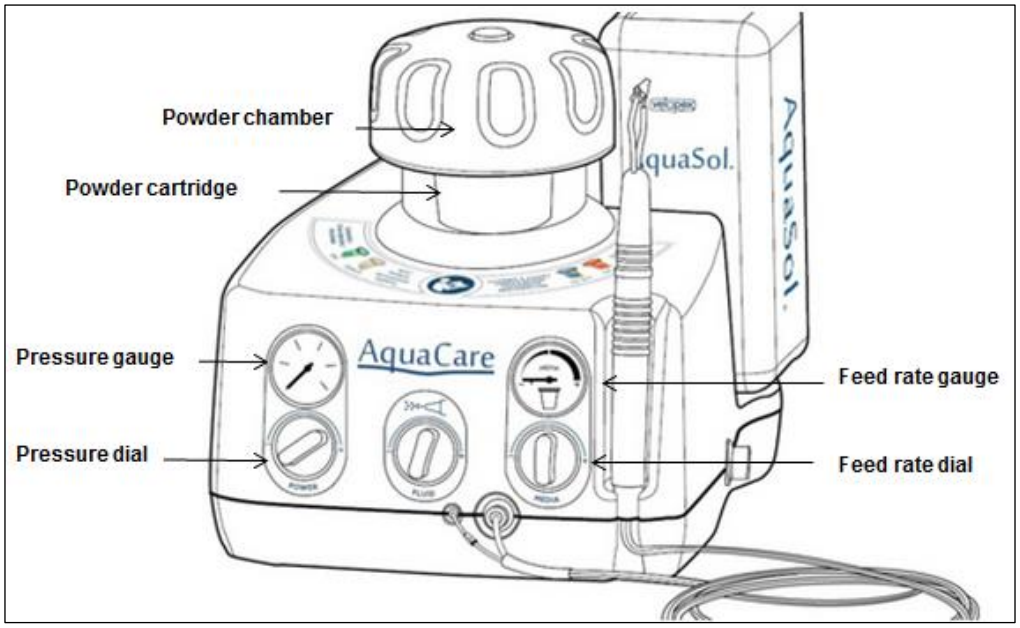

Figure 3.10: Schematic diagram of AquaCare-Dental air abrasion and polishing machine taken from https://www.dentaloperatoryequipment.com.

Three operating parameters were changed in this study and these include the air pressure (mechanics equipment variables), sample-nozzle distance and sample movement velocity (operator variables). However, the other parameters were all kept constant during the experiment in order to control the abrasion process. Additionally, the hardness of the bioactive glass particles, which is one of the relating variables to the powder properties, was also modified in the current experiment by changing the composition.

The nozzle-disc distance was determined by applying microscopic slides of a fixed thickness between the disc surface and the nozzle tip. The slides thicknesses were measured three times by a digital micrometre of 0.001 mm accuracy (Mitutoyo, Japan) in order to ensure the thickness accuracy Table (3.3). The nozzle of the hand piece was held by a clamp, fixed at a 90º tip angulation during the experiment and the distance was controlled by the gradual addition of the previously measured microscopic slides. The nozzle tip was kept in intimate contact with slide surface during the distance determination and removed before the abrasion procedure.

This step was to ensure the standardised distance and the accurate repetition of the procedure.

Table 3.3: Microscopic slides thicknesses.

Microscopic slide number	1	2	3	4	5
Thickness (mm)	1.03	1.04	1.03	1.03	1.04

Titanium discs, on the other hand, were fixed on a metal plate by double sided tape, placed on a motorised linear stage of 100 mm travel distance (Zaber Technologies, Vancouver, Canada) and the velocity was controlled by Zaber's computer software Figure (3.11). For pressure control, the pressure dial was set directly from the machine to give an output pressure between 0 and 7 bars.

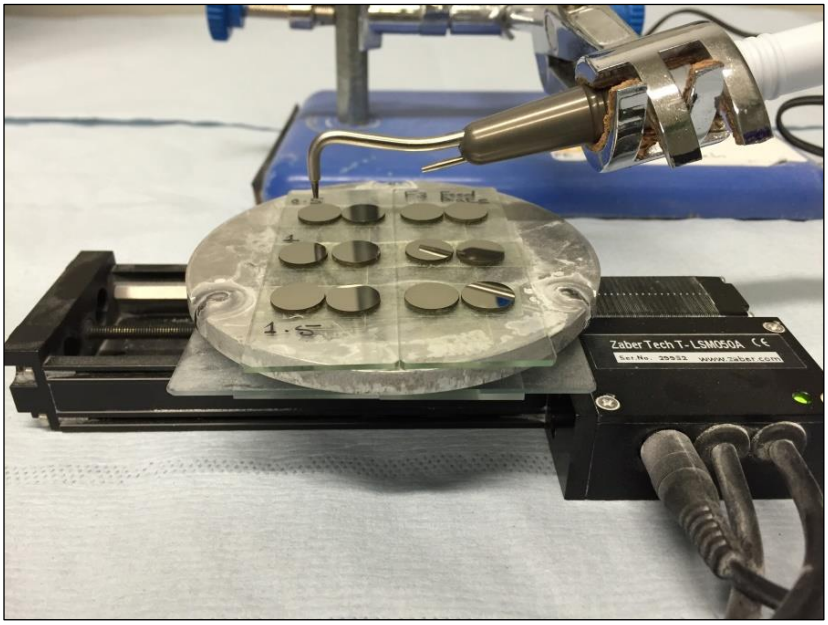

Figure 3.11: The grit blasting procedure. The handpiece nozzle is fixed with a clamp at a 90º angle; the titanium discs are fixed to a metal stage by double sided tape and placed on a programmed linear moving device.

Before the preparation of each experimental group, the powder plastic cartridge was loaded with a fixed amount of glass powder of about 45 g. This is to ensure the consistency of the powder flow during the abrasion and to standardise the abrasion rate. The cartridge was refilled to the same weight before the abrasion of the next group.

The coarse powder particles of a size range between 63 µm and 90 µm were used in this study. This is due to the results from the pilot study, which showed that the presence of small particles ≤38 µm causes agglomeration in the powder. This agglomeration resulted in an inconsistent powder flow output and this led to a non-homogenised and uneven abrasion across the titanium surface. Additionally, the powder feed rate dial was fixed to the middle value during the preparation of all the samples. This is to control the amount of powder emitted during the experiment and to control the abrasion efficiency by employing a constant PFR during the abrasion procedure.

In this study, three operating parameters were evaluated for each glass composition. When one variable was examined, the remaining parameters were kept constant, as show in Table (3.4).

Table 3.4: The evaluated operating parameters of the grit blast technique and their tested values.

Parameters	Nozzle distance (mm)	Sample velocity (mm/sec)	Air pressure (bar)
Nozzle distance	1, 3, 5	0.5	4
Sample velocity	3	0.25, 0.5, 1.0	4
Air pressure	3	0.5	2, 3, 4

Nine experimental groups of each glass composition were prepared, each with 4 samples giving a total number of 36 samples. Therefore, the total number for all compositions was 108 abraded samples Figure (3.12). These samples were investigated by WLP, SEM (image J) and SEM/EDX analysis. The samples were all prepared using a dry air abrasion system. This dry condition will preserve the bioactivity of the glass powder, as the bioactive glass is sensitive to water. In addition, it enhances the powder scattering on the substrate surface.

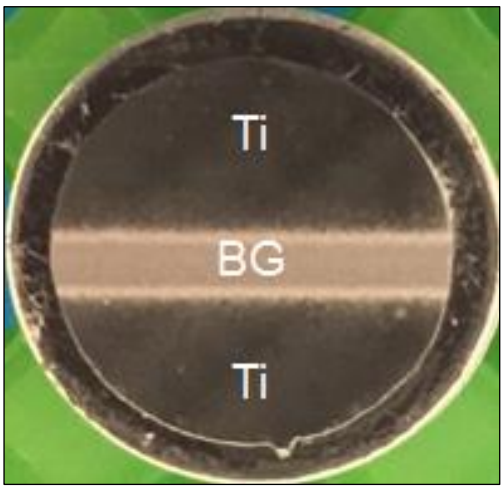

Figure 3.12: Titanium disc after grit blasting where the bioactive glass powder is embedded in the middle part of the disc leaving the sides intact.

The selected distance in this experiment was 3 mm. This is based on the SEM results of the pilot study, which showed that the abraded line border was well defined at that distance. In addition, there was good area coverage and even distribution of the glass particles across the abraded line. Regarding the velocity of the moving stage, the 0.5 mm/sec was programmed as the control speed. This was the acceptable velocity of the stage at which there was a good coverage of the disc without consuming a large amount of glass powder. The output pressure, on the other hand, was varied from 2 to 4 bar and with the selection of 4 bar as the control pressure during the experiment. This is due to the high efficiency of the glass powder to abrade and embed in the titanium surface at that pressure value, as concluded from the pilot study findings.

3.3.4 Abraded discs analysis

3.3.4.1 White Light Profilometry

For the analysis of the topographical surface changes of the abraded titanium discs, a Scantron, Proscan 2000 profilometer (Scantron industrial products Ltd, Taunton, UK) was used. It is a non-contacting optical device consisting of either laser or white light distance measuring sensor. This sensor scans the surface of the specimen without physical contact; therefore, there is no possible alteration in the surface of the samples. In this study S13/1.2 sensor was utilised, where S define as the type of the optical technique used which is chromatic light. The number 13 represents the maximum distance from which the sensor can measure the target area and its unit is in mm. While the second number is representing the measuring range which is 1.2 mm. In addition, the scanning resolution for this sensor is 0.025 µm and the spot size is 8.0 µm. The abraded discs were scanned by WLP with fixed setting parameters, such as, measurement frequency, average scan and step size. The recommended frequency for the specimens was 1000 Hz and this was due to the high reflectivity of the titanium. The metal surface was assigned 100 % reflected

light intensity during the measurements. For the purpose of decreasing the noise in the collected data, the average number of the scan was selected as 4. Regarding the step size, the sample was scanned with a step size of 20 µm.

The dimension of the tested area was (8 mm x 4 mm) and this included the abraded line and part of the “intact surface”. From the scan, three measurements were evaluated, such as, the abraded line width, depth and volume removal. The measurement was carried out using Proscan 2000 ver. 2.1.1.8+ software (Scantron industrial products Ltd, Taunton, UK). The line width was measured from the edge of the groove to the other edge as shown in Figure (3.13). Three measurements were taken across the abraded line for each tested disc. While for the depth evaluation, five points across the abraded line were measured. This was performed by calculating the depth from the edge of the groove to the deepest part as in Figure (3.14).

Figure 3.13: Cross sectional view of the abraded line showing the way of width measurement a) Starting point b) End point.

Figure 3.14: Cross sectional view of the abraded line showing the depth measurement a) Starting point b) Deepest point.

The volume of the titanium removal was calculated directly using the device software after determining the lowest and the highest point in the groove area, as see in Figure (3.15). Moreover, those measurements were taken for the same five points which have been selected for the depth measurements.

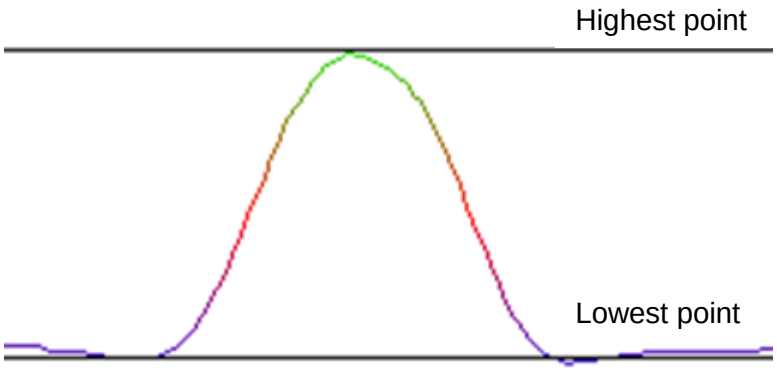

Figure 3.15: Cross sectional view of the abraded line and the software will calculate the volume automatically after determining the lowest and the highest point.

Regarding the measurements of the average surface roughness (Ra), three line scans were performed for both the abraded and the polished discs. The scan was done in the central part of the abraded line of the abraded discs and on the middle portion of the polished disc surface. The readings were taken after applying a filter of size 80 and this was to separate the roughness from waviness, which sometimes superimposes on each other.

3.3.4.1.1 Statistical analysis

The statistical analysis was conducted by using an IBM-SPSS software program (version 24). One-way analysis of variance (ANOVA) followed by Tukey post-hoc multiple comparison tests to evaluate the statistical significance at $(p \leq 0.05)$ was performed under the assumption of normally distributed measurements and equal variance between the groups.

3.3.4.2 SEM-EDX analysis

The surface topography of the polished and abraded titanium discs was characterised by using SEM microscope in a secondary electron (SE) mode. The discs were fixed on the stubs and scanned by SEM-SE (FEI Inspect F, Oxford Instruments, UK), using accelerating voltage 10 kV and working distance 10 mm.

For measuring the area coverage of the titanium discs with bioactive glasses, SEM-back scattered (BSE) images were utilised. The same setting which was used in the SEM-SE mode was also used in this mode. For each disc, four images with (1600X) magnification were taken from the central portion of different areas across the abraded line, two from the peripheries and two from the middle section. Then, those images were analysed for the measurement of the area percentage coverage by Image J software (Softonic). As there was a clear contrast between the titanium and the glass, the coverage percentage was calculated automatically by the program via selecting the black areas. The data were all analysed by one-way analysis of variance (ANOVA) followed by Tukey post-hoc multiple comparison tests to compare between the groups and to evaluate the statistical significance at $(p \leq 0.05)$. Additionally, the data were tested for normality using Shapiro-Wilk tests.

For the elemental analysis of the abraded discs, EDX line scans were used. This technique was carried out by drawing a line across the disc starting from the intact titanium part passing through the abraded line area and ended in the other end of the titanium surface. The detected elements were all presented in weight %.

3.3.5 Glass embedding and retention in Ti surface

The mechanical attachment of the glass particles to the titanium surface was determined by immersing the abraded discs in 0.1 M acetic acid. The solution was prepared by adding 6 mL of (100%) acetic acid (Analar normapur, VWR chemicals, France) to 900 mL of deionised water. Then, the pH was adjusted to 4.0 by sodium

hydroxide tablets (Fisher Scentific UK Limited, UK) and the total volume was filled to 1 L.

Six discs from each glass composition and with the abraded variables (distance 3 mm, velocity 0.5 mm/sec, and pressure 4 bars) were prepared and immersed in six tubes each containing 4 mL of 0.1 M acetic acid. The samples were kept in a shaking incubator for 3 to 6 h. Then, the discs were removed, left to dry for overnight in an incubator and tested by SEM-EDX analysis. The collected solutions were analysed for ions release by ICP-OES and F^--ISE.

3.3.6 Abraded discs bioactivity

The determination of the apatite formation on the glass abraded discs was evaluated in Tris buffer and SBF. Two titanium discs were blasted by QMFA1 glass at a distance 3 mm, velocity 0.5 mm/sec and pressure 4 bars. The bioactivity procedure was carried out by immersing one glass abraded disc in 4 mL of the testing solution. The discs were kept in a shaking incubator at 37 ºC for 3 days Figure (3.16). Then, the discs were collected, left to dry in an incubator for 12 h and scanned by SEM-EDX. Prior to scanning; the discs were fixed on a stub and coated with carbon. Then, the morphology of the apatite layer was evaluated by SEM in both SE and BSE modes and the element analysis was performed by SEM-EDX.

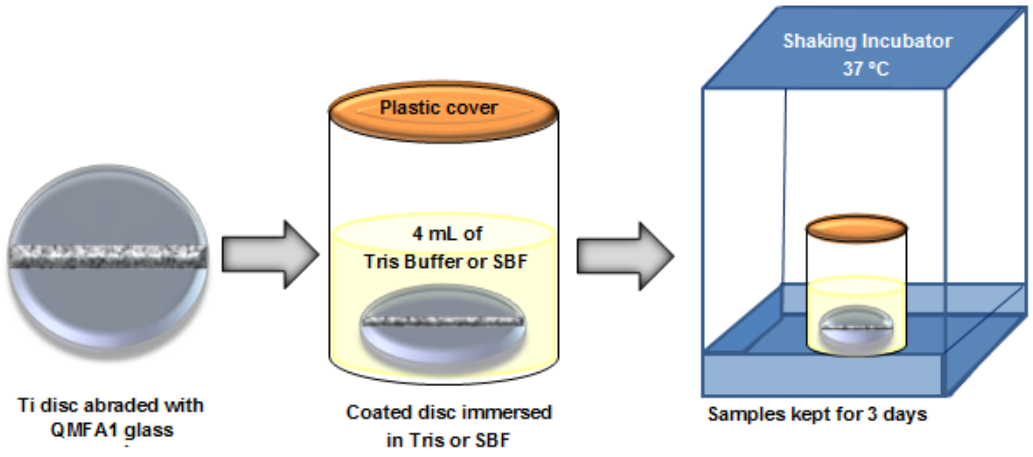

Figure 3.16: Schematic diagram of a glass abraded disc bioactivity study procedure.

3.4 Cell culture studies

MC3T3-E1 mouse preosteoblast cells (Public Health England, Porton Down, Salisbury, UK) was used in this study. This is due to the cell's ability to differentiate to osteoblasts and its responsibility in secreting the bone matrix for mineralisation. Moreover, the process of bone matrix calcification by this cell line is closely similar to the *in vivo* intramembranous osteogenesis (Sudo et al., 1983, Wang et al., 1999, Jeong and Jeong, 2016). MC3T3-E1 was cultured in T75 culture flasks in an incubator maintained at 37 ºC and 5% CO_2. The cells were grown in α-MEM media supplemented with 10% FCS, 1% penicillin/streptomycin and 1% L- glutamine. For the purpose of cell maintenance, the medium was changed every 3 to 4 days until confluence was reached. For the glass powder biocompatibility studies the cells were seeded at $1x10^4$ cells/mL, while for the titanium discs studies a density of $2x10^4$ cells/mL was used.

3.4.1 Glass powder biocompatibility

3.4.1.1 Quantitative assay of Alkaline Phosphatase (ALP) activity:

Prior to the ALP and DNA experiments, glass conditioned α-MEM was prepared from each glass composition. 75 mg of glass powder with a particle size ≤38 µm was immersed in 10% FCS supplemented α-MEM for 72 h at 37 ºC. After this time point, the solutions were centrifuged for 5 min at 800 rpm for glass separation, and filtered with 0.2 µm pore size filters for sterilisation. Then, these solutions were utilised to maintain the cells during the period of the experiments.

At 80% cell confluence in T75 flasks, the MC3T3-E1 cells trypsinised and seeded in 96-wells plate with a density of $1x10^4$ cells/mL and maintained with 2% FCS α-MEM for the first 24 h. After that, the media were changed with 10% FCS α-MEM for the control samples while for the test samples; 72 h glasses conditioned α-MEM media were used.

The cells were cultured and treated for specific time periods; 1, 3, 5 and 7 days, washed in phosphate buffer solution (PBS) and kept frozen until the assay was ready to be performed. This assay depends on the conversion of the p-nitrophenol phosphate into p-nitrophenol, which is a yellow coloured product the intensity of which is related to the action of alkaline phosphatase enzyme of the cells. The reaction solution of 2.5 mg/mL of 4-Nitrophenyl phosphate disodium salt hexahydrate in Tris buffer of pH (9.4) and 1 mM magnesium chloride (Sigma-Aldrich Company Ltd, Gillingham, UK) were prepared. After 1 h of thawing, 100 µL of the prepared reaction solution was added to each well and then the plates were stored in a 37 ºC temperature incubator for 45 min. After which the reaction was stopped by the addition of 50 µL of 0.5 M NaOH to each well. Then, the intensity of the coloured product was quantified by measuring the absorbance spectra at 405 nm. This experiment was conducted in triplicate to assess reproducibility.

3.4.1.2 Quantitative assay of DNA content:

This assay was used to quantify the number of cells and the proliferation rate by determining the DNA quantities in each well with fluorochrome bisbenzimidazole Hoechst 33258. The cells were cultured in 96-wells plate at a density of $1x10^4$ cells/mL, maintained in the same way as in 3.4.1.1 and treated with control or conditioned media for 1, 3, 5 and 7 days. Again, cells were washed in PBS and stored at -20ºC

At the assessment time, 100 µl of deionised water was added to each well after 1 h of thawing. This enhances the release of the DNA contents of the cells after their rupture due to the hypotonic environment. Then, 1:50 fluorochrome bisbenzimidazole Hoechst 33258 in TNE buffer, pH 7.4 with 10 mM Tris, 1mM EDTA and 2 M NaCl (Sigma-Aldrich Company Ltd, Gillingham, UK) was added to the wells. In the final step, the fluorescence intensity was measured on a plate reader at emission and excitation wavelengths of 460 nm and 350 nm respectively.

3.4.1.3 Statistical analysis

The data were reported as means ± SD and analysed by IBM SPSS program using one-way analysis of variance (ANOVA) followed by Tukey post-hoc test to evaluate the statistical significance at *($p \leq 0.05$)*.

3.4.2 Titanium discs biocompatibility

The glass abraded titanium samples were tested and compared for their *in vitro* biocompatibility against the polished titanium discs by using different assays. Each assay was performed to detect and evaluate a fundamental step in the bone formation process.

Due to the similarity in the glass properties and the insignificant difference between the abraded discs of different compositions, QMFA2 glass abraded discs were tested in the current study. The selected samples for the following experiments were prepared by the coating parameters (distance 3 mm, velocity 0.5 mm/sec and pressure 4 bars). 100 samples in total were prepared for the biocompatibility studies and this included both abraded and un-abraded titanium discs. All the discs were sterilised by a dry heat at 160 ºC for 1 h prior to the experiments.

3.4.2.1 Cell morphology

This study was carried out using SEM to ascertain the morphology of the osteoblast cells on both abraded and un-abraded titanium discs. Four samples from both un-abraded and abraded discs were placed in 24-well plates and seeded at a density of $2x10^4$ cells/mL. After 72 h, the media were removed and the cells washed twice with PBS. Next, the cells fixed with 2% glutaraldehyde (Sigma-Aldrich Company Ltd, Gillingham, UK) in PBS (pH 7.30) for 2 h at 4 ºC. After fixation, the cells subjected to a dehydration process using graded series of ethanol from 35%, 50%, 60%, 70% and 90%, each percentage was used for 5 min and repeated twice. Finally, the discs were immersed in 100% ethanol and kept at 4 ºC until they were ready to be used for the next step. Before SEM-scanning, the 100% ethanol was removed and 1 mL

of Hexamethyldisilazane (HMDS) (Sigma-Aldrich Company Ltd, Gillingham, UK) was added to each well plate for 5 min. Then, the discs were transferred to another well plate and left to dry for 2 h. The discs were scanned with SEM using SE mode at accelerating voltage 10 kV after coating with gold sputter (Agar Scientific, Elektron Technology UK Ltd, Essex, UK).

3.4.2.2 Qualitative and Quantitative assays of ALP activity

The qualitative ALP activity assay was evaluated by naphthol phosphate method. This method was carried out to compare the amount of ALP produced from the cells on the abraded part of the disc with that of the un-abraded part, as well as comparing the activity of cells on both pure titanium and glass abraded discs. The procedure was based on the reaction which takes place between the α-naphthol and the fast-blue RR (4-benzoylamino-2.5-diethoxybenzenediazoniumnchloride hemizinc chloride salt). This reaction will result in the production of insoluble blue precipitate which reflects the site of ALP activity.

For the qualitative ALP activity assay, three samples from each group were tested and this experiment was run in triplicate. The cells were seeded on the polished titanium and glass abraded samples with a density of $2x10^4$ and left to grow for 14 days in 10% α-MEM media which was changed every 3-4 days. After 14 days, each disc was washed twice with PBS and stained with 1 mL of fast blue stain solution. This solution was prepared by mixing of 0.4 mg/mL 1-Naphthyl phosphate monosodium salt monohydrate and 1 mg/mL Fast Blue BB salt (Sigma-Aldrich Company Ltd, Gillingham, UK) with a mixture of 8 mL of 0.1 M Tris (pH 9.2) and 15 µL of (0.05 M) $MgCl_2$. Finally, the samples were covered with aluminium foil at room temperature for 45 min. The reaction was stopped by repeated washing and samples were examined by reflected light microscope. ALP activity of cells on the glass abraded discs and control discs were compared using the quantitative assay.

In this experiment, the cells were seeded on the discs in the same manner as above and kept at the same time point.

After 14 days, both titanium and glass abraded discs were washed twice with PBS and treated with a solution consisting of 2.5 mg/mL of 4-Nitropheyl phosphate disodium salt hexahydrate in Tris buffer of pH (9.5) and 1mM magnesium chloride. The discs were transferred to clean 24-well plates and 400 µL of the prepared solution was added to each disc. The plates were covered by aluminium foil and kept in the incubator for 1 h. Then, 100 µL aliquots were transferred to the 96-well plates and the absorbance spectra were measured at 405 nm.

3.4.2.3 Detection and quantification of collagen type I formation

The MC3T3-E1 cells were seeded on the abraded and un-abraded titanium discs in the same manner as described in the previous studies. Six samples were used from both discs and the experiment was run in triplicate. The cells were left to grow for two weeks in 10% α-MEM medium. Then, this medium was changed with medium further supplemented with 50 µg/mL L-ascorbic acid, 5 mM β-glycerophosphate and 10 nM dexamethasone (Sigma-Aldrich Company Ltd, Gillingham, UK) to form osteogenic medium. The latter medium was used for maintaining the cells for the further two weeks and changed every 4-5 days.

After incubation, the seeded discs were washed twice with PBS and fixed with 4% glutaraldehyde for 30 min at room temperature. After fixation, the discs washed three times with PBS; stained with 1 mL of 0.1% Sirius red stain in 1.3% saturated picric acid (Sigma-Aldrich Company Ltd, Gillingham, UK) and kept in a dark place for 1 h at room temperature. Then, the discs transferred to a clean well plate, washed three times with deionised water and examined by reflected light microscope.

To quantify the intensity of the stain spectrophotometrically, the discs were treated with 0.1 M sodium hydroxide solution for 1 h at room temperature to elute the stain

from the samples. 400 µL of the solution was added to each well and then, 100 µL aliquots of the solution were transferred to 96-wells plate after disc removal. The absorbance was measured at 560 nm.

3.4.2.4 Detection and quantification of mineralisation nodules

For the detection of the calcified nodules on the seeded discs, the Alizarin Red S Stain was used. The seeding and treating procedure of the discs were performed in the same way as collagen formation study. However, in this study the discs were treated with the osteogenic medium for three weeks. After three weeks, the discs were washed twice with PBS, fixed with 4% glutaraldehyde for 30 min at room temperature and washed with PBS and deionised water each for two times. Then, the discs incubated with 1 mL of 40 mM Alizarin Red S (pH 4.1 Sigma-Aldrich Company Ltd, Gillingham, UK) in a dark place for 2 h. Later, the discs transferred to another plate, washed three times with deionised water and prepared for mineralisation nodules examination using reflected light microscope.

To quantify the amount of the stain in the treated discs, the Alizarin Red S stain was extracted. This procedure was carried out by treating the previously stained discs with 400 µL of 10% cetylpyridinium chloride in deionised water for 1 h at room temperature. Then, 100 µL aliquots were transferred to 96-wells plates and absorbance was read at 560 nm. In this study, three abraded discs were used per experiment, compared to three polished titanium discs as controls and the experiment run in triplicate.

3.4.2.5 Statistical analysis

All the data were presented as mean ± SD and they analysed by Excel 2010 software for statistical significant difference *($p \leq 0.05$)* using Student's *t-test*.

Chapter 4 Results and Discussion of Glass Characterisation

4 Results and discussion of glass characterisation

Modifying the glass composition can alter its physical, mechanical, thermal properties and bioactivity. This is due to the roles of each component in the glass structure. Therefore, it is essential to investigate the glass structure when designing a new glass composition.

4.1 XRD

From the XRD patterns Figure (4.1), it can be clearly observed that all the prepared glasses are amorphous in nature. There is a broad halo centred at around 25º- 35º (2θ) which indicates the amorphous structure. In QMFA3 glass, there is a small fraction of crystalline peak observed at around 31.5º (2θ) and this might be associated with the formation of a crystalline phase.

The confirmation of the amorphous structure of the glasses by XRD is fundamental prior to the bioactivity study. This is to ensure the glass rapid degradation which will result in changes that will take place in the XRD diffraction patterns after the immersion of the glasses in different testing solutions.

Optically, all glasses appear homogenous and transparent. This indicates that there is no phase separation in the prepared glasses on a light scattering scale (>0.2 micron).

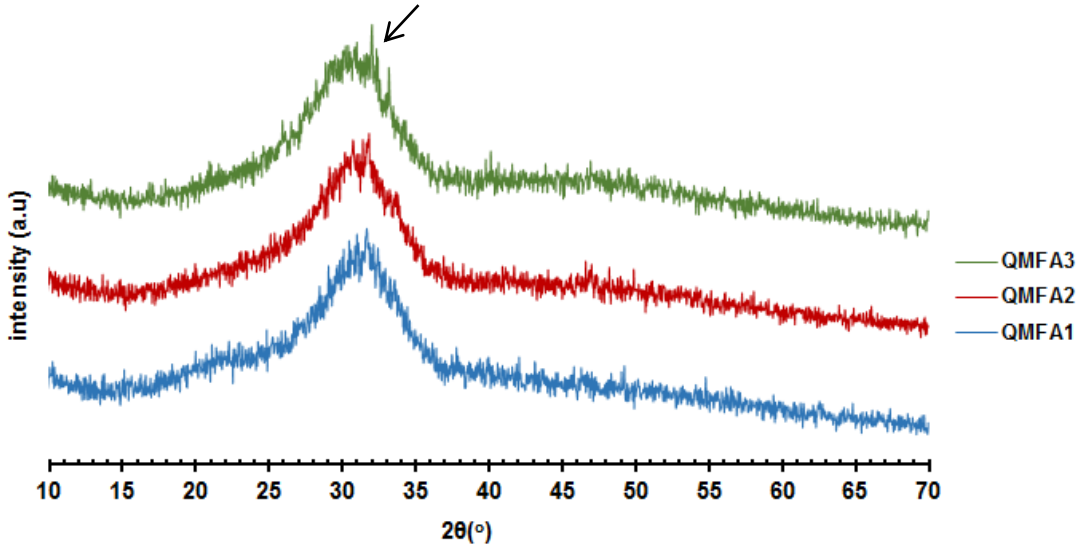

Figure 4.1: XRD patterns of the prepared glass powders showing a broad halo which is located between 25º-35º (2θ). The arrow points to the small crystalline peak at 31.5º (2θ) in QMFA3 glass (green pattern).

4.2 FTIR

Figure (4.2) shows the FTIR absorbance spectra of the prepared glasses. There are two dominant bands, one at 910 cm^{-1} and the second at 1020 cm^{-1} wavenumbers. These bands represent the $Si\text{-}O^{-}$ $alkali^{+}$ bands with the NBO bond and the BO stretching bands (Si-O-Si) respectively (Kim et al., 1989, Filgueiras et al., 1993b). There is also a broad band in the 550-600 cm^{-1} region, which represents the P-O bending vibration of PO_4 tetrahedron for the amorphous glasses and the Si-O-Si bending vibration band (O'Donnell et al., 2009). The spectra of the three prepared glasses are in agreement with those shown in the literature for the unreacted soda-lime glasses (Kim et al., 1989, O'Donnell et al., 2009, Mneimne et al., 2011). The bands are characteristic for the amorphous nature of the bioactive glasses and they will undergo distinct changes after the immersion of the glasses in different solutions. This will be interpreted and discussed in the bioactivity study in Chapter 5.

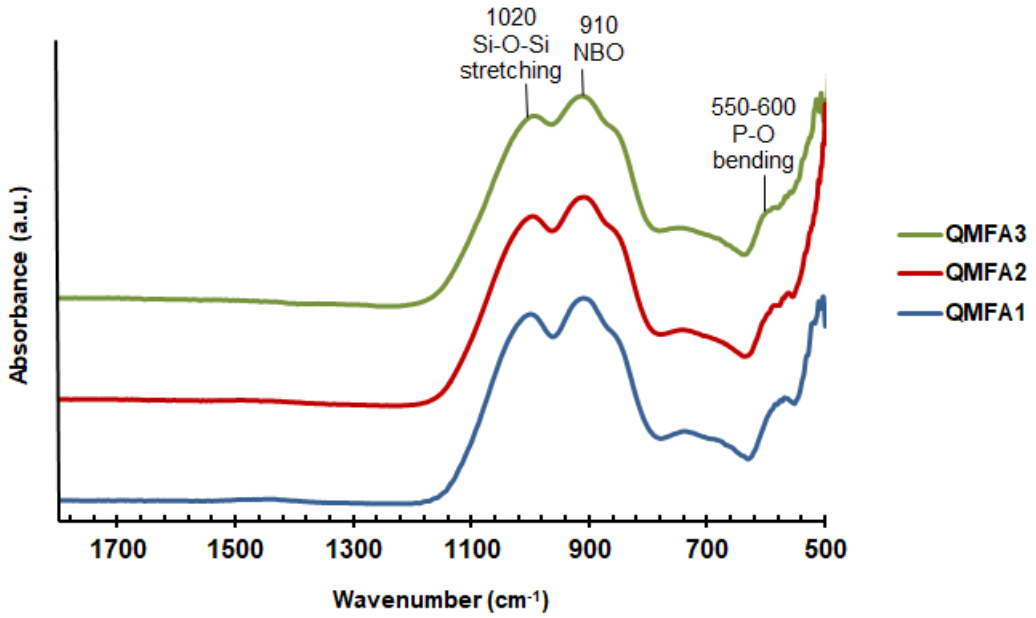

Figure 4.2: FTIR spectra of the prepared glass powders. The spectra show the presence of the prominent bands assigned to the amorphous structure of the glass powders.

4.3 ^{19}F and ^{31}P MAS-NMR

^{31}P MAS-NMR spectra of the prepared glasses are shown in Figure (4.3). These spectra demonstrate that the phosphate in all glasses exists as a separate orthophosphate species. This is due to the presence of a single symmetric peak in all spectra (Brauer et al., 2009). With decreasing the sodium content in the glasses, there is a shift in the ^{31}P peak position toward less positive values from 6.9 ppm to 5.6 ppm and to 4.5 ppm for QMFA1, QMFA2 and QMFA3 respectively. This shift suggests that there is a relation between the sodium content in the glasses and the orthophosphate species. The glass with more sodium content gives higher positive values and shifts the peak position toward the positive side. These results are consistent with the results of previous studies (Lockyer et al., 1995, Elgayar et al., 2005, Brauer et al., 2009). The shift is due to the lower electronic shielding of sodium in comparison to calcium and this causes the peak position of the phosphate to move toward higher chemical shift values with increase in sodium content.

In addition to the previous features, it can be seen that there is no change in the line width of all the peaks with changing the glass composition. This indicates that the phosphate in the glasses stays amorphous.

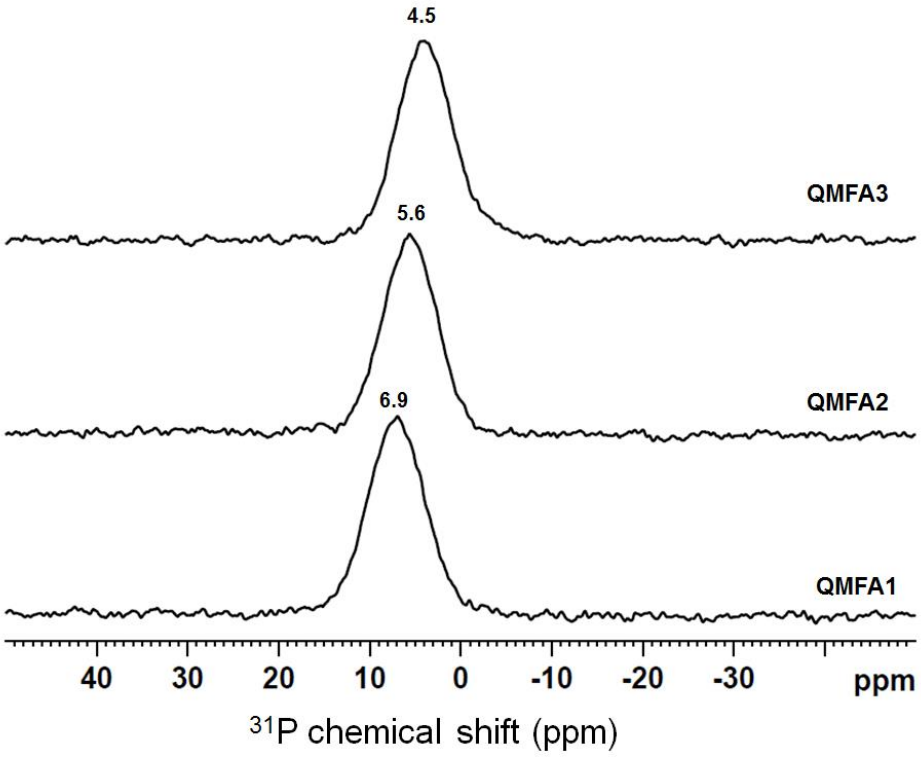

Figure 4.3: ^{31}P MAS-NMR spectra of the original glasses showing the presence of a broad signal, which represents the presence of a separate orthophosphate species.

Figure (4.4) demonstrates the ^{19}F MAS-NMR spectra of the prepared glasses. The peak positions of these glasses are varying between -131.8 ppm and -103.3 ppm and this range correlates with the presence of mixed species of sodium calcium fluoride (Hayashi et al., 2006).

Two peaks are clearly seen in QMFA1 glass, one is positioned at -170 ppm and this represents F-Ca(2) Na(2) species while the other, is at -131.8 ppm which is attributed to F-Ca(3) Na(1) (Brauer et al., 2009). Whereas, in the other two glasses QMFA2 and QMFA3, only one peak is present at position -117.4 ppm and -103.3 ppm respectively. Moreover, there is a clear chemical shift in the ^{19}F peak position toward zero value as the sodium content of the glass is decreased. This is related to

increase of calcium concentration in the glasses, which pushes the peak position towards an F-Ca (4) site (Brauer et al., 2009).

All signals in these ^{19}F MAS-NMR spectra are quite broad demonstrating an amorphous nature of the fluorine species in the glasses.

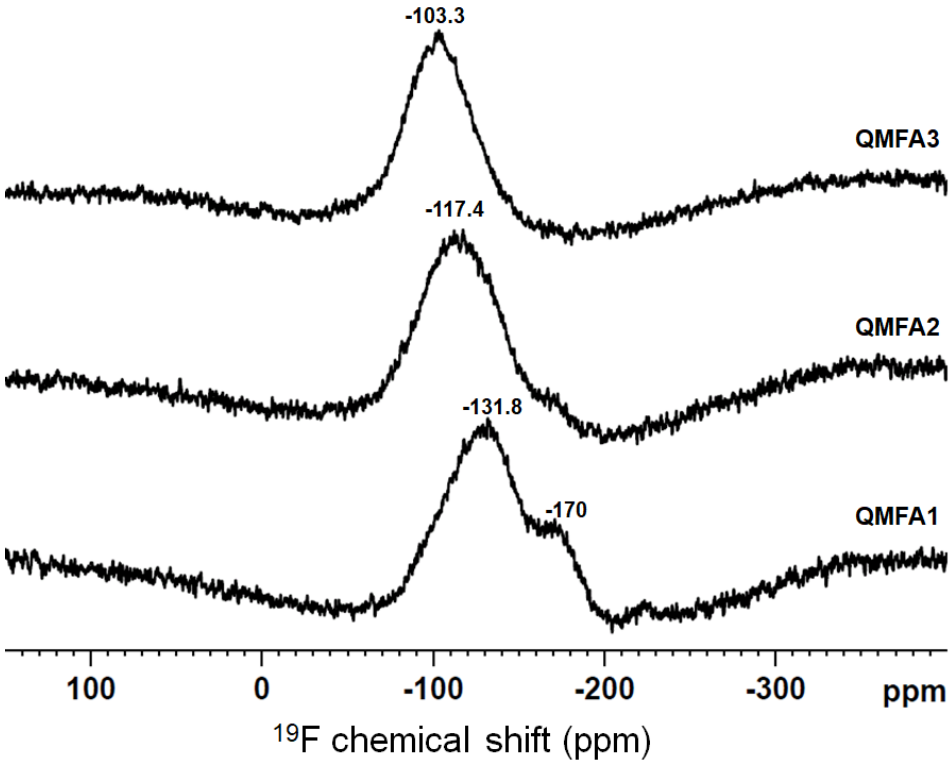

Figure 4.4: ^{19}F MAS-NMR spectra of the original glasses showing the presence of a broad signal, which refers to the amorphous fluorine species.

4.4 DSC

Glass transition temperature and crystallisation temperature of the unreacted glasses were analysed by DSC. Both temperatures were plotted as a function of the sodium oxide mole % in the glasses, as demonstrated in Figure (4.5) and Figure (4.6) respectively. The T_g of the lowest sodium contained glass (QMFA3) is 605°C and this value showed a decrease to 544°C and 488°C for QMFA2 and QMFA1 respectively. The same trend is also demonstrated with the T_c, where the values decrease from 766°C for QMFA3 to 601°C for QMFA1.

From both figures, it is clearly seen that there is a linear decrease in both temperatures with increasing the sodium content in the glasses. The linear correlation coefficient (R^2) for both relations is around 0.999 which confirms the strong linear relation. This behaviour was also found in the previous studies (Andersson, 1992, Wallace et al., 1999, Rajendran et al., 2002, Farooq et al., 2013).

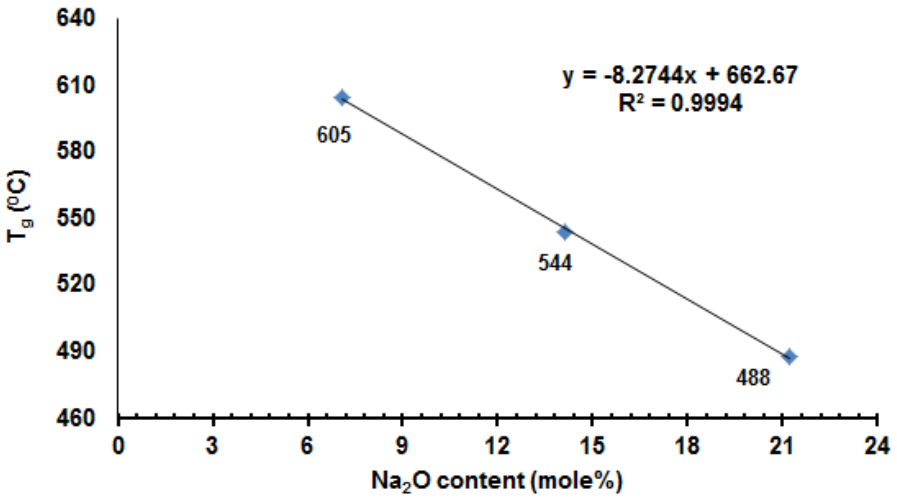

Figure 4.5: Graph illustrating the relationship between T_g (ºC) and Na_2O content (mole %) in the prepared glasses. The line represents the linear regression for T_g versus Na_2O content, R^2=0.999.

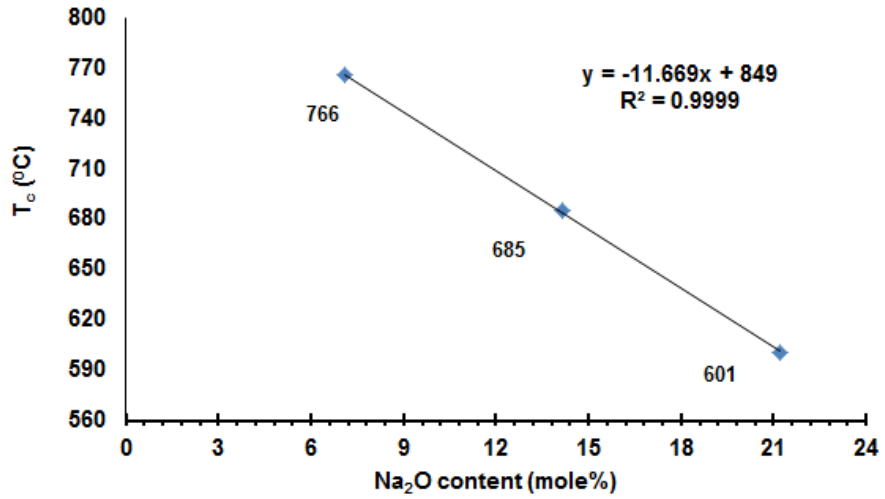

Figure 4.6: Graph shows the relationship between T_c (ºC) and Na_2O content (mole %) in the prepared glasses. The line represents the linear regression for T_c versus Na_2O content, R^2=0.999.

From these results, it can be revealed that the substitution of Na_2O for CaO has a great influence on the thermal properties of the glasses. The reduction in the T_g and T_c values is suggested to be related to the nature of the NBO bonds in the glass structure. It is known that both sodium and calcium cations are network modifiers and are lowering the T_g of the bioactive glass by opening up the glass structure (Elgayar et al., 2005). In case of the sodium substitution, there will be a replacement of one calcium cation with two sodium cations in the glass network. As sodium cation is a monovalent and bond with only one oxygen bond while, the calcium cation is a divalent and bond with two oxygen bonds. Therefore, in case of cations substitution there will be a consequent higher disruption in the structure of the network and a reduction in the crosslinking of the glass network, which will lead to a clear decrease in the T_g. This agrees with (Wallace et al., 1999, Farooq et al., 2013). The relation of the T_g and the sodium mole % with the glass hardness will be discussed later in section (4.7).

4.5 Particle size distribution of the abrasive glass powder

The means ± the standard deviations (SD) of the glasses particle size used in the grit blast technique are expressed as percentiles (10, 50 and 90%) in Figure (4.7). Moreover, a line graph presenting the distribution pattern of the glass particle size is seen in Figure (4.8).

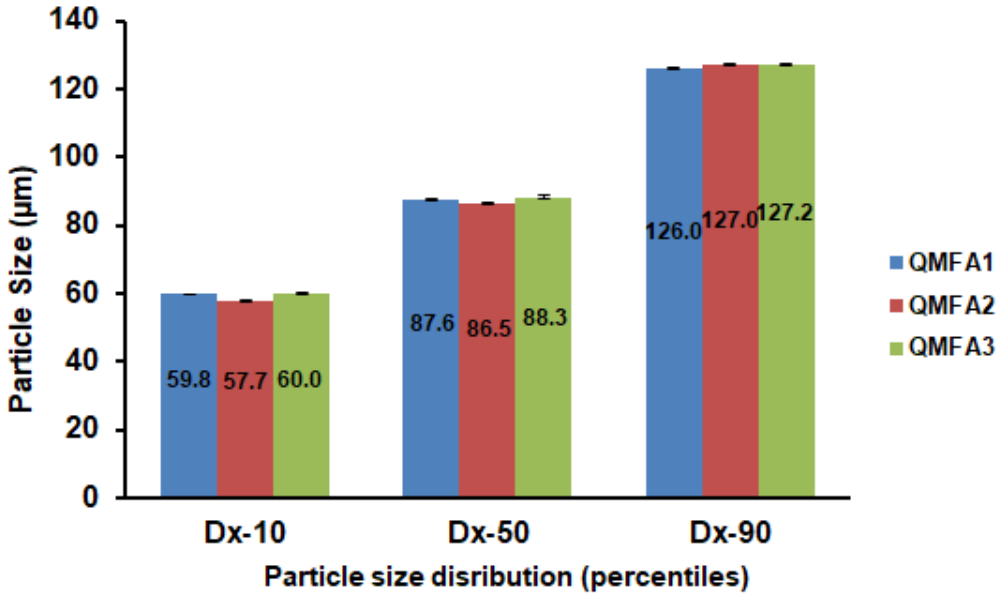

Figure 4.7: Mean ± SD of the glass particle size (µm) used in the grit blast technique, expressed as percentile classes.

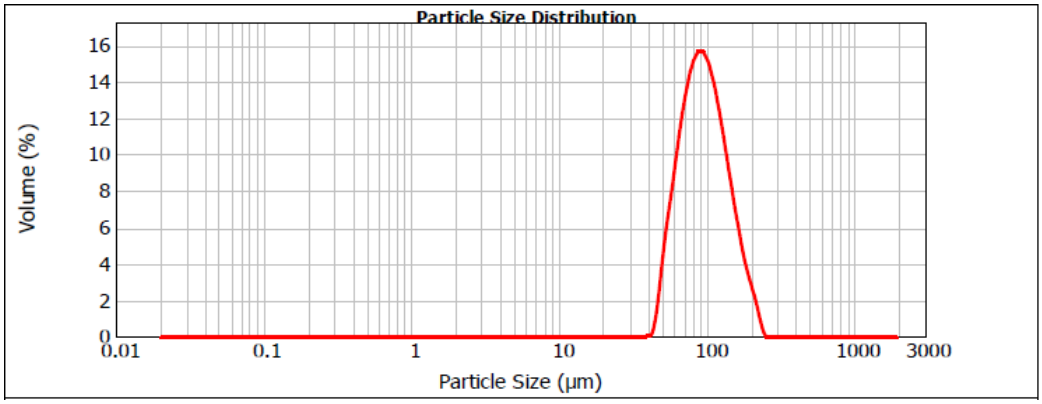

Figure 4.8: The particle size distribution of QMFA1 glass powder in volume %. The distribution of the particles is narrow in all glasses and indicates the coarse nature of the particles.

Generally, all the prepared glasses demonstrated narrow particle distributions and high values of particle size. The median particle size (D 50) of the glasses ranged between 86.5±0.0 µm to 88.3±0.2 µm, whereas the (D 90) percentile size of the sieved powders showed larger values than the used sieve mesh size. The values were between 126 µm and 127.2 µm for the glass particles, while the sieve mesh

size was 90 µm. This was suggested to be due to the tendency of the glass particles to adhere to each other during the running of the particle size experiment. This is because of the presence of particles in the submicron scale which might attach to the surface of the main particles and increase the formation of agglomerates. However, in these glasses there are not many particles in the submicron scale. Therefore, it is more likely to be related to the morphology of the glass particles. The glass particles are irregular in shape and they may pass through the mesh of the sieve in a longitudinal direction. The particle size analysis machine treats the particles as spheres during the analysis of the measurements as suggested by (Beuselinck et al., 1998) Figure (4.9). Thus, the machine will measure the irregular long glass particle as a sphere with a large diameter and this consequently will result in recording higher values of particle size dimension than the mesh size.

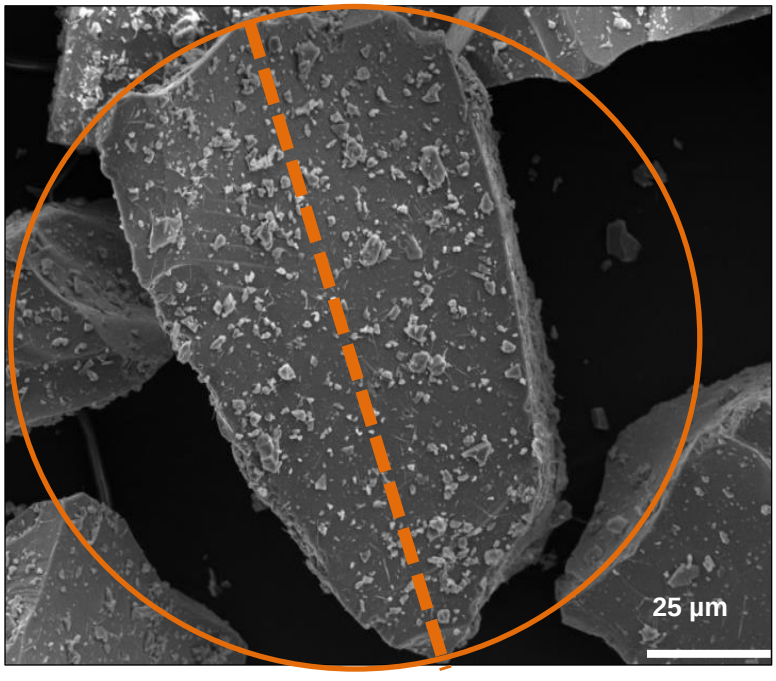

Figure 4.9: SEM image of QMFA1 glass particle (1600x magnification) showing the irregular shape of the particle and its prospective calculation as a sphere by the particle size analysis software.

Regarding the 10th percentile particle sizes of all the glasses, the results also exhibited large values which are 59.8±0.2 µm, 57.7±0.1 µm and 60.0±0.1 µm for QMFA1, QMFA2 and QMFA3 respectively. All findings indicate that all the glass powders are course in nature and they might result in a consistent smooth powder flow from the nozzle of the grit blast hand piece. Previous study reported that coarse particles enhance the flow of the abrasion stream (Koller et al., 2007). In addition, the large size of the powder particles affects the kinetic energy of the transferred particles in the air stream. The larger the particle mass, the higher the kinetic energy will be, therefore the cutting efficiency will be increased (Mount, 2009).

4.6 Abrasive glass powder morphology

The SEM micrographs of QMFA1, QMFA2 and QMFA3 glass powders of particle size range 63-90 µm are shown in Figures (4.10 a, b and c) respectively. From all the micrographs, it can be clearly seen that all the glasses particles have the same morphology. The particles are generally coarse in nature and they exhibit irregular shape with slightly rounded angular outline profile. However, there are submicron particles attached to the surface of the coarse particles. The findings from the SEM micrographs are consistent with the particle size data. The angular and the irregular shape of the glass particles were suggested to be due to the breakage mode which was used in the grinding of the glass frit. The Gyro mill technique depends on breaking the glass frit against the walls of the milling pot to produce small particles (Mahmood et al., 2014). Therefore, the massive fracture from this technique led to the production of irregular shaped particles. Determining the shape of the glass particles is considered as an important factor in determining the applications of the powder. Sharp and irregular glass particles are suggested to be used as an abrasive material and this is essential in this study (Kaya et al., 2002).

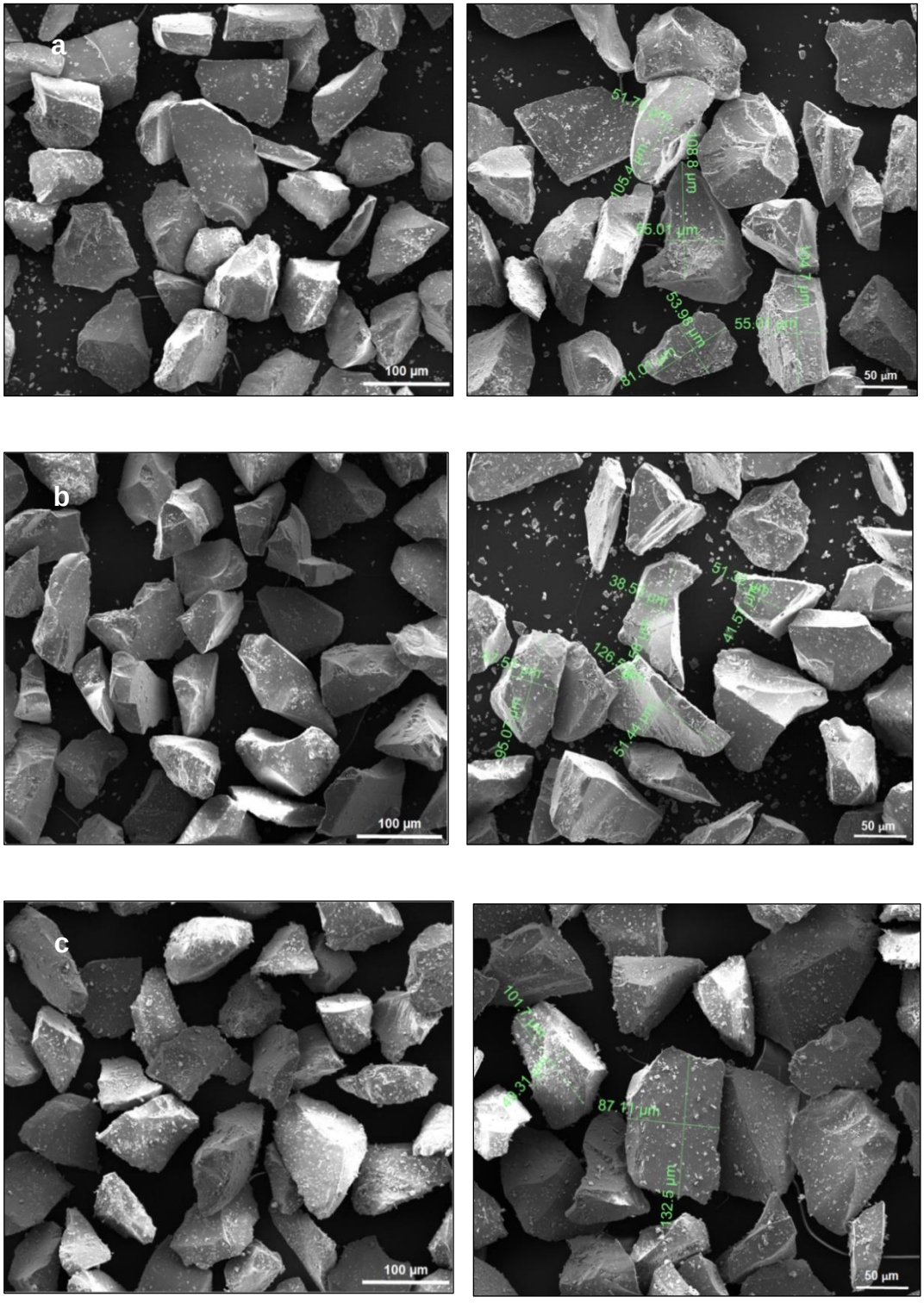

Figure 4.10: SEM micrographs of a) QMFA1 b) QMFA2 c) QMFA3 glass particles before air abrasion. The particles are irregular in shape with round angular outline. There are submicron particles attached to the surface of the coarse particles. The scan was performed by accelerating voltage: 10 kV, working distance: 10 mm and magnifications: 500x and 600x).

4.7 Glass hardness and density

Table (4.1) shows the hardness values of the prepared glasses and the statistical differences between the groups *(P≤0.001)* (see appendix 1 (10.1) for the detailed statistical values). The hardness of the high sodium content glass (QMFA1) is 4.19±0.14 GPa and it is significantly lower than that of the low sodium contained glass (QMFA3), which is 5.11±0.33 GPa. The hardness of the QMFA2 glass showed a middle value of 4.59±0.12 GPa. Figure (4.11) demonstrates the relation between glass hardness and the sodium content in the prepared glass compositions. The analysed data indicate that there is a linear relationship between the sodium content and the hardness values, as the correlation coefficient is 0.994. The higher the sodium content in the glass, the lower is the hardness value.

Table 4.1: Mean ± SD of Vickers hardness values (GPa) with the Na_2O mole % of the prepared glasses. Different symbols indicate a significant difference between the glasses *(P≤0.001)*.

Glasses	Na_2O mole %	Mean hardness (GPa)	Standard deviation
QMFA1	21.2	4.2^a	0.1
QMFA2	14.1	4.6^b	0.1
QMFA3	7.1	5.1^c	0.3

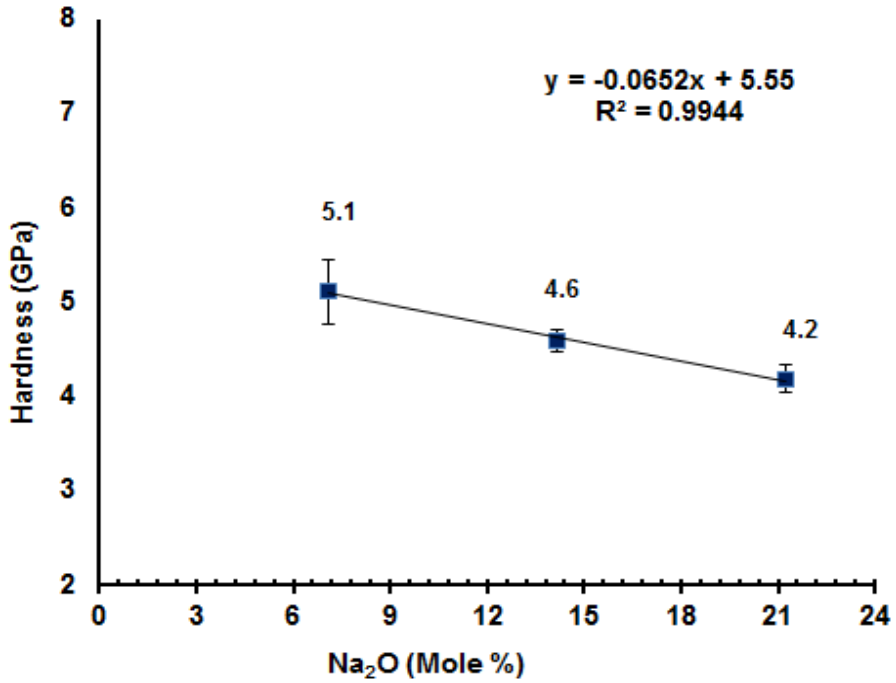

Figure 4.11: Graph demonstrates the relation between the glass hardness (GPa) and the Na_2O mole% in the glasses. The line represents the linear regression for hardness versus Na_2O content, R^2=0.9994.

The results of the current study are compared to the results of (Farooq et al., 2013) study Figure (4.12). In the previous study the glasses were prepared with sodium content from 0-10 mole %. The same trend was also appeared between the hardness and the sodium content. The lower the sodium content in the glasses, the harder is the glass. However the fluoride content in both studies is slightly different, but similar linearity is clearly demonstrated. The fluoride mole % in the Farooq et al. study was approximately 3 mole %, while in the present study it is 4.5 mole %.

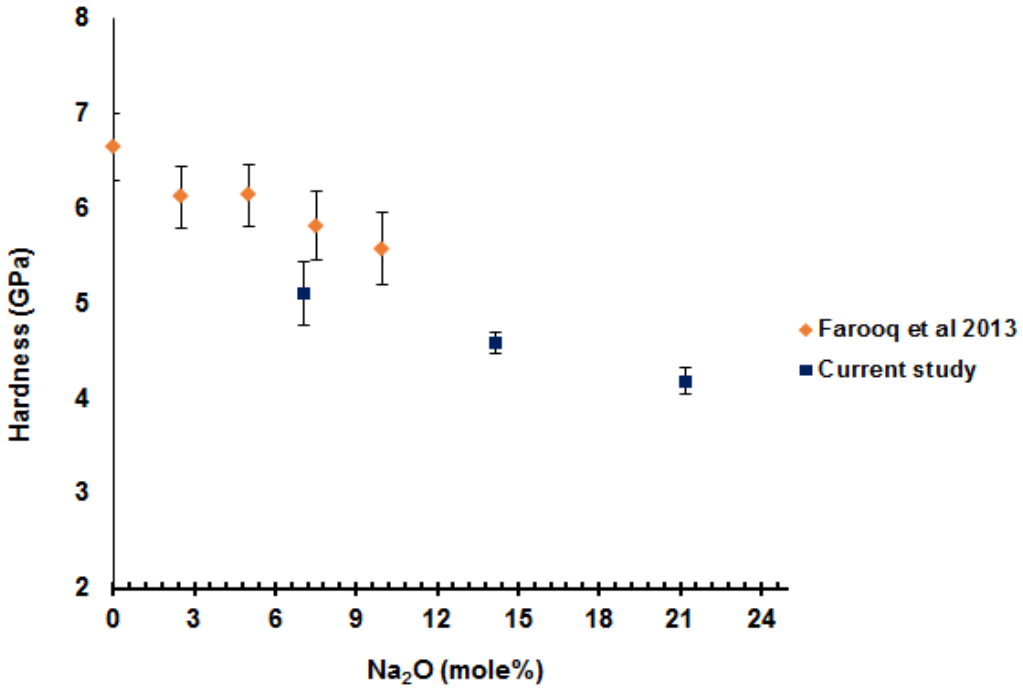

Figure 4.12: Graph shows the comparison of Vickers hardness relation with Na_2O between the prepared glasses (blue squares) and the glasses produced by (Farooq et al., 2013) (orange diamond-shaped).

As mentioned earlier in section 4.4 that there is an inverse relationship between glass T_g and sodium content. The same relationship is also seen with the glass hardness. This suggests that there could be a correlation between glass T_g and hardness. From Figure (4.13), it can be shown that there is a linear correlation between glass T_g and hardness, where the coefficient of correlation is around 0.997. This reveals that the glass hardness decreases with decreasing the glass T_g. This correlation was also proposed by (Baesso et al., 1999, O'Donnell, 2011, Farooq et al., 2013).

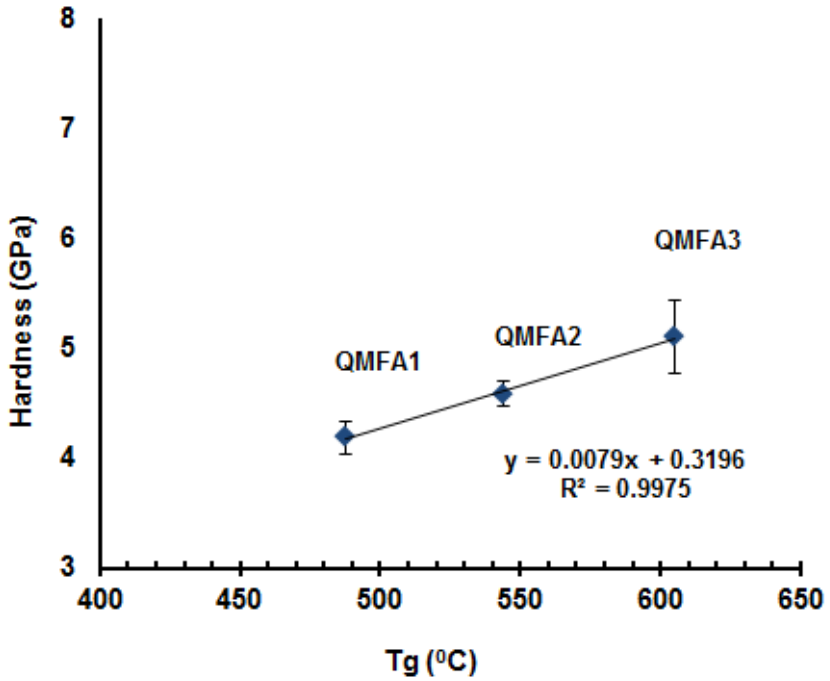

Figure 4.13: Graph shows the relationship between Vickers hardness (GPa) and T_g (ºC) of the prepared glasses. The line represents the linear regression for hardness versus T_g, R^2=0.997.

In addition to the glass hardness, the glass bulk and oxygen densities are also affected by the sodium content in the prepared glasses. Both densities revealed a linear decrease with increasing the sodium content Figure (4.14). The correlation coefficients of both glass and oxygen densities relations are 0.981 and 0.989 respectively. QMFA1 has both lower bulk and oxygen densities than QMFA2 and QMFA3 glasses. The bulk density of QMFA1 is around 2.78±0.01 gcm^{-3} while for QMFA2 and QMFA3 glasses, the bulk densities are 2.84±0.01 and 2.92±0.01 gcm^{-3} respectively. The oxygen densities of the glasses are around 1.19 gcm^{-3}, 1.23 gcm^{-3} and 1.27 gcm^{-3} for QMFA1, QMFA2 and QMFA3 respectively.

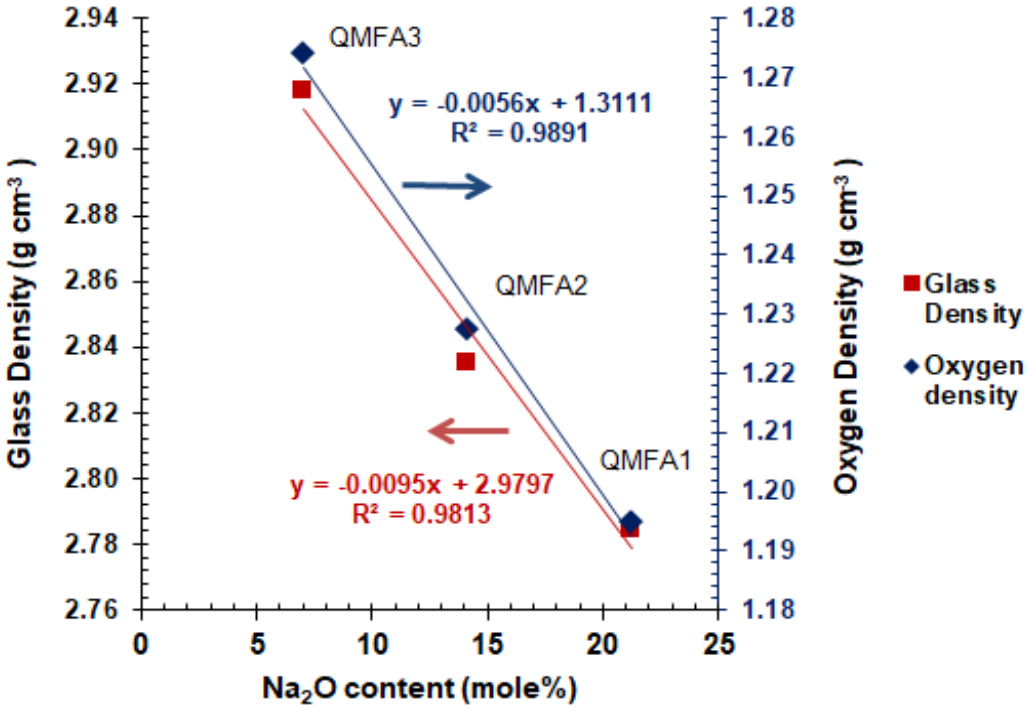

Figure 4.14: Graph shows the relation between the glass density (g cm^{-3}) (red squares) and the oxygen density (g cm^{-3}) (blue diamond-shaped) versus the Na_2O content in the glasses. The error bars are smaller than the point sizes. The red line represents the linear regression for glass density versus Na_2O content, R^2=0.981 and the blue line represents the linear regression for oxygen density versus Na_2O content, R^2=0.989.

These results were compared to the results of (Farooq et al., 2013) Figures (4.15) and (4.16). The same trend is seen in both studies. However, the glass density of QMFA1 and QMFA2 glasses are less than those of the glasses in the previous study. On the other hand, the oxygen densities of the prepared glasses are higher than the oxygen density values of Farooq et al study. This might be related to the difference in the calcium fluoride concentrations in both studies. Fluoride ions form complexes with sodium and calcium ions in the glass structure and not to the silica. Therefore, this results in a clear reduction in the density of the current study glasses in comparison to the previous glasses. This agrees with what has been reported in the literature (Brauer et al., 2008, Brauer et al., 2009, Brauer et al., 2010).

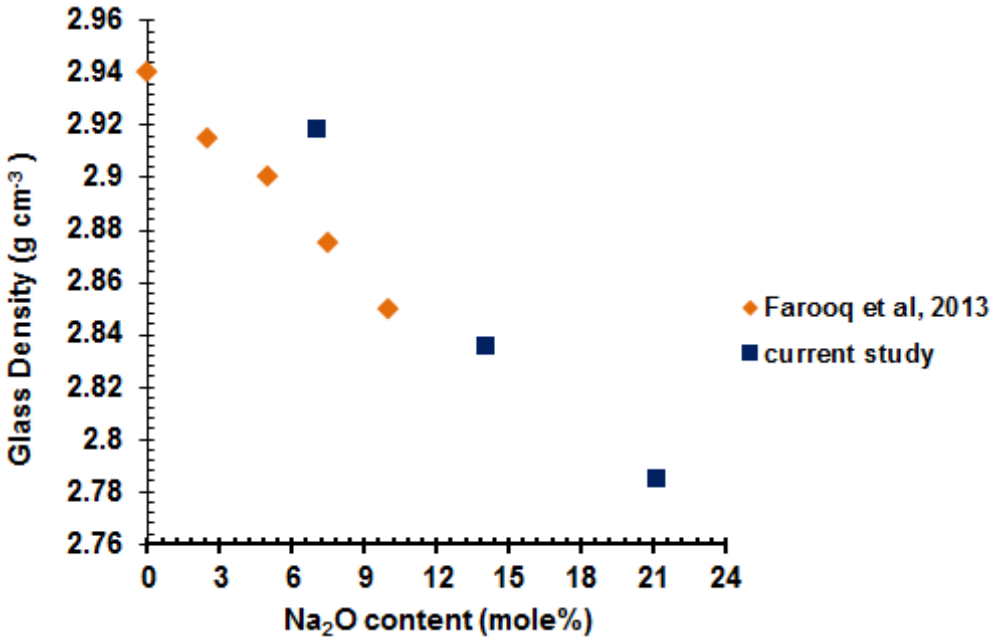

Figure 4.15: Graph shows the comparison between the glass densities (g cm^{-3}) of the current study (blue squares) and those prepared by (Farooq et al., 2013) (orange diamond-shaped) with the Na_2O content.

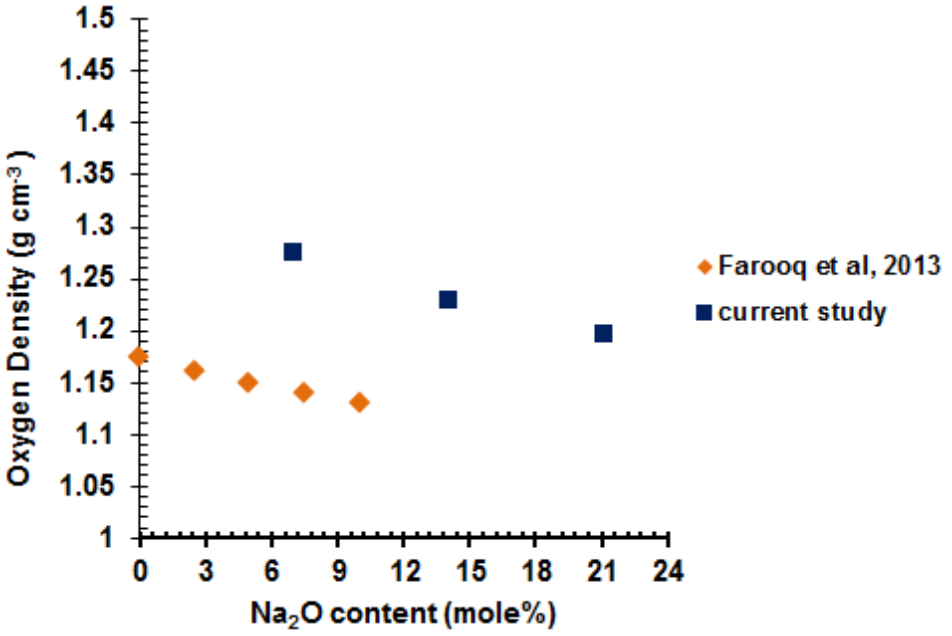

Figure 4.16: Graph illustrates the comparison between the oxygen densities (g cm^{-3}) of the current study (blue squares) and (Farooq et al., 2013) study (orange diamond-shaped) with the Na_2O content.

The same relation between the sodium concentration and the bulk density is also detected in the density and compactness of the abrasive glass powders. These properties together with the powder flow rate test are important to be investigated. This is because of the direct relation between these properties and the glass powder flow through the grit blast hand piece. In Table (4.2), QMFA1 glass powder shows the lowest density and compactness values among the three glasses. The powder density of QMFA1 is around 1.29±0.01 g/cm^3 followed by QMFA2 and QMFA3 with 1.32±0.02 g/cm^3 and 1.43±0.02 g/cm^3 respectively. These results are consistent with the density values of the glass monoliths. Therefore, the compactness of QMFA1 is lower than the other glasses and it is around 0.46.

Table 4.2: Mean ± SD of the glass powder densities (g/cm^3) and the measured compactness of the glass powders. Different symbols indicate a significant difference between the glasses *(p≤0.05)*.

Glasses	Powder density (g/cm^3)	SD	Compactness of glass powder
QMFA1	1.29^a	0.01	0.46
QMFA2	1.32^b	0.02	0.47
QMFA3	1.43^c	0.02	0.49

The substitution of the Na_2O for the CaO on molar bases does not modify the glass network structure, but it affects the glass density (Elgayar et al., 2005). The glass density depends on the compactness of the glass structure and the degree of crosslinking. The replacement of one Ca^{2+} ion by two Na^+ ions as an element substitution in the designed glasses causes decrease in the glass density and oxygen density. This was suggested to be due to the disruption of the silica network by the two sodium ions, where these two ions can cause an expansion in the silica network and lowering in the degree of packing of the atoms (Ray, 1974, Wallace et al., 1999).

The glass density showed an effect on the hardness property, as can be seen in the results of this study and (Farooq et al., 2013) study. Decreasing the compactness of the glass network showed a clear decrease in the hardness values. Moreover, the glass hardness and the T_g are also affected by the bond strength of the glass network. As more Na_2O included in the glass network, there is weaker ionic bond between the components of the glass. Therefore, the weak bonds and the low atomic packing result in low hardness and T_g.

4.8 Summary

The designed glasses are characterised by different techniques and they showed an amorphous structure. The phosphorus species in the glasses is presented as orthophosphate as detected by the ^{31}P MAS-NMR. The ^{19}F MAS-NMR confirms the presence of mixed sodium calcium fluoride species in all glass compositions. The partial substitution of Na_2O for CaO decreases both glass T_g and T_c. The compactness of the glasses, as well as the hardness is decreased with increasing the Na_2O mole %. The glasses, which are sieved between 63 μm and 90 μm mesh sizes, are angular and irregular in shape in addition they possess a narrow distribution of their particle size. Therefore, these glasses can be used successfully in the bioactivity study, as they are amorphous. The course and sharp particle glass powders are potentially attractive in the grit blast technique.

Chapter 5 Results and Discussion of Glass Powder Bioactivity

5 Results and discussion of glass powder bioactivity

Bioactivity refers to the dissolution ability of the glass in the surrounding environment and the formation of apatite on its surface. The glass solubility and the rate of apatite formation can be affected by the glass structure and composition (Hill, 1996). Therefore, altering the glass composition might increase or decrease its bioactivity and this could affect the rate of osseointegration.

5.1 Immersion of the glass powders in Tris buffer

5.1.1 FTIR results:

The FTIR spectra of the investigated glasses before and after their immersion in Tris buffer for 3, 6, 9, 24 h, 3 and 7 days are shown in Figure (5.1 a, b, c). In general, the trend of the degradation process is the same for all the glasses. The spectra of the treated glasses change significantly compared to the spectrum of the original glasses. These changes started after 3 h and became more pronounced with time. As mentioned in Chapter 4 that the original glasses had two main bands. These bands reveal distinct changes after the immersion of the glasses in Tris buffer. The NBO Si-O^- stretching band at 910 cm^{-1} disappears after 3 h immersions, while the P-O stretching band at 1020 cm^{-1} shifts and sharpens with the longer reaction times. At the same time, another Si-O-Si band also appears in the spectra at 790 cm^{-1}. These changes are all related to the dissolution of the glass powder in the testing solution, in which the sodium and the calcium ions from the glasses are released. The ions are released via ion exchange with the protons (H^+ /H_3O^+) in the testing solution, which will lead to the formation of the Si-OH group. This group acts as a nucleation site for the formation of the crystalline apatite (Li et al., 1994, Oliveira et al., 2002, Mami et al., 2008). Moreover, the sharpening of the band at 1033 cm^{-1} and the

appearance of Si-O-Si band at 790 cm^{-1} are also assigned to the development of this silica gel layer and the precipitation of the apatite crystals (Hench, 1991, Jones et al., 2001, Brauer et al., 2010). Therefore, from this step it can be indicated that all the investigated glasses have the ability to dissolve rapidly in this solution enabling the early formation of apatite.

Accompanied with the previous changes, the tetrahedral PO_4^{-3} or the P-O bending band at the region between 550 cm^{-1} and 600 cm^{-1} also showed marked changes after 3 h. This band demonstrates a minute split at the beginning of the immersion time and then the intensity of this split band increases with time. This indicates either the replacement of the ACP layer by a crystalline apatite phase or the formation of nano-sized apatite crystals on the surface (Fowler, 1974, Kim et al., 1989, Brauer et al., 2010, Mneimne et al., 2011, Chen et al., 2014a). Moreover, the high intensity of both P-O bending and P-O stretching bands suggests the further formation or the growth of the apatite crystals on the surface of the glass powder.

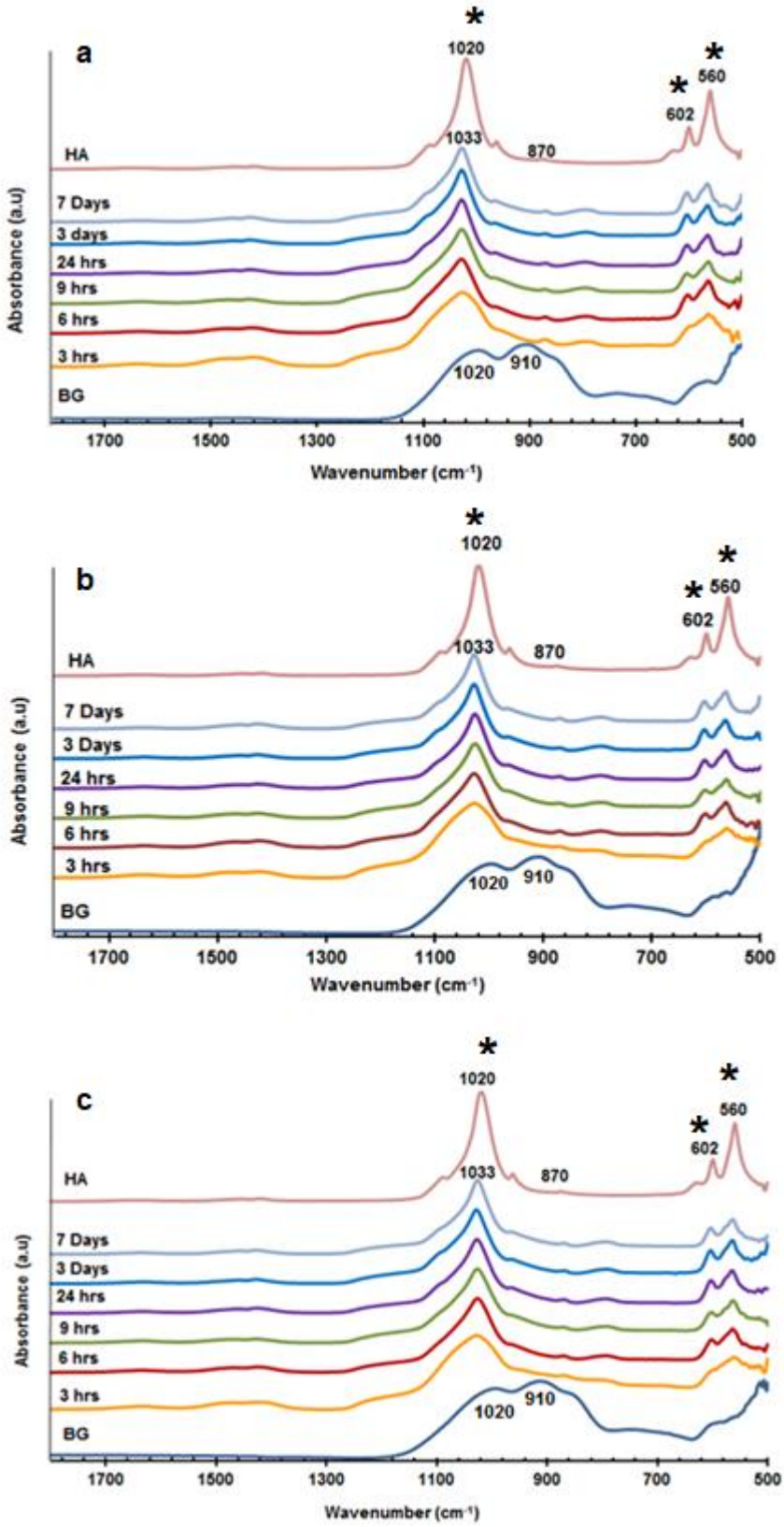

Figure 5.1: FTIR spectra of a) QMFA1 b) QMFA2 c) QMFA3 before immersion (bottom) and after immersion in Tris buffer up to 7 days. The spectra are compared to the spectrum of the HAP reference (top) and the apatite is marked by an asterisk.

5.1.2 XRD results:

The XRD patterns of the glasses immersed in Tris buffer demonstrate a narrowing and shifting of the amorphous halo with the appearance of a small diffraction peak at 26º (2θ) after 3 h immersion. After 6 h, another diffraction peak appears at 32º (2θ) in addition to the sharpening of the 26º (2θ) peak Figure (5.2 a, b, c). With longer times, these diffraction peaks become more pronounced and are assigned to a crystalline apatite, as these patterns are all matched the HAP (ICDD file number 01-074-0565) and FAP (ICDD file number 00-003-0736) reference patterns. However, from these illustrated patterns it can be seen that the peak at 32º (2θ) is broad and this represents the superimposition of three diffraction lines of (211), (112) and (300) at 31.8 º, 32.19º and 32.9º respectively. This feature was also shown in previous studies (Müller and Müller, 2006, Mneimne et al., 2011) and it was explained as the formation of disordered or nano-size crystals in the apatite structure (Manjubala et al., 2001, Brauer et al., 2010).

In addition to the above findings, it can also be seen that at the 3 h immersion time point, the intensity of the peaks in the low sodium containing glass QMFA3 is slightly higher than those in the other two glasses. This suggests the earlier dissolution of QMFA3 glass in Tris buffer, where the ions are released at a higher rate within this media as it will be discussed in section (5.1.4). This might be due to the slight crystallinity of the glass, which initiates the early formation of apatite or due to the presence of high calcium content, which provides more calcium to form apatite at a faster rate. Therefore; the peaks of the crystalline phase appeared earlier and with a distinct intensity in QMFA3 glass. However, at longer immersion periods, the intensity of the major crystalline peaks of apatite increases for all the glasses and at the same time additional minor diffraction peaks for apatite become more evident.

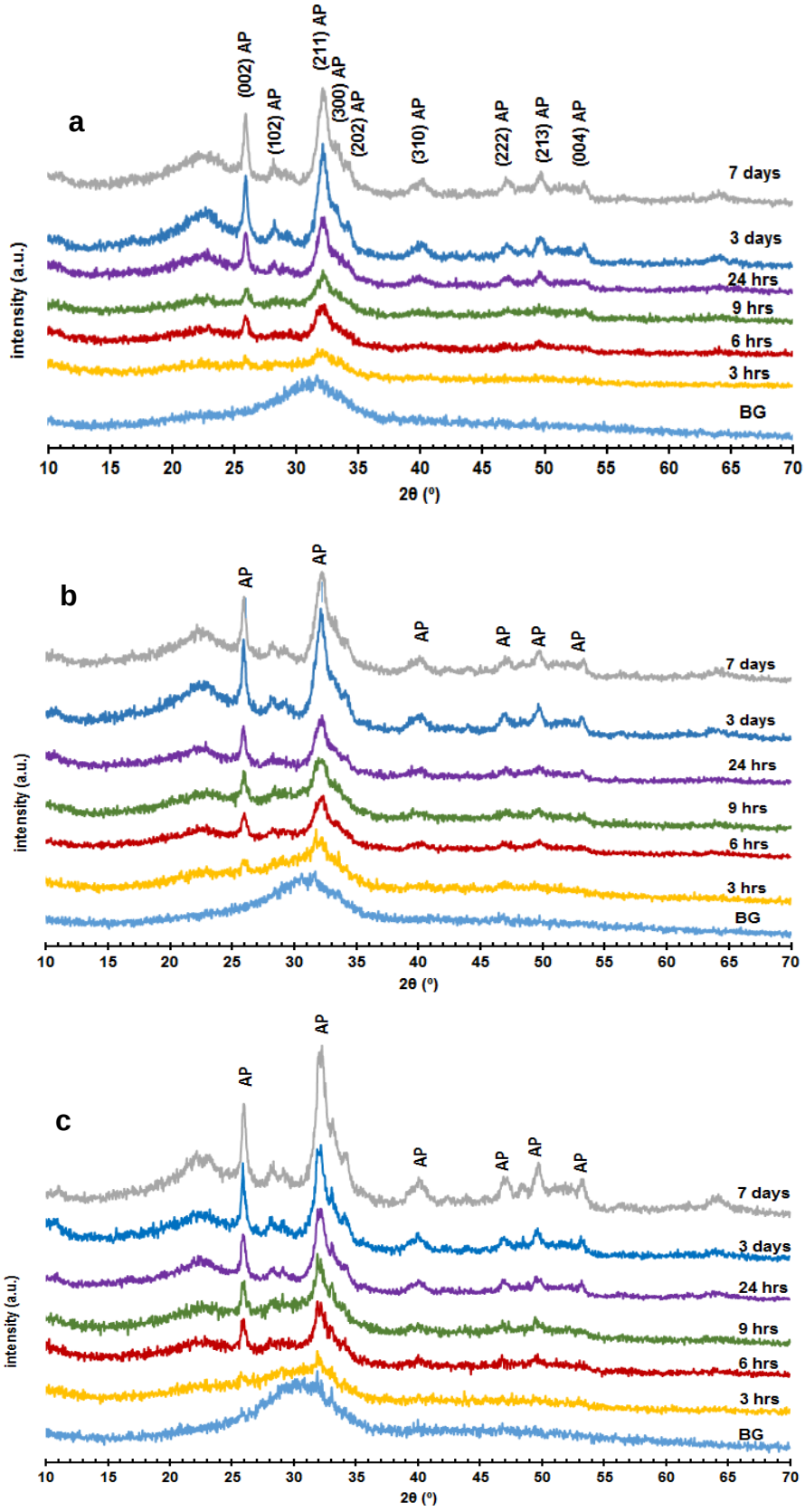

Figure 5.2: XRD patterns of a) QMFA1 b) QMFA2 c) QMFA3 before immersion (bottom) and after immersion in Tris buffer for 7days. (AP) refers to the apatite peaks.

From both FTIR and XRD results, it cannot be confirmed whether the apatite crystals formed on the surface of the glass powder in this study are HAP or FAP. This is due to the similarity between the both diffraction patterns and the FTIR spectra. Some authors report that there is a slight difference in the XRD pattern of the FAP and the HAP. The FAP pattern showed a shift in both (002) and (300) peaks in which the (002) was shifted toward the lower angle value while, the other toward the higher angle value (Manjubala et al., 2001). This suggested that these differences were represented the substitution of the F^- for the OH^- in the lattice. However in this study, this difference cannot detect by the XRD only. This is because of the formation of small nano-sized crystals, as well as the broadening of the peaks and this is in agreement with (Nikčević et al., 2004). Therefore, from the above reasons ^{19}F MAS-NMR was carried out.

5.1.3 ^{19}F MAS-NMR results:

^{19}F MAS-NMR is a sensitive technique used to confirm the formation of the fluoride-substituted apatite by the detection of FAP in different phases, such as, amorphous, crystalline and adsorbed phase (Yesinowski and Mobley, 1983). From Figure (5.3), it can be seen that there is a dominant peak at -102 ppm for all the glasses after their immersion in Tris buffer for 7 days. This peak represents the coordination of the F^- with three calcium cations, F-Ca (3). Therefore, it indicates the presence of the fluoride in the apatite structure and confirms the formation of FAP, as this peak corresponds to the channel fluoride ions which are assigned to the FAP structure (Mason et al., 2009, Mneimne et al., 2011, Yi et al., 2013).

The investigated glasses contain CaF_2 in their composition and this gives a high possibility for the formation of FAP. The incorporation of the fluoride can be performed by the release of the fluoride ion via its exchange with other ions in the solution. This exchange can lead to the contribution of the fluoride in the apatite formation (Yesinowski and Mobley, 1983).

The detected peak is broad and asymmetric in nature; there is a shoulder at around -88 ppm to -90 ppm. This shoulder is also seen in the SBF samples and it contributes about 8% of the fluorine content. This peak corresponds to a second fluoride environment in the apatite structure (Wang et al., 2009). The -88 ppm signal only appeared in carbonate rich apatite structures and it corresponds with a B-type carbonate substitution (Mason et al., 2009) . The F^- ion will occupy the vacant space of the oxygen site when the CO_3^{2-} replaces the PO_4^{3-} in the apatite structure (GH and Lehr, 1969, Reigner et al., 1994, Yi et al., 2013).

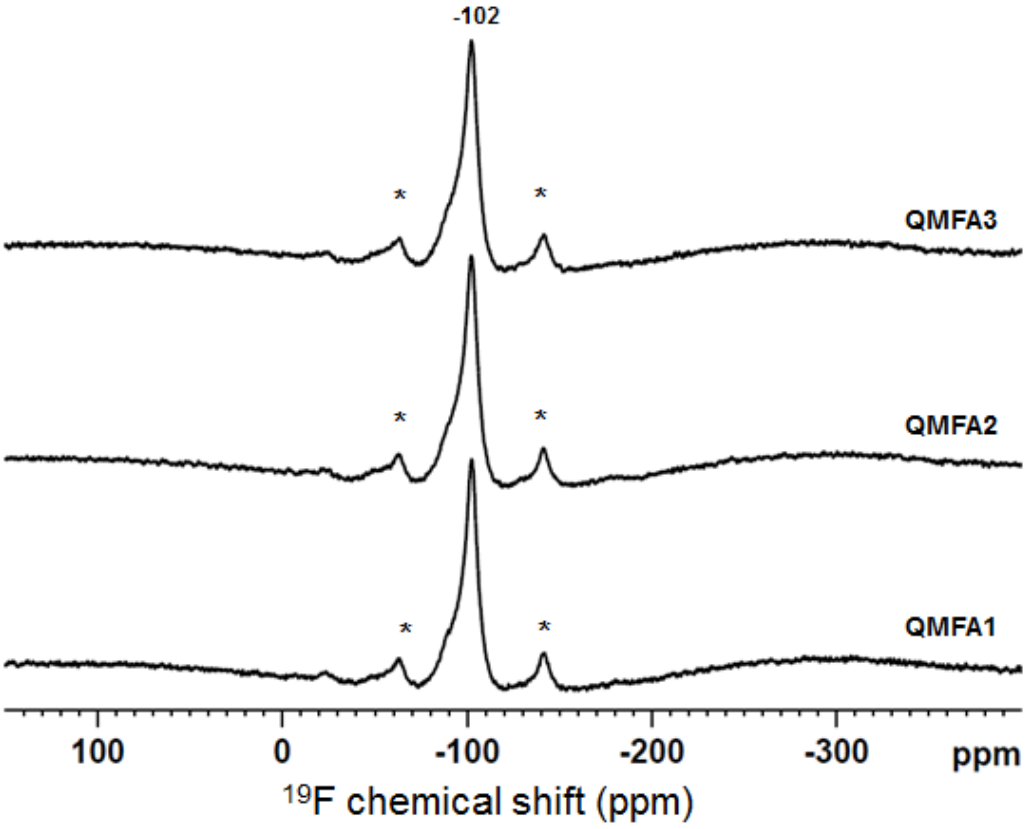

Figure 5.3: ^{19}F MAS-NMR spectra of QMFA1, QMFA2 and QMFA3 glasses after 7 days immersion in Tris buffer. The main resonance at -102 ppm corresponds to the fluoride in the apatite structure (FAP) and the shoulder at -88 ppm corresponds to the presence of carbonate in the apatite structure. Spinning side bands are marked by an asterisk.

5.1.4 pH changes and ion release in Tris buffer:

It is known from the literature that all the soda-lime bioactive glasses cause a rise in the pH of the solutions in which the glasses are immersed. This pH rise is important in the process of apatite formation however; sometimes the high alkalinity may bring some adverse effect on the surrounding tissues (Aina et al., 2009).

Figure (5.4) illustrates the pH changes in the Tris buffer with the immersion time. For all glasses, it can be observed that the pH of the Tris buffer rises gradually with time and this rise starts from the initial value 7.4±0.02 reaching a maximum 7.9±0.03 after 24 h. Then during the remaining period of the glass immersion, the pH remains approximately constant. The initial increase in the solution's pH during the first 24 h immersion can be explained by the ion exchange process that occurs on the surface of the glasses. The Na^+ and Ca^{2+} ions in the glass are exchanged with the H^+ from the solution leading to a clear increase in the pH of the testing solution (Lusvardi et al., 2009, Mneimne et al., 2011). It is also observed that, the level of the pH rise is slightly higher in the glass with higher sodium content in comparison to the other glasses. This might be due to the presence of the larger number of monovalent cations that weaken the crosslinking bonds with the network formers (Wallace et al., 1999). Thus, this leads to more H^+ ions from the solution being replaced by Na^+ cations from the glass surface. This might result in an increase in the hydroxyl group concentration in the solution and subsequent rise in its pH level.

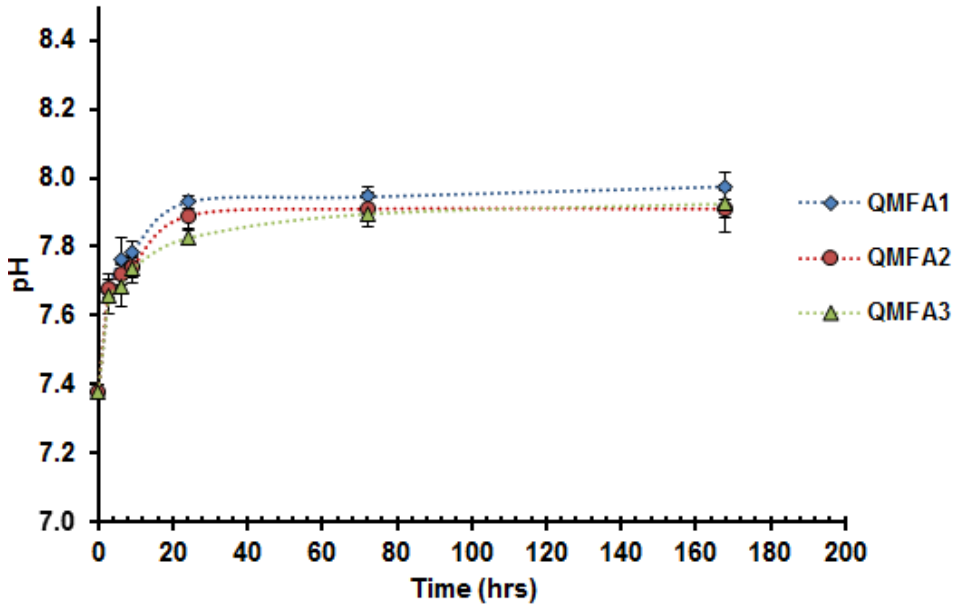

Figure 5.4: Graph shows the pH changes of Tris buffer after the immersion of the glasses for 7 days (Lines are drawn as visual guides).

However, the pH rise in Tris buffer is not exceeding a value of 8 and this is because of the actions of other ions in this solution; such as, the release of the fluoride ions from the glasses. As can be seen in Figure (5.5) that, the fluoride concentration in the Tris buffer increases rapidly within the first 6 hr of glass immersion reaching to 10.3±0.02 ppm, 8.7±0.02 ppm and 7.7±0.03 ppm for QMFA1, QMFA2 and QMFA3 respectively. The fluoride release from the glasses is consequently compensated with the hydroxyl group of the solution resulting in a less pronounced rise in the pH. At longer immersion times, the fluoride concentration reduces suggesting the consumption of the fluoride ion in the formation of the FAP (Mneimne et al., 2011). Therefore, besides the action of the fluoride in lowering the pH rise of the solution, it contributes to the formation of FAP.

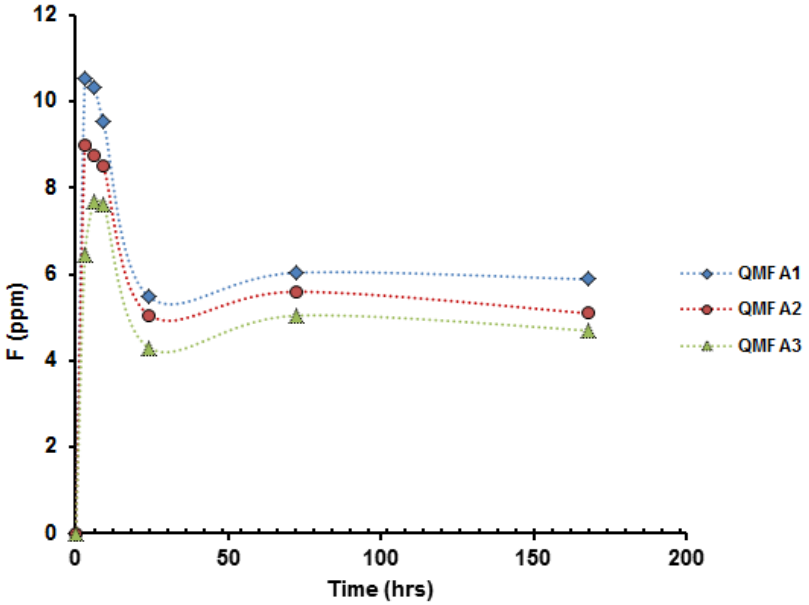

Figure 5.5: Elemental concentrations of (F) in Tris buffer after the immersion of the glasses for 7 days (Lines are drawn as visual guides). The error bars are smaller than the point size.

Calcium concentrations also showed a considerable increase within the first 6 h reaching 134±1.7 ppm, 165.7±2.5 ppm and 192.3±1.4 ppm in QMFA1, QMFA2 and QMFA3 respectively, as shown in Figure (5.6). This increase is consistent with the increase in the pH of the solution. This indicates that the glass is degraded in the solution and the released Ca^{2+} is taking part in the ion exchange process. However, the release of the Ca^{2+} from the QMFA3 glass is slightly higher than that from the other two glasses and this is due to the substitution of the Na^{+} with the Ca^{2+}. These findings are consistent with results of the XRD patterns regarding the apatite formation. Therefore, it can be indicated that during the first period of immersion, there is a consumption of calcium ions for the formation of apatite. With the immersion time, the concentration of Ca^{2+} reaches a constant level and this level is above the baseline. This suggests the presence of an excess calcium content in the compositions of the glasses which is not taking part in the apatite formation process.

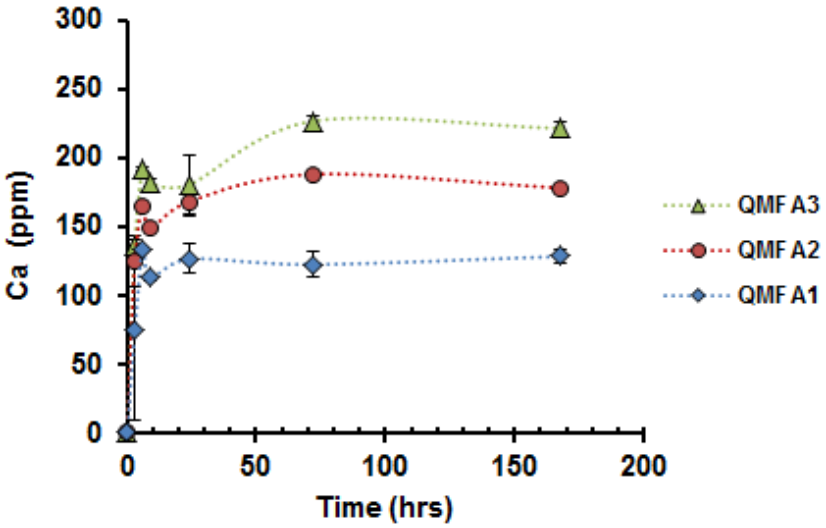

Figure 5.6: Elemental concentrations ± SD of (Ca) in Tris buffer after the immersion of the glasses for 7 days (Lines are drawn as visual guides).

Phosphorus, on the other hand, shows an evident high release within the first 6 h of glasses immersion and after that it sharply drops as in Figure (5.7). This might indicate the consumption of phosphate from the glass compositions in the precipitation of the apatite crystals. Therefore, the amount of phosphate was considered as a critical factor in the formation of apatite as suggested by (Mneimne et al., 2011).

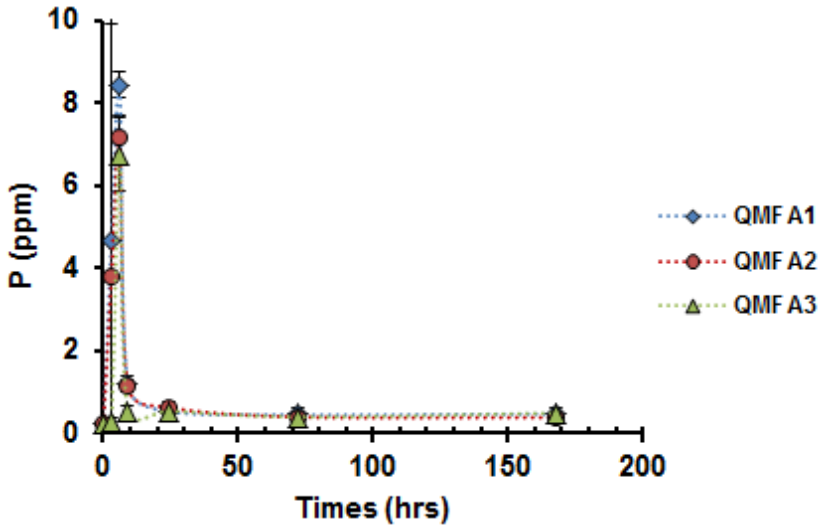

Figure 5.7: Elemental concentrations ± SD of (P) in Tris buffer after the immersion of the glasses for 7 days (Lines are drawn as visual guides).

The silicon concentration as a function of immersion time for all the prepared glasses is shown in Figure (5.8). In the previous study by (Brauer et al., 2010), it was reported that the silicon has a solubility limit which is about 60 ppm. In case of the glass dissolution, if the silicon concentration in the tested solution reached that limit, there will be a drop in the phosphate concentration. This drop indicates the formation of apatite phase and related to the formation of the silica- gel layer. In this study, the silicon concentration reaches the solubility limit at the 9 h immersion for all the glasses.

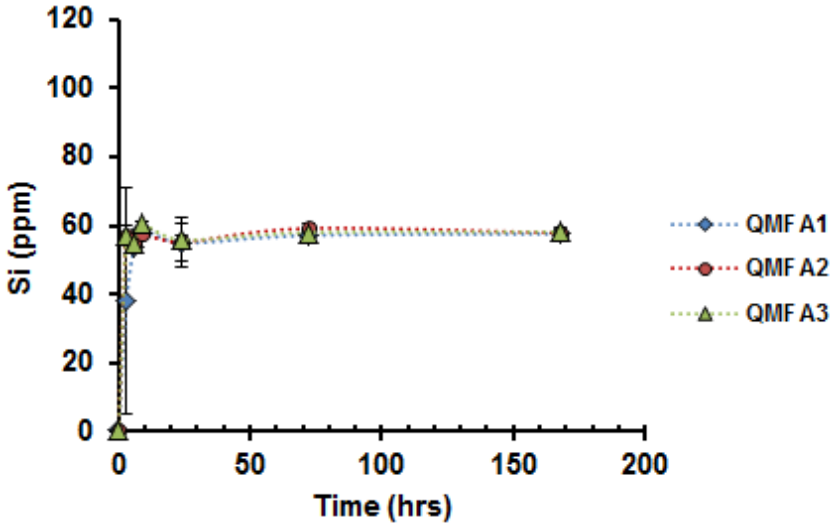

Figure 5.8: Elemental concentrations ± SD of (Si) in Tris buffer after the immersion of the glasses for 7 days (Lines are drawn as visual guides).

All of the above findings are consistent with the findings from the FTIR and XRD. The rise in the solution's pH is accompanied with the increase in the concentrations of the calcium, phosphate, fluoride and silicate ions during the first hours of the glass immersion correspond with the disappearance of the NBO bands in the FTIR spectra. Also, at the same time there are narrowing of the amorphous halo signal and appearance of the apatite diffraction peaks in the XRD patterns. Therefore, it can be confirmed that all the investigated glasses dissolve in Tris buffer and release all their ions. At longer immersion time, there is a clear stability in the pH

accompanied with the stability in the calcium, fluoride ions and silicon species level. However, the concentration of the phosphate ion shows a sharp reduction in its level. All these features match with the prominence and the splitting of the P-O bands in the FTIR spectra and the sharpness of the apatite peaks at 26º and 32º (2θ) in the XRD patterns. Thus, the second findings confirm the participation of the ions in the precipitation and the formation of the crystalline apatite layer on the surface of the glass powder. The formation of the FAP phase was demonstrated by the ^{19}F MAS-NMR.

5.1.5 SEM results:

Figure (5.9 a and b) shows the SEM micrographs of QMFA1 glass powder at different magnifications after soaking in Tris buffer for 7 days. A needle-like apatite structure is seen on the surface of the glass powder. This needle structure is compacted as flowers with small and highly numerous crystals. The same features are also detected when the glasses are immersed in SBF. The presence of fluoride ions in the soaking solution has a considerable effect on the configuration of the crystal structure. If the fluoride was added to the SBF solution this gives rise to a needle-like apatite structure (Li et al., 1993). Moreover, the addition of the fluoride in the bioactive glass composition can result in the formation of FAP species directly without forming the octacalcium phosphate (OCP) as a first precursor phase in the process of apatite formation (Shah et al., 2014).

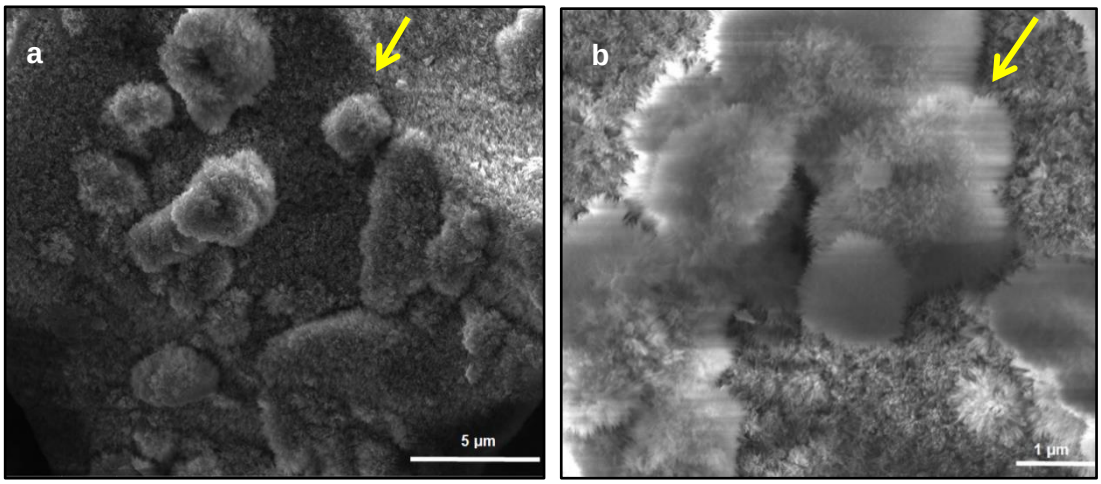

Figure 5.9: SEM micrographs of QMFA1 glass powder after immersion in Tris buffer for 7 days a) at 12000x magnification b) at 24000x magnification. The arrow points to the needle-like apatite structure, which consists of a flower like arrangement with small and highly numerous crystals on the surface of the glass powder.

5.2 Immersion of the glass powders in SBF

5.2.1 FTIR results:

Figure (5.10 a, b, c) shows the FTIR absorbance spectra of the untreated and treated glasses for 3, 6, 9, 24 h, 3 and 7 days. Generally, the dissolution features of the glasses immersed in SBF are similar to that of the glasses soaked in Tris buffer. However, the rate of the degradation process of the glass powders in the former solution is considerably slower than that in the latter solution.

The NBO Si-O^- alkali band at 910 cm^{-1} displays gradual disappearance within the first 9 h of soaking time until it totally disappears at 24 h. At the same time, the phosphate band at 1033 cm^{-1} shows a progressive increase in its intensity with the longer immersion time. The first finding is suggested to be related to the depletion of the silica gel layer for the formation of the apatite crystals at the 24 hr time point, therefore; the band is completely disappeared at that time point.

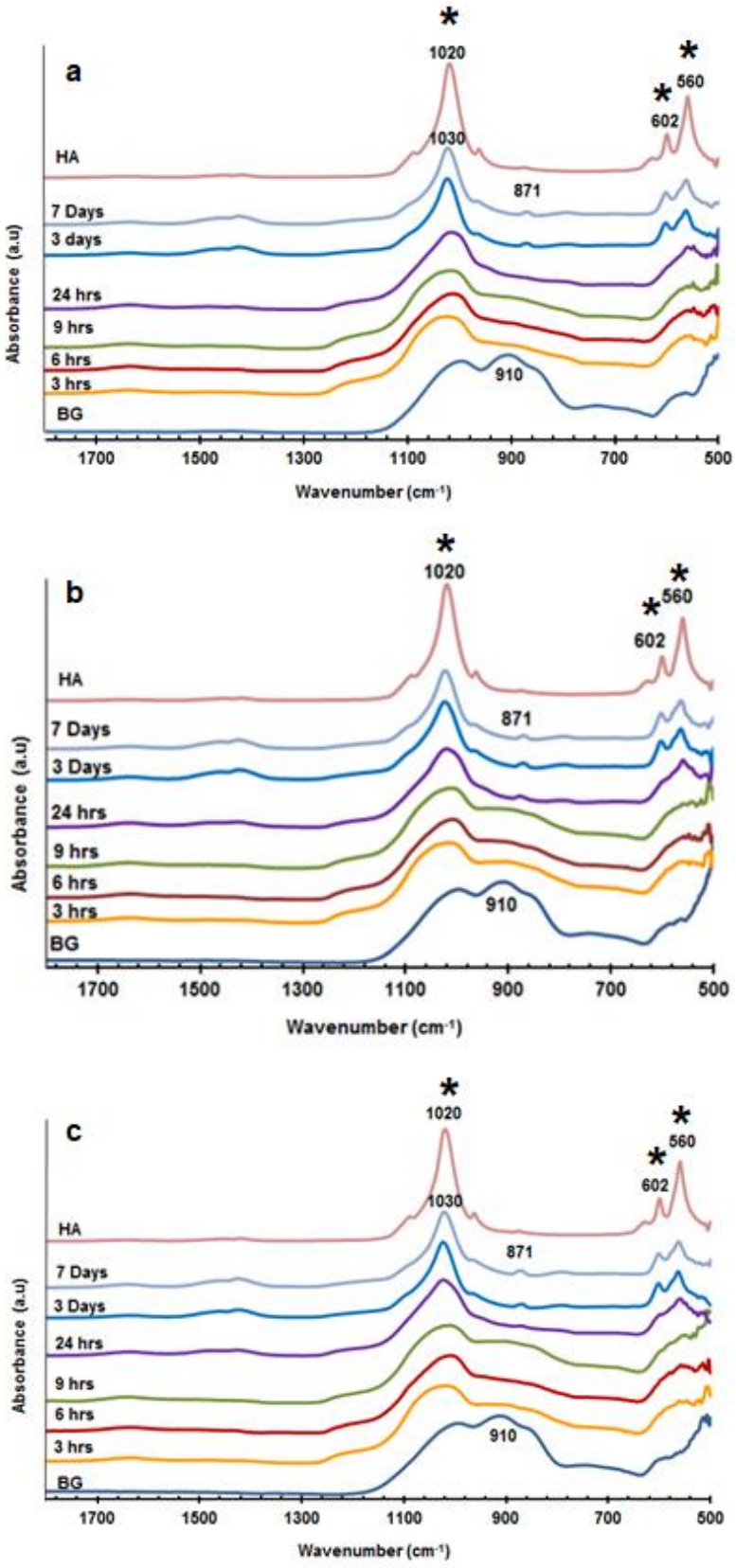

Figure 5.10: FTIR spectra of a) QMFA1 b) QMFA2 c) QMFA3 before immersion (bottom) and after immersion in SBF solution up to 7 days. The spectra are compared to the spectrum of the HAP reference (top) and the apatite is marked by an asterisk.

On the other hand, the sharpening of the other band corresponds to the precipitation and the crystallisation of the Ca-P layer (Mami et al., 2008). Moreover, the P-O bending vibration band at the region between 560 cm^{-1} and 602 cm^{-1} appears as a single broad peak during the first 9 h immersion, which indicates the existence of ACP or nano-sized crystals. Subsequently, this band starts to split into two peaks and become more evident after 24 h. This split indicates the growth of the apatite crystals on the glass surface (Karlsson et al., 1989). Some authors stated that the split of this peak is typical for the existence of the orthophosphate lattice and not the HAP phase (Maçon et al., 2015).

In addition to the previous findings, there is also another interesting feature in the FTIR spectra of the glasses immersed in SBF, which is the presence of the carbonate group. However, this feature is less pronounced in this solution in comparison to the cell culture media as SBF has much lower carbonate content than the α-MEM media. Therefore, it can be seen from the spectra that there is an existence of two carbonate bands. The C-O bending and C-O stretching bands at around 870 cm^{-1}, 1426 cm^{-1} and 1457 cm^{-1} respectively (Mami et al., 2008, Maçon et al., 2015). These bands are assigned to the existence of the B-type carbonated apatite as the orthophosphate is substituted by carbonate.

From the above results, it can be concluded that the investigated glasses slowly dissolve in the SBF solution and form apatite crystals at a slower rate than in Tris buffer. The suggested reason for this phenomenon is related to the existence of the magnesium ions in SBF. This ion exhibits a retardation effect on the process of apatite layer formation. This occurs by blocking of the active sites on the surface of the crystals preventing the further growth of the apatite crystals (Hench and Wilson, 1993, Filgueiras et al., 1993a, Diba et al., 2012). The retardation effect of the Mg^{2+} ion can lead to the formation of a poorly crystalline Ca-P layer as reported by (Habibovic et al., 2002).

5.2.2 XRD results:

Figure (5.11 a, b, c) shows the XRD patterns of the three glass powders before and after their immersion in SBF solution for 7 days. Generally, it can be seen that there is no appearance of any diffraction peaks during the first 9 h of immersion. However, there is a slight shift in the amorphous halo position toward higher (2θ) accompanied with the appearance of a small hump at around 22º (2θ). This suggests the slow reaction of the glass powder in this solution and this finding is consistent with the FTIR results. After 24 h immersion, a small Bragg peak (002) is noticeable at 26º (2θ) besides the subsequent narrowing and shifting of the amorphous halo peak at 32º (2θ). These features indicate the formation of small nano-sized crystals of apatite on the surfaces of the glass powders (Mneimne et al., 2011). With time, the major Bragg peaks at 26º (2θ) and 32º (2θ) demonstrate a significant sharpening in their intensities in addition to the appearance of the other diffraction apatite peaks, which all indicate the subsequent growth of apatite crystals with time.

In addition to the above findings, it can also be seen that the rate of apatite formation is slightly higher in the low sodium contained glass. The shift of the amorphous halo peak and the sharpening of the (002) apatite peak are more prominent in QMFA3 glass in comparison to the other glasses. These features were also detected in Tris buffer results, although the features are more pronounced in SBF. This finding might be related to the presence of a higher calcium content in comparison to the others, which in turn reveals a noticeable enhancement in the precipitation of apatite crystals on the glass surfaces.

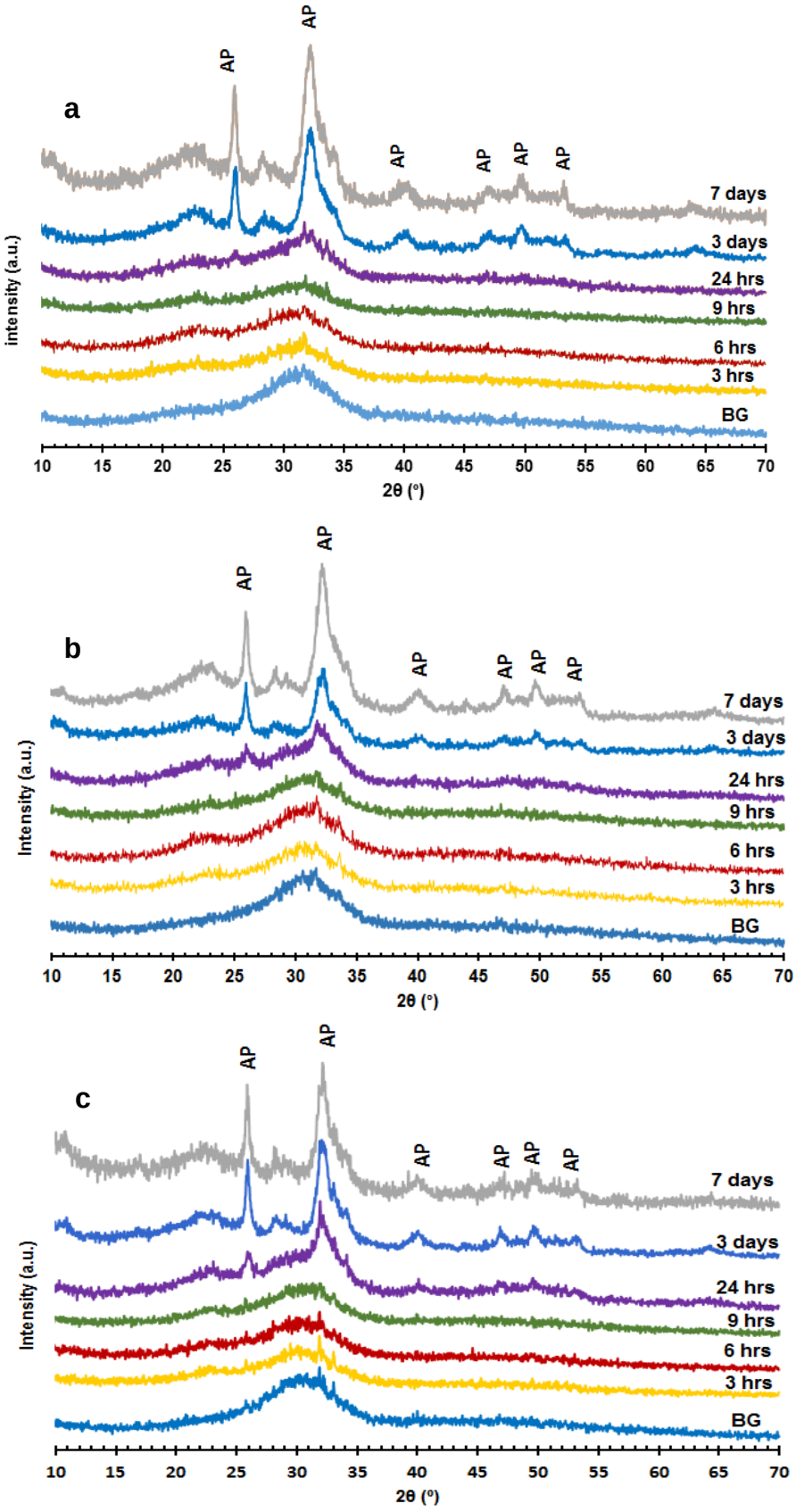

Figure 5.11: XRD patterns of a) QMFA1 b) QMFA2 c) QMFA3 before immersion (bottom) and after immersion in SBF for 7 days. (AP) refers to the apatite peaks.

The results of this study are in agreement with (Mneimne et al., 2011) study, in which it has been reported that the precipitation of apatite crystals was faster in the high calcium content glasses. Kokubo proposed that the nucleation and the apatite crystal growth are triggered by the interaction of the calcium cation of the glass with the H_3O^+ of the solution. This interaction could lead to the formation of the silica gel layer at a faster rate, which in turn accelerates the nucleation process of the apatite formation process (Rámila and Vallet-Regı, 2001).

Previous studies reported that the presence of a high sodium concentration in the glass composition had a noticeable effect on the solubility of the glass and they explained their results depending on the role of the sodium ion in the silica network. Sodium acts as a modifier in the glass network and it can cause a reduction in the crosslinking of the network and consequent rise in solution pH. Therefore, it accelerates the reaction of the glasses in the immersion solutions (Elgayar et al., 2005, Brauer et al., 2010). In contrast, this study showed that the high sodium glass has a slight deceleration in the dissolution rate in comparison to the others. The sharpening of the apatite peaks at 26º (2θ) and 32º (2θ) for QMFA1 is slightly lower than QMFA2 and the latter is lower than QMFA3 and this feature is only pronounced at 24 h immersion time point. However, after that period all the glasses show the same trend and intensity rise.

Besides the above results, there is another detected feature in the XRD patterns, which is the slow rate of apatite formation in SBF. This finding was also mentioned in the FTIR results. Although Tris buffer is ion free and the SBF is saturated with ions, the apatite peaks appeared earlier in Tris buffer. The results of the current study disagree with what has been stated by (Chen et al., 2014a), in which the SBF supported the apatite precipitation. Therefore, it can be concluded that the glasses with high phosphate and calcium contents in their compositions can form apatite earlier in the SBF. However, the rate of apatite detection is slower in SBF in

comparison to Tris buffer. The apatite is formed at 24 h immersion in SBF while, in Tris the apatite was detected at 3 h immersion. The reason for this might to be related to the presence of Mg^{2+} in the SBF , which was reported to have a retardation effect on apatite formation (Brauer, 2015). Thus, despite from the presence of calcium and phosphate ions in the SBF, the apatite features were more obvious in Tris buffer.

5.2.3 ^{19}F MAS-NMR results:

The ^{19}F NMR spectra of the glasses immersed in SBF for 7 days are presented in Figure (5.12). The spectra show a distinct chemical shift at the position ~ -102 ppm which is close to the FAP apatite peak position. The slight deviations in the positon is suggested to be due to the substitution of some ions with other ions from the glass structure, such as, the substitution of the fluoride with the hydroxyl group and the carbonate with the phosphate group (Hill et al., 2015). Besides the chemical shift, the fluorine signal is prominent and asymmetric in nature and there is a shoulder at around -88 to -90 ppm. This shoulder also appeared in the ^{19}F NMR spectra of the glasses immersed in Tris buffer. This indicates the existence of the carbonate type B substitution as reported by (Mason et al., 2009, Yi et al., 2013). However (Chen et al., 2014b) stated that this signal represents the presence of different fluoride species in the residual glass. Moreover, (Brauer et al., 2010) reported that the appearance of a single peak at the position of -89 is related to the presence of the F-Ca (n) group in the glass network.

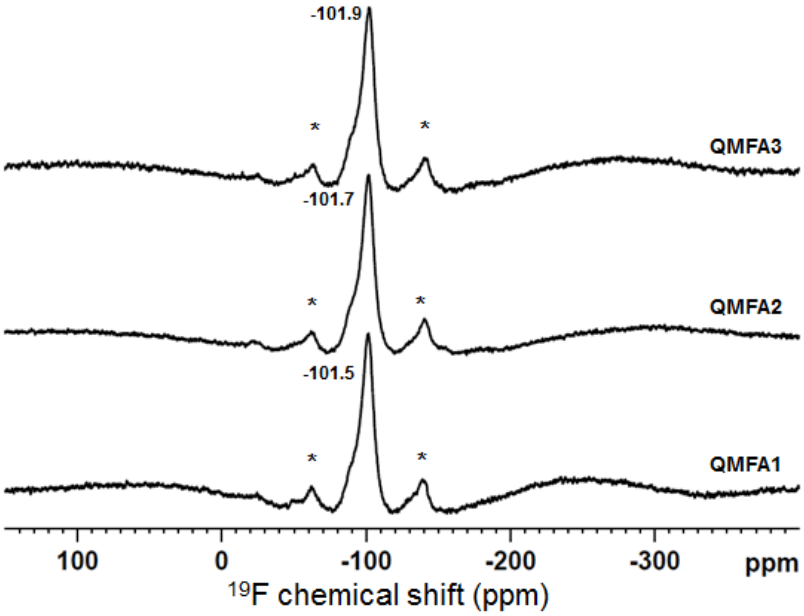

Figure 5.12:^{19}F MAS-NMR spectra of QMFA1, QMFA2 and QMFA3 glasses after 7 days immersion in SBF. The main resonance at about -102 ppm is corresponds to the fluoride in the apatite structure (FAP) with minor ion substitution. Spinning side bands are marked by an asterisk.

5.2.4 pH changes and ion release in SBF:

All the bioactive glasses show a pH rise during their immersion in SBF from about 7.4±0.02, which is the initial pH of the solution, to about 7.8±0.03 at 24 h. The pH continues to increase slightly to about 7.9±0.03 at day 3 and stays constant for the remaining time of the experiment Figure (5.13). This pH rise trend is nearly similar to that in Tris buffer however; the level of the rise is slightly higher in SBF than Tris buffer. This may be due to the buffering action of the Tris buffer. It was reported that the pH rise depends on several factors; one of them is the buffering capacity of the testing solution. Therefore, the pH rise in Tris is less pronounced than that in SBF (Mneimne et al., 2011). Interestingly, it can also be seen that the pH level of the solution is not decreasing at longer times instead; it stays constant at a high value of about 7.9±0.03. This might be related to the cation content in the composition of the original glasses (Maçon et al., 2015).

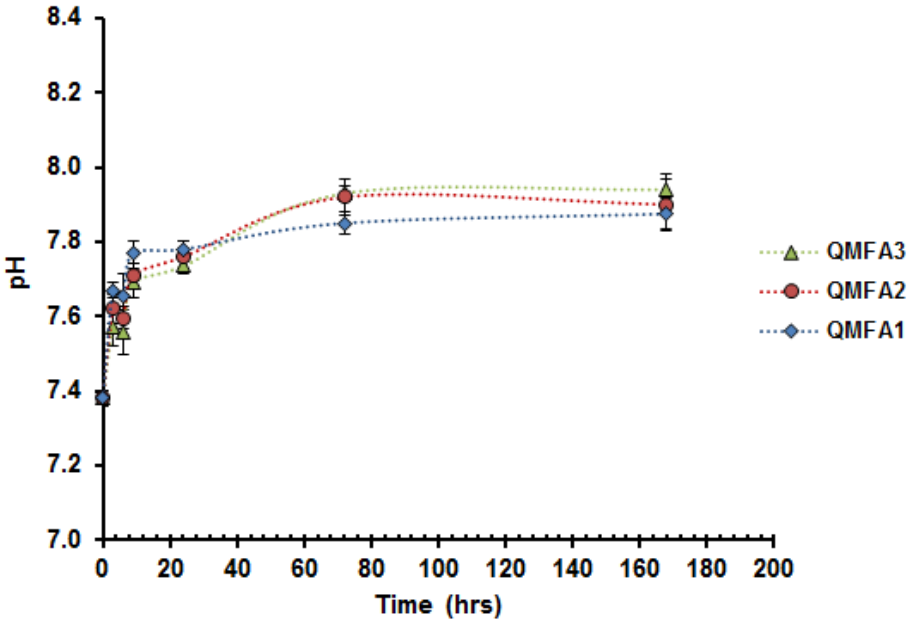

Figure 5.13: Graph shows the pH changes of SBF after the immersion of the glasses for 7 days (Lines are drawn as visual guides).

In a previous study by (Lu and Leng, 2005), it was stated that the rate of apatite nucleation and formation was highly depended on the value of the pH rise. However, the presence of ions in the testing solution might also have an effect on the rate of apatite formation. As SBF solution has Ca^{2+} and PO_4^{3-} ions and their concentrations are nearly similar to that in human body plasma. Therefore, the release of Ca^{2+} is started form a baseline value of 141 ppm unlike Tris buffer where the release starts from 0 ppm. Moreover, the release profile of the Ca^{2+} in SBF involves both the calcium from the solution and the calcium from the glass composition. Thus, the concentration of the calcium release in SBF is appeared higher than that in Tris. Also, from the above finding it can be suggested that the higher calcium release form the glass can cause higher rise in the pH. Figure (5.14) shows the calcium release profile in SBF for 7 days. There is a general rise in the Ca^{2+} concentration during the period of glasses immersion reaching the maximum of 236.5±4.3, 313±0.8 and 402±32.3 ppm in QMFA1, QMFA2 and QMFA3 respectively at day 3. Then, these concentrations demonstrate a slight decrease at day 7. However at 9 h

immersion time, there is a slight drop in the calcium level and this indicates the consumption of the calcium for the precipitation of the Ca-P layer (Sepulveda et al., 2002).

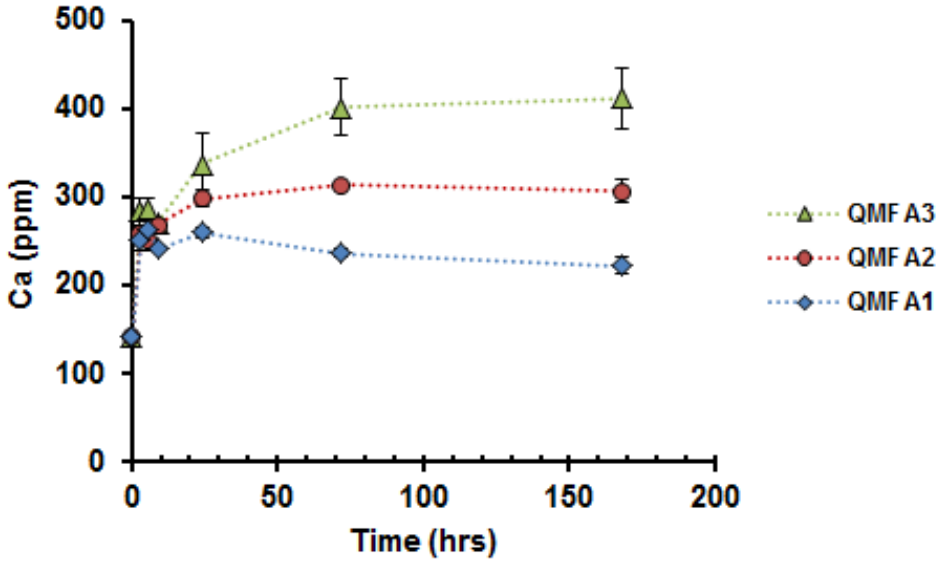

Figure 5.14: Elemental concentrations ± SD of (Ca) in SBF after the immersion of the glasses for 7 days (Lines are drawn as visual guides).

At the same time period, the phosphorus concentrations of all the reacted glasses show an overall continuous decrease in their values with immersion time in SBF as in Figure (5.15). This decrease might indicate the uptake of the phosphorus ion from the solution for the precipitation of the apatite layer on the surface of the glass powders (Maçon et al., 2015). Interestingly, from the above finding, it can be seen that there is a clear difference in the trend of phosphorus release in Tris buffer and SBF. This is suggested to be due to the deficiency of the ions in Tris buffer, where the ions are entirely derived from the glasses and not from the media. However this difference is clearly detected between the two solutions, the rate of apatite formation is faster in Tris than in SBF as described previously by FTIR and XRD techniques.

This delay might again be related to the presence of the Mg^{2+} in the SBF (Hench and Wilson, 1993, Brauer, 2015).

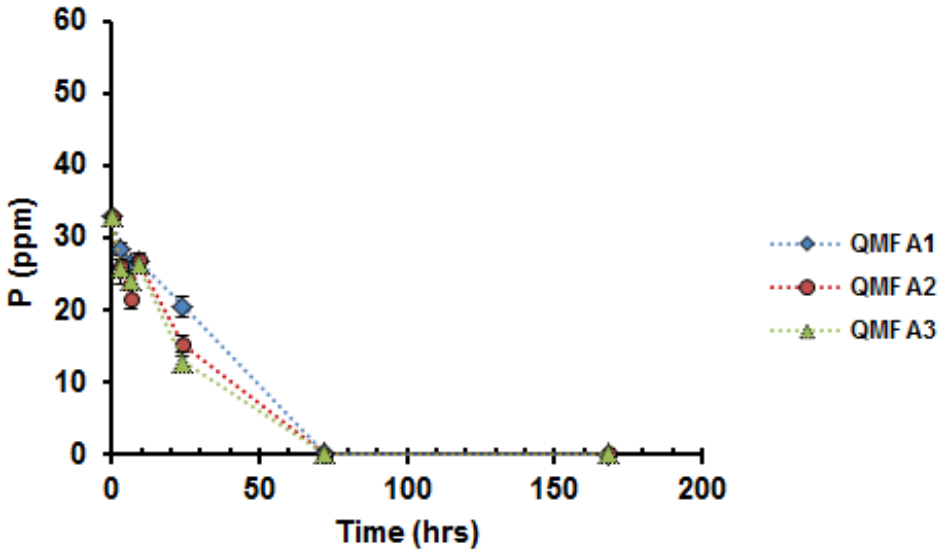

Figure 5.15: Elemental concentrations ± SD of (P) in SBF after the immersion of the glasses for 7 days (Lines are drawn as visual guides).

Furthermore, the profile of phosphorus release in SBF is similar for all the reacted glasses unlike the Ca^{2+} release. This is due to the presence of the same phosphate content in their compositions. While, the calcium content in the QMFA3 glass is relatively higher than that in the other glasses. Therefore, the trends of the ions release are different for both ions.

The depletion in the phosphorus concentration with the longer immersion time suggests the formation of the Ca-P layer on the surface of the glasses. This layer promotes the nucleation process of the apatite and leads to the consumption of the phosphate from both the glasses and the solution to form the crystalline apatite. This finding is consistent with the findings from the Si concentrations in SBF Figure (5.16). During the soaking time, the silicon concentration in all glasses increases

continuously and it reaches the solubility limit at 24 h immersion. Therefore, the formation of the silica gel layer is clearly detected after that time period.

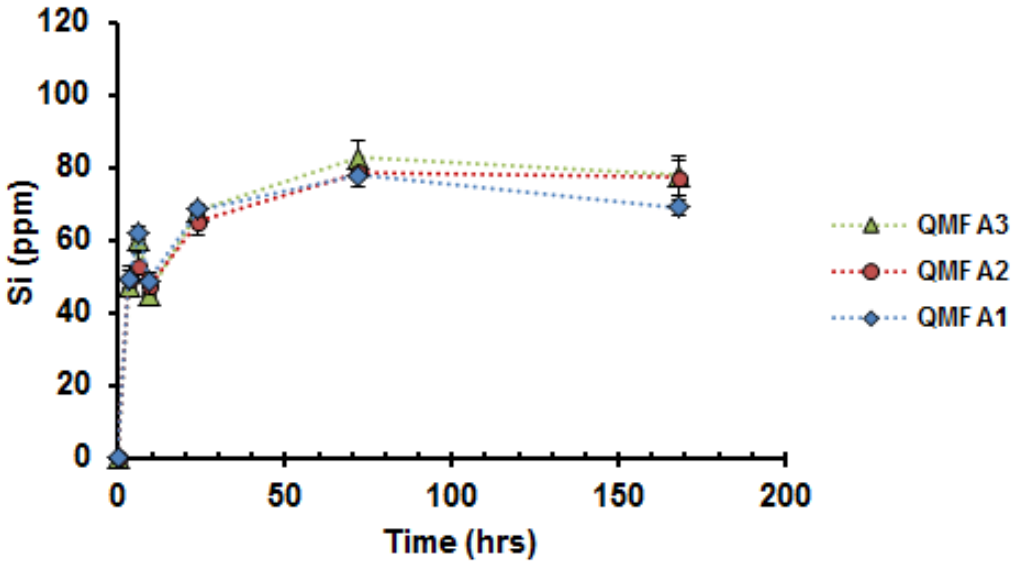

Figure 5.16: Elemental concentrations ± SD of (Si) in SBF after the immersion of the glasses for 7 days (Lines are drawn as visual guides).

Regarding the fluoride release in SBF, the same trend is clearly seen in this solution as that in Tris buffer Figure (5.17). However, the concentration of the F^- ions is much lower in the SBF solution where, the concentrations reach to the maximum of 8.3±0.03, 7.3±0.05 and 6.2±0.02 ppm for QMFA1, QMFA2 and QMFA3 respectively after 9 h. While in Tris buffer, the concentrations reach to 1.5 ppm more than that in SBF and for the same time period. Moreover, in SBF there is a continuous reduction in the fluoride concentration after 9 h immersion unlike the fluoride profile in Tris, where there is a slight increase after the dipping point. This feature might be related to the presence of other ions in SBF, which could take part in the ion exchange process and slow down the action of the fluoride ion in the formation of apatite.

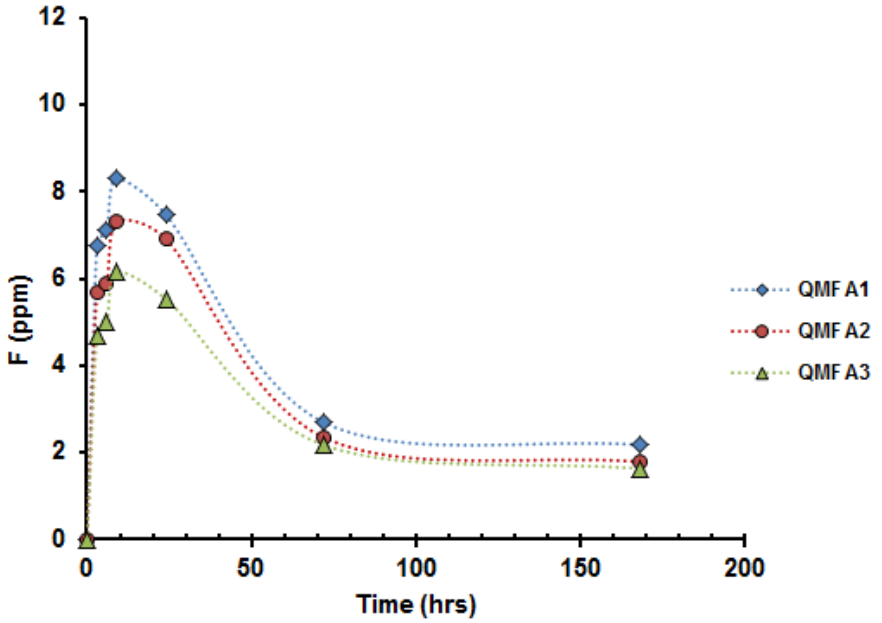

Figure 5.17: Elemental concentrations of (F) in SBF after the immersion of the glasses for 7 days (Lines are drawn as visual guides). The error bars are smaller than the point size.

5.2.5 SEM results:

SEM observation shows clear changes in the surface morphology of the QMFA1 glass after immersion in SBF for 7 days. In Figure (5.18 a and b), the micrographs show the formation of needle-like apatite structure on the surface of the glass powder. The crystals are small and numerous in natures. Thus, it can be concluded that the FAP species are successfully formed on the glass surfaces when they immersed in SBF. This is because of the high weight % of the Ca, P and F ions which are deposited on the surface of the glass particles as detected by the EDX Table (5.1). However, the characteristic FAP flower configuration is less obvious in SBF than in Tris buffer. This might be due to the slow rate of glass degradation and the late formation of the apatite phase in this solution. Consequently, there might be a large chance for the apatite crystals to grow enormously and become more oriented in Tris buffer in comparison to SBF, as the former showed apatite precipitation within the first 3 h immersion.

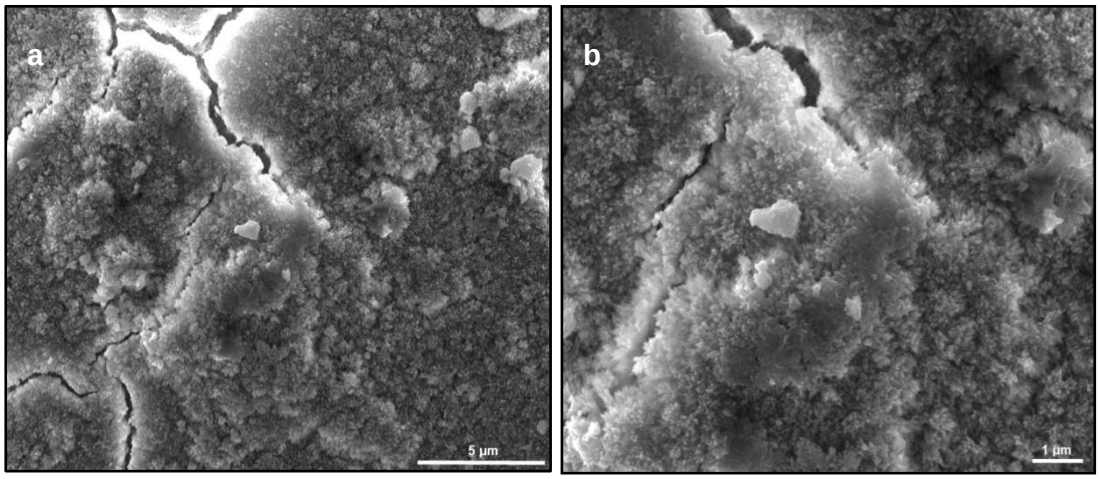

Figure 5.18: SEM micrographs of QMFA1 glass powder after immersion in SBF for 7 days a) at 12000x magnification b) at 24000x magnification. The needle-like apatite crystals are spread on the entire surface of the glass powder.

Table 5.1: SEM/EDX analysis of QMFA1 powder before and after its immersion in Tris buffer, SBF, SFα-MEM and Sα-MEM testing solutions for 7 days and 1 month. All the concentrations are in weight %.

Solution media	C	O	F	Na	Mg	Si	P	Ca	Cl	S
Original glass QMFA1	0.0	41.4	4.4	14.9	0.0	15.7	5.6	18	0.0	0.0
Tris buffer (7 Days)	5.2	45.2	6.3	0.0	0.0	11.9	9.6	21.5	0.3	0.0
SBF (7 Days)	0.0	38.0	4.5	0.9	0.6	11.9	13.3	29.4	1.1	0.3
SFα-MEM (7 days)	8.5	29.0	1.0	2.7	0.3	18.4	10.2	30.0	0.0	0.0
SFα-MEM (1 month)	14.1	42.4	0.7	0.0	0.6	0.2	1.2	40.7	0.0	0.0
Sα-MEM (7 days)	2.4	37.6	3.7	4.0	0.2	19.8	7.7	24.5	0.0	0.0
Sα-MEM (1 month)	4.8	31.7	1.9	3.4	0.4	17.8	10.6	29.5	0.0	0.0

5.3 Immersion of the glass powders in SFα-MEM media

5.3.1 FTIR results:

The use of SBF as an *in vitro* media to predict the *in vivo* bioactivity of the materials is controversial. The soaking of the glass powder in SBF might give false negative and false positive results (Bohner and Lemaitre, 2009). Previous studies reported that the structure of the apatite formed in SBF is different in its composition to that formed in the human body tissue and this is due to the lower carbonate content of the SBF (Kim et al., 1999, Kim et al., 2001). Thus for these reasons, cell culture medium was used. The FTIR absorbance spectra of the glasses immersed in a SFα-MEM medium show several changes within the two months immersion period, as seen in Figure (5.19 a, b, c). These changes are relatively similar to that in Tris buffer and SBF solutions however, the period of the glass degradation and Ca-P crystallisation are distinctly delayed in this media.

The complete disappearance of the NBO band is detected after 14 days immersion time. The P-O stretch peak at 1035 cm^{-1} starts a gradual increase in its intensity from day 3 and continues within the rest period of the experiment. At day 14, the single P-O bending vibration band is splits into two peaks at the 560cm^{-1} and 602cm^{-1} region, indicating the formation of the crystalline apatite.

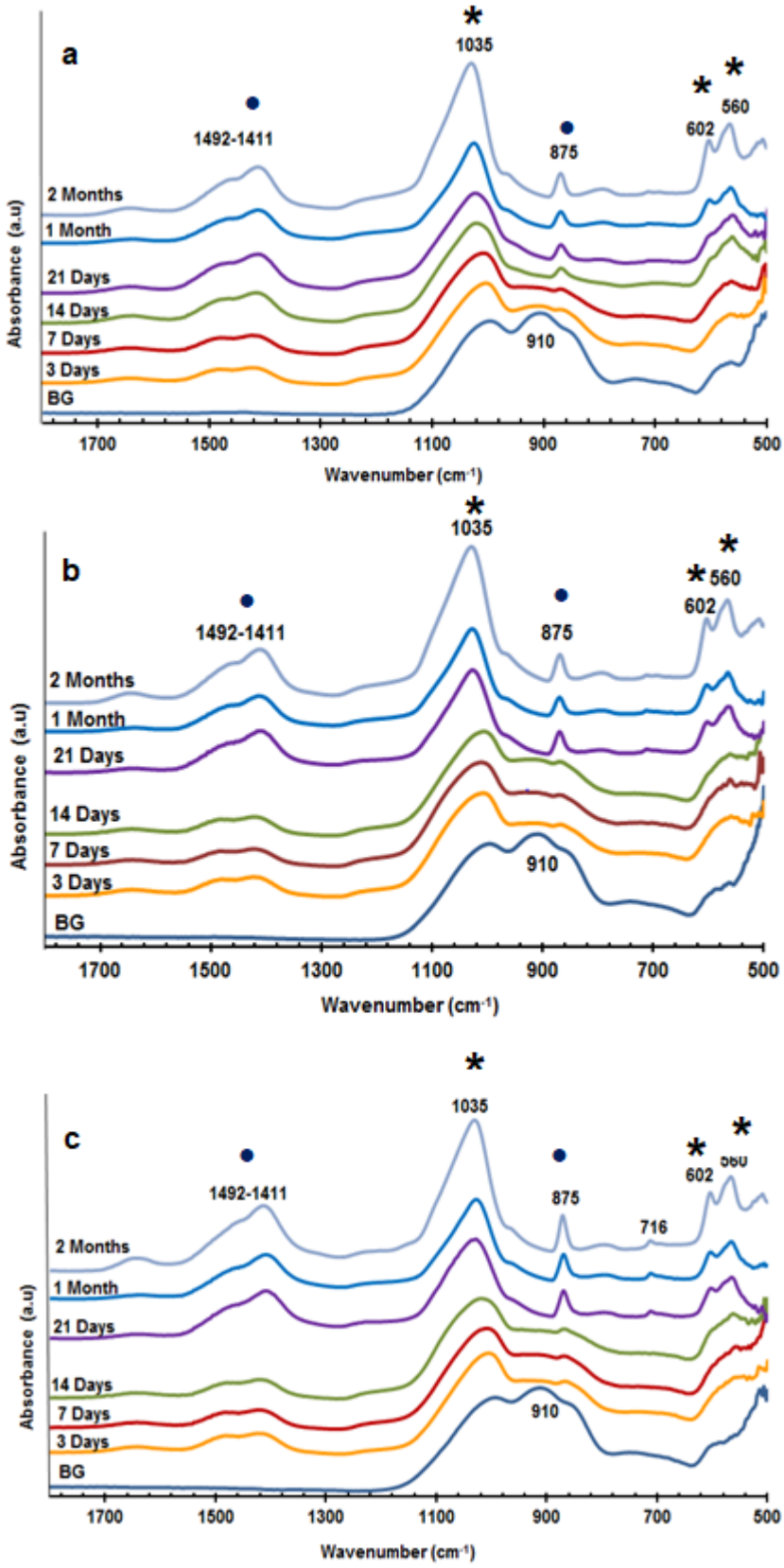

Figure 5.19: FTIR spectra of a) QMFA1 b) QMFA2 c) QMFA3 before immersion (bottom) and after immersion in SFα- MEM up to 2 months. (⁎) represents apatite and (●) represents carbonate band.

As α-MEM is rich in carbonate content Table (5.2), therefore the carbonate bands clearly exist in the absorbance spectra. However, these bands also appeared in the FTIR spectra of the SBF solution but, they are more pronounced in the cell culture media. The carbonate concentration in the cell media is 1571.4 ppm and it is approximately four times more than the carbonate concentration in the SBF solution, which is 256.2 ppm. Thus, the intensity of the carbonate bands in the cell media is higher than that in the SBF. These bands were reported to be an indicator of the formation of carbonated apatite by the substitution of either the $(PO_4)^{3-}$ group or the (OH^-) group by $(CO_3)^{2-}$ group (Heughebaert et al., 1988, Radin and Ducheyne, 1993, Müller and Müller, 2006, Mami et al., 2008). Previous studies suggest that there are two different carbonated fluorapatite structures and these are type-A and type-B. This depends on the site of the CO_3^{2-} substitution, if it is substituted for the OH^- then, it is known as type-A. If the substitution is for the PO_4^{3-} group thus, the apatite type is B. The indication of which type of apatite is formed in this study can be related to the location and the intensity of the C-O bands in the spectra. The CO_3 stretching bands appeared at 1411 cm^{-1} and 1492 cm^{-1} and they are accompanied with high peak intensities. Besides, there is also a CO_3 bending band which is detected at 874 cm^{-1}. These findings indicate the formation of type-B carbonated fluorapatite as more carbonate groups are present in the solution and this leads to more carbonate at the B-site of the apatite structure (Reigner et al., 1994, Yi et al., 2013). Additionally, there is another C-O absorption band in these spectra which is at around 716 cm^{-1}. (Reigner et al., 1994) found that the presence of this band in the FTIR spectra of the synthetic the carbonated fluorapatite indicates the occurrence of the $CaCO_3$ precipitates. This finding agrees with the results of this study as the $CaCO_3$ is clearly formed in the association with the carbonated fluorapatite structure as this band is clearly detected. From the above features it can be concluded that the type of the formed apatite in this media is different from the previous immersion solutions in which more carbonate groups are substituted at the B-site of the apatite structure.

In addition to the above, it can also be concluded that the cell media has a considerable effect on the glass dissolution process, where it can cause a distinct delay in the glass degradation. This might be related to the presence of Mg^{2+} and other ions in its composition or the adsorption of the solution amino acids on the glass surface, both of which can slow down the apatite precipitation (Radin et al., 1994, Radin et al., 1997) .

Table 5.2: Concentrations of some ions in SBF and SFα-MEM Cell Culture media presented in (ppm) and (mmole/L).

Elements	Ion Conc. in SBF		Ion Conc. in Cell media	
	(ppm)	(mmole/L)	(ppm)	(mmole/L)
Ca^{2+}	100.0	2.5	72.2	1.8
P^{+5}	31	1.0	31.5	1.0
Mg^{2+}	36. 5	1.5	19.8	0.8
K^{+}	195.0	5.0	209.7	5.4
Na^{+}	3266.0	142.0	3245.6	141.1
HCO_3^{-}	256.2	4.2	1571.4	25.8

5.3.2 XRD results:

The XRD analyses of the glasses immersed in SF α-MEM medium for 2 months are presented in Figure (5.20 a, b, c). The X-ray diffraction patterns demonstrate no clear shifts in the position of the amorphous halos during the first 14 days of glass immersion. However, at this time point few diffraction peaks are appeared in the spectra of the QMFA1glass. These peaks are located at 29.4º, 36º, 40º and 43.2º (2θ) and corresponded to the crystalline calcite ($CaCO_3$) peaks, as these patterns are compared to the calcium carbonate reference (ICDD file number 00-005-0586). Therefore, the appearance of these peaks may indicate the formation of carbonate substituted hydroxyapatite. After 21 days immersion, the characteristic apatite

diffraction peaks are present at 26º (2θ) and 32º (2θ) besides the subsequent increase in the intensities of the previously identified calcite peaks. These results matched with the FTIR spectra, where the carbonated bands became more pronounced after 21 days immersion in addition to the split in the apatite peaks. With the longer immersion time, all the apatite diffraction peaks show a considerable increase in their intensities and this suggests the significant growth of the apatite crystals.

The delay in the appearance of the apatite diffraction peaks and the prominence of the calcite peaks when the glasses are immersed in SFα-MEM are likely related to the calcium, phosphate and carbonate quantities in the testing medium. The calcium content in the culture media is around 1.8 mM and it is lower than that in the blood plasma and the SBF, which is around 2.5 mM. While, the carbonate content in α-MEM is nearly similar to the blood plasma at around 27 mM. This concentration level is higher than that in the SBF which is around 4.2 mM. Therefore, it can be suggested that Ca/P ratio in the cell media is not supersaturated to produce HAP; in contrast it is supersaturated to produce calcite and ACP as reported by (Rohanová et al., 2014). This is because of the lower Ca/P ratio in the cell media in comparison to the human blood plasma. The presence of high carbonate content in the solution of about 27 mM may lead to the formation of the $CaCO_3$ precipitate. This is because of the competition between the HPO_4^{2-} and the CO_3^{2-} for the PO_4^{3-} position. This competition in turn lead to the charge imbalance and this can be compensated by the formation of the $CaCO_3$ (Jalota et al., 2006).

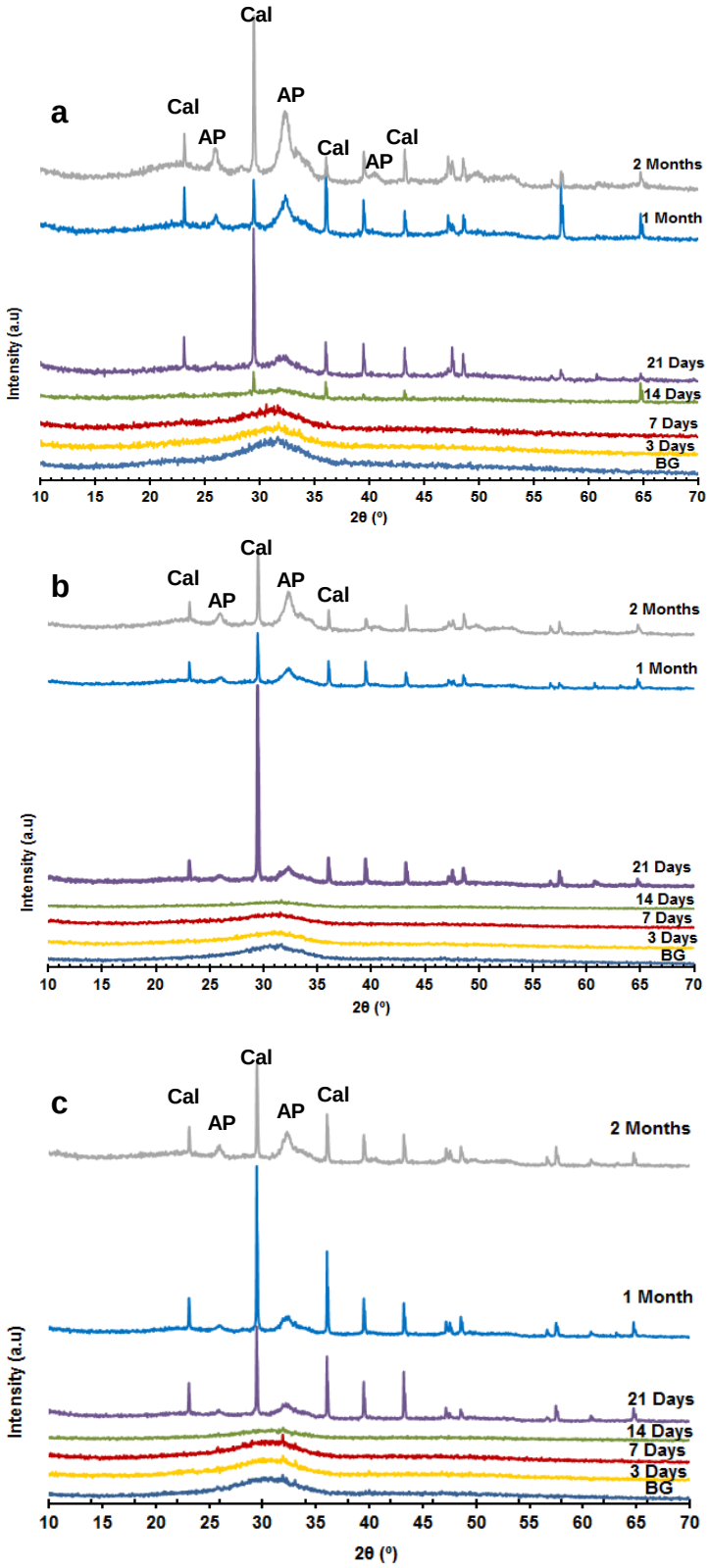

Figure 5.20: XRD patterns of a) QMFA1 b) QMFA2 c) QMFA3 before immersion (bottom) and after immersion in SFα- MEM up to 2 months. (AP) refers to the apatite peaks and (Cal) refers to the calcite peaks.

5.3.3 ^{19}F and ^{31}P MAS-NMR:

^{19}F MAS-NMR was run on the SFα-MEM treated glasses for specific time periods up to 2 months. Figure (5.21) displays the ^{19}F MAS-NMR spectra of the untreated and treated QMFA1 glass. After 3 days immersion the spectra show the appearance of a shoulder at -101 ppm besides the original two peaks of -132 and -170 ppm. With the longer immersion time, this shoulder peak transformed into a clearer peak at the position slightly shifted towards zero ppm accompanied with a noticeable decrease in peak width and increase in intensity. The peak position after 2 months immersion is at -97 ppm and this in turn becomes the main peak in the spectra. At the same time, the peak at -132 ppm shows reduction in its intensity. This indicates the existence of the remaining amount of the original glass besides the apatite crystals. The same changes are also taken place in the ^{19}F MAS-NMR spectra of the QMFA2 and QMFA3 glasses after their immersion in this media; however the original glasses spectra show the existence of one main peak unlike the QMFA1 glass, which has a shoulder peak accompanied with the main peak. This was related to the presence of higher sodium content in the structure of the QMFA1 glass in comparison to the other glasses. The peaks in QMFA2 and QMFA3 are gradually shifted and reach the same -97 ppm peak position after 2 months immersion Figure (5.22) and (5.23). The shifting in the peak position towards -97 ppm is related to the glass reaction and the formation of the carbonated type-B fluoroapatite. As mentioned earlier that the peak around -88 ppm is corresponded to the presence of fluoride associated with a carbonate group in the apatite lattice at the B-site. However, the carbonate content in this media is relatively high therefore; the formation of carbonate substituted fluorapatite is likely. The presence of high carbonate content in the solution will give the possibility to the F^- ion to bond with the Ca^{2+} to form CaF_2. Also, F^- ion combines with the carbonate of the solution and form fluorocarbonated apatite. As these two peaks are close to each other, there will be a

chance of the peaks overlapping. This overlapping may lead to the presence of one peak at -97 ppm as opposed to two peaks at -88 ppm and -102 ppm.

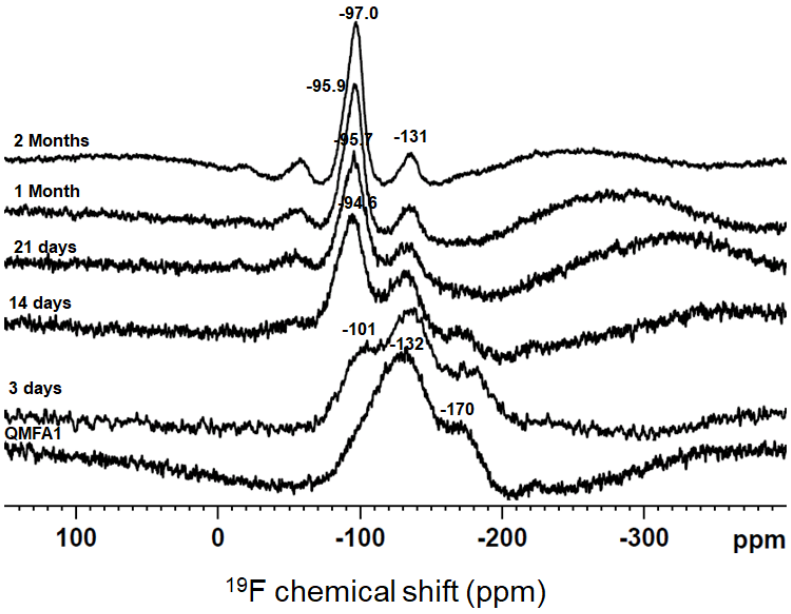

Figure 5.21:^{19}F MAS-NMR spectra of QMFA1glass before immersion (bottom) and after immersion in SFα-MEM for 2 months. The peak position is shifted from-101 ppm to -97 ppm, which is related to the presence of carbonate in the apatite structure.

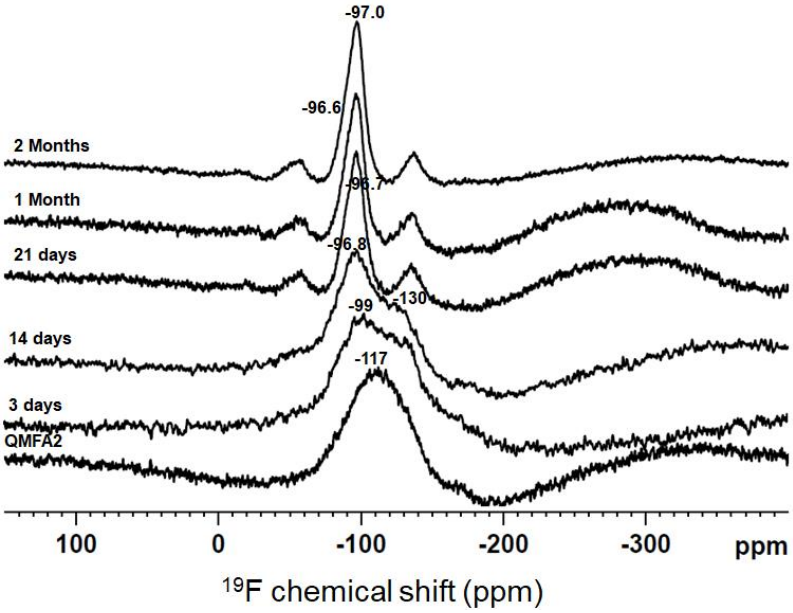

Figure 5.22:^{19}F MAS-NMR spectra of QMFA2 before immersion (bottom) and after immersion in SFα-MEM for 2 months. The peak position is shifted from-112 ppm to -97 ppm, which is related to the presence of carbonate in the apatite structure.

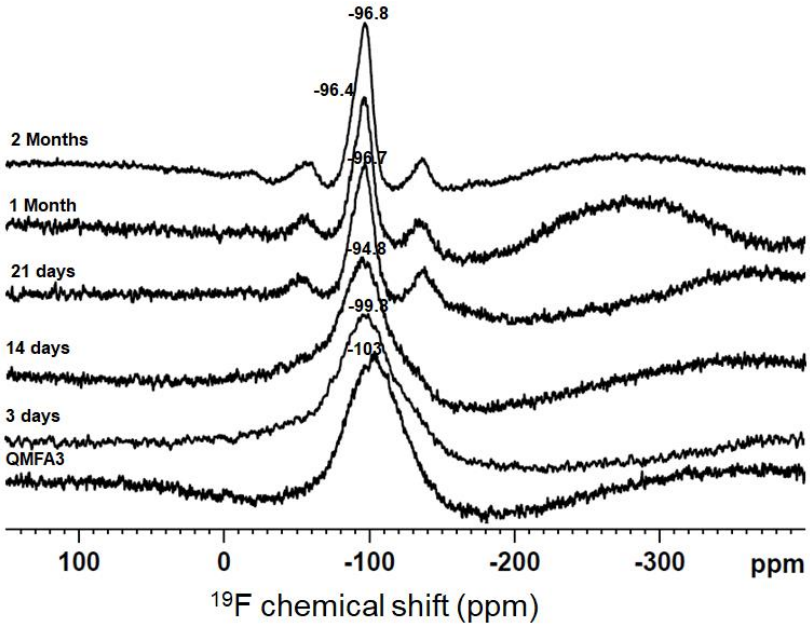

Figure 5.23:^{19}F MAS-NMR spectra of QMFA3 before immersion (bottom) and after immersion in SFα-MEM for 2 months. The peak position is shifted from-103 ppm to -96.8 ppm, which is related to the presence of carbonate in the apatite structure.

Regarding the ^{31}P MAS-NMR, Figure (5.24 a, b, c) demonstrates the changes in the phosphorus peak position in the untreated and treated glass powders. The width of the ^{31}P NMR lines for all the glasses shows a gradual narrowing with the immersion time where the signal becomes sharper and narrower after 2 months immersion in comparison to the original spectra. This sharper peak indicates the consumption of the phosphates from both the glasses and the medium for the formation of the apatite phase (Brauer et al., 2010). Moreover, the sharp peaks in all glasses show relative shift in position toward the lower values and the centres of the peaks are located at around 2.9-3.05 ppm. This peak position with the reduced linewidth corresponds to the formation of crystalline apatite phase (Chen et al., 2014a).

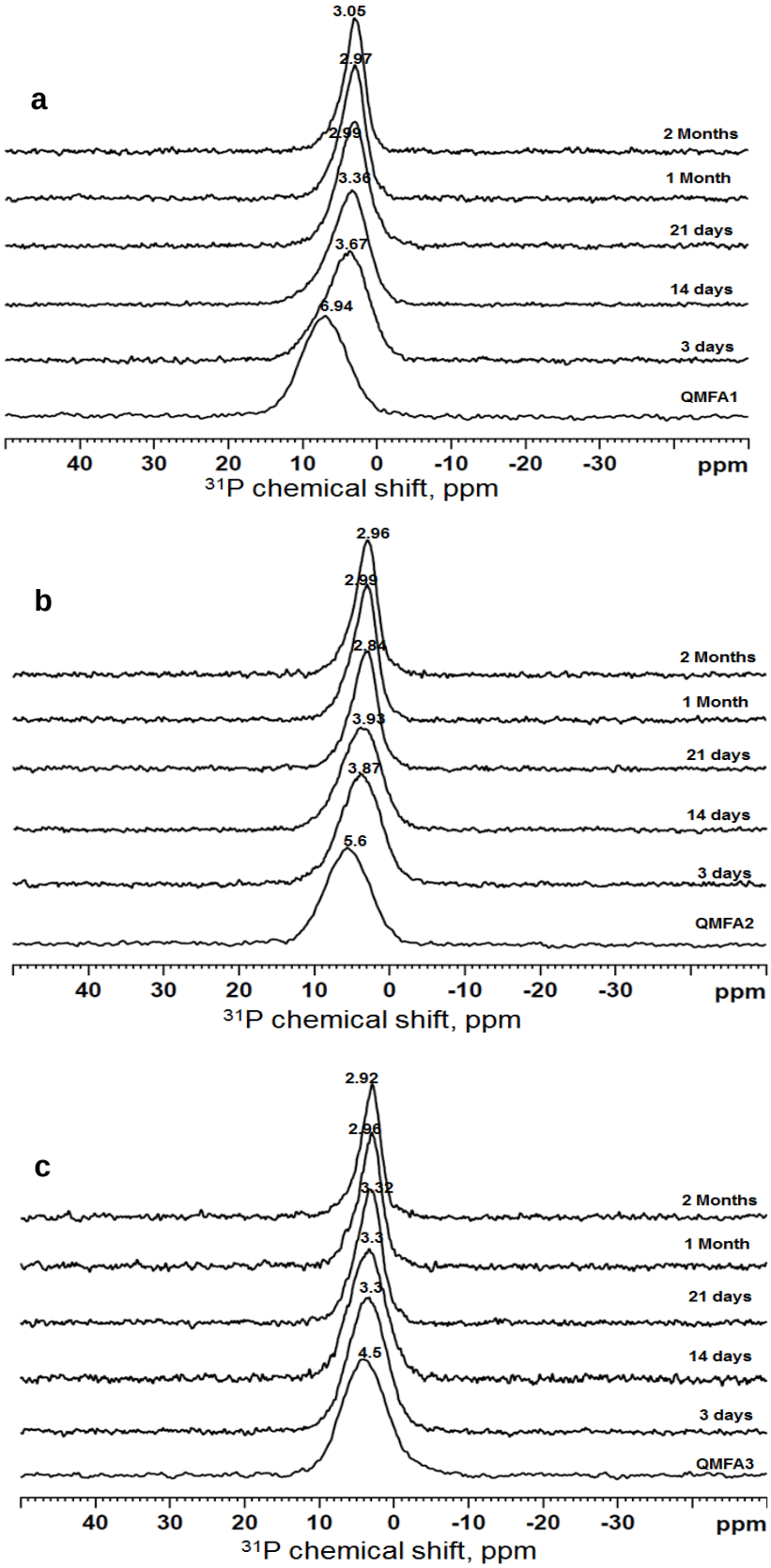

Figure 5.24: ^{31}P chemical shift spectra of a) QMFA1, b) QMFA2, c) QMFA3 glasses before immersion (bottom) and after immersion in SFα-MEM up to 2 months. The main resonance at -2.92 to -3.06 ppm corresponds to the presence of fluoride substituted apatite.

5.3.4 pH changes and ion release in SFα-MEM:

The medium pH changes over time of the experiment when all the glasses are immersed in SFα- MEM as shown in Figure (5.25). During the first 3 to 14 days of the immersion period, the pH of the SFα- MEM shows a noticeable rise in its value and this rise reaches to about 8.5±0.04 for QMFA1 and 8.4±0.05 for both QMFA2 and QMFA3 glasses. This higher pH level promotes the existence of the CO_3^{2-} ions in the media (Cerruti et al., 2005). This is due to the existence of a high concentration of HCO_3^- in this medium in comparison to the previous solutions. The HCO_3^- decomposes with time releasing the CO_3^{2-} in the media and raising the pH of the solution (Müller and Müller, 2006). Thus, the pH rise in this media is higher than Tris and SBF and the values reach to 8. After this time point, the pH show a sharp drop in its level and this might be related to the formation of the calcium carbonate. This is due to the reaction between the calcium hydroxide and HCO_3^-, which leads to the formation of $CaCO_3$+H_2O and causes the sharp reduction in the solution pH.

Other studies suggest that the drop in the solution pH is related to the precipitation of the Ca-P layer and the $CaCO_3$ layer by the uptake of the CO_3^{2-} and the PO_4^{3-} from the HCO_3^- and HPO_4^{2-} respectively. This ion uptake process pushes the equilibrium to the apatite and the calcite side, where more H^+ is present in the solution and this in turn decreases the pH of the media (Cerruti et al., 2005).

These results are consistent with the previous results from the FTIR, XRD and NMR, where the formation of apatite phase is clearly detected after 14 days.

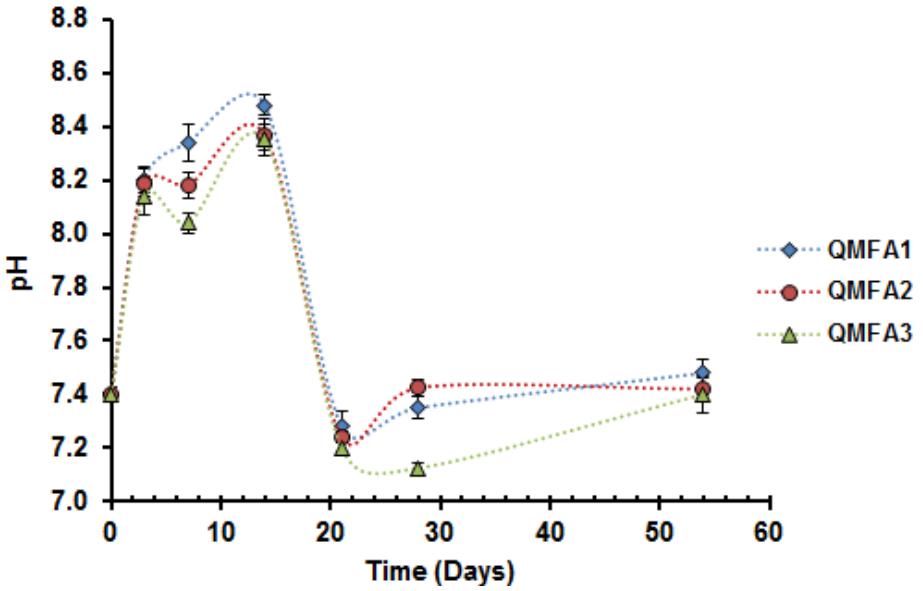

Figure 5.25: Graph shows the pH changes of SFα-MEM after the immersion of the glasses for 2 months (Lines are drawn as visual guides).

The pH changes are also consistent with the changes in the release profiles of all the ions within this media. The concentration of calcium cation shows a considerable increase during the first 7 days, where it reaches the maximum values of about 80.0±3.6 ppm, 98.5±2.3 ppm and 118.9±4.5 ppm for QMFA1, QMFA2 and QMFA3 respectively Figure (5.26). This indicates the release of this cation in the solution for the ion exchange process. Then at 14 days, the calcium concentration in all the glasses demonstrates a noticeable drop in values. This signifies the consumption of the calcium for the formation of the calcite phase.

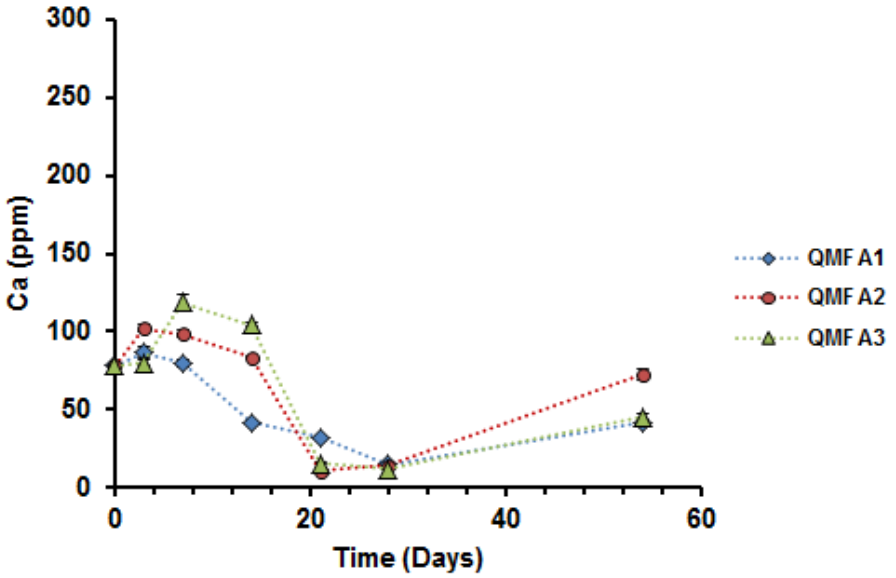

Figure 5.26: Elemental concentrations ± SD of (Ca) in SFα-MEM after the immersion of the glasses for 2 months (Lines are drawn as visual guides).

During the same time period, the phosphorus concentration shows a clear decrease Figure (5.27). The concentrations reach the lowest values at 21 days, where the values approximate to 6.4±0.1 ppm, 5.0±0.2 ppm and 4.1±0.1 ppm for QMFA1, QMFA2 and QMFA3 respectively. Then, after this time point the concentrations demonstrate a constant level for all the glasses for the rest of the experimental period. This release profile is nearly similar to the phosphorus release profile in SBF solution. However, in the former solution there is a clear delay in the period of the phosphorus drop. This drop, as mentioned earlier in the SBF section, is attributed to the incorporation of phosphate to form the Ca-P layer on the surface of the glass powder.

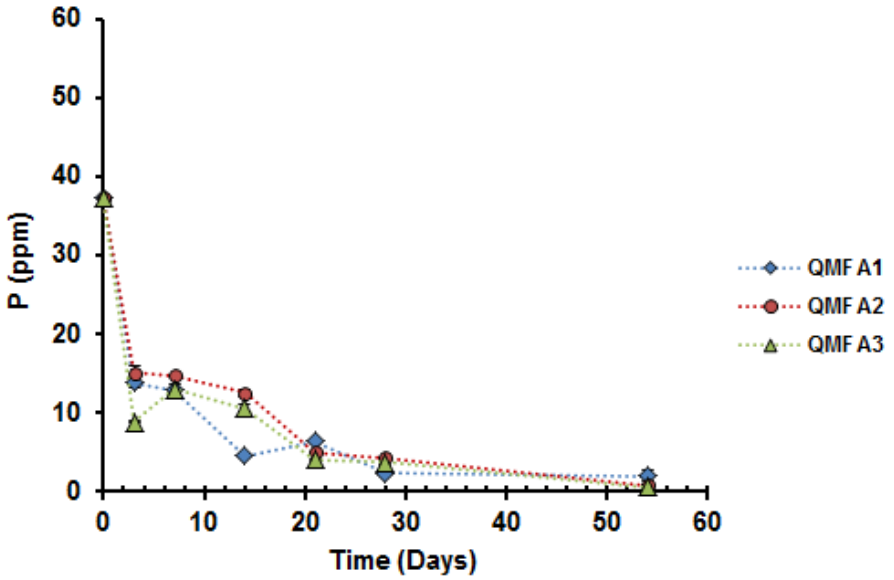

Figure 5.27: Elemental concentrations ± SD of (P) in SFα-MEM after the immersion of the glasses for 2 months (Lines are drawn as visual guides).

The Si concentration in the SFα-MEM, on the other hand, shows a continuous increase with the immersion time as seen in Figure (5.28). However at the day 14 of glasses immersion, QMFA2 and QMFA3 glasses demonstrates a slight decrease in the concentration values, the values reaches 37±0.4 ppm and 39±0.9 ppm respectively and this is around 6-7 ppm lower than the values at day 7. This might be corresponded to the earlier formation of the $CaCO_3$ phase in the QMFA1 glass. As this glass reaches the Si solubility limit, which is around 60 ppm, at that time period. While, for the other two glasses the solubility limit is reached after this time point.

Interestingly, it can also be noticed from the Si release profile that the Si release concentration in this medium is higher than in the other testing solutions. This is related to the higher pH of this medium which reaches to approximately 8.5. In this high pH level the formation of the supersaturated solution of silicic acid can be promoted and the excess of this acid is can be polymerised to colloidal particles. Therefore, higher concentration of Si is clearly detected in this medium (Iler, 1979).

The solubility of the Si species is correlated with the pH level of the solution. The pH drop at day 21 causes the solubility of the Si species to decrease. This reduction can consequently result in the presence of high Si concentration.

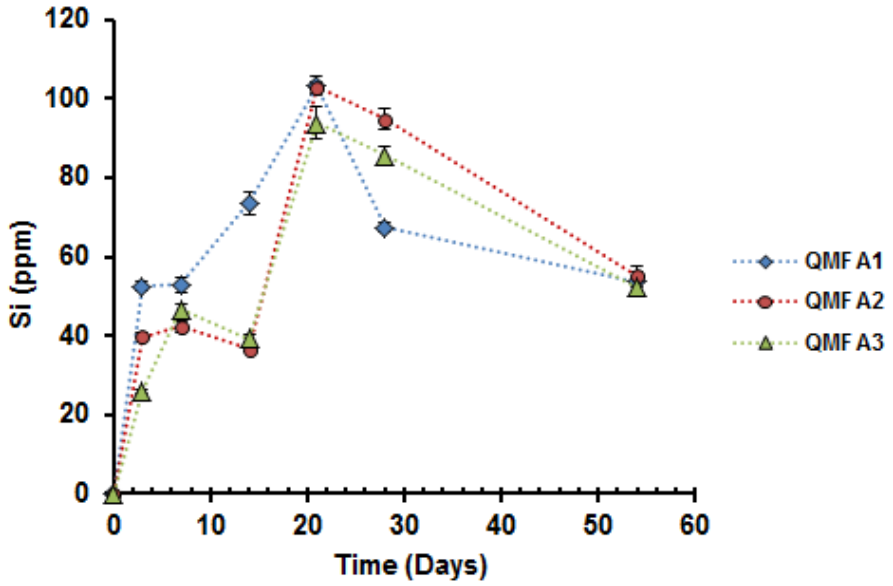

Figure 5.28: Elemental concentrations ± SD of (Si) in SFα-MEM after the immersion of the glasses for 2 months (Lines are drawn as visual guides).

The same trend is also seen with the fluoride release in SFα-MEM. The concentration of the fluoride in all glasses rises with time, though there is slight decrease in the values at days 7 and 14 and this is clearer in QMFA2 and QMFA3 Figure (5.29). This slight dip might be related to consumption of fluoride in the formation of the FAP crystals. At day 21, the fluoride concentration rises and reaches the maximum value of 11.4±0.3 ppm, 9.0±0.2 ppm and 8.5±0.2 ppm for QMFA1, QMFA2 and QMFA3 respectively. With the longer time the concentration drops sharply, and this might suggest the depletion of the fluoride ion in the solution for the formation of the fluorcarbonated FCO_3 apatite.

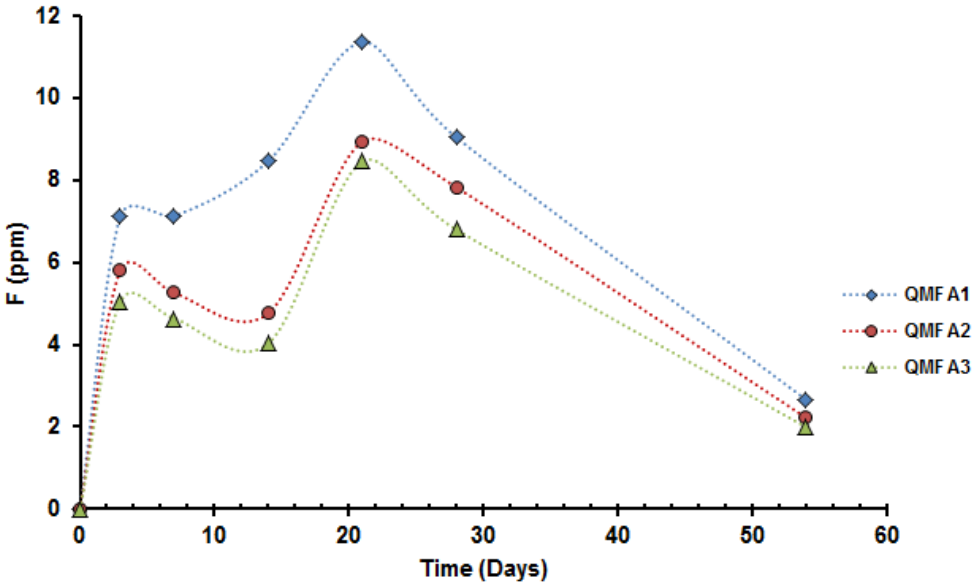

Figure 5.29: Elemental concentrations ± SD of (F) in SFα-MEM after the immersion of the glasses for 2 months (Lines are drawn as visual guides). The error bars are smaller than the point size.

5.3.5 SEM results:

The changes on the surfaces of the glass powders after their immersion in SFα-MEM media for 7 days and 1 month are demonstrated as SEM micrographs of two different magnifications in Figure (5.30 a, b, c and d).

In day 7, it can be seen that there is a deposition of small crystals on the surface of the glass powder and these crystals grow with longer immersion time Figure (5.30 a and b). After one month, these crystals undergo subsequent changes in their morphologies, where they become more numerous and packed in nature Figure (5. 30 c and d). Moreover, these crystals grow as a cauliflower-like morphology and this is in agreement with (Rohanová et al., 2014), who detected the same morphology of the deposited crystals, but on the surface of a glass-ceramic scaffold immersed in serum containing DMEM cell media.

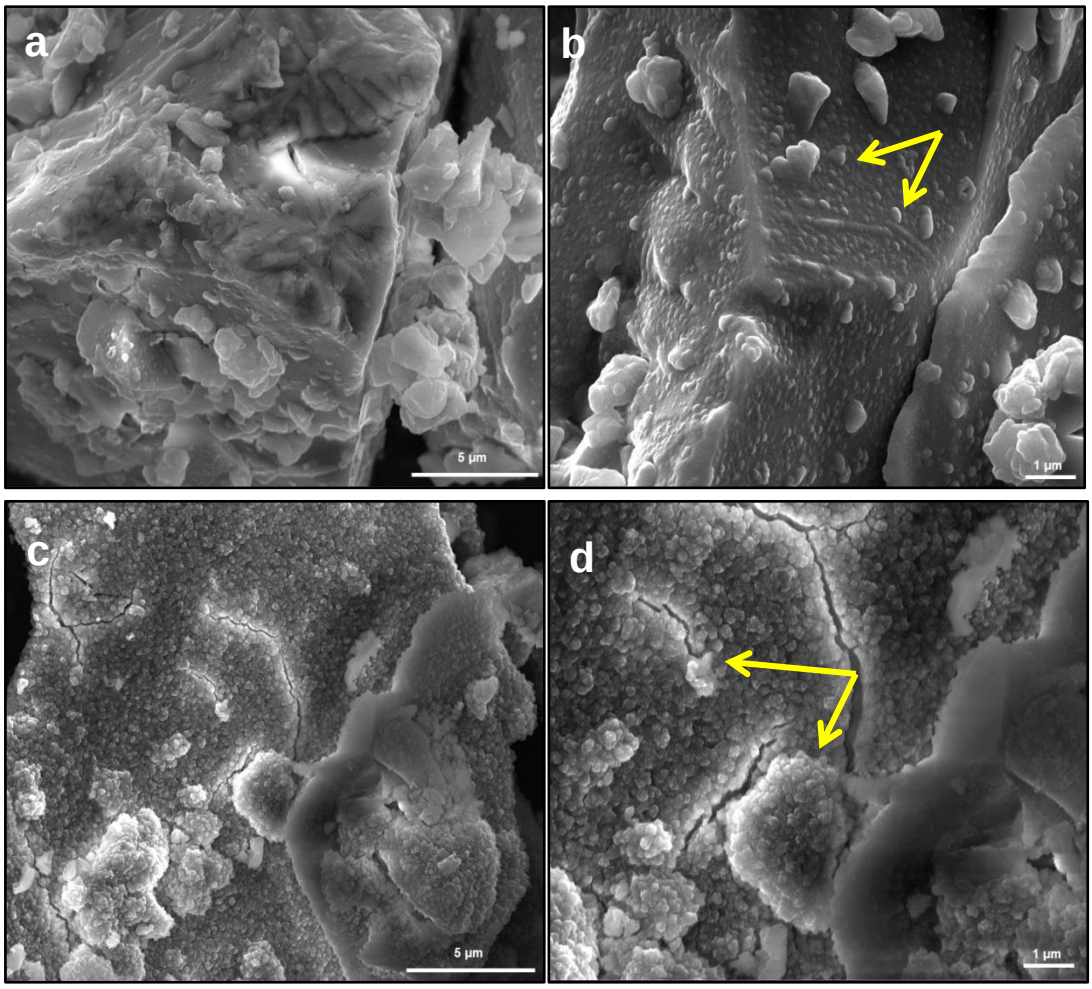

Figure 5.30: SEM micrographs of QMFA1 glass powder after immersion in SFα-MEM for a, b) 7 days (12000x and 24000x magnification) where small crystals are deposited on the glass surface. c, d) 1 month immersion (12000x and 24000x magnification, the crystals grow as a cauliflower-like morphology.

It was suggested that the white aggregated globules were ACP depositions covered with $CaCO_3$ phase and this related to the high Ca concentration on the surface of the scaffold as detected by EDX. The same result is also appeared in this study, where the detected calcium concentration on the surfaces of the glass powders is higher in values in one month immersion than that in day 7, as can be seen by the EDX analysis in Table (5.1, page 160). Subsequently, the detected phosphate concentration is depleting at the longer immersion time and this might indicate the

formation of the Ca-P phase underneath the $CaCO_3$ phase. All the findings from the SEM and EDX are coincide with the apatite formation and ICP-OES results.

Interestingly, the morphology of the crystals which are aggregated on the surface of the glass powder after their immersion in SFα-MEM media are different than the shape of the crystals formed in Tris and SBF. In the former solution the morphology of the crystals are cauliflower in shape with packed globules while, in Tris and SBF the crystals are flower in shape with needle-like nature. This corresponds to the formation of the $CaCO_3$ phase in the former solution and not in the latter solutions. Moreover, the detected concentration of calcium on the surface of the glass powder by the EDX is higher in this solution than the other two solutions which confirm the precipitation of the calcite layer. However, the immersed glasses are known to release fluoride ion in the surrounding solution during their dissolution process and this in turn promote the formation of the needle like shape. This feature is not clearly demonstrated in the culture media. This might be due to the presence of high carbonate content in the solution, which might hide the needle structure of the FAP. Therefore, the cauliflower shape is abundant in this media. It can be also seen that the detected fluoride concentration is higher on the surface of the glass powders when they immersed in Tris and SBF while; in the SFα-MEM media the concentration is low. This might indicate the incorporation of the fluoride in the formation of the outer layer of the deposited crystals.

5.4 Immersion of the glass powders in Sα-MEM

5.4.1 FTIR results:

The FTIR spectra of the glasses immersed in Sα-MEM for a time period ranged from 3 h to 2 months are displayed in Figure (5.31 a, b, c). Generally, it can be clearly seen that there is a noticeable delay in the process of glass degradation and dissolution with no clear appearance of the characteristic peaks for apatite formation.

The NBO peak at 910 cm^{-1} shows partial disappearance during the two months period, while the P-O stretching band at 1033 cm^{-1} exhibits a slight increase in its intensity. Furthermore, there is an existence of a broad hump at 560-602 cm^{-1} region which is related to the presence of the ACP layer (Pereira et al., 1994, Radin et al., 1997). Therefore, it can be indicated that the glasses are not dissolved completely in the Sα-MEM. Although, the glasses are releasing their sodium and calcium ions in the media to form the silica gel layer, the complete features of apatite formation is not clearly seen. These features are true for QMFA1 and QMFA2 glasses. However, in QMFA3 the P-O bending shows a minute split at the 2 months with the disappearance of the NBO peak and the appearance of the carbonate peak at 870 cm^{-1}. This suggests the starting of the apatite formation in this prepared glass.

The reason for the delayed apatite formation in all glasses is related to the presence of the serum proteins in the media. These proteins cause substantial interference to the process of apatite formation by their adsorption on the surface of the glass particles during their first stages of reaction with the media. This phenomenon can occur due to the presence of differences in the surface charges between these two materials. Thus, a clear delay in the formation of apatite layer is carried out (Radin et al., 1997, Lobel and Hench, 1998, Sepulveda et al., 2002). The dissolution behaviour of the glasses in this medium is different than in SBF and the same feature is also appeared in (Sepulveda et al., 2002) study.

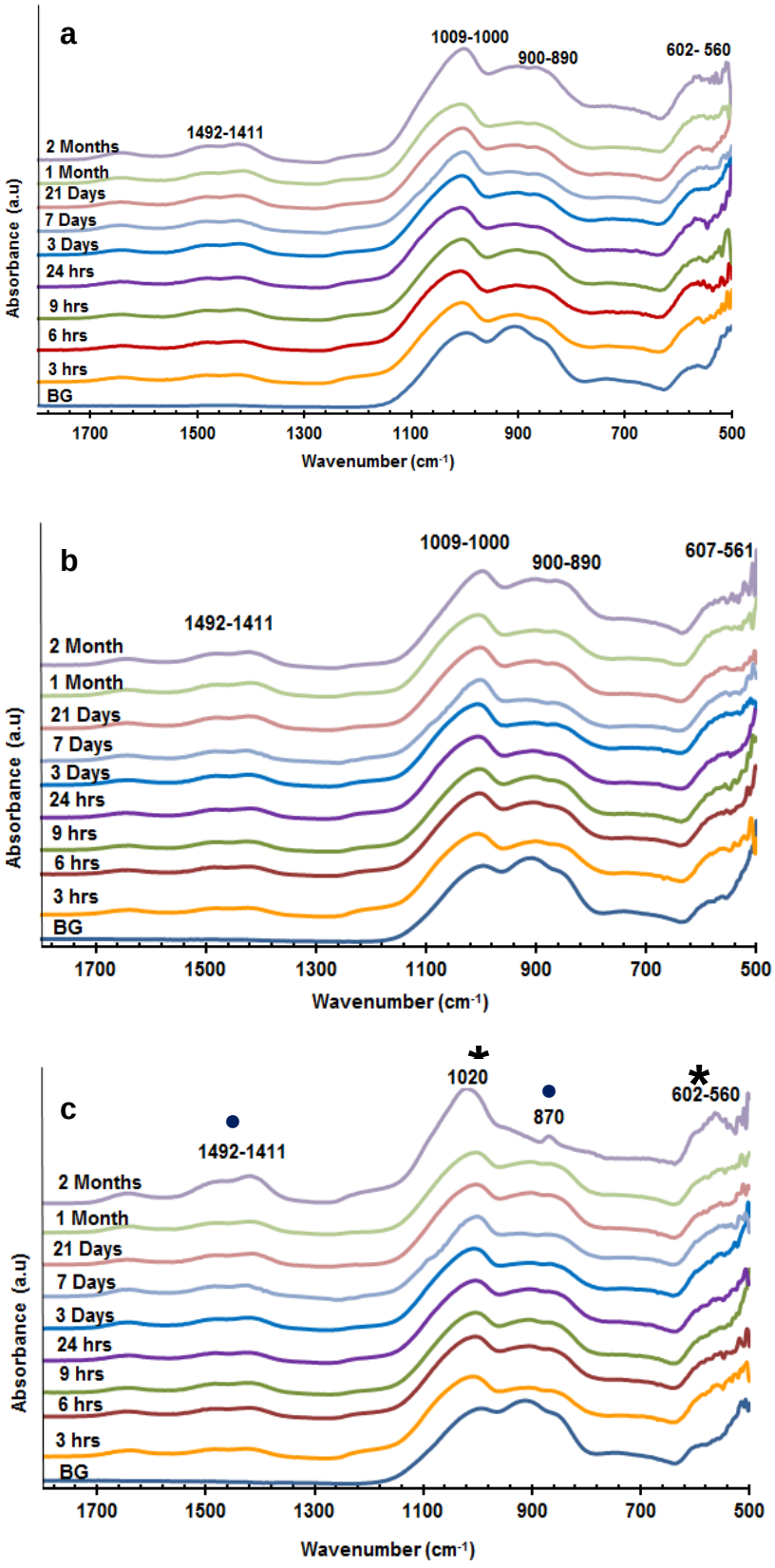

Figure 5.31: FTIR spectra of a) QMFA1 b) QMFA2 c) QMFA3 before immersion (bottom) and after immersion in in Sα- MEM media up to 2 months. (⁎) represents apatite and (●) represents carbonate band in QMFA3 glass only.

Regarding the carbonate group in the Sα-MEM, the C-O bending peak at the lower energy region is not detected in QMFA1 and QMFA2, while the C-O stretching peak at the higher energy region 1411 cm^{-1} and 1492 cm^{-1} is clearly shown in all glasses. However, they are not as prominent as that in the SFα-MEM. Another difference between the Sα-MEM and SFα-MEM is the appearance of new bands at approximately 1650 cm^{-1}, 1500 cm^{-1} and 1442 cm^{-1} region. These bands are slightly overlapped and they represent the C=O bonds, C-N-H band and CH_2 bands respectively. These bands are reported to be related to the presence of proteins and the organic phases on the surface of the powder particles (Sauer and Wuthier, 1988, Radin et al., 1997, Gebhardt et al., 2012).

5.4.2 XRD results:

The XRD patterns of the immersed QMFA1 and QMFA2 glasses in Sα-MEM demonstrate no appearance of any diffraction peaks for apatite during the whole period of immersion Figure (5.32 a and b). However, at the range of 20º- 23º (2θ) there is an appearance of a slight hump. This intensity hump is suggested to be related to the degradation of the glasses in the media and the formation of the silica gel layer (Al-Noaman et al., 2012b, Miola et al., 2015). The XRD pattern of the low sodium containing glass QMFA3 at 2 months shows a slight shift in the amorphous halo towards the higher (2θ) values with a subsequent prominence in its intensity. Moreover, a low intensity calcite peaks are also become evident in this pattern Figure (5.32 c). This might be related to the high calcium content in the QMFA3 glass which enhances the deposition of apatite crystals as discussed before in section (5.2.2). Therefore, these features suggest the formation of nano-crystalline apatite as the silica gel layer is enriched in calcium and phosphate and it can act as a starting point for the apatite deposition and nucleation. The presence of the serum in the culture media could suppress the dissolution of the glass-ceramic but not the crystallisation of calcite and the formation of ACP (Rohanová et al., 2014).

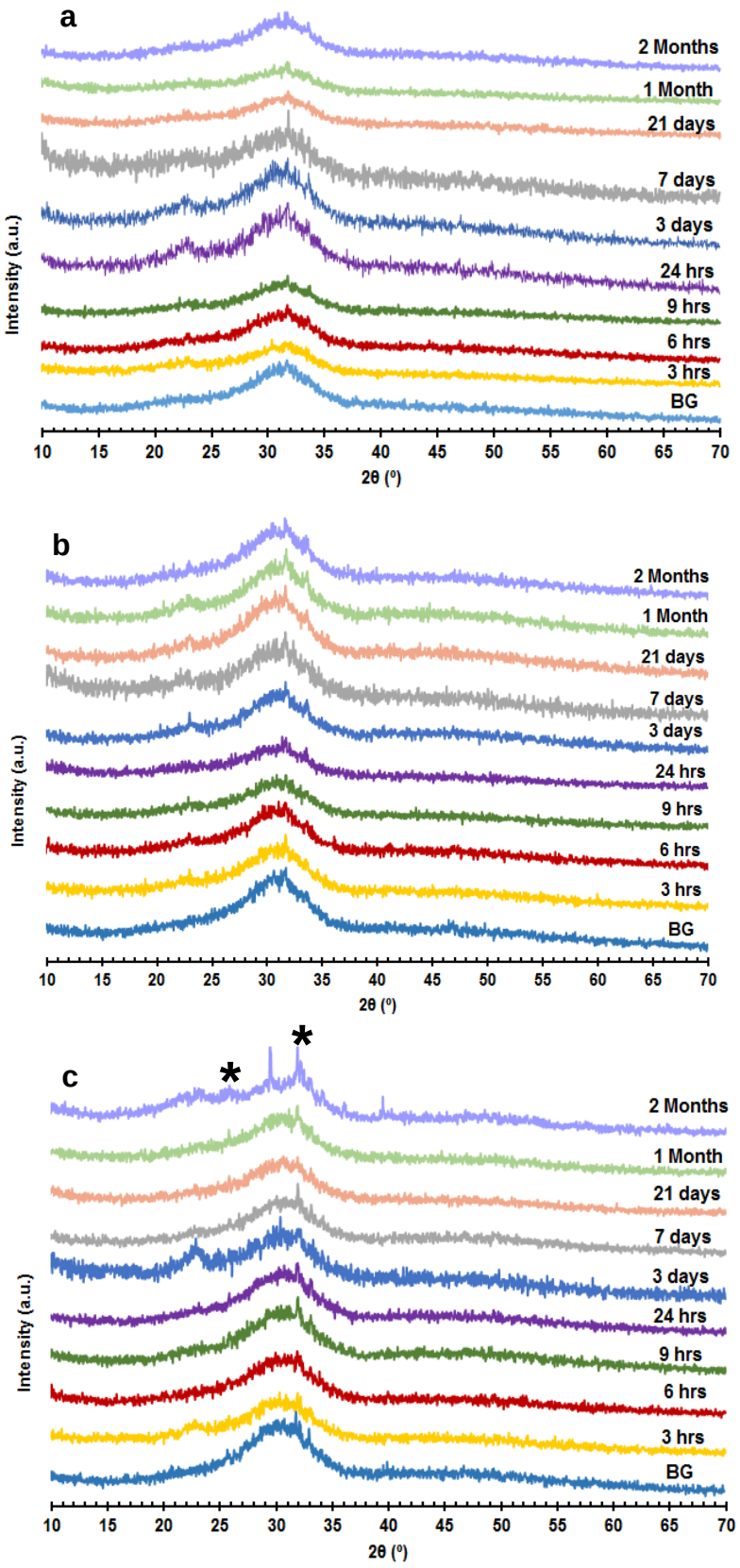

Figure 5.32: XRD patterns of a) QMFA1 b) QMFA2 c) QMFA3 before immersion (bottom) and after immersion in Sα-MEM up to 2 months. (⁎) represents crystalline phase in QMFA3 glass.

5.4.3 ^{19}F and ^{31}P MAS-NMR results:

^{19}F MAS-NMR spectra in Sα-MEM show small changes in both peak positions and signal widths for all the glasses during the whole period of immersion. In QMFA1 glass Figure (5.33), there is an appearance of a small shoulder peak at -101 ppm with increase in immersion time in addition to the slight shift of the other peaks toward the left side compared to the ones in the unreacted glass. In QMFA2 and QMFA3 glasses Figure (5.34) and (5.35), the peak positions at -117.4 ppm and -103.3 ppm are also shifted slightly toward the positive side. However, the width of the spectra line for all the glasses is stayed wide during the experiment. These findings suggest that there is a reaction between the solution and the glasses, but there is a great amount of unreacted glass powder which is remaining. These peaks could contribute to a mixed sodium calcium fluoride species or a complex of calcium sodium fluorine species adsorbed on the original glass powder (Brauer et al., 2009, Mneimne et al., 2011).

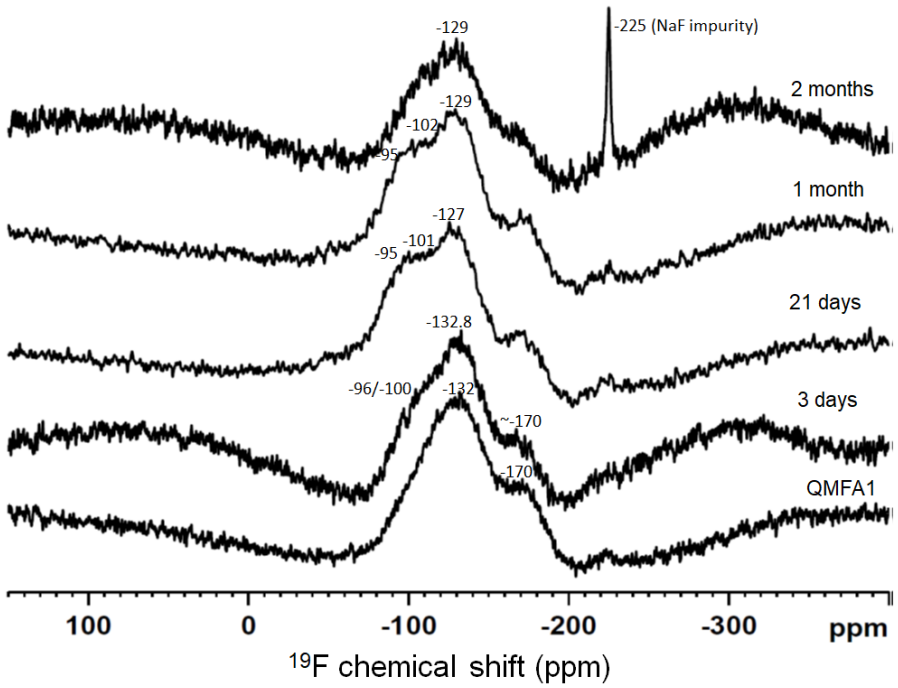

Figure 5.33: ^{19}F chemical shift spectra of QMFA1 before immersion (bottom) and after immersion in Sα-MEM for up to 2 months. Peak at -225 ppm corresponds to the contamination of the zirconia rotor by NaF solution.

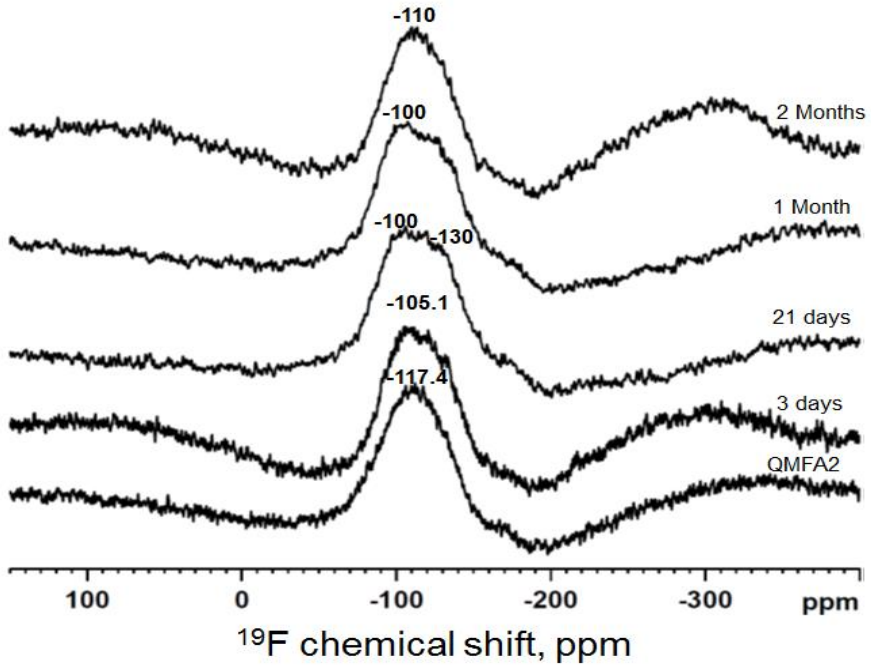

Figure 5.34: ^{19}F chemical shift spectra of QMFA2 before immersion (bottom) and after immersion in Sα-MEM for up to 2 months.

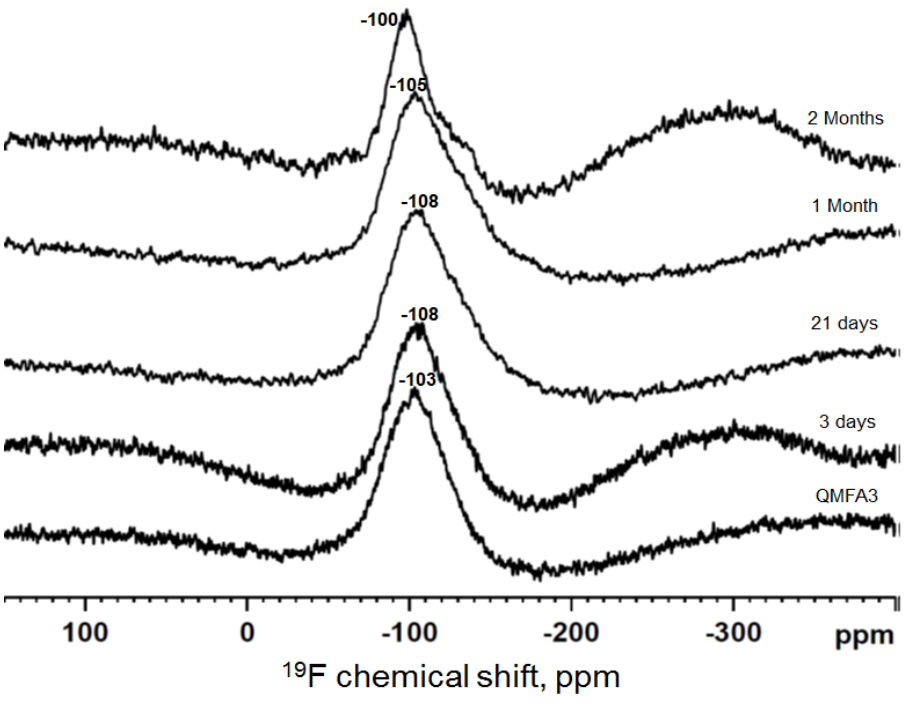

Figure 5.35: ^{19}F chemical shift spectra of QMFA3 before immersion (bottom) and after immersion in Sα-MEM for up to 2 months.

Figure (5.36 a, b, c) displays the ^{31}P MAS-NMR spectra of the three treated glasses. The spectra reveal relatively broad peaks with positions shifted from 6.94, 5.6 and 4.5 ppm to 4.46, 4.1 and 3.11 ppm for QMFA1, QMFA2 and QMFA3 glass respectively within the 2 months immersion time. The broad line widths might be corresponding to the presence of the orthophosphate species of the original glasses. While, the shifted peak position indicates the slow glass disintegration in the modified cell media. However in the third glass, the centre of the peak position is located at 3.11 ppm and this value is close to the peak position of the crystalline apatite which is about 3.0 ppm. Therefore, this peak suggests the formation of the amorphous calcium orthophosphate (Chen et al., 2014b).

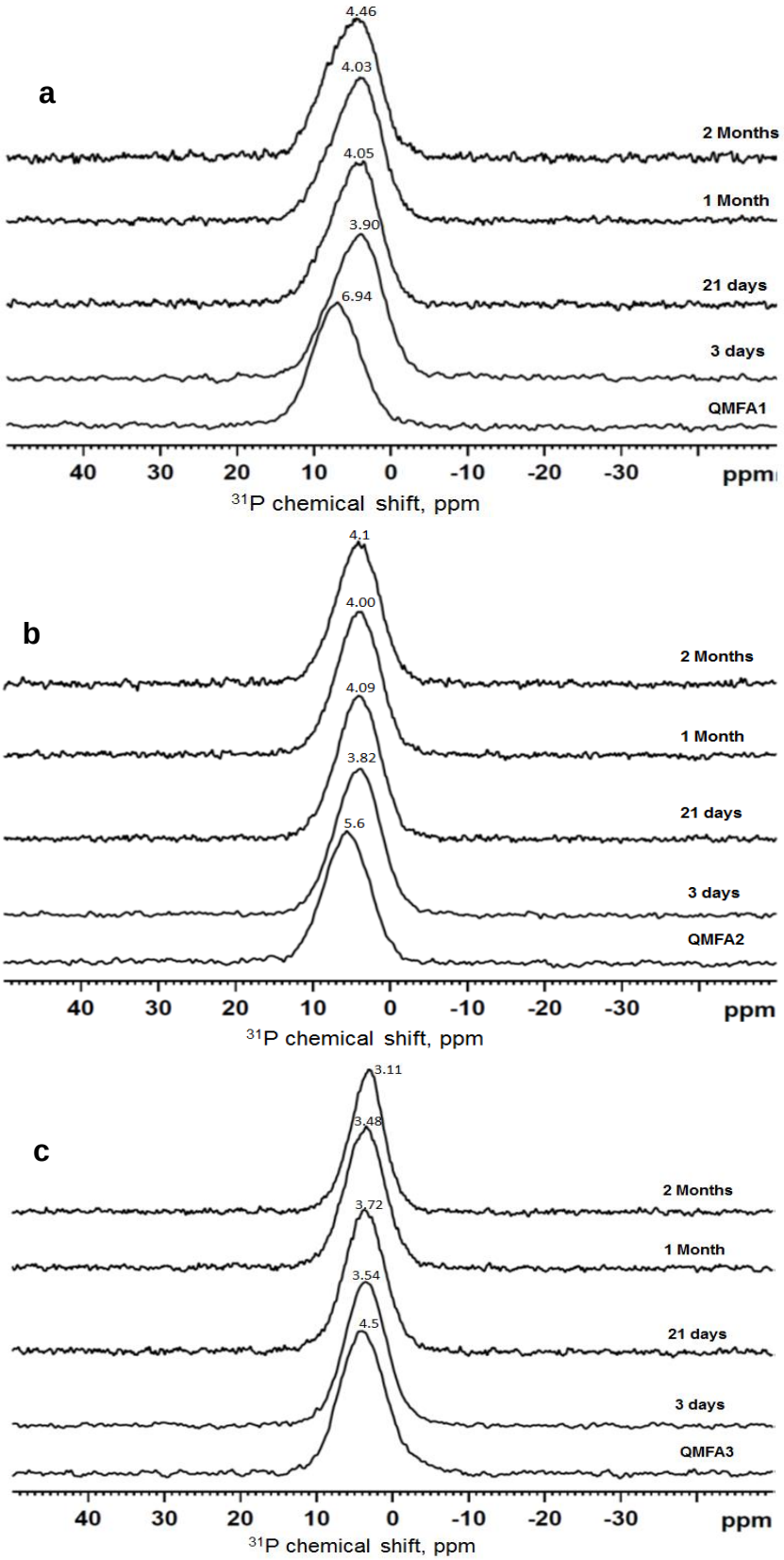

Figure 5.36: ^{31}P chemical shift spectra of a) QMFA1, b) QMFA2, c) QMFA3 glasses before immersion (bottom) and after immersion in Sα-MEM up to 2 months.

5.4.4 pH changes and ion release in Sα-MEM:

Figure (5.37) demonstrates the pH changes of the Sα-MEM medium after the immersion of the glass powders at different time points. The general trend is similar for all the treated glasses. After 3 days immersion, the pH of all solutions shows a distinct increase in value from 7.4±0.03 to 8.2±0.05 for QMFA1 and to 8.0±0.04 for QMFA2 and QMFA3. Then, the pH level stays nearly constant afterword until 1 month immersion, where the value rises again to the maximum level of about 8.5±0.03-8.4±0.05. This trend is relatively different than that in the SFα-MEM in which the latter showed a sharp decrease in the pH value after 21 days and it reached to 7.35±0.04. At that time point the features of the apatite deposition appeared clearly with the formation of the $CaCO_3$ phase. However, in this media there are no noticeable features of apatite formation appear in the XRD and FTIR spectra during the period of the experiment. The difference between these two media can be corresponded to the addition of the 10% of the serum protein to the SFα-MEM. This in turn suggests that there is an evidence of the ion release in the serum contained medium, but with no clear participation of the ions in the apatite precipitation.

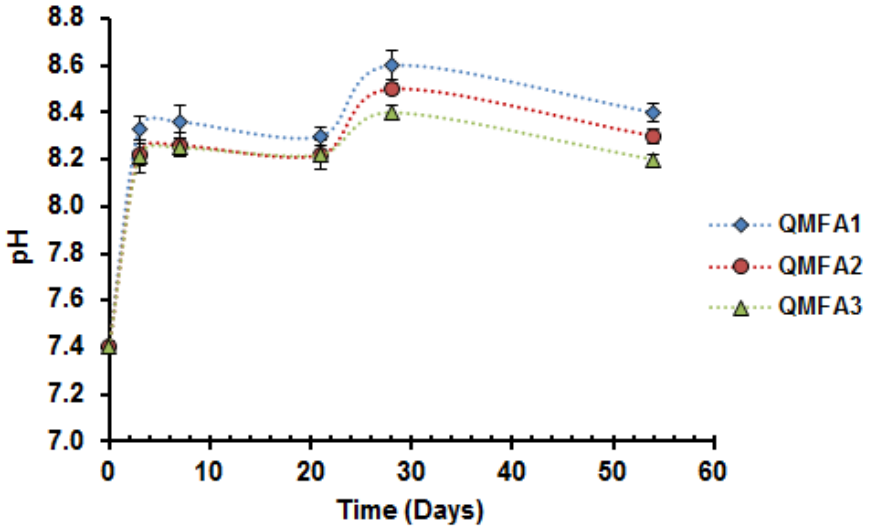

Figure 5.37: Graph shows the pH changes of Sα-MEM after the immersion of the glasses for up to 2 months (Lines are drawn as visual guides).

The pH change features are in agreement with the ion release data. Both calcium and fluoride concentrations show a slight dip at the 21 days of the immersion period and this dip appears after the maximum rise level. This might be related to the consumption of some of the released ions in the formation of the ACP phase Figure (5.38 and 5.39).

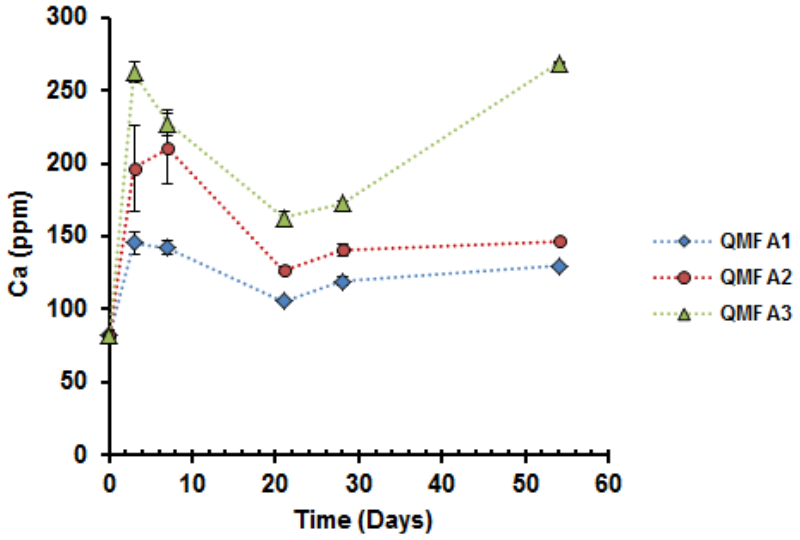

Figure 5.38: Elemental concentrations ± SD of (Ca) in Sα-MEM after the immersion of the glasses for up to 2 months (Lines are drawn as visual guides).

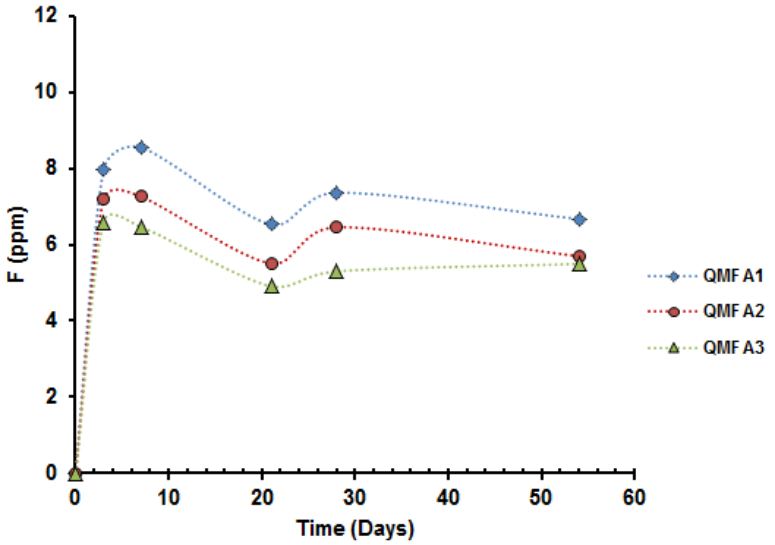

Figure 5.39: Elemental concentrations ± SD of (F) in Sα-MEM after the immersion of the glasses for up to 2 months (Lines are drawn as visual guides). The error bars are smaller than the point size.

At the same time, the phosphorus concentrations demonstrate decrease in values during the immersion time which also indicate the release of the ion in the solution. However, their concentrations do not reach the same minimum level at the longer immersion period as was seen before in the previous solutions Figure (5.40). This signifies that the phosphorus is consumed in the previous solutions and not in this medium. Moreover, it can be seen that the concentration of the calcium release in the SFα-MEM media is much lower than the concentration in this media which indicates the clear retardation of the release process in the latter media.

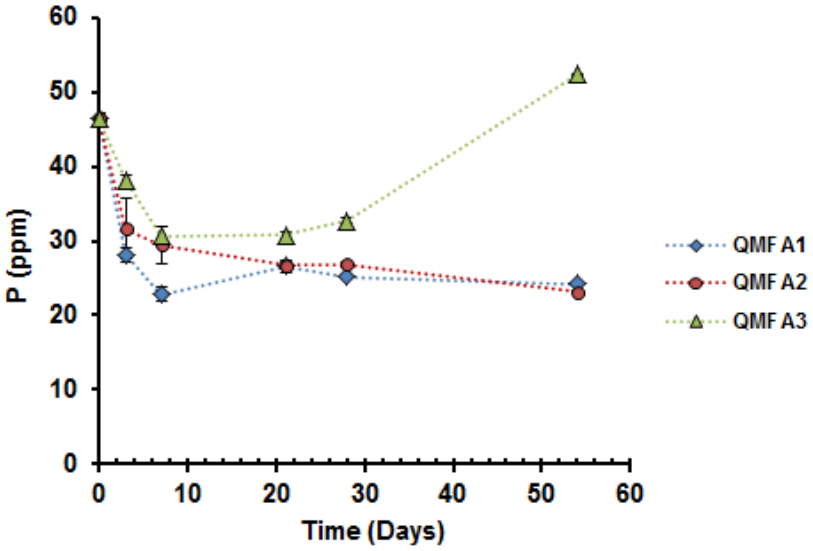

Figure 5.40: Elemental concentrations ± SD of (P) in Sα-MEM after the immersion of the glasses for up to 2 months (Lines are drawn as visual guides).

Regarding the Si release, the solubility limit is reached at day 7 of the glasses immersion, where the concentrations are about 60±2.9, 69±5.9 and 66±1.5 ppm for QMFA1, QMFA2 and QMFA3 respectively, as seen in Figure (5.41). This indicates the formation of the silica gel layer as reported by (Brauer et al., 2010). However, in this study there is no evidence of apatite formation on the surface of the QMFA1 and QMFA2 glass powders with the formation of this layer. Therefore, it can be

suggested that the serum has a retardation effect on the deposition of the ions on this layer which cause delay in the apatite formation process.

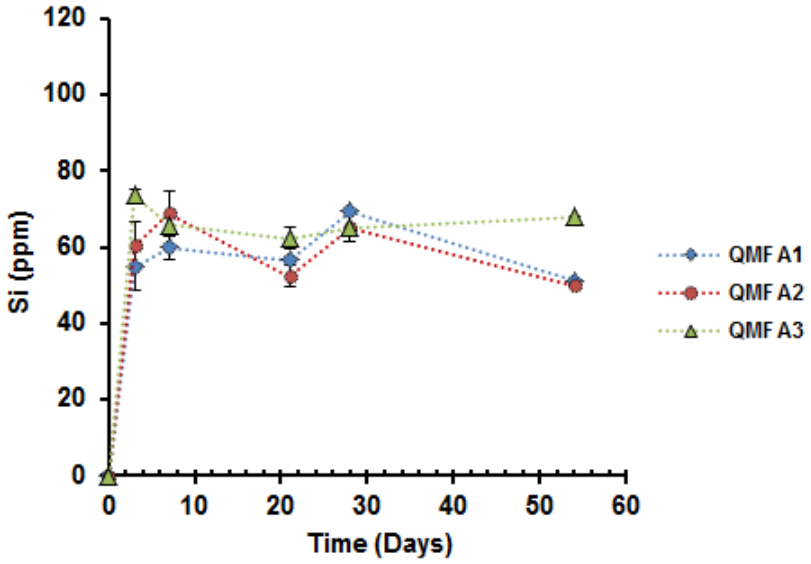

Figure 5.41: Elemental concentrations ± SD of silicon in Sα-MEM after the immersion of the glasses for up to 2 months (Lines are drawn as visual guides).

5.4.5 SEM results:

Figure (5.42) shows SEM micrographs of the surfaces of the bioactive glass powder after soaking in Sα-MEM for 7 days and 1 month. It can be noticed from the 7 days immersion micrographs Figures (5.42 a and b) that there is no appearance of the typical globular apatite-like structures on the surfaces during the period of the experiment. The surfaces are relatively smooth with no existence of the crystals agglomeration. However, after 1 month immersion the concentrations of the calcium and phosphorous on the surface of the glass particles show an increase in values to approximately 29.45 and 10.64 weight % as detected by the EDX analysis Table (5.1, page 160). This indicates the formation of the reaction layer which is the Ca-P rich layer on the surface of the glass powder.

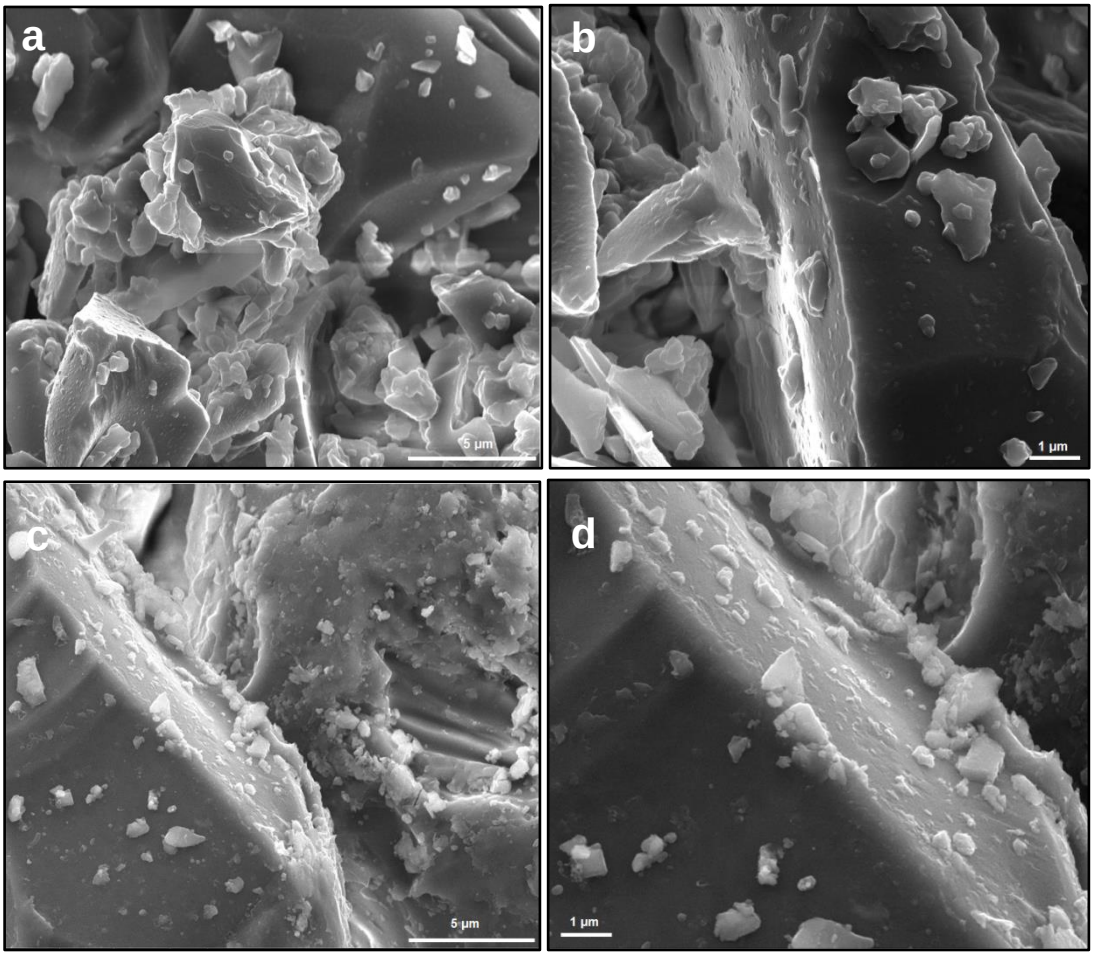

Figure 5.42: SEM micrographs of QMFA1 glass powder after immersion in Sα-MEM for a, b) 7 days (12000x and 24000x magnification) c, d) 1 month immersion (12000x and 24000x magnification). There is no appearance of the apatite-like structure on the surface of the glass particles.

5.5 Summary:

Glass composition has an important role in determining the glass bioactivity. The prepared glasses are immersed in four different solutions. These solutions are varied in their ions content, in addition to the serum protein which is added to the cell culture media. After immersion, the glasses cause a clear rise in the solutions pH as they release ions into the tested solutions. These ions are participating in the formation and crystallisation of the apatite layer. In Tris buffer the apatite formation

is detected after 3 h immersion while, in SBF the glasses start to form apatite after 24 h. In SFα-MEM, the formation of apatite is extensively delayed and it is identified after 21 days. However, the picture is completely different in the Sα-MEM where the glasses show limited evidence of apatite formation during the 2 months immersion. The apatite, which formed in these solutions, is much less obvious due to the different composition of the solutions. The apatite in Tris and SBF is predominantly FAP with minor proportion of carbonate substitution as can be seen from the ^{19}F NMR results. The asymmetric peak is related to the existence of the carbonate group in the lattice. In SFα-MEM, the apatite demonstrates the formation of carbonated B-type FAP, where the carbonate group is more dominant in the structure of this apatite. The SEM micrographs are consistent with the all findings where the shape of the formed apatite in the cell media is relatively cauliflower in shape, while in Tris and SBF the crystals are needle-like in nature. All glasses show the same trend in dissolution process in each medium, though QMFA3 glass shows earlier features of apatite formation than the other two glasses.

Chapter 6 Results and Discussion of Titanium Discs Study

6 Results and discussion of titanium discs study

Coating the titanium implants with bioactive glasses using grit blast technique depends on their ability to embed physically into the surface. This can potentially be related to the hardness of the glass particles. Investigating the glass ability to abrade the titanium surface and their successful retention within the surface is the primary aim of this chapter.

6.1 Powder flow rate results

The PFR is one of the effective parameters in controlling the cutting characteristics of the abrasive stream and determining the quality of abrasion (Banerjee and Watson, 2002, Banerjee et al., 2008). Therefore, it is important to measure the amount of particles output at every pressure parameter during the blasting process. This is to ensure a constant flow of the glass powder through the grit blast nozzle during the experiment time. Moreover, it can help in predicting the titanium removal from the surface.

The means and the SD of the glass PFR according to the propellant air pressure are illustrated in Figure (6.1). The results show that there is a small reduction in the PFR with increasing the air pressure for each glass composition. The difference is insignificant between all the groups within QMFA2 and QMFA3 compositions *(P≥0.05)* see appendix 1 (10.2). However, the PFR in QMFA1 at pressure 2 bars is around 2.11±0.14 g/min and this is significantly higher than that at pressure 4 bars. By comparing the three glass compositions at the same pressure variable, the results show that the flow rate is significantly higher in QMFA1 glass in comparison to the other two glasses at all pressures. However, the difference is insignificant between the QMFA2 and QMFA3 glasses at pressure 2 and 3 bars.

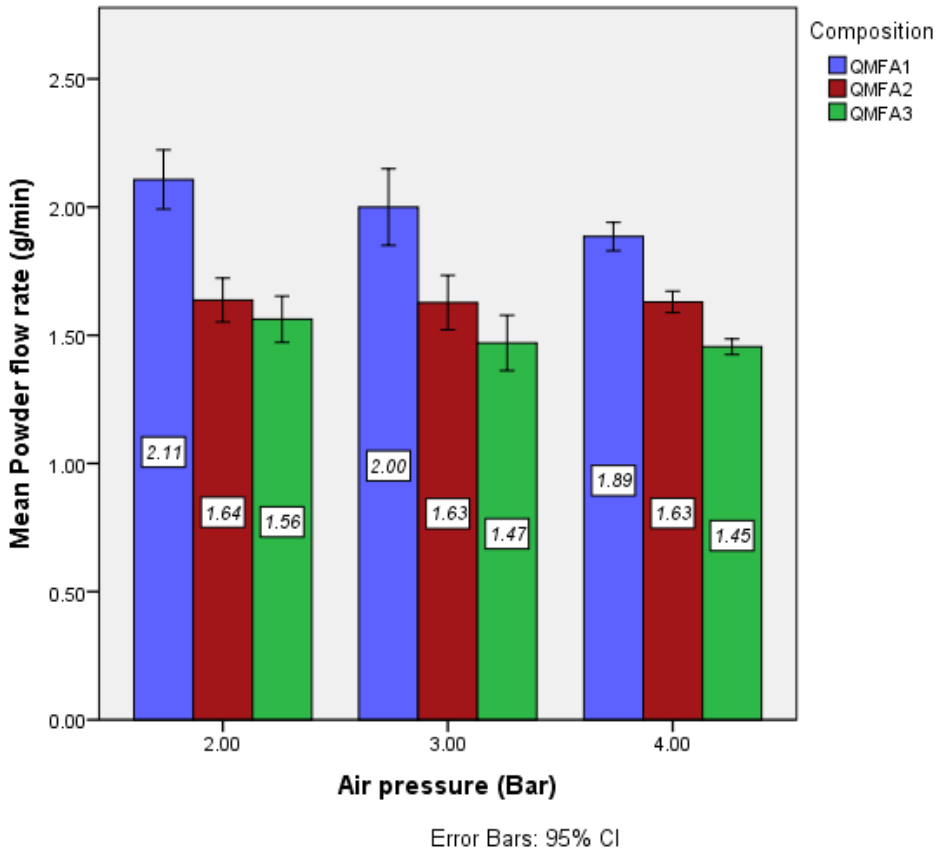

Figure 6.1: Mean ± SD (g/min) of the glass powder flow rates according to different propellant air pressures (feed rate dial was fixed at the middle setting).

From these results, it can be concluded that all the glass powders are flowing easily through the nozzle of the grit blast hand piece. This is due to the high flow rate values and the small standard deviation. The smooth powder stream output could be related to the particle size distribution of the glass powder. As mentioned earlier in Chapter 4 section 4.5, that the distribution pattern of the particle size was narrow in all glass compositions. The average particle size ranged between 58 and 127 μm and this gives rise to a smooth and consistent flow output. This is due to the absence of small particles in the glass powder, which can cause clogging of the powder stream. Moreover, the glass composition might have an effect on the PFR, as higher sodium content glasses are sensitive to the humid atmosphere and it can cause clogging in the powder output. Thus, the glass powders were subjected to high temperature drying at 120 ºC before sieving to ensure complete dryness.

Regarding the relation between the PFR and the propellant air pressure, this study shows that the PFR of the glass powders decreases with increasing the pressure. These results disagree with what had been reported by (Milly et al., 2014). They stated that the PFR of the 45S5 glass remained constant at different propellant pressures and this is related to the mode of mixing of the powder with the air stream. The Aquacut^{TM} air abrasion machine relies on the vibrational mode of mixing and this could not be affected by changing the air pressure. Although, the AquaCare unit is a new version of air abrasion machine designed by the same company (Velopex), different findings were obtained. This difference might be correlated to the shape of the glass particles. As the shape and size of the glass particles have a major effect on the cutting abilities of the powder stream and the flow rate (Horiguchi et al., 1998). The high air pressure might cause the particles to compete with each other during their passage through the narrow nozzle opening. These competitive forces result in fewer particles being emitted from the nozzle.

By decreasing the pressure dial of the machine less competitive forces are generated between the glass particles and this increases the field for the particles to pass. Therefore, the PFR increases by lowering the pressure dial of the machine.

Glass composition also shows a considerable effect on the PFR, where QMFA1 glass powder gives the highest PFR values at all pressures. The reason for this might be related to the powder density and compactness. As mentioned in Chapter 4 section 4.7 that the QMFA1 has the lowest powder compactness among the glasses. This means that there are large spaces between the glass particles and this may lead to an increase in the powder flow, whereas QMFA3 showed the highest compactness and lowest flow.

6.2 WLP results:

The cutting efficiency of the abrasive powder can be controlled by many parameters. These parameters determine the amount of material deposition on the surface and the amount of substrate removal (Paolinelis et al., 2008). The selected operating parameters in the study were sample-nozzle distance, substrate movement velocity and propellant air pressure. By modifying these parameters, it is possible to modify the surface of the titanium substrate and to control the amount of the glass deposition and the titanium abrasion. The novelty of this study is in designing new bioactive glasses which differ in their hardness and investigating the effect of glass hardness's on the abrasion and embedding characteristics.

The effect of each operating parameter on the abrasion efficiency and its subsequent relation to the dimension of the abraded trough and/or line and the surface roughness were all examined by the WLP.

All the statistics regarding this section are included in the appendix 1 (10.3). This is to provide easy and subsequent flow of information.

6.2.1 Effect of sample-nozzle distance on the abraded line width

Figure (6.2) shows the means and SD of the abraded line width as a function of the substrate-nozzle distance for all glass compositions. By changing this parameter intensive changes are clearly seen in the width of the abraded lines. The line width in QMFA1 glass abraded samples is significantly increased from 0.75±0.02 mm to 1.21±0.02 mm when the nozzle distance increased from 1 mm to 5 mm. The same profile is also seen with QMFA2 and QMFA3 glass abraded samples, but with width range between 0.78±0.01 mm and 1.31-1.30±0.03 mm respectively. This increase is both statistically and clinically significant *($p \leq 0.05$)* Figure (6.3). This result suggests that there is a relation between changing the distance of the substrate and the spread pattern of the glass particles on the sample surface.

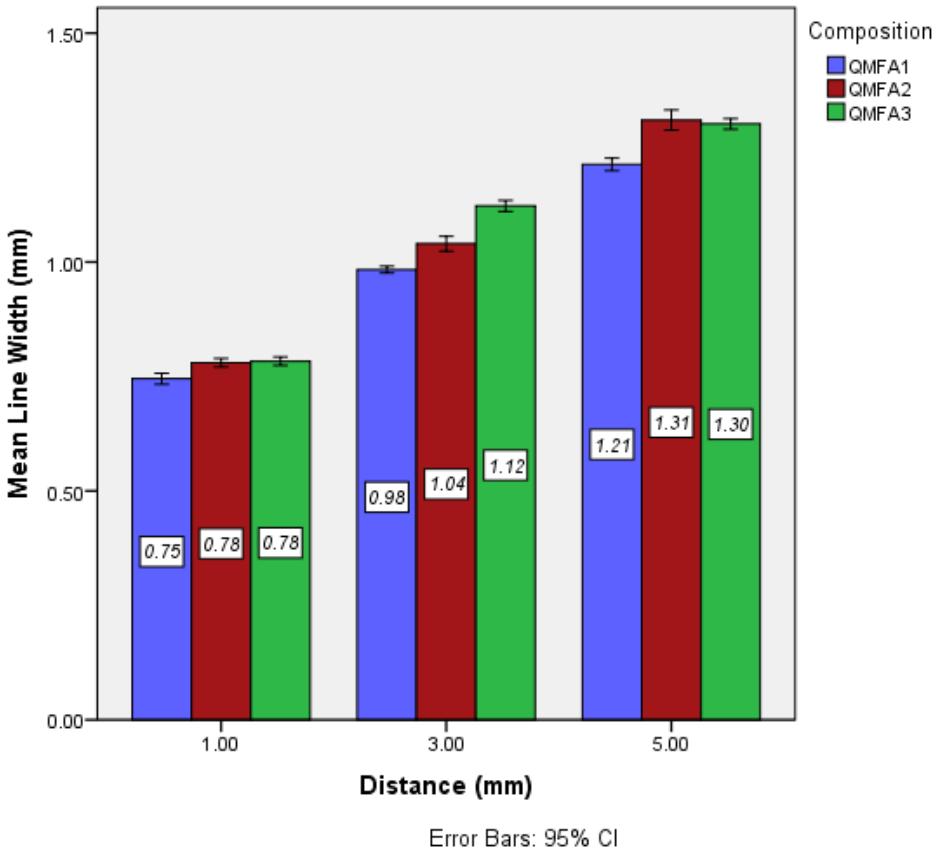

Figure 6.2: Mean ± SD of the abraded line width (mm) in QMFA1 (blue), QMFA2 (red) and QMFA3 (green) glass abraded samples with varying sample-nozzle distance.

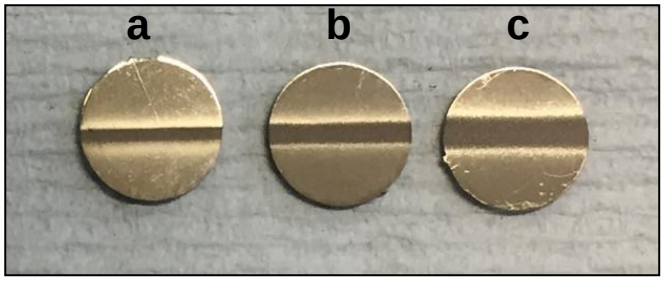

Figure 6.3: Image shows the spread pattern or the width of the abraded line by QMFA1 glass powder on the titanium discs at sample-nozzle distance a) 1 mm b) 3 mm c) 5 mm.

Figure (6.4) demonstrates that there is a proportional linear correlation between the distance and the abraded line width. The correlation coefficient (R^2) is around 0.976, 0.999 and 0.968 for QMFA1, QMFA2 and QMFA3 glass abraded discs respectively.

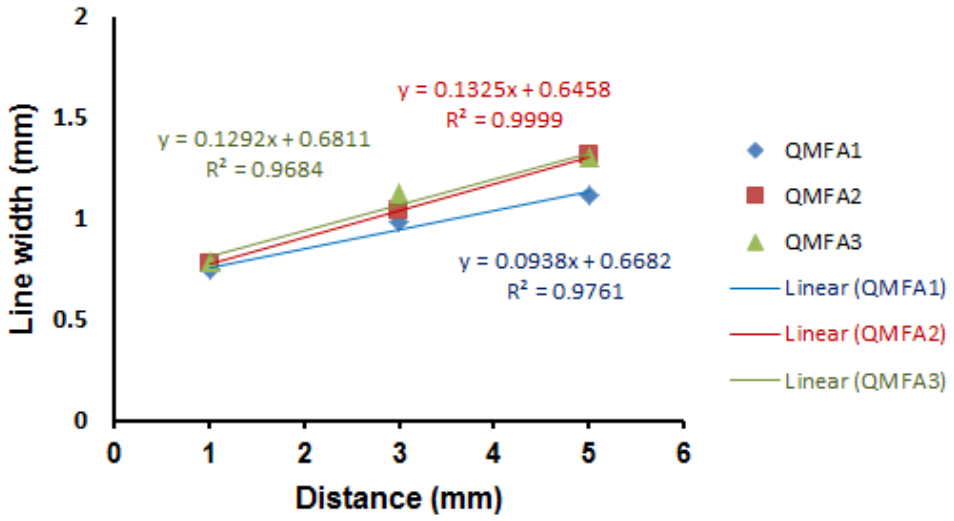

Figure 6.4: Graph shows the relation between the abraded line width (mm) and the distance parameter (mm) in all glass abraded compositions. The lines represent the linear regression for line width versus distance, R^2=0.976, 0.999 and 0.968 in QMFA1 (blue), QMFA2 (red) and QMFA3 (green) abraded samples respectively.

These findings agree with (Al-Ani, 2013) study, who found that the furthest distance forms a broad area of abrasion. However, the condition of samples preparation is totally different in both studies, the same outcome is observed. In this study, the samples prepared by dynamic abrasion method, while in Al-Ani study a static abrasion condition was used. Furthermore, the particle size and the powder composition are different in both studies.

The reason for the wide abrasion might be related to the divergence of the particles from the nozzle opening. The spread pattern of the powder from the nozzle of the sandblasting machine is cone in shape. The diameter of this cone shape will increase with the far nozzle distance. This means that the particles will scatter over a wider area (Ishikawa et al., 1997) Figure (6.5).

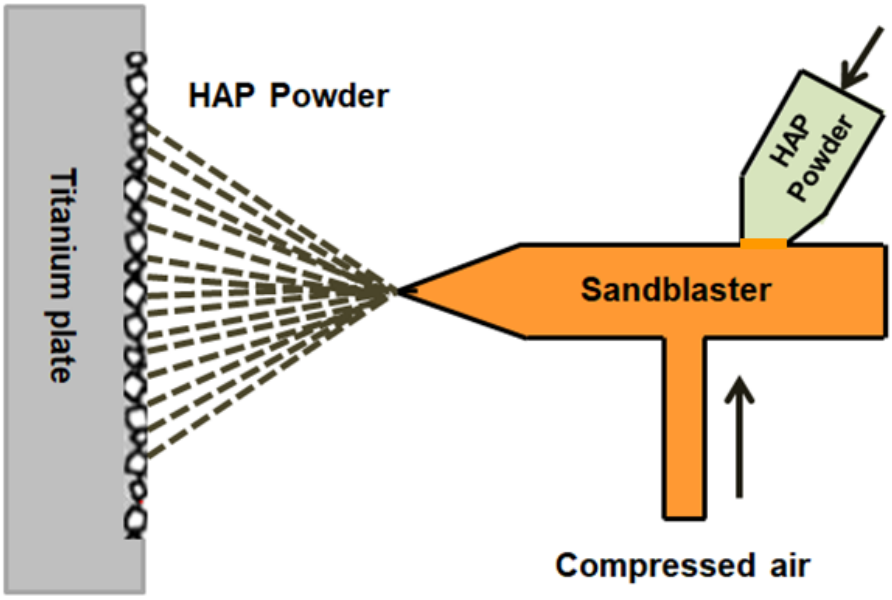

Figure 6.5: Schematic diagram illustrates the shape of the blasting pattern of the particles on the titanium surface by sandblaster (Ishikawa et al., 1997).

However, the spread pattern of the powder by using air abrasion method is different from that of the sandblasting technique. The spread pattern in the former technique is more focussed and well defined in comparison to the latter method (Black, 1945). To confirm this finding, the relation between the cone diameter and the nozzle distance were plotted Figure (6.6). We assumed that the cone diameter at distance 0 mm is 0.6 mm, which is the actual nozzle diameter. The correlation coefficient (R^2) of this relation is 0.994 and this indicates the proportional linear relationship between the line width and the distance. The results of this study agree with what have been stated in the literature. However, the findings from the literature all related to human teeth and not on titanium substrate, but the same outcome is detected. The width of the cavity preparation in primary teeth by using the air abrasion is affected by the diameter of the nozzle and the distance from the nozzle. The width of the cavity showed a significant increase when the distance from the tooth surface increased from 2 mm to 5 mm (Peruchi et al., 2002).

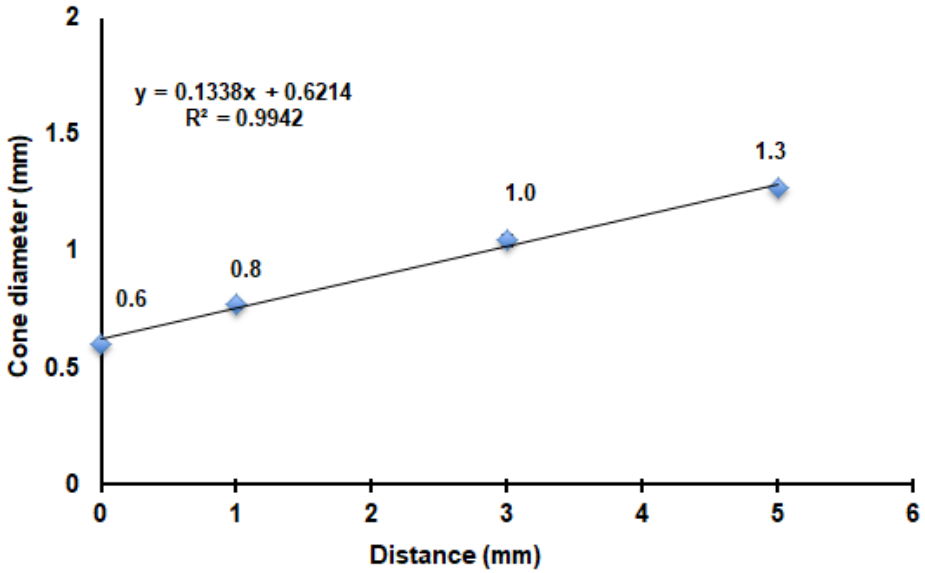

Figure 6.6: Graph shows the relation between the average cone diameter of the abrasion pattern in all glasses abraded samples (mm) and the sample-nozzle distance (mm). The line represents the linear regression for cone diameter versus distance, R^2=0.994.

Regarding the glass composition and its effect on the abraded line width, it can be seen that the QMFA1 abraded samples demonstrate the lowest values of line width in comparison to QMFA2 and QMFA3 abraded discs. This indicates that the scattering pattern of the harder glass (QMFA3) is wider and more divergent in comparison to the others. This difference is statistically significant with *($p \leq 0.05$)*, but it can be considered clinically as small and negligible. This is because of the extremely small difference between all the groups, in which the differences are less than 0.1 mm. Therefore, practically this small difference cannot be critical in the abrasion process regarding the scattering patterns of the particles.

6.2.2 Effect of sample-nozzle distance on the abraded line depth

Besides measuring the width of the abraded line, it is essential to quantify the depth of that line. This is because of the importance of this scale in determining the abrasivity of the glass particles. Depth measurement can give information whether the designed glass powder is abrasive and hard enough to remove material from the titanium surface.

The hardness of the titanium discs is around 3.9±0.2 GPa, as measured by Zwick/Roell hardness test machine. This value is lower than the hardness values of the designed glasses. The glass hardness is around 4.2 GPa, 4.6 GPa and 5.1 GPa for QMFA1, QMFA2 and QMFA3 respectively. Thus, from these measurements it can be hypothesised that the glasses are able to abrade the surface of the titanium discs.

In Figure (6.7) it can be seen that the means of the line depth in all glass abraded groups are decreasing significantly with increasing the nozzle distance. The mean line depth in QMFA1 glass abraded discs is decreasing from 14.70±0.61 μm to 12.74±1.07 μm when increasing the sample-nozzle distance from 1 mm to 5 mm. QMFA2 and QMFA3 abraded discs also demonstrated the same trend, but with lower values in comparison to QMFA1 samples. The means of the line depth are around 12.98±0.74 μm and 12.49±0.87 μm and 12.40±0.85 μm and 11.22±0.48 μm for QMFA2 and QMFA3 abraded discs at distances 1 and 5 mm respectively. Additionally, there is a correlation between the mean abraded line depth and the nozzle distance. The coefficient values of the relation are around 0.851, 0.998 and 0.810 in QMFA1 QMFA2 and QMFA3 abraded discs respectively Figure (6.8). This indicates the linear relationship between this operating parameter and the extent of the abrasion.

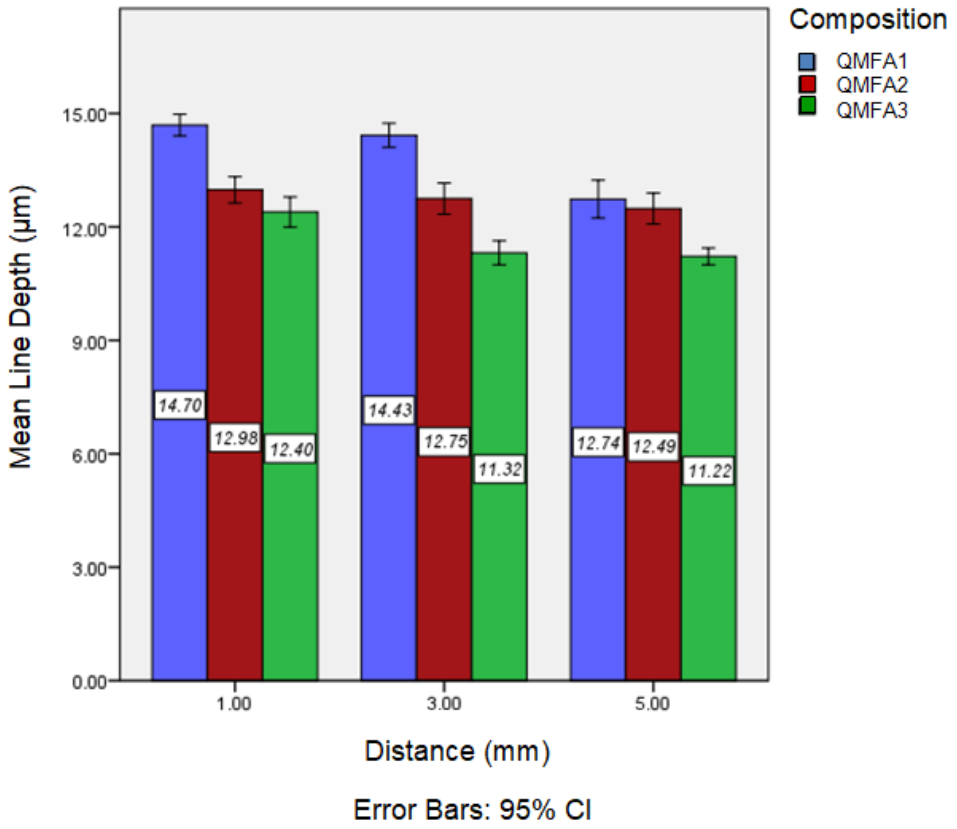

Figure 6.7: Mean ± SD of the abraded line depth (µm) in QMFA1 (blue), QMFA2 (red) and QMFA3 (green) glass abraded samples with varying sample-nozzle distance.

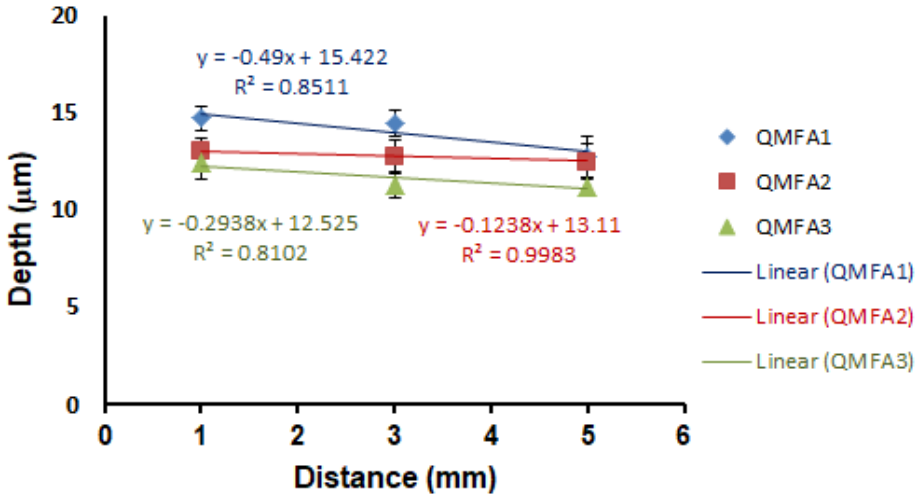

Figure 6.8: Graph demonstrates the relation between the mean abraded line depth (µm) and the nozzle distance parameter (mm) in all glass abraded compositions. The lines represent the linear regression for line depth versus distance, R^2=0.851, 0.998 and 0.810 in QMFA1 (blue), QMFA2 (red) and QMFA3 (green) abraded samples respectively.

The reason for depth reduction when increasing the distance parameter might be related to the particles velocity. According to the principle of the grit blast method, the powder particles are carried by a stream of compressed air. This particles stream bombards the substrate surface and creates an abrasion or a deformation to the target surface. The particles will obtain a high velocity when leaving the abrasion nozzle. This velocity will decelerate when the target distance increases. Therefore, the cutting efficiency of the particles will decrease. This is due to the lower ability of the particles to further penetrate into the substrate surface. Thus, a consequent reduction in depth values is recorded. The results of this study agree with (Bailey and Phillips, 1950), who found that the particles cutting efficiency decreases with increasing the distance from the tooth surface. Moreover, the same findings are also seen by (Al-Ani, 2013), but with strontium containing glass composition of high hardness. Some studies, relate this reduction to the spread pattern of the powder particles (White and Eakle, 2000). The wider the spread pattern of the particles the less their cutting efficiency and this is consistent with our results regarding the abraded line width. The wide spread pattern will reduce the impact of the particles on the surface, as the force is going to be distributed over a wide area. This is true because it agrees with the cross sectional view results of the abraded line. The abrasion pattern of the substrate surface at distance 1 mm is relatively sharp and narrow Figure (6.9 a). However, the profile of the abrasion is becoming gradually wider and with a less well-defined border when the distance increases to 3 mm and 5 mm Figure (6.9 b and c).

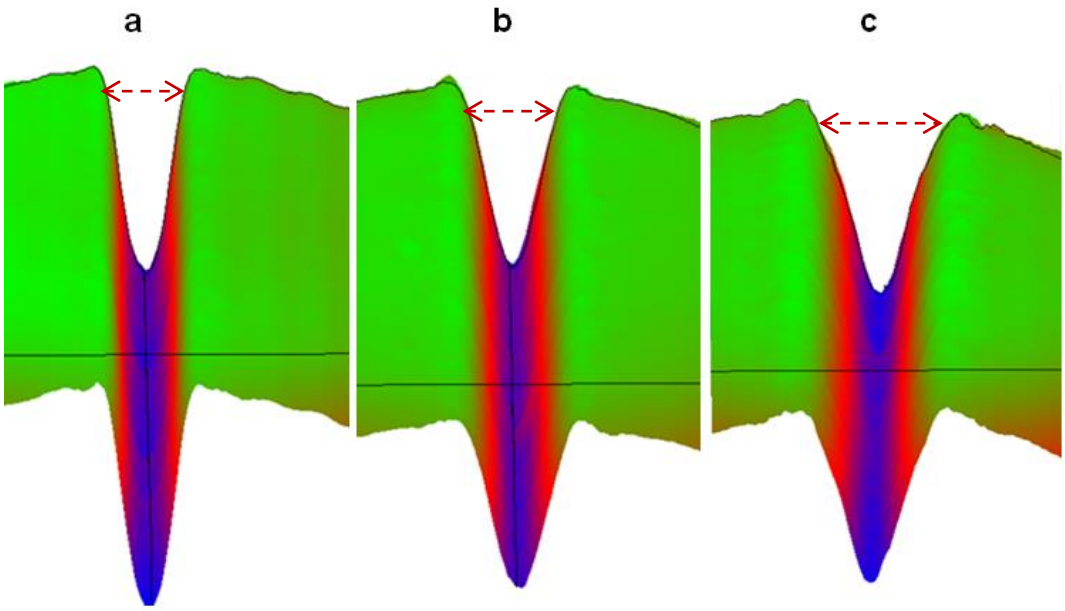

Figure 6.9: 2-D profile showing the cross section of the abraded line in QMFA1 samples and its relation to the nozzle distance a) at distance 1mm, the cutting profile is narrow and well-defined b) at distance 3mm, the abrasion is wider than distance 1mm c) at distance 5mm, the profile of the abrasion are wider at the top with a poorly defined margin.

Regarding the change in glass composition and its relation to the depth of the abraded line, the results show that the difference in glass hardness is effective in controlling the extent of material removal from the titanium surface. QMFA1 glass powder produces the highest depth at all distances followed by QMFA2 and QMFA3. The difference between the three glass compositions at each distance is statistically significant with *($P \leq 0.001$)*. This finding indicates that the glass with the lowest hardness is abrading more from the titanium surface. However, this finding is counter intuitive and this is due to the fact that the harder the material the more the abrasion of the substrate surface is expected. This could be due to the kinetic energy of the particles. Modifying the mass of the particles will modify their kinetic energy and this can cause either decrease or increase in the particles impact on the target surface. All the designed glasses obtained the same particle size and

distribution profiles. However, the composition is different where the calcium oxide is substituted by the sodium oxide. The atomic mass of the calcium is about 40 and for the sodium the atomic mass is about 23. In total, the atomic mass of QMFA1 glass powder is the highest among the other glasses followed by QMFA2 and QMFA3. Thus, according to the equation (6.1) the QMFA1 particles will have the highest kinetic energy and will produce the highest abraded line depth.

Equation 6.1

$$Kinetic\ energy = \frac{1}{2} mass \times Velocity^2$$

However, there is another fact about the grit blast process which is the concept of embedding the particles into the substrate surface besides its abrasion. From this concept the idea of using the bioactive glass in the grit blast technique was created by (Koller et al., 2007). When the abrasive stream strikes the target surface, the glass particles will embed into that surface. The exposed part of the embedded particles will be subjected to a drastic cleavage, when the second line particles hit them. Therefore, this embedded part will protect the substrate surface from further abrasion Figure (6.10). This feature suggests that QMFA3 composition has the ability to embed deeply into the titanium surface thus protecting it from further abrasion.

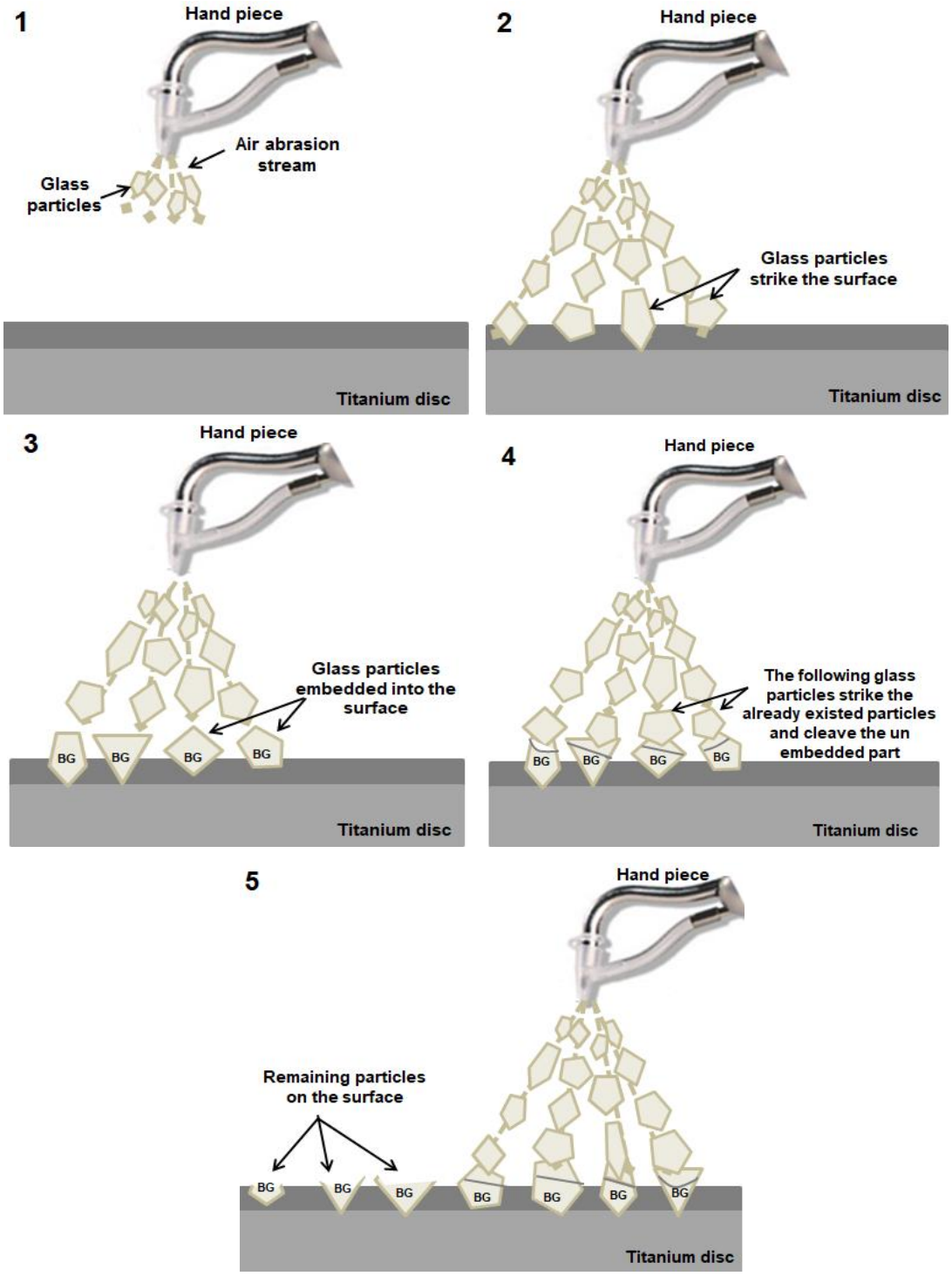

Figure 6.10: Schematic diagram showing the sequence of the abrasion process on the titanium surface and the cleavage of the embedded particles by the second line particles.

Regarding this suggestion it can be seen that the cross section of the abrasion is different between the three glasses Figure (6.11). This difference is more clearly seen at distance 1 mm than the other distances. The cross section of the abraded line, when QMFA1 glass powder was used, appears narrow with a pointed bottom Figure (6.11 a). While, in QMFA3 abraded samples the profile of the abrasion is more U-shape and with wide rounded bottom Figure (6.11 b). QMFA2 powder produces a profile in between. This difference is somehow small, but it might suggest that the particles are embedding more in case of the QMFA3 abraded samples, as the bottom of the abraded line is with round cut profile.

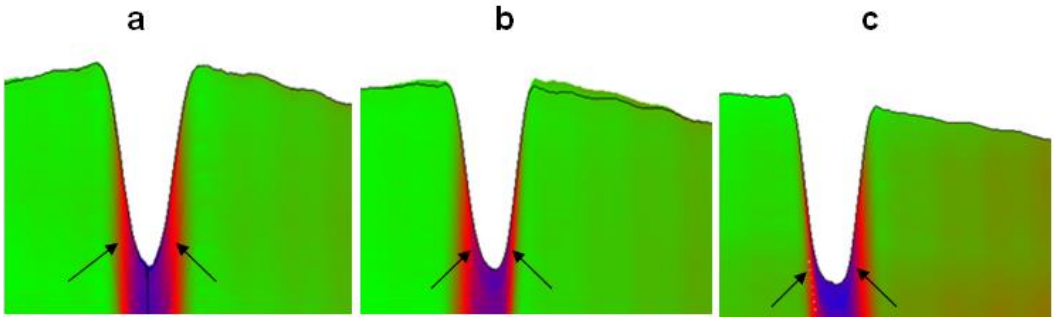

Figure 6.11: 2-D profile showing the cross section of the abraded line at distance 1 mm in a) QMFA1 abraded sample b) QMFA2 abraded sample c) QMFA3 abraded sample. The bottom of the abraded line is becoming more rounded with QMFA3 abraded samples.

6.2.3 Effect of sample-nozzle distance on the titanium removal volume

Measuring the volume of the titanium loss is substantially associated with the depth measurements. From both measurements, it is possible to evaluate the glass efficiency in abrading the surface of the titanium discs in the association with the changing in the operating parameters.

The means and SD of the abraded line volume according to the substrate-nozzle distances are demonstrated in Figure (6.12). From this bar chart, it can be clearly seen that in each glass composition there is a small reduction in the amount of volume removed when increasing the distance from 1 mm to 5 mm. This reduction is statistically significant between the tested groups of the same composition. These results are consistent with the line depth measurements. There is an inverse relationship between the glass abrasion efficiency and the sample-nozzle distance. The further the distance from the substrate surface the less the material loss from the sample and the less the powder abrasion efficiency. This agrees with (Bailey and Phillips, 1950), who found that the enamel loss is higher with the closer distance. However, an opposite relation was found by (Paolinelis et al., 2009, Milly et al., 2014), who reported that the volume of the substrate removal is increasing with increasing the nozzle distance. The first study used alumina as an abrasive agent and the tooth enamel as a substrate material. While Milly et al, used both alumina and 45S5 glass as abrasive agents and Macor® as a substrate material. Moreover, the measurement methodologies in the previous studies are different to what have been used in the current study. Thus, it can be concluded that due to the presence of many differences between the previous studies and the current study making comparisons relatively difficult to perform.

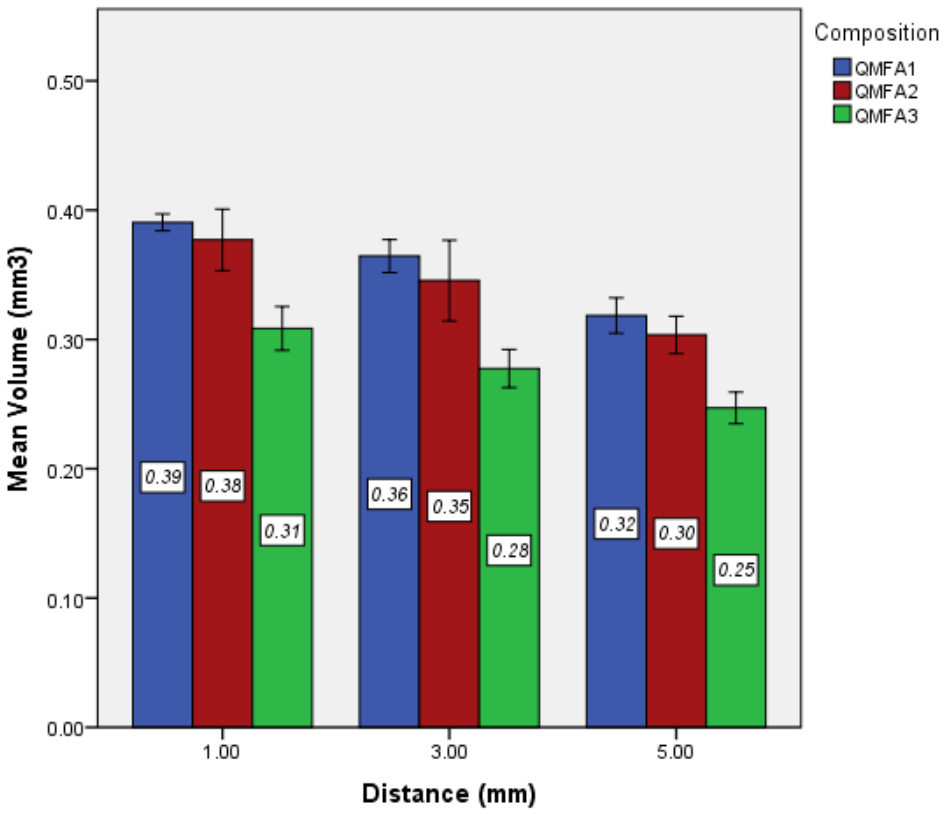

Figure 6.12: Mean ± SD of the abraded line volume (mm^3) in QMFA1 (blue), QMFA2 (red) and QMFA3 (green) glass abraded samples with varying sample-nozzle distance.

The volume of titanium removal is also affected by changing the composition of the glass. Similar to what has been reported in the abraded line depth measurements. The glass of the lowest hardness produces the highest volume removal values. This finding is clearly seen at all sample-nozzle distances. The volume of titanium lost in the QMFA1 glass abraded samples is ranged between 0.39±0.02 mm^3 and 0.32±0.03 mm^3 at distance 1 mm and 5 mm respectively. While, QMFA3 glass powder produces the lowest values of titanium volume removal. The measurement values are between 0.31±0.05 mm^3 and 0.28±0.25 mm^3. These differences are statistically significantly between both QMFA1 and QMFA2 glass abraded samples with the QMFA3 glass abraded groups at all distances with *($p \leq 0.001$)*. While, there is an insignificant difference between QMFA1 and QMFA2 glass abraded groups at all nozzle distances *($p \geq 0.05$)*.

These findings together with the abraded line depth results suggest the possibility of the presence of two processes, which are the abrasion process and the embedding process. The incidence of both processes might take place at the same time of the coating procedure. Therefore, the recorded measurements are not only reflecting the results of the abrasion process, but it might reflect the results of the embedding process. This hypothetical suggestion could be confirmed by measuring the surface coverage of the titanium with the glass particles *i.e.* investigating the coverage of the particles embedded in the titanium surface after the abrasion.

6.2.4 Effect of sample movement velocity on the abraded line width, depth and titanium removal volume

The velocity of the moving stage, where the titanium samples were placed, is the second operating parameter in the abrasion process. This parameter represents the exposure time at which the sample will be subjected to the abrasive particles. It can be used in controlling the dimension of the abraded line and in modifying the abrasion rate of the abrasive stream. Thus, from this parameter we can estimate the minimum time, which is effective in the abrasion and the embedding processes.

Figure (6.13) illustrates the mean ± SD of the abraded line width by changing the substrate velocity with the three glasses. Generally, increasing the velocity of the moving stage, results in a decrease in the width of the abraded line in all samples. The measured width in the QMFA1 abraded samples is decreasing from 1.04±0.02 mm at velocity 0.25 mm/sec to 0.86±0.01 mm when the velocity increased to 1 mm/sec. The same profile is also demonstrated with QMFA2 and QMFA3 abraded samples, but with slightly higher abrasion width values. The differences between the groups in each glass composition are statistically significant with *($p \leq 0.0001$)*. Also, this difference is clear and effective clinically.

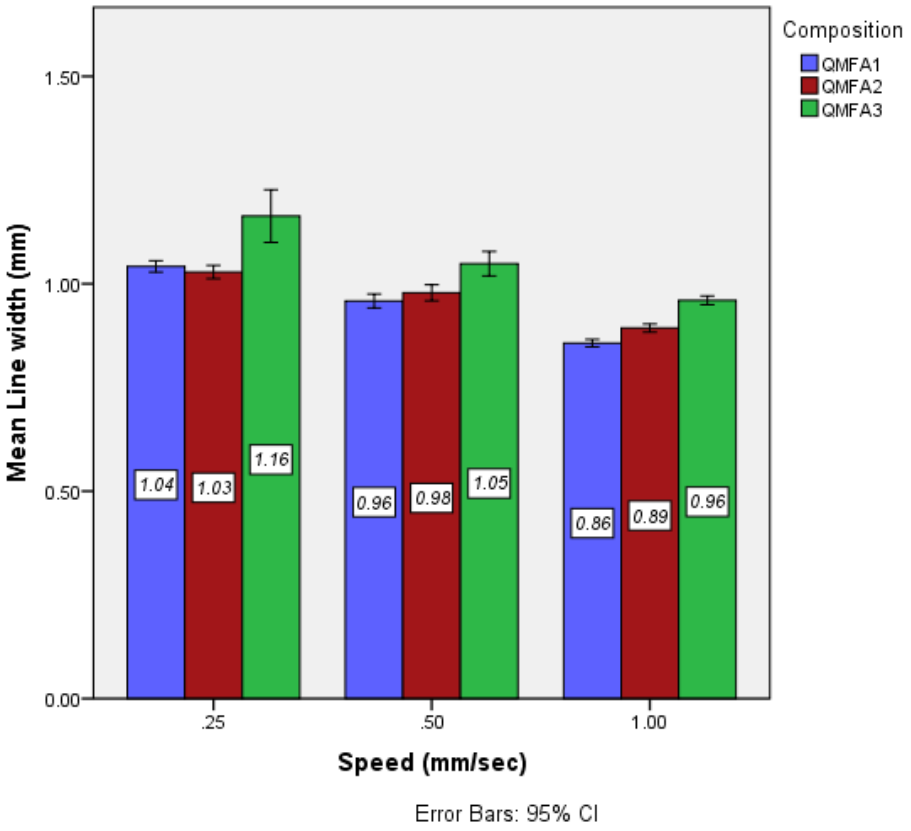

Figure 6.13: Mean ± SD of the abraded line width (mm) in QMFA1 (blue), QMFA2 (red) and QMFA3 (green) glass abraded with varying sample movement velocity.

The spread pattern of the particles is wider in samples prepared with the slowest velocity in comparison to that of the same composition, but with highest substrate velocity Figure (6.14). This suggests that the more the time the samples are subjected to the abrasive particles, the wider is the spread pattern of the particles on the surfaces. This is due to the sample surface exposure to large number of particles per second and this can lead to a wide spread of the particles on the target surface.

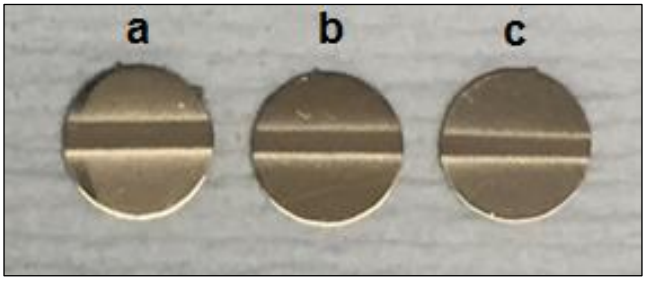

Figure 6.14: Image shows the spread pattern or the width of the abraded line by QMFA1 glass powder on the titanium discs at sample movement velocity of a) 0.25 mm/sec b) 0.5 mm/sec c) 1 mm/sec.

The relationship between this operating parameter and the line width is an inverse linear relationship Figure (6.15). The R^2 of this correlation is around 0.982, 0.998 and 0.931 for QMFA1, QMFA2 and QMFA3 glass abraded discs respectively. This indicates the effectiveness of this parameter on determining the spread pattern of the glass particles. The higher the advancement rate, the lower the width of the abrade line across the sample surface.

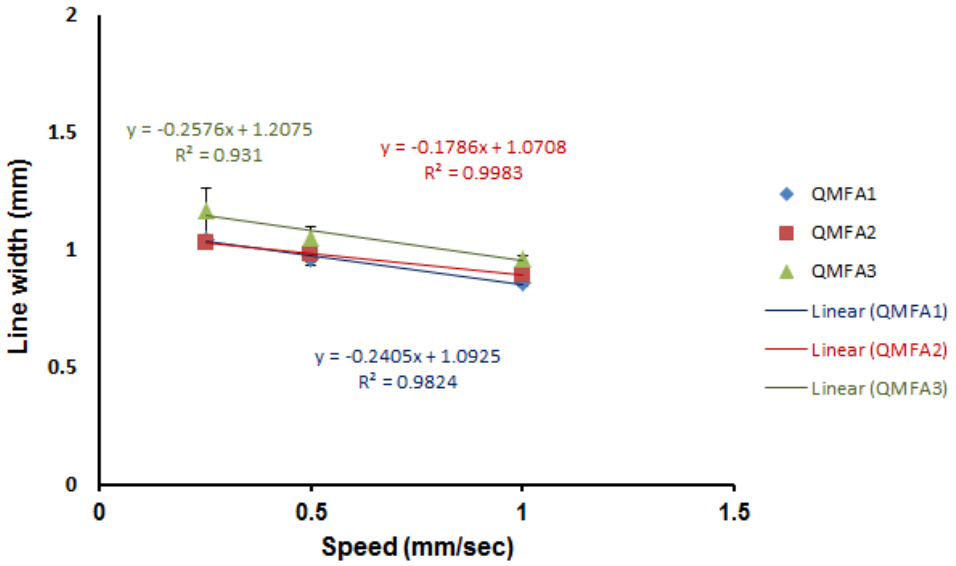

Figure 6.15: Graph shows the relation between the abraded line width (mm) and the velocity of the moving stage (mm/sec) in all glass abraded compositions. The lines represent the linear regression for line width versus velocity, R^2=0.982, 0.998 and 0.931 in QMFA1 (blue), QMFA2 (red) and QMFA3 (green) abraded samples respectively.

Regarding the change in glass composition and its relation to the abraded line width, QMFA3 produces a wider width at all velocities in comparison to the other glasses. The width values of this composition at stage velocity 0.25 mm/sec and 1 mm/sec are 1.16±0.10 mm and 0.96±0.02 mm respectively. This wider width might be related to the difference in the nature of the particles abrasivity, as well as their embedding abilities. QMFA3 particles were suggested to embed more and spread widely in the titanium surface in all abrasion conditions. The difference between the compositions is statistically significant, but not probably clinically relevant. Therefore, from this finding it can be suggested that the change in glass composition at a fixed exposure time has no critical effect regarding the width of the abraded area.

The effect of the sample velocity and its relation to the abraded line depth and the amount of titanium removal were also investigated. Figures (6.16) and (6.17) show the mean ± SD of the abraded line depth and volume by changing the apparatus velocity for all composition coatings. The results show that there is a massive decrease in both measurements with increasing the velocity of the moving stage in all samples.

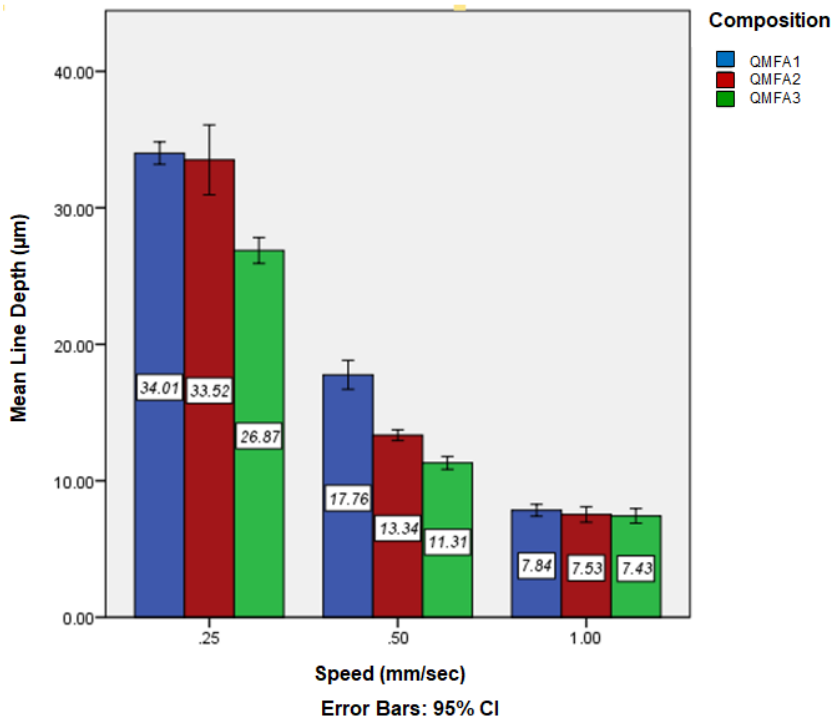

Figure 6.16: Mean ± SD of the abraded line depth (µm) in QMFA1 (blue), QMFA2 (red) and QMFA3 (green) glass abraded samples with varying sample movement velocity.

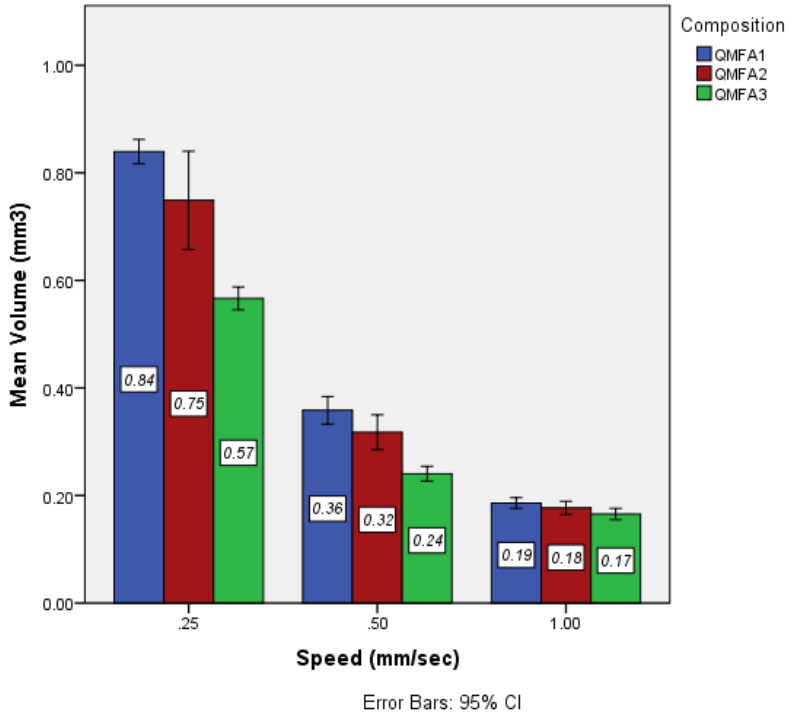

Figure 6.17: Mean ± SD of the abraded line volume (mm^3) in QMFA1 (blue), QMFA2 (red) and QMFA3 (green) glass abraded samples with varying sample movement velocity.

The longer the time the sample is exposed to the abrasive particles, the deeper the depth of the abraded line produced and the more titanium removed from the surface. Increasing the velocity to 1 mm/sec shows a significant reduction in both line depth and volume and the values are nearly quarter the values of the samples prepared at velocity 0.25 mm/sec stage velocity. This might be related to the fewer number of particles impacting the surface of the titanium discs per unit time. Therefore, it can be suggested that less particles are embedding into the sample surface in case of fast advancement rate.

Moreover, these findings indicate that there is an inverse relationship between the velocity parameter and both measurements, as can be seen in Figure (6.18). This relation is not linear, but the effect is quite clear and massive. This low R^2 value might suggest that there is an inconsistent loss in the amount of material in relation to the time of the sample exposure. Again QMFA1 glass produces the highest depth and volume removal followed by QMFA2 and QMFA3 at all velocity values. The differences between the glass compositions are insignificant specifically at velocity value of 1 mm/sec. This insignificance might be due to the short time of the sample exposure to the particles in which the effect is becoming less clear in comparison to the longer time. The difference in the glass hardness is clearly detected at the slowest velocity and this effect is reduced with decreasing the time for the sample abrasion.

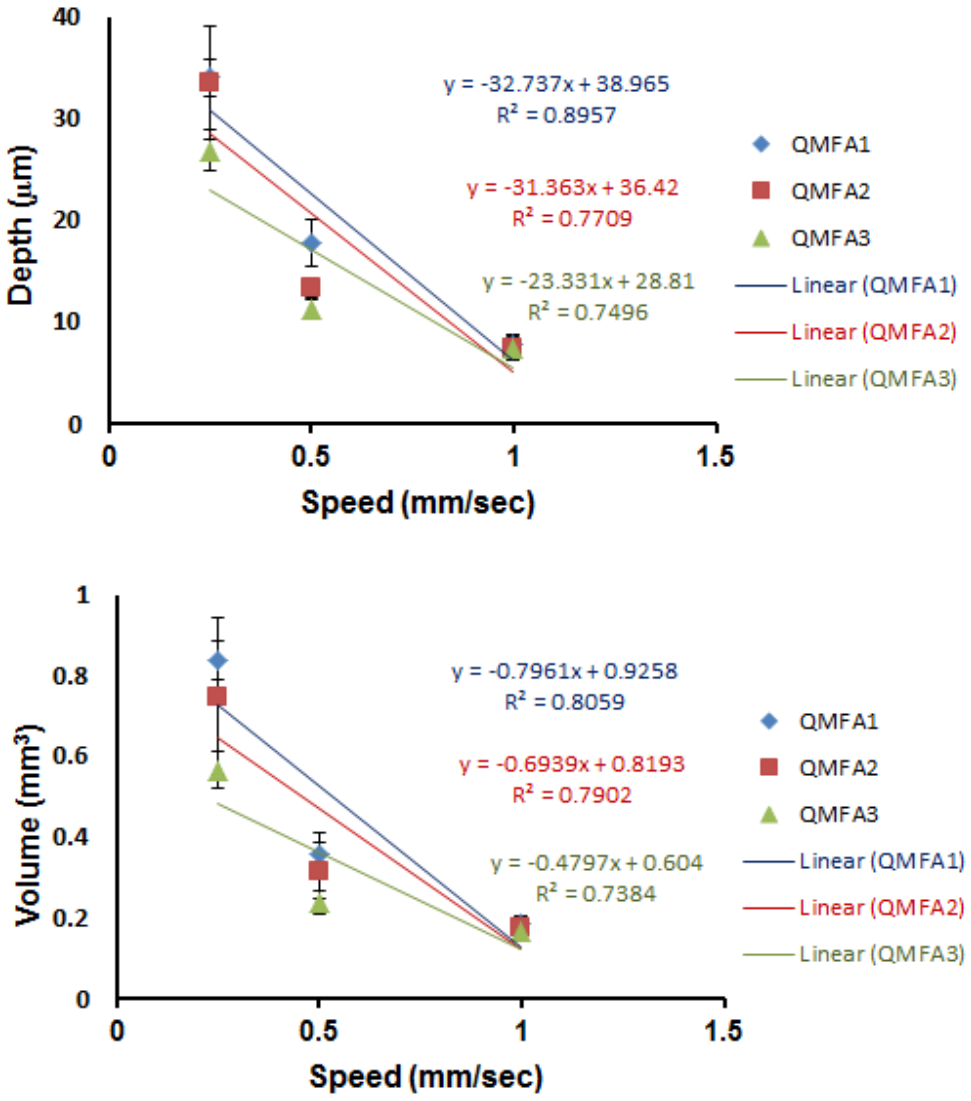

Figure 6.18: Graphs show the relation between the abraded line depth (µm) and line volume (mm^3) with the velocity of the moving stage (mm/sec) in all glass abraded compositions. The lines represent the linear regression for line depth and volume versus velocity.

From these results, it can be indicated that the substrate velocity is clinically effective in controlling the extent of titanium removal and determining the abrasion dimension. This finding disagrees with what has been reported in the literature, in which it's been stated that the time has no effect in determining the dimension of the abraded area. The difference in the amount of enamel loss by increasing the time of exposure from 5 to 15 min is small and not effective as reported by (Bailey and Phillips, 1950).

Other authors stated that the change in time is less effective than the change in distance on determining the width and depth of the cavity preparation in human teeth (Peruchi et al., 2002). Both studies were performed on human enamel unlike this study which accomplished on the titanium of fixed hardness. Additionally, the operating distances in those previous studies were greater than 5 mm. Therefore, the effect of time is less clear on the cutting rate of the abrasive material. Other studies stated that the increase in the advancement rate leads to an increase in the amount of abrasion rate (Paolinelis et al., 2009). This result is opposite to what have been found in this study, in which the decrease in exposure time leads to a less extent of material removal and lower preparation dimensions.

6.2.5 Effect of propellant air pressure on the abraded line width, depth and titanium removal volume

The particles abrasion ability depends on their kinetic energy and their travelling velocities. These two factors can be controlled by the applied air pressure, the size and the mass of the particles, the distance of the abrasion and finally on the diameter of the grit blast nozzle (White and Eakle, 2000). Therefore, the effect of the propellant pressure on the degree of particles impact on the target surface was investigated.

Figure (6.19) shows the effect of the pressure on the width of the abraded line in all glass composition abraded discs. The increase in the pressure dial of the grit blast machine results in a minute increase in the width of the abraded line. The mean line width of the QMFA1 abraded discs is increasing from 0.88±0.02 mm to 0.95±0.02 mm when the air pressure dial increases from 2 bars to 4 bars. The same trend is also seen with the other two composition abraded discs.

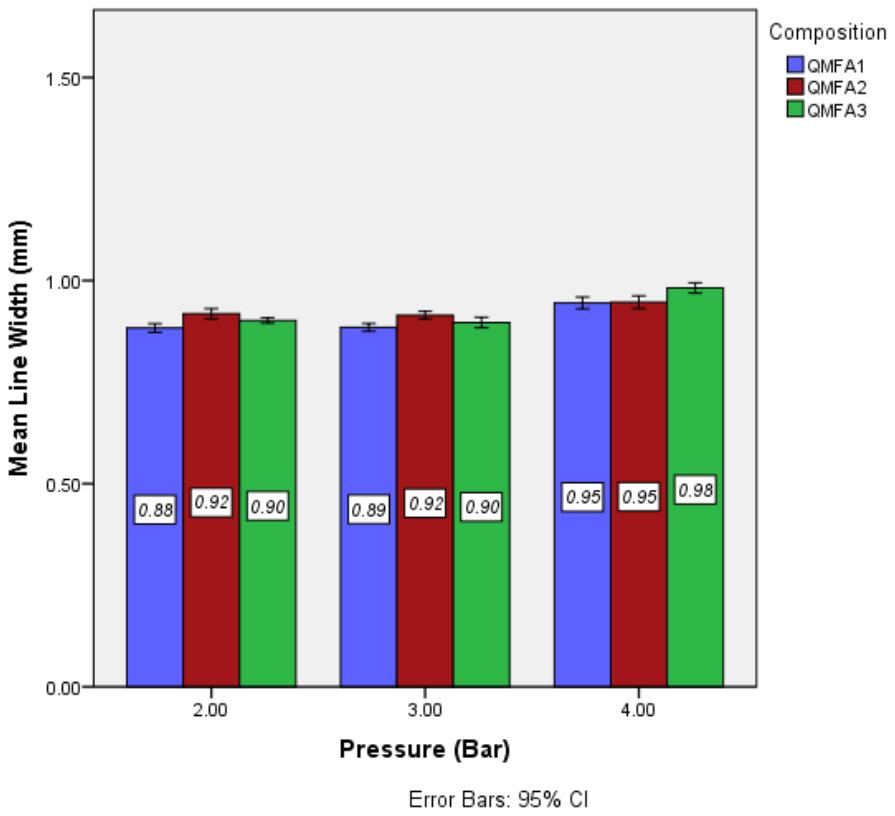

Figure 6.19: Mean ± SD of the abraded line width (mm) in QMFA1 (blue), QMFA2 (red) and QMFA3 (green) glass abraded samples with varying air pressure.

The difference between the tested groups of the same composition is statistically significant, but it is not clinically relevant. This suggests that the air pressure has an unclear effect regarding the abraded line width. The correlation coefficient (R^2) value of this relation is quite small and it is around 0.770, 0.662 and 0.703 for QMFA1, QMFA2 and QMFA3 glass abraded discs respectively. This small coefficient values indicates that this parameter has less effect on the spread of the particles. The spread pattern is nearly the same at all pressure values and it is less affected by changing the velocity of the particles Figure (6.20). The same finding is also seen when changing the composition of the glass powder. However, statistically there is a difference between the groups at 2 and 3 bars with those of the higher pressure 4 bars. Clinically, the spread pattern of the particles across the sample surface is nearly similar.

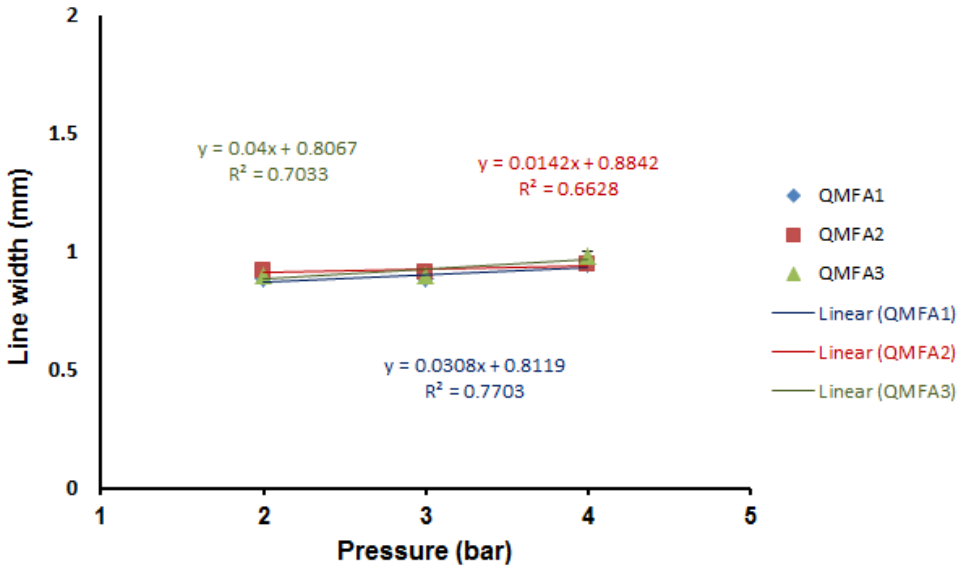

Figure 6.20: Graph shows the relation between the abraded line width (mm) and the air pressure (bar) in all glass abraded compositions. The lines represent the linear regression for line width versus pressure, R^2=0.770, 0.662 and 0.703 in QMFA1 (blue), QMFA2 (red) and QMFA3 (green) abraded samples respectively.

The effect of the air pressure is more clear and effective on the abraded line depth and the extent of titanium removal. In all compositions, the increase in the pressure causes an increase in both depth and volume measurements Figure (6.21) and Figure (6.22). A large amount of material was removed from the titanium surface when the pressure dial increased from 2 bars to 4 bars. The range of the line depth and volume in QMFA1 glass abraded discs, when increasing the pressure from 2 to 4 bars, are between 7.57±0.40 μm and 15.76±2.96 μm and between 0.17±0.01 mm^3 and 0.37±0.04 mm^3 respectively. This range is significantly higher than the range of the other glass composition groups. QMFA3 produces the smallest values in both measurements among the other compositions. The depth ranges between 4.79±0.38 μm and 13.83±2.27 μm at 2 and 4 bars respectively. While, the volume removal ranges between 0.13±0.01 mm^3 and 0.30±0.04 mm^3 at the same pressure dials.

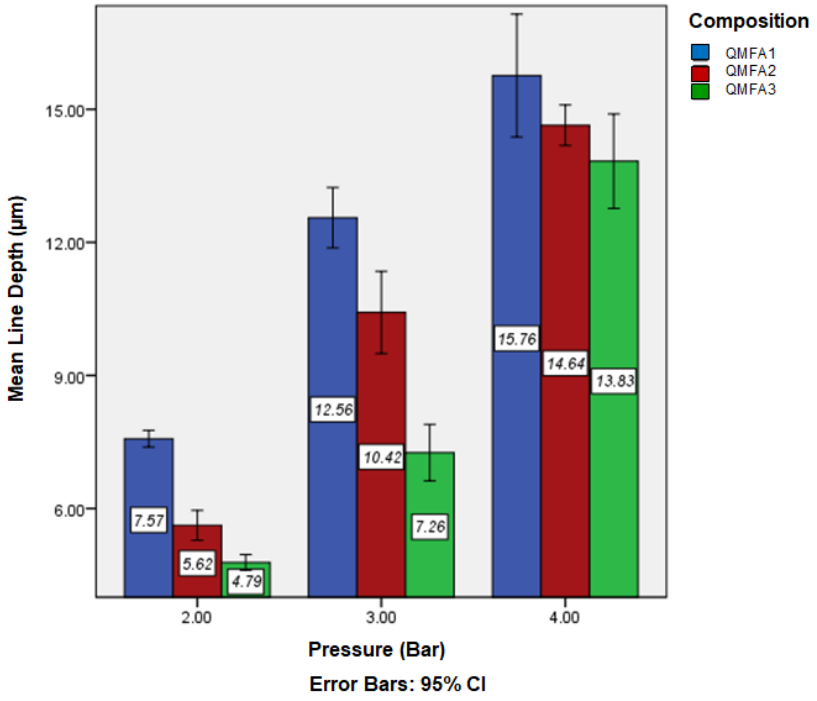

Figure 6.21: Mean ± SD of the abraded line depth (µm) in QMFA1 (blue), QMFA2 (red) and QMFA3 (green) glass abraded samples with varying air pressure.

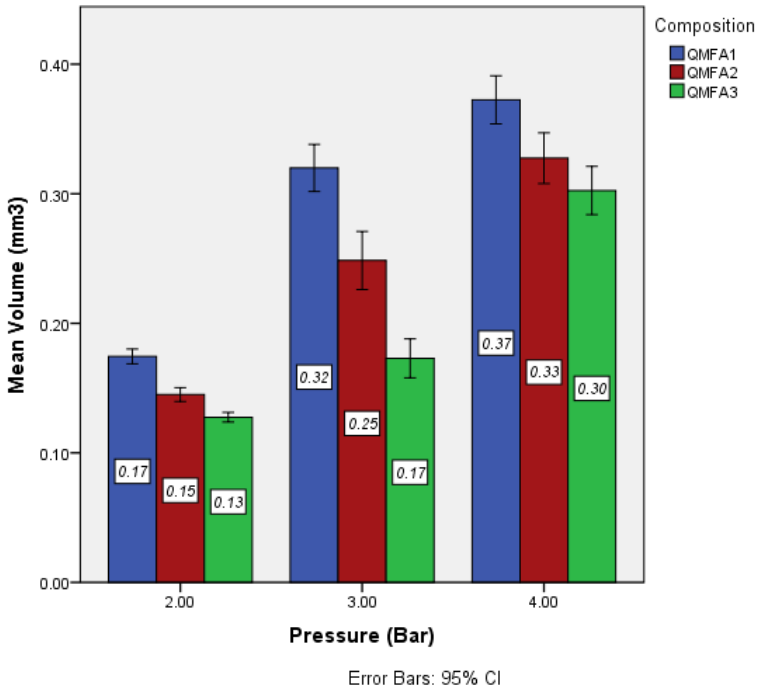

Figure 6.22: Mean ± SD of the abraded line volume (mm^3) in QMFA1 (blue), QMFA2 (red) and QMFA3 (green) glass abraded samples with varying air pressure.

The relationships between this operating parameter and the abraded line depth and volume are shown in Figure (6.23) and Figure (6.24). The correlation coefficient values in the depth relation are about 0.984, 0.998 and 0.936 for QMFA1, QMFA2 and QMFA3 abraded discs respectively. The same high R^2 is also seen in the volume relation. These high R^2 values indicate the proportional relationship between this parameter and both measurements. The higher the pressure, the deeper the depth and the greater the volume removed from the surface. These findings agree with (Black, 1945, Banerjee and Watson, 2002, Peruchi et al., 2002).

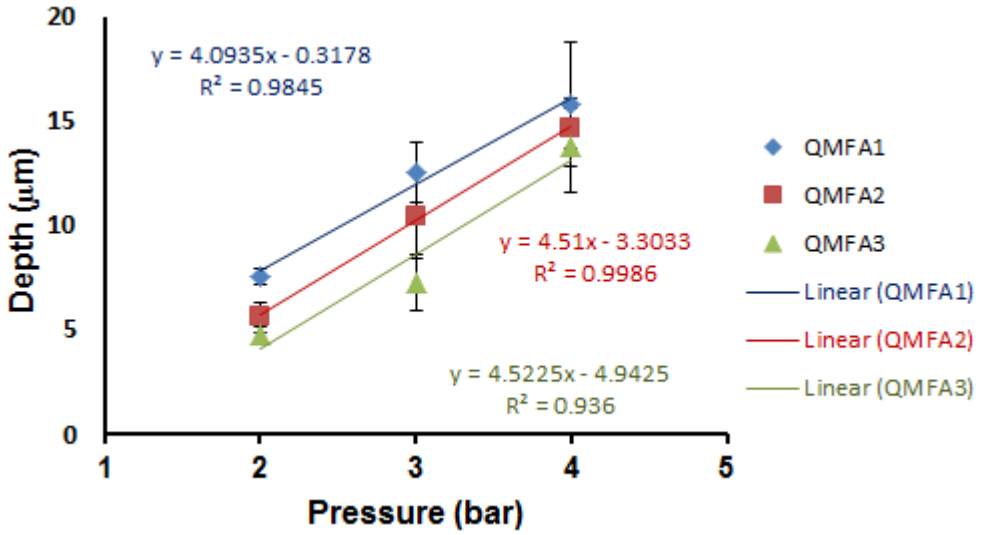

Figure 6.23: Graph shows the relation between the abraded line depth (µm) and the air pressure (bar) in all glass abraded compositions. The lines represent the linear regression for line depth versus pressure, R^2=0.984, 0.998 and 0.936 in QMFA1 (blue), QMFA2 (red) and QMFA3 (green) abraded samples respectively.

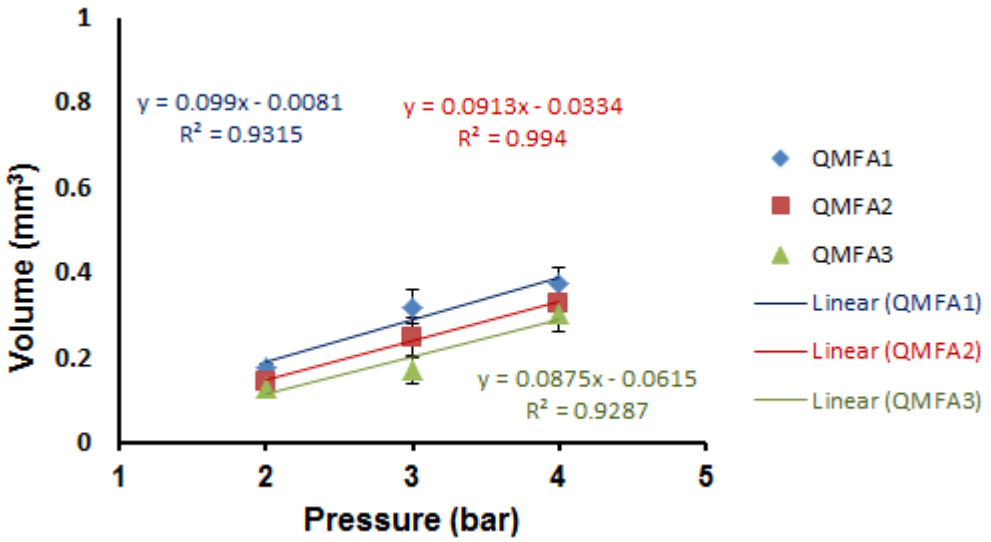

Figure 6.24: Graph shows the relation between the abraded line volume (mm^3) and the air pressure (bar) in all glass abraded compositions. The lines represent the linear regression for line volume versus pressure, R^2=0.931, 0.994 and 0.928 in QMFA1 (blue), QMFA2 (red) and QMFA3 (green) abraded samples respectively.

Previous studies found that large powder particle sizes and high air pressure are effective in removing more material from the tooth surface (Horiguchi et al., 1998). The same relation between the pressure and the cutting depth and volume removal on the enamel surface and Macor® material were also reported by (White and Eakle, 2000, Paolinelis et al., 2009, Milly et al., 2014). The reason for the higher rate of material removal is related to the speed and the kinetic energy of the particles. When the pressure of the air stream increases the velocity of the abrasive particles will increase. Accelerating the air stream will increase the kinetic energy and the velocity of the particles. Therefore, high energy impacts will occur at the target surface and this will result in more material being removed from the target surface.

Regarding the difference in glass composition, again the same profile is seen with QMFA1. These higher measurements might be related to the high atomic mass of this composition or its low embedding ability. However, there might be another

suggestion for this finding, which is the powder flow rate. As mentioned in section 6.1 that QMFA1 obtains the highest PFR at all pressures parameters. This means that large number of particles is ejected from the nozzle opening and more particles are striking the target surface. Thus, large extent of material is removed from the surface and higher depth measurements are recorded. This disagree with (Farooq et al., 2013), who reported that the pressure has a pronounce effect with high sodium containing glasses and the cutting time for these glasses was high due to the low hardness

All these are possible suggestions to what has been found in this study; however the subsequent experiments might clarify the explanations for these findings.

6.2.6 Effect of operating parameters on the surface roughness of the titanium discs

The surface roughness of implants plays a crucial role in determining the success of the implant *in vivo*. Investigating the effect of changing the operating parameters on the surface roughness is important in determining which factor is more powerful in enhancing the roughness.

Generally, abrading the titanium surface by the glass particles shows a significant increase in the surface roughness values. The Ra value of the smooth titanium discs before the abrasion is around 0.1 μm and after the abrasion the number increases to ≥1 μm. Changing the operating parameters result in a significant increase in the Ra values, but to different extents.

In Figure (6.25), it can be seen that increasing the abrasion distance results in an increase in the roughness values. The Ra value of the samples abraded at distance 1 mm is in the range between 1.34±0.05 μm and 1.36±0.07 μm. This is significantly lower than that recorded in samples prepared at distance 5 mm. The roughness

ranges between 1.61±0.04 μm and 1.62±0.07 μm. Theoretically, the former group should obtain higher roughness in comparison to the group of the further distance.

This is because of the condense pattern of particles which hit the target surface at the close distance. However, the measurements were all taken from the central portion of the abraded line and this reflects the area where the particles are embedded. The higher roughness might be due to the existence of glass particles on the top surface of the disc, as they are less deeply embedded with the greater distance.

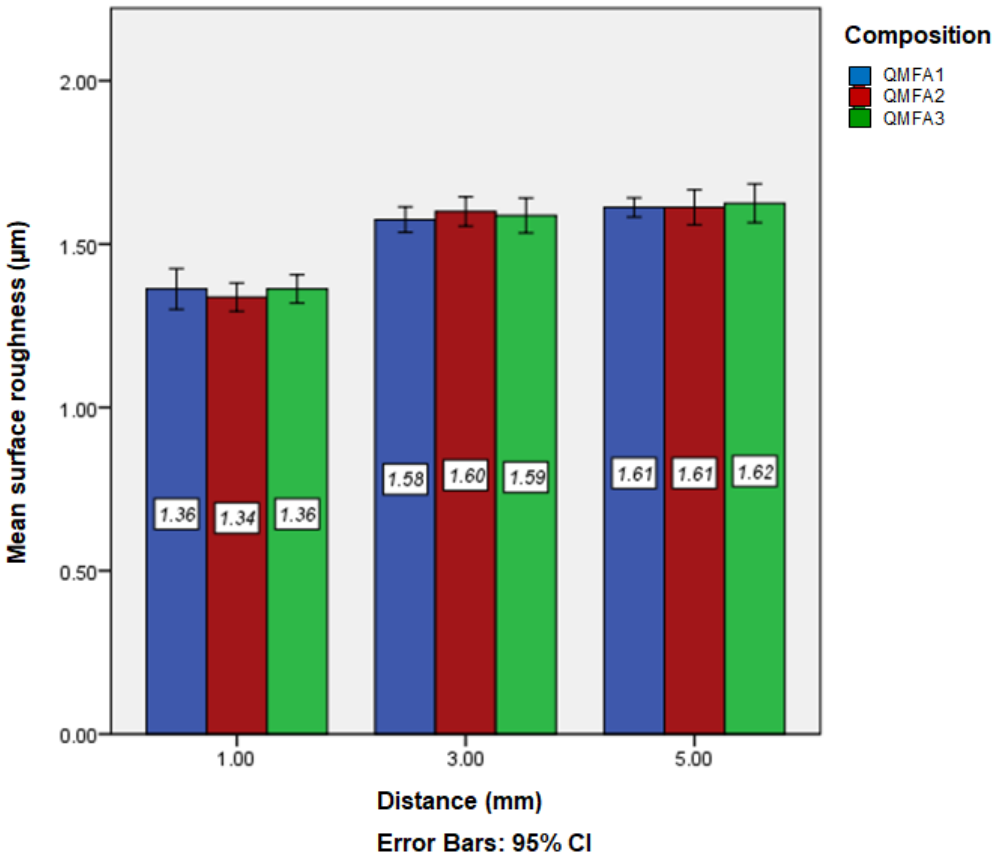

Figure 6.25: Mean ± SD of the titanium surface roughness (μm) abraded with QMFA1 (blue), QMFA2 (red) and QMFA3 (green) glasses at varying sample-nozzle distance.

Increasing the stage velocity causes an insignificant reduction in the Ra values of the abraded samples. The Ra value decreases from 1.59±0.1 μm to 1.51±0.08 μm in QMFA1 abraded discs, when the substrate velocity increased from 0.25 mm/sec to 1mm/sec Figure (6.26). This might be related to the less number of particles which are hitting the target surface per unit time. Therefore, the roughness is higher with the slowest travelling velocity.

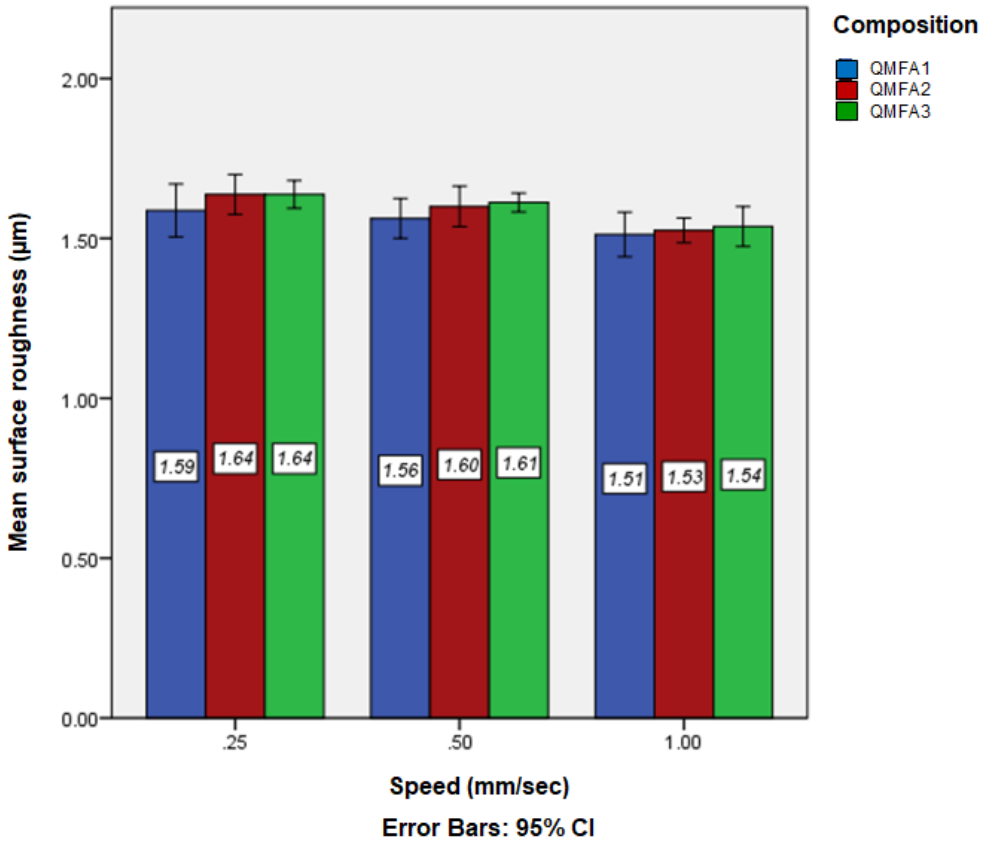

Figure 6.26: Mean ± SD of the titanium surface roughness (μm) abraded with QMFA1 (blue), QMFA2 (red) and QMFA3 (green) glasses at varying stage velocity.

The surface roughness is also increased when increasing the air pressure Figure (6.27). The increase is significantly higher in the samples prepared with 4 bar pressure in comparison to the other groups. The Ra ranges between 1.58±0.07 μm and 1.60±0.09 μm in QMFA1, QMFA2 and QMFA3 abraded discs respectively. This increase is suggested to be related to the higher abrasivity of the particles with the

higher pressure. As high pressure, the particles causes in an extensive deformation to the surface topography, this agrees with (Black, 1950).

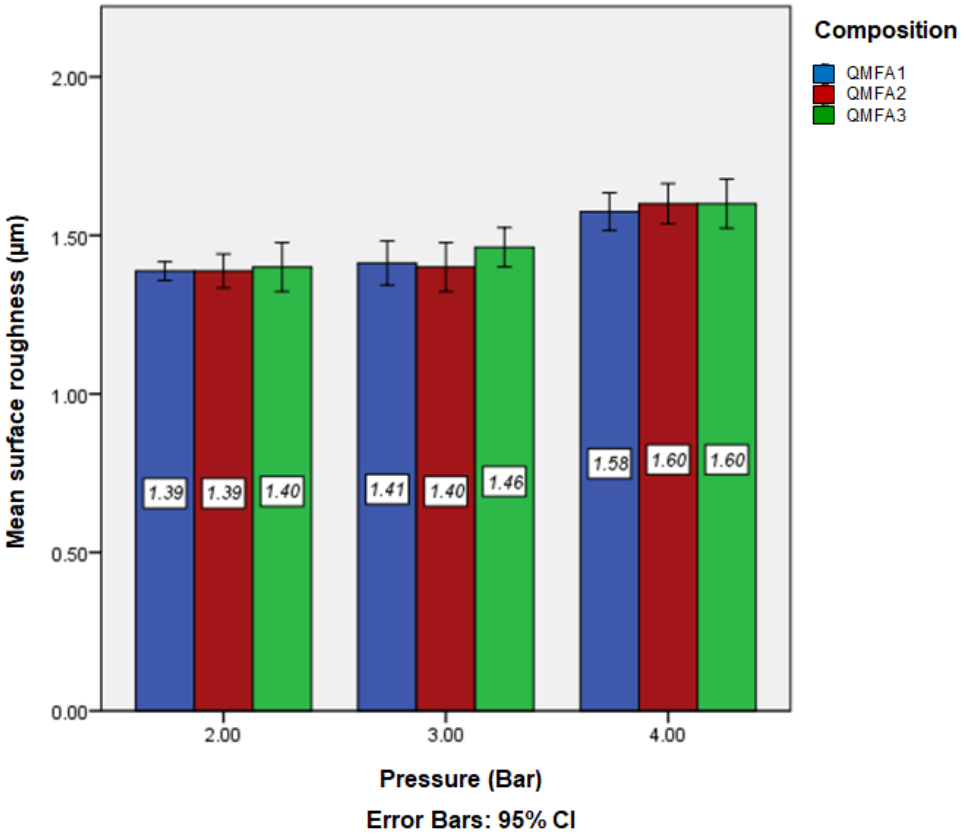

Figure 6.27: Mean ± SD of the titanium surface roughness (µm) abraded with QMFA1 (blue), QMFA2 (red) and QMFA3 (green) glasses at varying air pressure.

Interestingly, at all operating parameters it can be seen that there is small difference between the glass abraded compositions regarding the surface roughness. The roughness is insignificantly higher in QMFA3 abraded samples in comparison to QMFA1 and QMFA2 compositions. All the values are within the same range and this may be due to the insignificant difference in the size of the particles. The large particle size of the powder can result in a clear increase in the surface roughness and percentage of area coverage and this agrees with (Rønold and Ellingsen, 2002, Udomlertpreecha et al., 2014). However, there may be more embedded particles of QMFA3 in the surface which give rise to a higher roughness values.

6.3 SEM-surface coverage

The nature and the strength of bond between the implant and bone tissue is highly affected by the implant surface topography. The smooth implant surface may lead to a formation of weak bond with bone due to the formation of the fibrous tissue. While the rough surface forms a strong attachment to the bone by providing a wide area for cell attachment (Thomas and Cook, 1985, Feighan et al., 1995). To investigate the changes in the surface of the titanium discs after their abrasion by bioactive glasses, SEM-SE mode was used. The surface topography of the titanium discs demonstrates a plastic deformation after its abrasion by the glass particles. As can be seen from Figure (6.28 a) that the disc has a smooth surface before the abrasion process. After the abrasion, the surface becomes physically modified by the glass particles, as shown in Figure (6.28 b). The abraded surface appears rough with the presence of elevations and depressions. These irregularities indicate the effectiveness of the glass particles in roughening and modifying the titanium surface. This finding is visually confirming the higher Ra values of the samples after the abrasion when using the WLP.

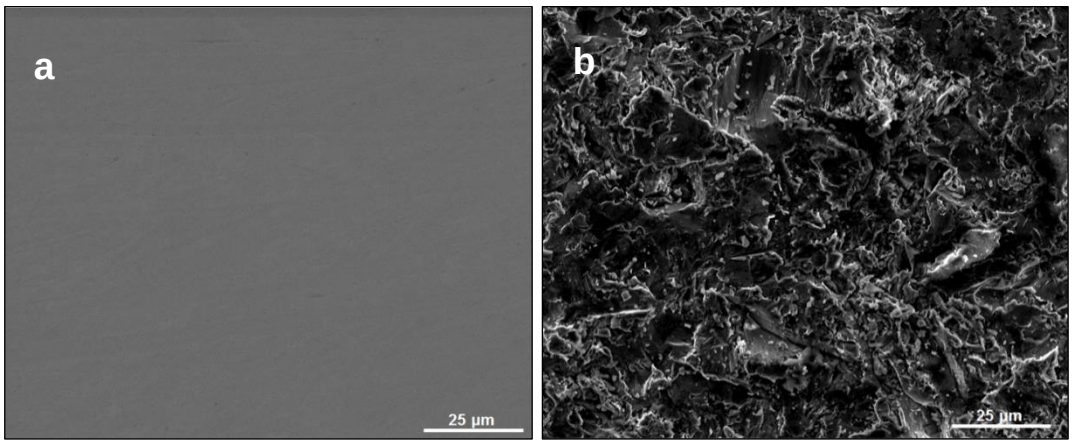

Figure 6.28: SEM micrographs of titanium discs in SE mode showing the surface morphology of the disc a) before abrasion (polished) b) after abrasion (abraded) with magnification (2000x). The surface is smooth with no irregularities in the polished discs while, the abraded surface appears irregular with multiple elevations and pits.

In the SE mode imaging, it is difficult to differentiate between the glass particles and the titanium in the prepared samples: therefore, SEM-BSE mode was carried out. The contrast in the BSE mode depends on the difference in the atomic number density between the two materials. In Figure (6.29), the glass particles appear as black patches spreading through the white titanium surface. This indicates the embedding and the spread of the glass particles on the titanium surface in a homogenised pattern. Interestingly, the sizes of the embedded particles are much smaller than the actual abrasive particles. The size of the prepared particles was between 58 µm and 127 µm. After the abrasion, the measured size of the glass areas is ≤25 µm. This signifies the suggested principle of the particles cleavage by the other particles in the powder stream.

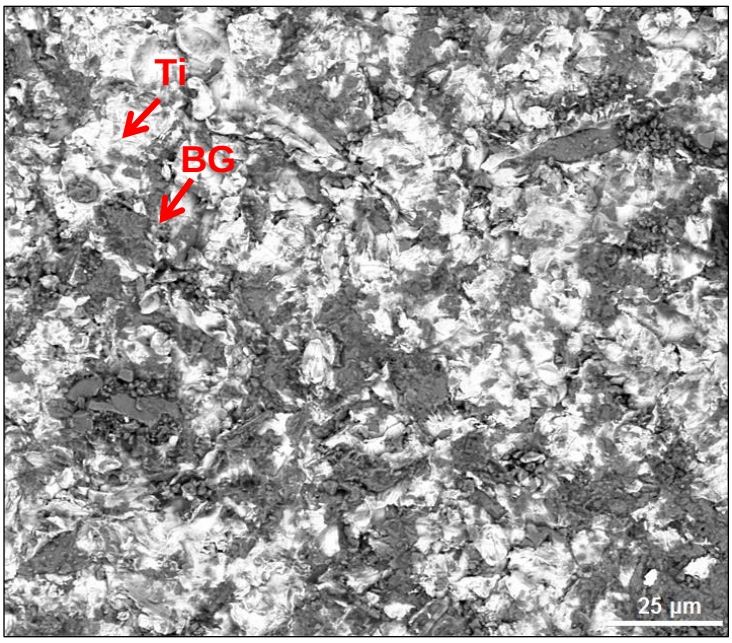

Figure 6.29: SEM-BSE micrographs of the titanium disc after abrasion showing the embedded glass particles (BG: grey) into the titanium surface (Ti: white) and their sizes (1600x magnification).

However, from these SEM-BSE micrographs, it is possible to measure the percentage of area covered by the glass across the abraded line. The percentage coverage was calculated by using image J software and the results were presented as means ± SD for all the samples with varied parameters (distances, velocities and pressures). The central portion of the abraded area was selected for the area coverage measurements and four areas were selected across the line. This is because of the high abrasion efficiency of the particles ejected from the central part of the nozzle cone in comparison to the particles ejected from the peripheral part (Watson et al., 2008). It can be hypothesised that by modifying the operating parameters the percentage of coverage may be varied. This is because of the differences which have been seen in the WLP measurement between the investigated groups.

Figure (6.30) demonstrates the means and SD of the area percentage coverage in all abraded samples with varying sample-nozzle distance. There is a significant increase in the percentage of the covered area in all compositions when increasing the distance from 1 mm to 5 mm, see appendix 1 (10.4.1). Percentage areas in QMFA1, QMFA2 and QMFA3 abraded discs are about 52.42±1.60%, 54.55±2.12% and 58.26±1.90% respectively at sample distance 1 mm. These values increase at distance 5 mm and the range of the increase is between 2%-6% in comparison to distance 1 mm.

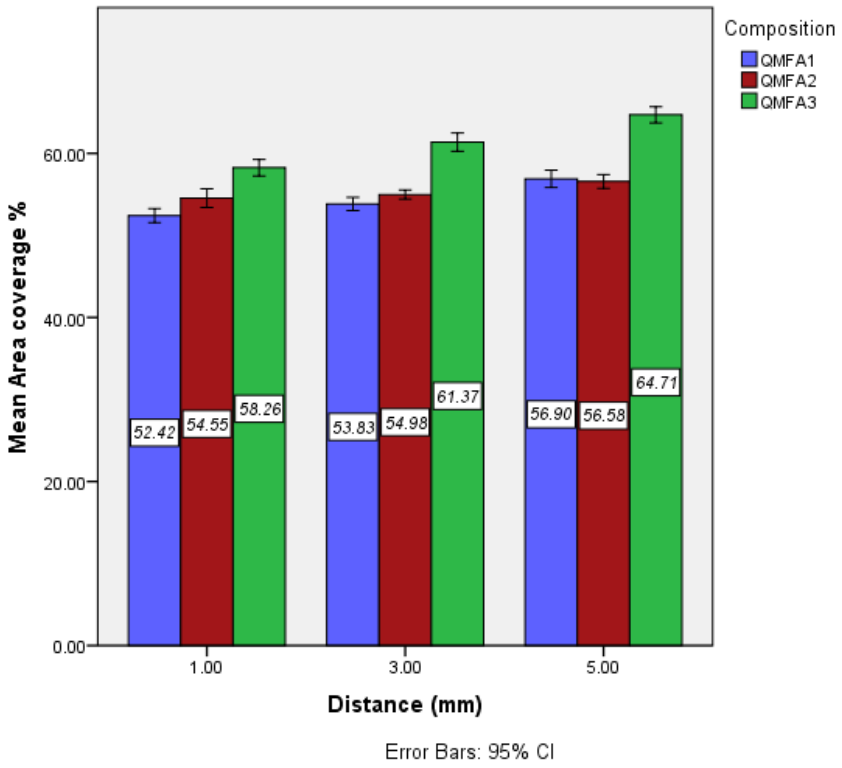

Figure 6.30: Mean ± SD of the surface area percentage coverage in QMFA1 (blue), QMFA2 (red) and QMFA3 (green) glass abraded samples with varying sample-nozzle distances.

The higher coverage at greater sample distances might be related to the low abrasion efficiency of the particles and their wide spread on the target area. Figure (6.31 a) show the spread of QMFA1 particles on the titanium surface at sample distance 1 mm. The particles appear with less surface area, as they might be embedded further into the titanium surface or might be cleaved by other close particles. The particles on the titanium surface at distance 5 mm appear wide and flattened and this indicates the low abrasion efficiency Figure (6.31 b). These results are consistent with the surface roughness measurements.

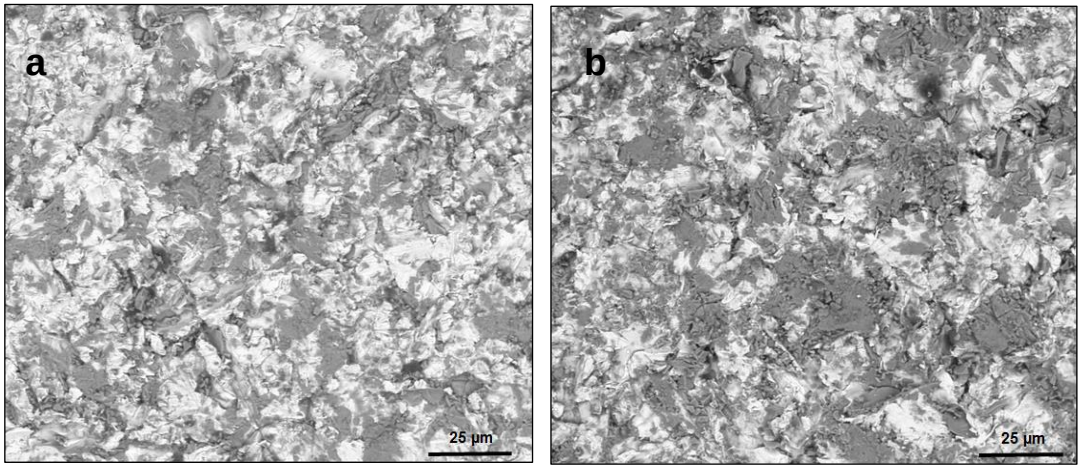

Figure 6.31: SEM-BSE micrograph of QMFA1 glass abraded titanium disc showing the pattern of particles distribution and coverage at a) distance 1 mm b) distance 5 mm (1600x magnification).

The fast sample velocity results in a significant reduction in the percentage of area coverage in all composition abraded discs. The covered area percent at velocity 0.25 mm/sec in QMFA1, QMFA2 and QMFA3 abraded samples is 57.82±2.18%, 61.47±2.15% and 62.31±2.35% respectively Figure (6.32). These values are significantly higher than that at 1 mm/sec *($p \leq 0.05$)*, see appendix 1 (10.4.2). However, the difference between the groups at 0.5 mm/sec and that at 1 mm/sec in all compositions is statistically insignificant. The highest area coverage with the slowest sample velocity might be related to the longer the abrasion and the more the particles embedded into the abraded area.

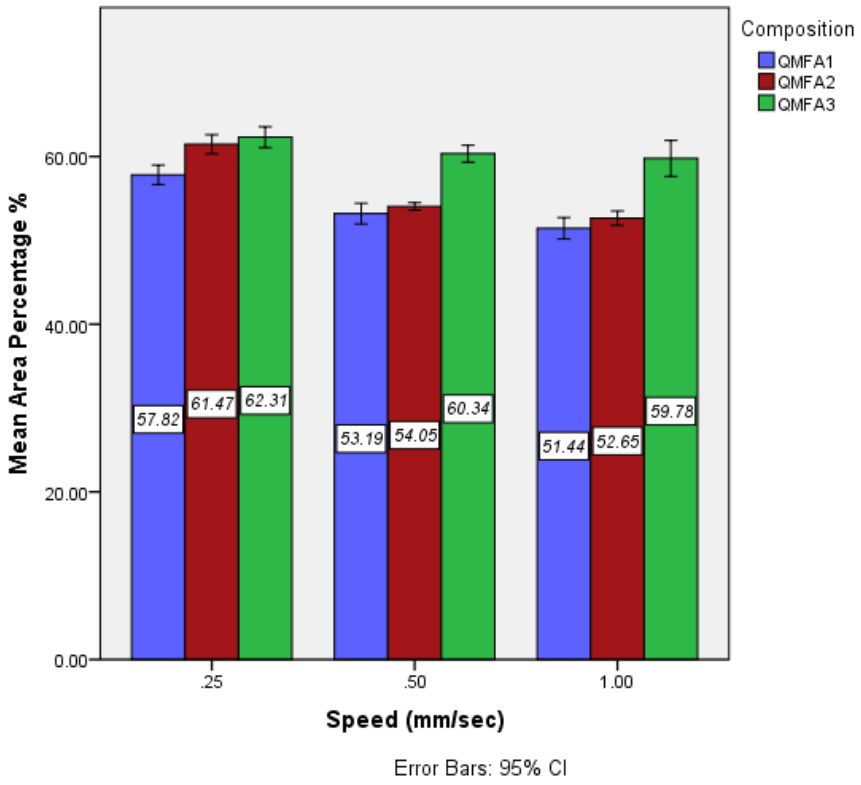

Figure 6.32: Mean ± SD of the surface area percentage coverage in QMFA1 (blue), QMFA2 (red) and QMFA3 (green) glass abraded samples with varying stage velocity.

At all velocities, QMFA3 abraded samples show the highest percentages coverage. The same result was also seen in the nozzle distance parameter. This suggests that the hardest glass has a higher embedding ability into the titanium surface.

Increasing the air pressure causes an increase in the percentage of area coverage in all composition groups Figure (6.33). This is due to the higher abrasion efficiency of the particles. Again, the effect is more apparent with the QMFA3 abraded samples in comparison to the other compositions. With the pressure rise from 2 bars to 4 bars, the coverage percentages of QMFA3 abraded samples are significantly increased from 57.03±2.13% to 62.64±%. While, in the QMFA1 and QMFA2 glass abraded samples the percentages values are increased from 52.74±1.31%, 52.52±2.16 % to 53.64±1.98%, and 54.53±2.37%. These results indicate the softer

glass gives a lower coverage in comparison to the hardest glass. This agrees with the surface roughness findings; however the effect is highly significant in the surface coverage, rather than the insignificant difference between the groups in the surface roughness.

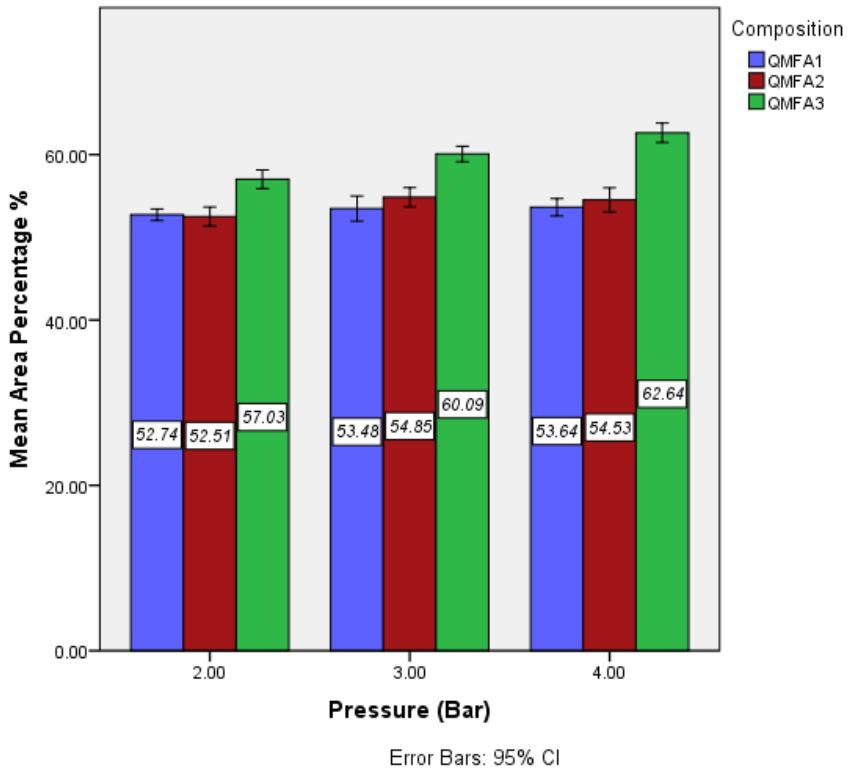

Figure 6.33: Mean ± SD of the surface area percentage coverage in QMFA1 (blue), QMFA2 (red) and QMFA3 (green) glass abraded samples with varying air pressure.

From all the above findings, it can be indicated that the amount of area covered by the glass particles is relatively high. Greater than 50% of the abraded area is covered by the glass particles and this could be related to the large size of the particles. The larger the particle size the greater the percentage of coverage and this agrees with (Rønold and Ellingsen, 2002, Udomlertpreecha et al., 2014).

6.4 Results of glass embedding and retention in Ti surface

As the Ti discs were successfully abraded by the glass particles and a good percentage of area coverage was detected. Microanalysis by EDX was conducted on the abraded surface. This is to confirm the presence of the glass on the disc surface and to determine the elemental analysis of the samples depending on the characteristic X-Ray peaks for each element.

SEM-EDX line scans were carried out on the surface of the abraded samples across the intact and abraded areas. Figure (6.34) shows EDX-Line scan of the abraded Ti disc in SEM-BSE mode where the QMFA1 glass is located in the central part of the disc. The results are presented in weight % and they indicate the presence of fluoride, sodium, silicon, phosphorus, calcium and oxygen elements in the abraded area. These elements represent the chemical composition of the bioactive glass. However, in the intact areas titanium becomes the abundant element at these regions.

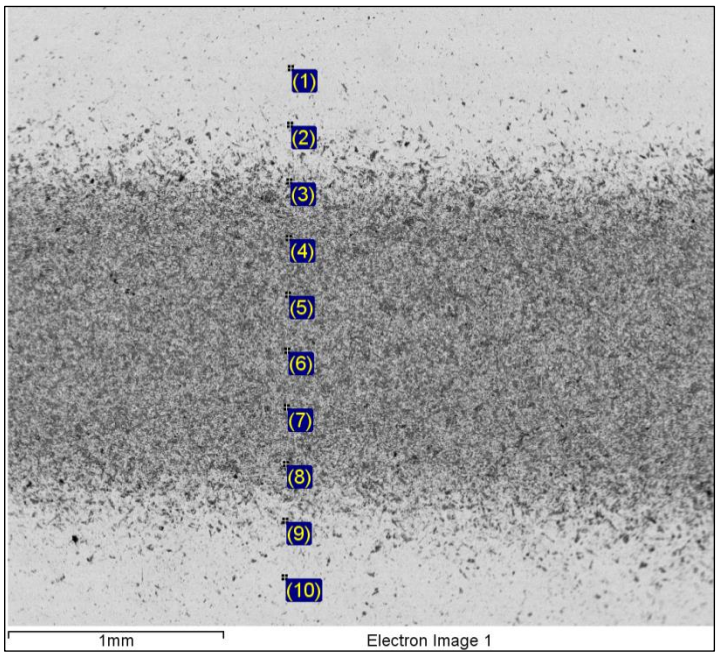

Spectrum	In stats.	C	O	F	Na	Si	P	Ca	Ti	Total
(1)	Yes								100.00	100.00
(2)	Yes								100.00	100.00
(3)	Yes								100.00	100.00
(4)	Yes	3.55	42.65	5.11	9.33	14.49	4.56	20.30		100.00
(5)	Yes		20.04		5.34	11.10	4.12	16.62	42.78	100.00
(6)	Yes		24.61		2.35	2.63	0.75	3.88	65.77	100.00
(7)	Yes	2.21	34.62	3.02	5.60	7.93	3.01	12.79	30.82	100.00
(8)	Yes		32.16	2.46	4.49	5.65	1.97	8.86	44.41	100.00
(9)	Yes		19.06		1.69	2.03	0.83	2.56	73.83	100.00
(10)	Yes								100.00	100.00

Figure 6.34: SEM micrograph with the EDX line scan analysis of QMFA1 glass abraded disc after grit blast. The table illustrates the detected elements at the selected points all in weight %.

The distribution profile of the glass particles in the titanium surface is also presented by plotting the weight percent of the detected elements against the selected points Figure (6.35). There is a decline in the weight % of the detected titanium element at the central portion of the disc. This part represents the area where the glass particles existed. This is clear from the appearance of glass elements at the abraded region. Thus, it can be confirmed that the glass is not only abrading the surface of the Ti disc, but it is also embedding into it. This embedded glass can result in a chemical modification to the titanium surface. Therefore, the surfaces of the titanium

discs are altered, both physically and chemically by the abrasion and the embedding processes respectively. Both modifications are important in enhancing the integration of the implant with bone tissue.

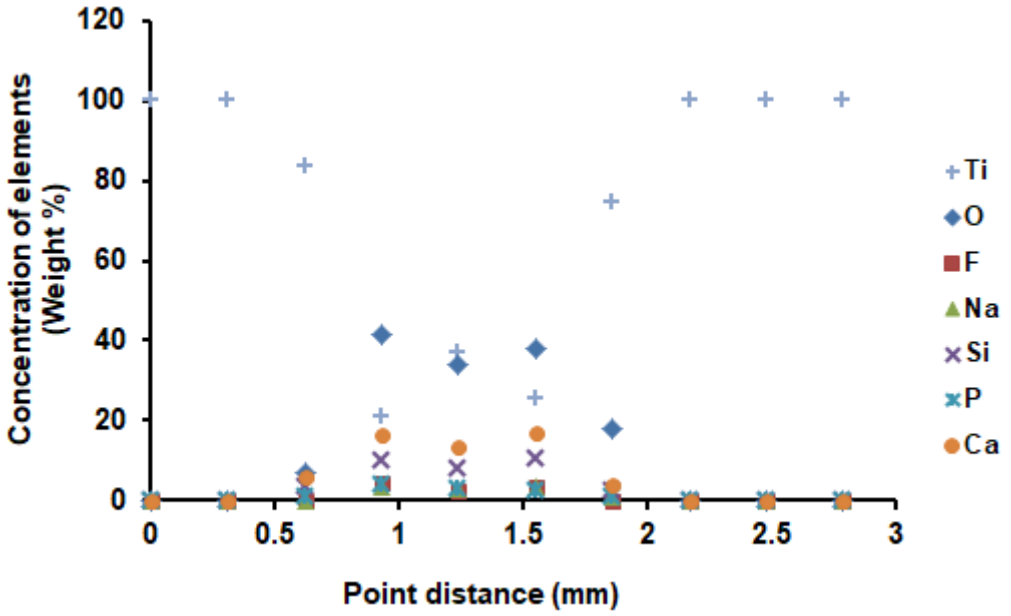

Figure 6.35: Graph shows the distribution of the glass elements and the titanium at the EDX selected points across the scanned titanium disc.

The results of this study agree with what have been reported regarding the embedding of the glass in the titanium surface (Koller et al., 2007, Al-Ani, 2013). The EDX mapping in the previous studies showed the presence of the glass elements in the abraded area and confirmed their distribution in homogenised form. However, the extent of the glass particles embedding and the strength of their attachment to the surface were not investigated. The immersion of the abraded samples in weak acid was suggested to be as a method for their determination. However, this method is not very accurate; there is a possibility to assess the resistance of the glass components to the dissolution in weak acid media. The resistance might give information about the strength of the particles attachment to

the surface. After the first 3 h of the disc immersion, the glass particles show a fast dissolution in the acid. This is indicated from the EDX analyses of the immersed disc, which demonstrate the absence of the glass elements from the surface. Only Si is detected on the surface besides the titanium and oxygen Figure (6.36).

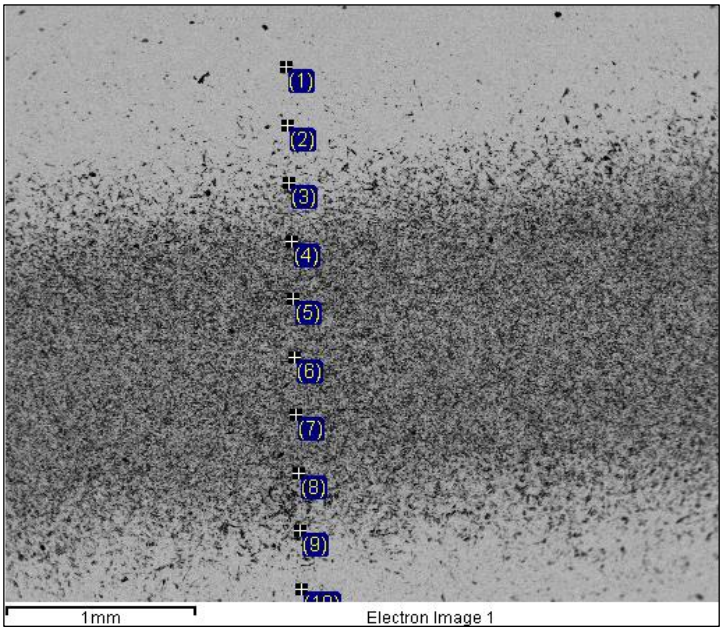

Spectrum	In stats.	C	O	Si	Ti	Total
(1)	Yes				100.00	100.00
(2)	Yes				100.00	100.00
(3)	Yes				100.00	100.00
(4)	Yes		46.18	15.23	38.59	100.00
(5)	Yes		31.41	12.10	56.49	100.00
(6)	Yes	0.98	32.36	11.48	55.18	100.00
(7)	Yes			1.14	98.86	100.00
(8)	Yes		12.76	4.29	82.95	100.00
(9)	Yes				100.00	100.00
(10)	Yes				100.00	100.00

Figure 6.36: SEM micrograph with the EDX line scan analysis of QMFA1 glass abraded disc after immersion in acetic acid for 3 h. The table illustrates the detected elements at the selected points all in weight %.

After 6 h of immersion, the same results are also seen, but with lower Si concentrations across the line scan. The titanium concentrations, on the other hand, are becoming higher with the immersion time, as can be seen in Figure (6.37). This indicates the exposure of the underneath titanium surface.

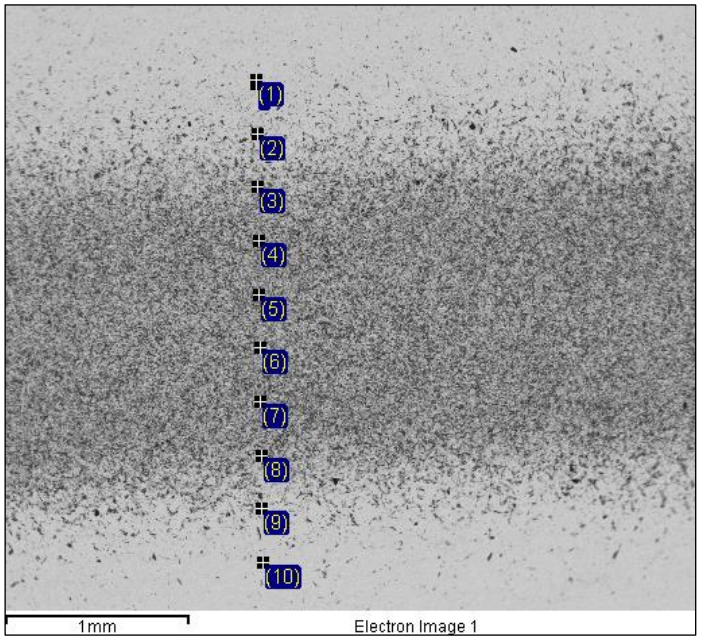

Spectrum	In stats.	O	Si	Ti	Total
(1)	Yes			100.00	100.00
(2)	Yes			100.00	100.00
(3)	Yes		0.44	99.56	100.00
(4)	Yes	19.66	5.18	75.16	100.00
(5)	Yes	18.31	21.78	59.91	100.00
(6)	Yes	15.94	4.39	79.67	100.00
(7)	Yes	31.10	6.00	62.90	100.00
(8)	Yes		0.93	99.07	100.00
(9)	Yes			100.00	100.00
(10)	Yes			100.00	100.00

Figure 6.37: SEM micrograph with the EDX line scan analysis of QMFA1 glass abraded disc after immersion in acetic acid for 6 h. The table illustrates the detected elements at the selected points all in weight %.

Therefore, there is a good retention of the bioactive glass to the titanium surface. This is because of the resistance of the Si element to the dissolution as they still attached to the surface and this reflects the deep retention of the particles to the surface.

To confirm this finding, ICP-OES analysis was used. This method determines the difference in the amount of embedded glass between the three compositions-abraded samples. Figure (6.38) shows the mean and SD of the concentrations of the released Ca, P and Si ions from all compositions of abraded discs after 6 h immersion in acetic acid. The results demonstrate that the Ca^{2+} release is about 11.10±1.95 ppm in QMFA3 composition abraded samples followed by 8.53±1.31 and 6.51±0.39 ppm for QMFA2 and QMFA1 abraded samples respectively. The same profile is also shown with P and Si species where, the highest values are detected in QMFA3 abraded discs of about 1.61±0.35 and 1.54±0.27 ppm respectively. For the fluoride release, the concentration in all the composition coatings is quite small and it is around 0.0005 ppm. Therefore, the data are not shown in the graph.

From all results, it can be confirmed that the discs, which abraded by QMFA3 glass have the highest amount of embedded particles into their surface and this consistent with the SEM surface coverage results.

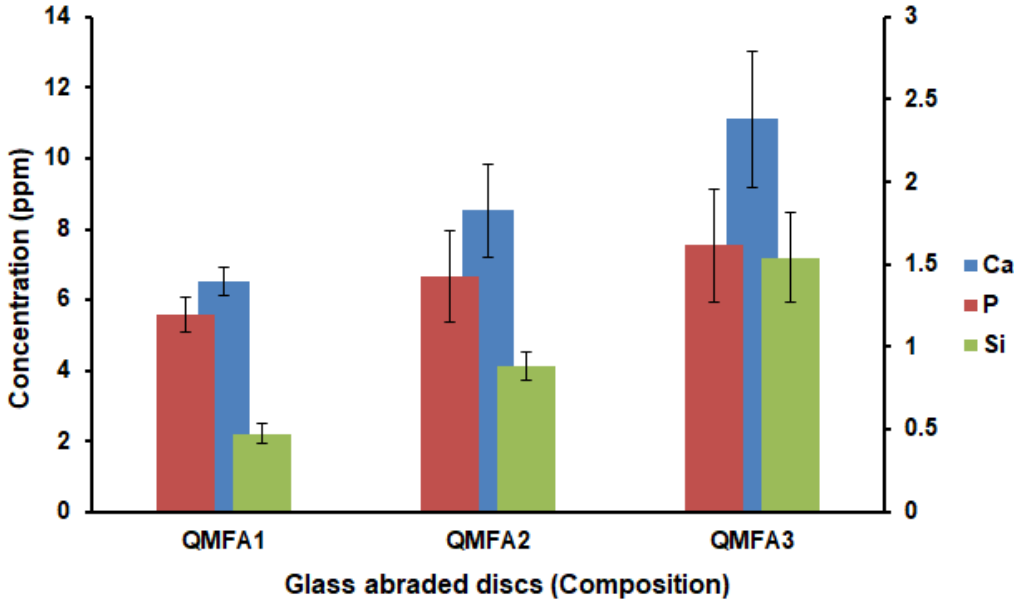

Figure 6.38: Mean ± SD of the Ca (blue), P (red), Si (green) concentration (ppm) in the three composition coatings after immersion in acetic acid for 6 h. Phosphorus and silicon are plotted on the right hand y-axis.

6.5 Abraded discs bioactivity results

The bioactivity of the glass powders in different solutions were discussed in details in Chapter 5. The abrasion process of the titanium discs might affect the glass bioactivity, as the glasses are sensitive to the humidity of the atmosphere. Humidity causes partial crystallization to the glass powder and this result in a reduction in the reactivity. Therefore, the ability of the glass abraded samples to form apatite on their surfaces was investigated. The discs were immersed in Tris buffer and SBF for 3 days. The experiment was conducted by using only one glass composition, which is QMFA1. This is due to the similarity in reactivity of all the compositions as described previously. The glass abraded titanium discs demonstrate clear changes in the surface morphology after their immersion in Tris and SBF. In the SEM-SE mode Figure (6.39), the immersed samples show a deposition of a crystal layer on their surfaces when compared to the samples before immersion.

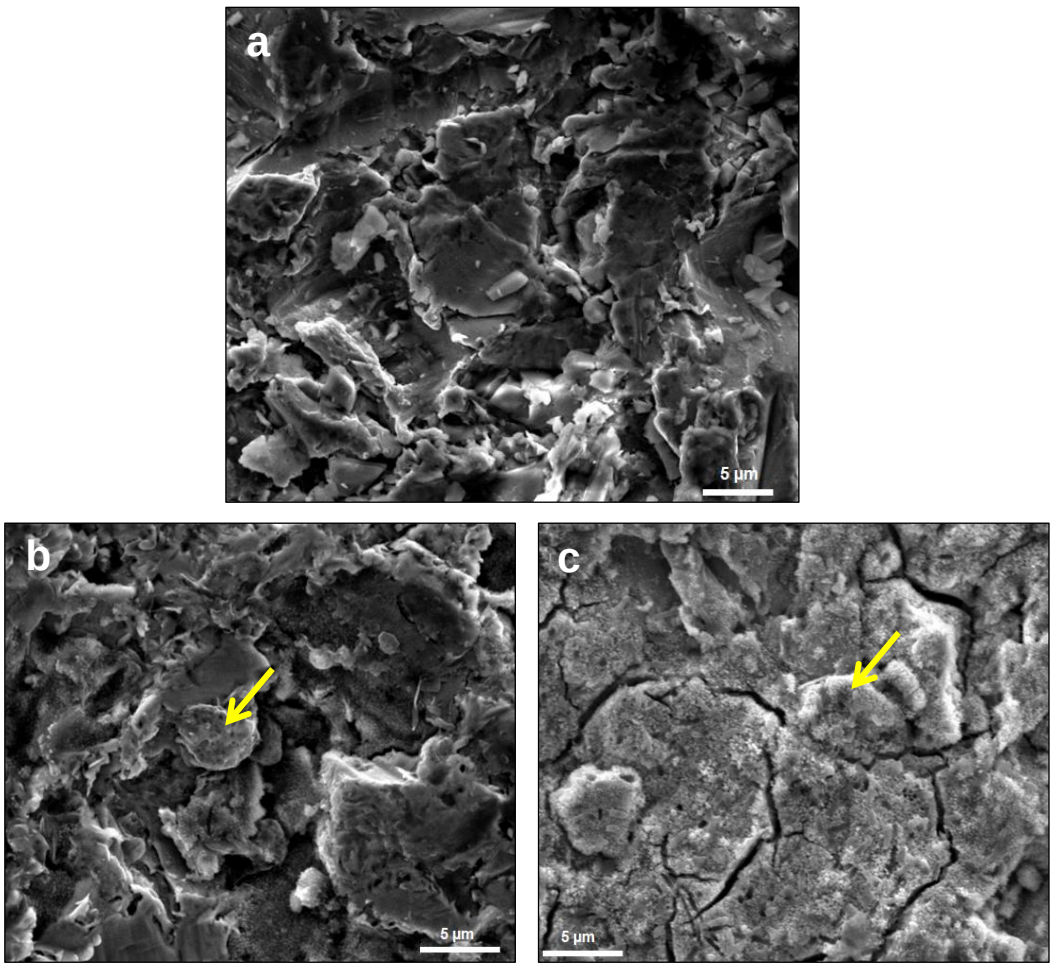

Figure 6.39: SEM micrographs of the glass abraded titanium discs in SE mode showing the surface morphology of the Ti disc (a) before immersion (b) after immersion in Tris buffer for 3 days (c) after immersion in SBF for 3 days. The arrow points to the apatite deposition.

However, there is a difficulty in detecting whether the crystal layer is formed on the whole surface of the sample or on the glass part only. SEM-BSE mode was performed for this purpose. In this mode, it is clearly seen that the crystal layer is formed on the glass particles and not the pure titanium surface Figure (6.40).

This indicates that this layer reflects the reaction of the glass particles with the testing solution and establishes their bioactivity.

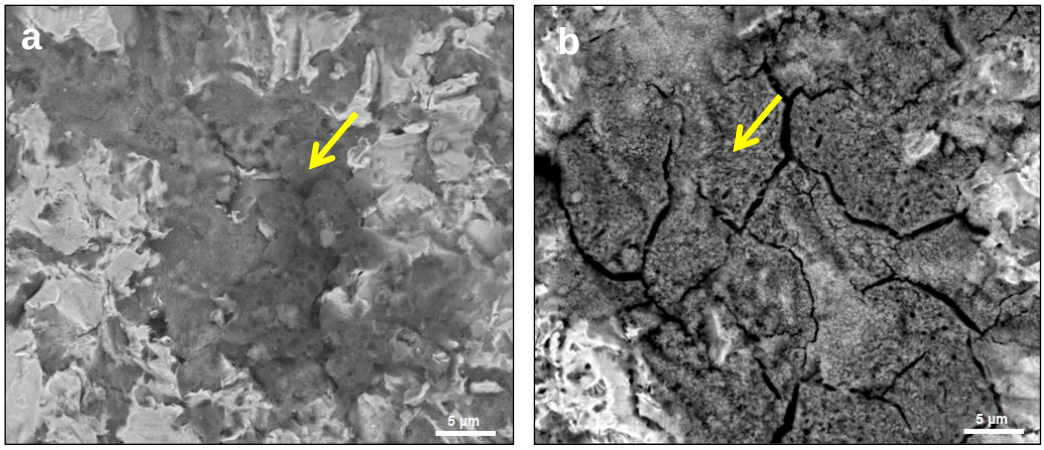

Figure 6.40: SEM micrographs of the QMFA1 glass abraded titanium discs in BSE mode showing the formation of apatite on the surface of the glass particles (a) after immersion in Tris buffer for 3 days (b) after immersion in SBF for 3 days.

To confirm whether this deposited layer is apatite or not, EDX analysis was performed. The element scan analysis of the crystal layer on both Tris and SBF treated samples revealed that there is a presence of high Ca and P on the surface in addition to other elements. The Ca/P ratio in this embedded particle is around 2.0-2.5 and this ratio is close to the apatite weight ratio of 2.5. This indicates the formation of Ca-P rich layer on the surface of the embedded particle Figure (6.41). Therefore, the glass coatings still maintained their compositional properties and not affected by the abrasion process and the atmosphere.

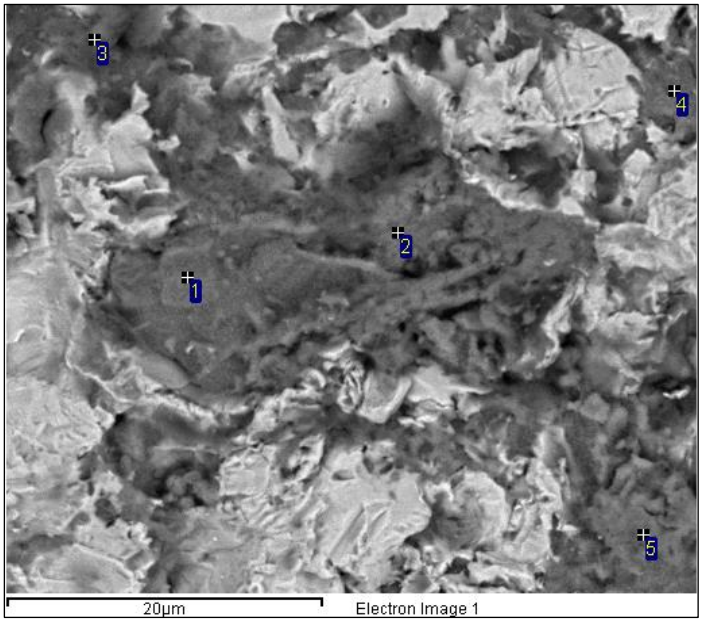

Spectrum	In stats.	O	F	Al	P	Cl	Ca	Ti	Fe	Total
1	Yes	36.43	3.44	0.38	12.69	5.45	25.55	16.06		100.00
2	Yes	27.92	2.56		15.54	11.44	31.00	11.53		100.00
3	Yes	24.32			10.38	19.90	18.44	21.89	5.08	100.00
4	Yes	38.92	3.73		10.22	2.02	20.00	25.12		100.00
5	Yes	39.42	3.93	0.41	16.07	6.67	30.96	2.55		100.00

Figure 6.41: SEM micrograph associated with EDX element analysis of QMFA1 glass abraded titanium disc immersed in Tris buffer for 3 days. The table illustrates the detected elements on the glass particle surface and all of them in weight %.

6.6 Summary

Modifying the surface of the titanium implant is one of the essential aims that many implant companies are seeking for in their design of implants. The surface topography and roughness are important in providing strong osseointegration. In this study, three operating parameters were modified and their effect on the quality of the coating was investigated.

Increasing the sample distance and its travelling velocity both resulted in a significant reduction in the dimension of the abrade line and the amount of titanium

removal. However, the surface roughness and the percentage of area coverage were increased with increasing the distance. In contrast, both features were decreased with increasing the sample velocity. On the other hand, all the mentioned measurements demonstrated a significant increase by increasing the pressure of the machine.

The existence and the retention of the particles in the surface of the titanium discs were investigated by SEM-EDX analysis. The Si, Na, Ca, P, O and F elements were all detected in the abraded area and these represent the glass elements. Moreover, Ti element was detected in higher weight % at the intact areas. Furthermore, the abraded discs were also investigated for their bioactivity in Tris and SBF. The results showed that the discs were still conserving good bioactivity by forming apatite on the surface after 3 days immersion.

Chapter 7 Results and Discussion of Cell Culture Study

7 Results and discussion of cell culture study

7.1 Glass biocompatibility

The designed glasses showed good bioactivity *in vitro* when immersed in physiological solutions. However, it is important to obtain thorough information regarding the biological responses of the cells to the prepared glasses. Therefore, the effect of the glass conditioned media on the cell proliferation and differentiation was investigated.

7.1.1 DNA content and ALP activity results of MC3T3-E1 cells cultured in glass conditioned media

These two experiments were performed in order to test the biocompatibility of the glass powders *in vitro*. The DNA content assay reflects the proliferation of the seeded cells, while ALP activity is a marker for osteoblasts and it indicates the degree of cell differentiation and their response to the treated media.

The results of the osteoblast cell proliferation in the control α-MEM medium and 72 h glass conditioned media are presented in Figure (7.1). In general, the number of cells which survived during the period of treatment is relatively high. In day 1 treatment, there is no difference in DNA content between control and conditioned media. However with the longer culture time periods, the proliferation of cells becomes insignificantly higher in control media in comparison to the conditioned media. This may be due to the longer period that the cells are subjected to the glass extract. The proliferation of the cells is slightly affected by the type of glass conditioned media, specifically at the longer culture period of 7 days.

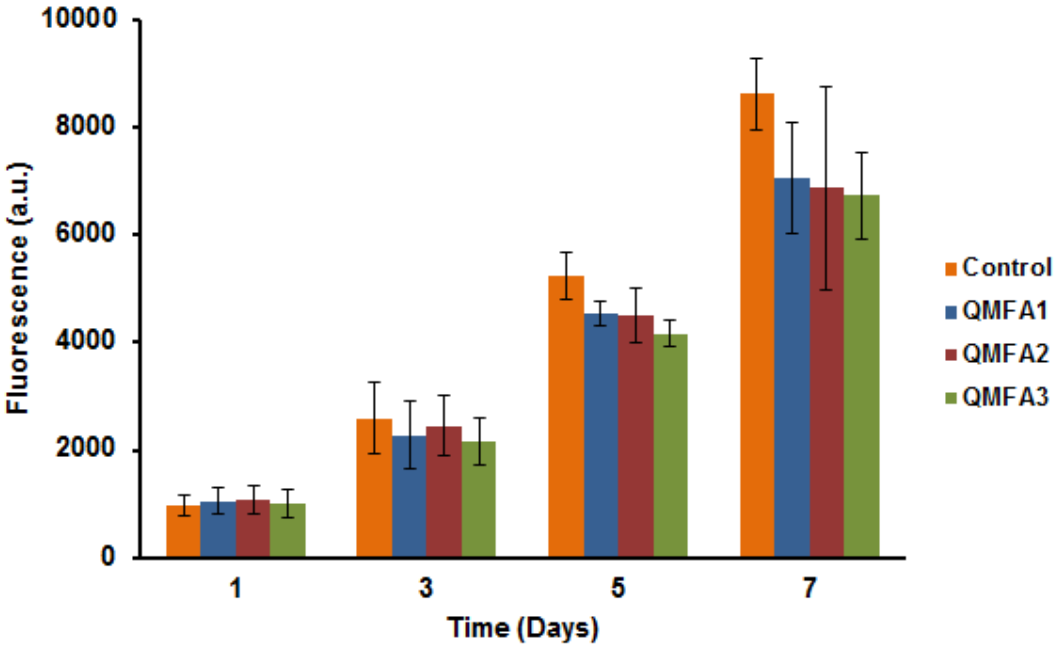

Figure 7.1: Effect of the glass conditioned media on the cell number and proliferation of MC3T3-E1 cells at 1, 3, 5 and 7 days. Each bar represents the mean of three experiments (each with 10 samples) ± their standard deviations. There is no statistical difference between the groups at the same time point *(P≥0.05)*.

The same profile is also seen with the ALP cell differentiation experiment. After treatment by the three conditioned media for 3, 5 and 7 days, the ALP activity of the MC3T3-E1 in these media is becoming lower than that in the control α-MEM. However, the ALP activity is higher in the first day of the glass conditioning when compared to the control, as see in Figure (7.2). The ALP activity of this cell line is known to be as low during the growth phase. However, the activity of ALP becomes higher when the cells reach confluence (Sudo et al., 1983). The results of the ALP experiment are consistent with the proliferation results, as both are decreased with the longer culture time by the effect of the glass condition. This might be related to the impact of the medium pH on both processes. As reported previously that the local environment, where the cells are grown, can be affected by the dissolution of the implanted material (Shen et al., 2012).

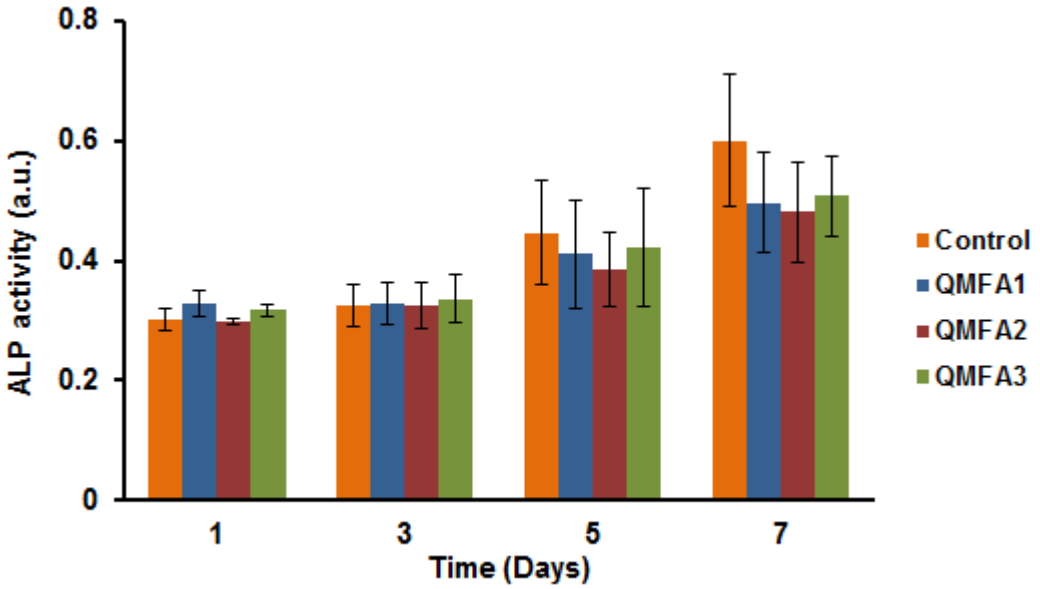

Figure 7.2: Effect of the glass conditioned medium on the MC3T3-E1 cells differentiation at 1, 3, 5 and 7 days. Each bar represents the mean of three experiments (each with 10 samples) and their standard deviations. There is no statistical difference between the groups at the same time point *(P≥0.05)*.

The rapid dissolution of the bioactive glass in the *in vitro* cell environment may adversely affect the osteoblast behaviour and function. This is due to the release of the ions from the glass surface, which causes an increase in the pH of the *in vitro* environment and this can be cytotoxic to the osteogenic cells (Varanasi et al., 2009). Various authors have reported that the alkaline environment of the physiological fluid is beneficial in the osteogenesis and mineralisation process, as this condition can enhance the function of the osteoblast cells (Chakkalakal et al., 1994, Silver et al., 2001, Shen et al., 2012). Others have suggested conditioning the glass powder in SBF medium before its usage in the *in vitro* study. This is to stabilise the medium pH and to reduce the effect of the high alkalinity of the glass material (Foppiano et al., 2007, Varanasi et al., 2009). Conditioning the glass can lead to a good stimulation of the cell markers. Interestingly, in this study the designed glass powders did not produce a highly alkaline environment, as they contained 6 mole % of phosphate in their compositions. The high phosphate content in the glass composition results in reducing the alkalinity of the media by releasing the

phosphate into the surrounding medium, which causes buffering to the alkaline environment (O'Donnell et al., 2008, O'Donnell et al., 2009). Therefore, the high phosphate content was suggested to enhance osteogenesis. Additionally, the glass powders were conditioned for 72 h in the cell medium prior to the proliferation and differentiation experiments. The pH of the conditioned media at that time period ranged between 8.2 and 8.3. This conditioning process was performed based on the results from (Liu et al., 2016), who found that the toxicity of the media that is conditioned by the fluoride containing bioactive glass for 72 h is the least for the earlier time points (8 and 24 h). Therefore, the conditioning was performed at these time points in order to have a stabilised condition. From the results Figure (7.2), it can be seen that the ALP activity of the osteoblasts and their proliferation rate are increased with the culture time for all treated media. This indicates the biocompatibility of the material. In spite of this finding, the ALP activity and the cell numbers are lower in the conditioned medium than the control medium in day 3, 5 and 7 of the cells culture. This might be related to the presence of the high concentration of fluoride in the conditioned media. The presence of a high concentration of calcium fluoride of about 5-7 mole % in the glass composition was reported to suppress the osteogenic response of the MC3T3-E1 cells (Liu et al., 2016). However, there is a clear difference in the concentration of the fluoride between the current study and Liu t al. study; the same finding is also recorded but with less effect. The measured fluoride concentration in the QMFA1, QMFA2 and QMFA3 media after 72 h conditioning is about 7.9 ppm, 7.2 ppm and 6.6 ppm respectively. These concentrations are significantly lower than the concentration of the fluoride found in Liu et al. study where the concentration was 12-16 ppm. Therefore, in the present study there is a mild effect on the cells osteogenic response unlike the huge cell suppression which found by Liu et al., 2016. Many studies have reported that fluoride in low doses is effective in enhancing the proliferation of the osteoblast cells. This positive effect would lead to the stimulation

of the bone formation and increasing the density of the bone by facilitating the retention of the calcium to the bone tissue (Rich and Ensinck, 1961, Kleerekoper and Mendlovic, 1993, Aaseth et al., 2004).

7.2 Titanium discs biocompatibility

Titanium is a bioinert material due to the presence of the TiO_2 layer on its surface. This layer is responsible for its biocompatibility *in vivo*, as it protects the surface from corrosion and it minimises the adverse reaction of the body (Okazaki and Gotoh, 2005, Lorenzetti et al., 2015, Wang et al., 2016). Modifying the surface of the Ti was used to create a functional surface with good surface properties and positive biological responses. Thus, it is essential to investigate the effect of the glass abrasion on the cell attachment, differentiation and bone matrix formation.

7.2.1 Cell morphology

Cell morphology is considered as an effective parameter in understanding the biocompatibility of an implant material, as the osteoblasts respond in a different manner, depending on the implant surface (Schmidt et al., 2002). The results of this study indicate and compare the 'behaviour' of the MC3T3 osteoblast cells on the pure titanium and the glass abraded titanium discs after 3 days in culture.

SEM micrographs demonstrate that both abraded and un-abraded discs are suitable environments for osteoblast-like adhesion and spreading. The spread pattern of the cells on the pure titanium discs is polygonal and flattened in shape Figure (7.3 a and b). The cells are well attached to the smooth titanium surface by their lamellar protrusions. However, this pattern is quite different from that on the glass abraded samples. The cells are attached on the glass surfaces by a thin cytoplasmic protrusions or filopodia, which extend from the base of the cells. The cell body is spindle shape and it is not attached to the glass surface Figure (7.3 c and d).

Additionally, it can be seen that the cells on both surfaces show an enormous proliferation and their borders start to connect and form a monolayer Figure (7.4).

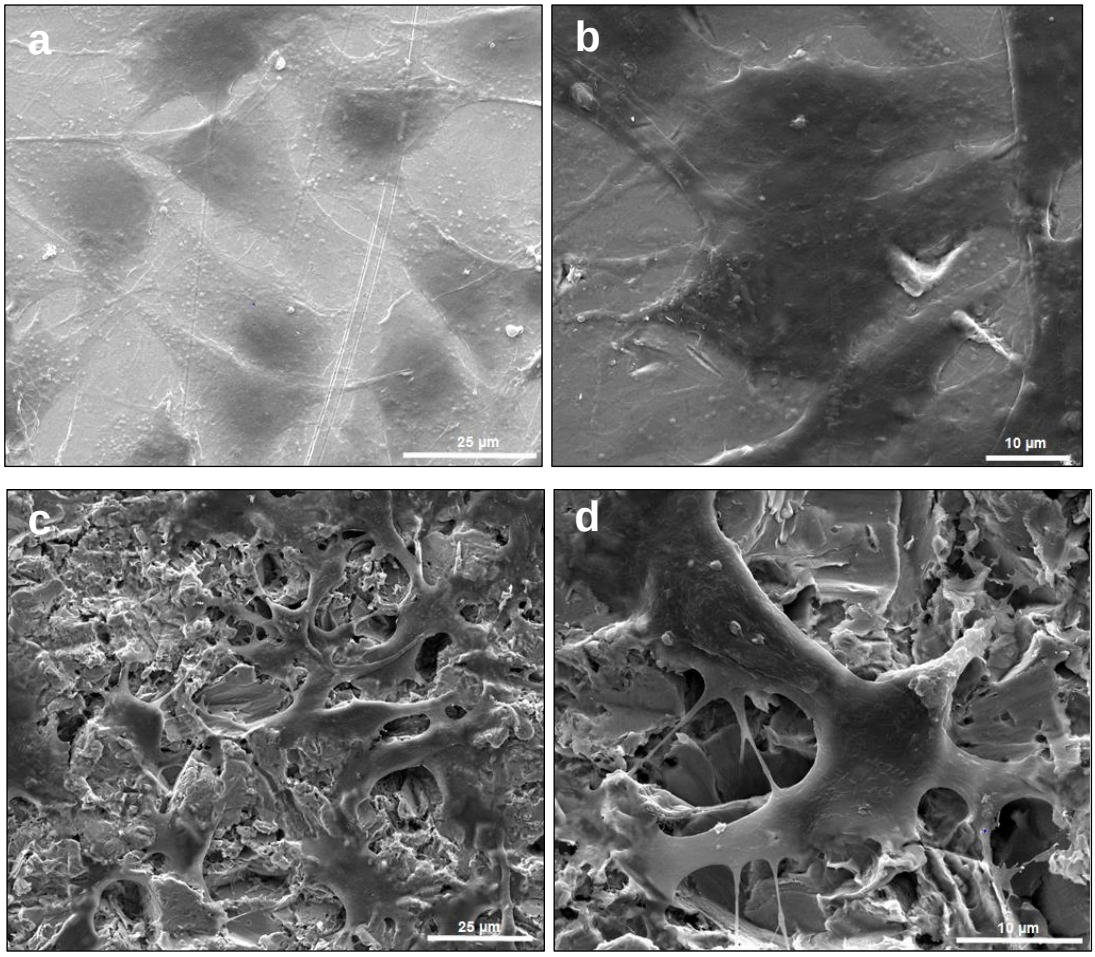

Figure 7.3: SEM micrographs of MC3T3-E1 osteoblast morphology on smooth titanium surface (a) at 2500x magnification (b) at 4000x magnification and on QMFA2 glass abraded surface (c) at 2500x magnification (d) at 4000x magnification after 3 days incubation. The cells on the smooth surface are flat polygonal in shape, while on the abraded rough surface the cells are spindle shape with multiple thin cytoplasmic protrusions.

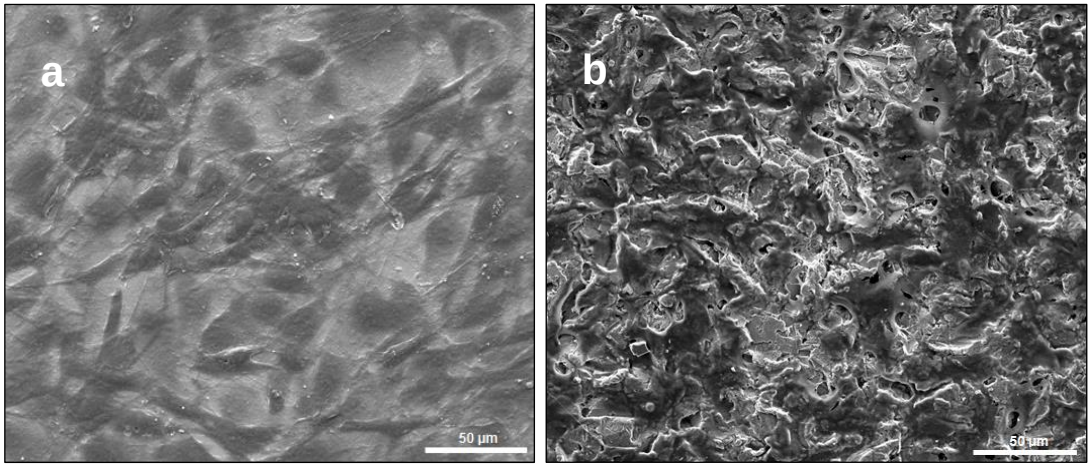

Figure 7.4: SEM micrographs of MC3T3-E1 osteoblasts spread on (a) smooth titanium surface (b) glass abraded surface after 3 days incubation (1000x Magnification). The cells are numerous and start to form a monolayer on both surfaces.

However, this feature is more clearly seen on the smooth pure titanium surface than on the glass treated surface. The small variation in the cell morphology and the attachment on both materials could be due to the difference in the surface topography and the surface roughness of the two samples. Apart from the surface chemistry of the material, the surface physical characteristic of the sample can affect the cells morphology and orientation (Flemming et al., 1999). In the current study, the pure titanium discs have smooth surface features with R_a value around 0.1 µm and this is quite different from the irregular rough surface of the abraded discs. Therefore, the cells on the control samples are spreading randomly and in a flat orientation while, the cells on the rough glass surface try to extend in a manner that connects the peaks of the surface. This bridging effect was also seen in previous studies (Groessner-Schreiber and Tuan, 1992, Locci et al., 1997, Anselme et al., 2000, Schmidt et al., 2002, Hakki et al., 2012). They reported that the osteoblasts grow in a three dimensional morphologies on the rough surface while on the smooth surface, they spread in flattened manner and in a morphology similar to the flattened fibroblast cells.

Although the findings were the same between the previous studies and this study, the direct comparison is relatively difficult. This is due to the differences in the cell type and the experimental methods that are used in all studies.

The presence of a rough surface could provide a preferable environment for the cells to produce good osseointegration with the implant material because of the formation of the 3-dimensional network (Schmidt et al., 2002). (Locci et al., 1997) found that the cells which grow on the titanium surface have the same morphological features to those grown on plastic surfaces. Other studies discussed the effect of the chemistry of the implant coating on the cell behaviour. The cells show high level of cell activation when they grow on 45S5. This was detected from the shape of the cells and the multiple microvilli that protruded from the cell bodies, as this phenotype is reflecting the good activity and biological response (Xynos et al., 2001). In the initial stages of the cell response to bioactive glass, the cells proliferate slowly and this mode of growth is similar to the *in vivo* bone repair (Henstock et al., 2015). Therefore, it can be indicated that both abraded and un-abraded samples are biocompatible and they allow for the attachment and the growth of the osteoblast cells.

7.2.2 Qualitative and quantitative results of ALP, collagen type I and mineralised nodule formation assays

ALP is a marker for cell differentiation, and contributes to the initial stages of the hard tissue formation (Harrison et al., 1995). ALP is an enzyme located in the outer surface of the plasma membrane of osteoblast cells. This enzyme is known to have an important role in the mineralisation process of bone tissues, as it enhances the calcification of bone tissues. However, the exact role, and the absolute mechanism of this enzyme in the mineralisation and calcification processes, is still controversial and not completely understood (Glimcher, 1986, Yoon et al., 1989, Golub et al., 1992).

Figure (7.5 a and b) shows the light microscopy images of the ALP activity of the osteoblast cells on pure titanium and glass abraded titanium discs after 14 days incubation. From both images, it can be seen that the osteoblasts are spread as clusters across the entire surface of both samples. This is clear from the spread of the blue precipitates on the surfaces, as these precipitates represent the ALP activity of the seeded cells. Therefore, it can be indicated that both abraded and un-abraded samples are enhancing the proliferation and differentiation of the osteoblasts. However, the intensity of the blue precipitates is slightly different between the two surfaces and this might be related to the difference in the surface topography of both samples. Moreover, the chemical structures of both surfaces are different and this might affect the biological behaviour of the osteoblast cells. The surface of the un-abraded disc is composed mainly of pure titanium, while the abraded disc is composed of titanium and bioactive glass materials. These differences may affect the proliferation and differentiation rates of the osteoblast cells. Therefore, in order to determine this difference numerically, and to investigate which surface is more simulative to the osteoblasts, a quantitative ALP assay was carried out. The results of this assay were collected after 14 days of cells incubation and the data were presented as means and SD of the ALP activity of the osteoblast cells on abraded and un-abraded samples, as can be seen in Figure (7.6).

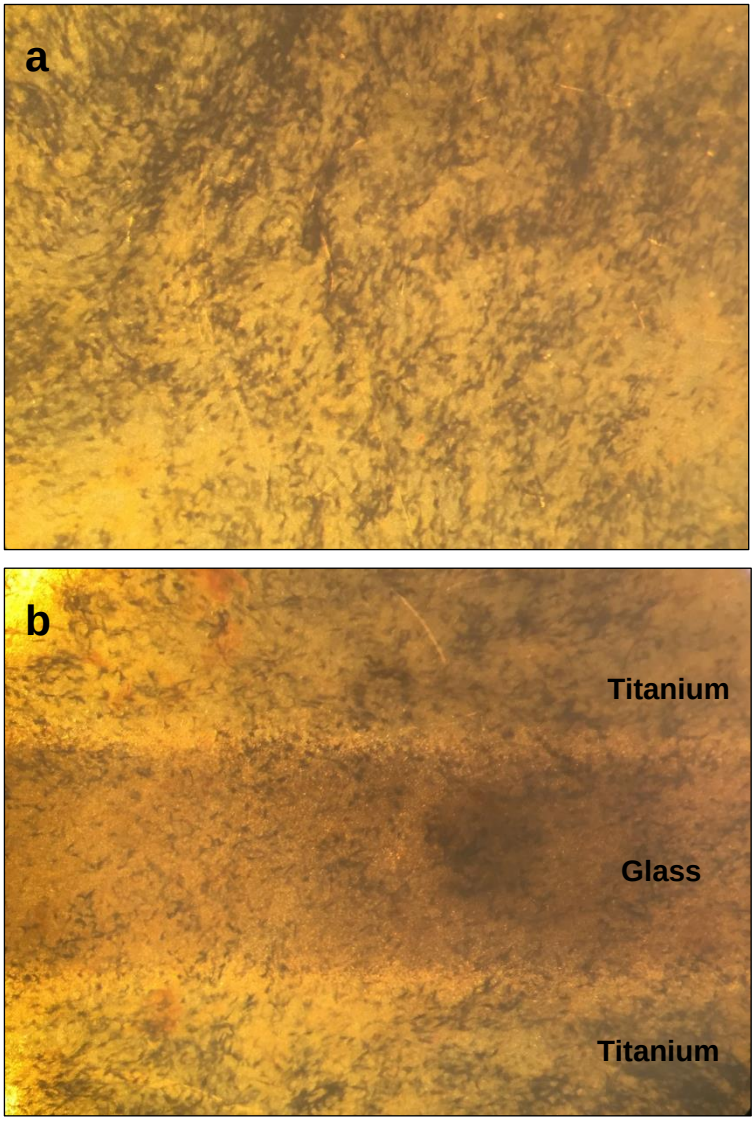

Figure 7.5: Light microscopy images showing the ALP activity of MC3T3-E1 osteoblast cells, as blue precipitates on (a) smooth titanium surface (b) glass abraded surface after 14 days incubation. The intensity of the blue precipitates on smooth Ti surface is slightly higher than the abraded surface.

In general, the results show that the ALP activity of the osteoblasts on the glass abraded discs is slightly higher than that on the smooth pure titanium discs. However, the *t-test* analysis shows that the difference between the ALP activities on both discs is not significant *(P≥0.05)*. This might be due to the small percentage of area coverage by the glass powder, as only 25% of the total titanium surface is covered by the glass particles. This partial coating might not give a clear picture to

the effect of the glass particles on the cells as would be the case with the total coverage. Therefore, this feature can be considered as one of the limitations in this study, as the abrasion procedure needs a large amount of glass powder to be prepared in order to perform the full coverage of the total area.

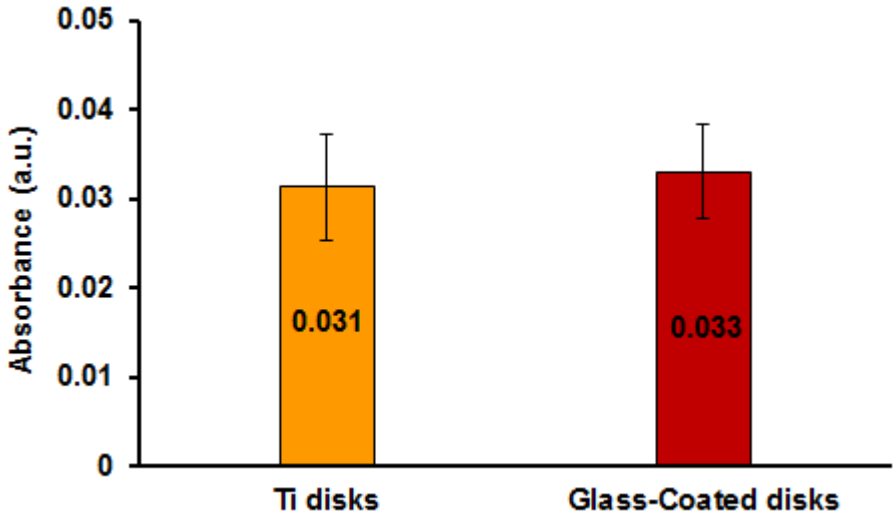

Figure 7.6: Quantitative results of ALP activity of MC3T3-E1 cells on smooth titanium surface and glass abraded surface after 14 days incubation period. Each bar represents the mean of three experiments (each with 3 samples) and their standard deviations. Student *t-test* shows that there is no statistical significant difference between the two groups *(P≥0.05)*.

Regarding the collagen type I assay, many studies reported that the process of new bone formation in the bone-implant interface is affected by the amount of collagen fibres formed in this area. Collagen type I is synthesised by the osteoblast cells and it forms 90% of the total bone proteins. Moreover, this protein is considered as an important marker in the formation of the bone matrix and it forms the backbone protein of the mineralised tissue (Franceschi and Iyer, 1992, Quarles et al., 1992, Franceschi et al., 1994, Zambonin et al., 2000). The osteogenic medium, which was used for the maintenance of the osteoblast cells for 2-3 weeks during the cell culture work, contains ascorbic acid and glycerophosphate. Ascorbic acid is involved in the

binding and the crosslinking of the collagen fibrils, while the second component is responsible for providing the cells with organic phosphate (DiGirolamo et al., 1999, Beck, 2003). This media was used due to the lack of phosphate source in the un-abraded titanium discs. ALP enzyme in the osteoblasts will extract the phosphate from the glycerophosphate and enrich the media with organic phosphate. This element will participate in the apatite formation and stimulate bone calcification.

The qualitative study of Sirius red stain shows that the stain on the glass abraded samples is presented as connected beads of collagen nodules across the abraded surface. However, on the pure titanium discs the collagen nodules are diffuse and separated in comparison to the glass abraded samples, as can be seen in Figure (7.7 a and b). Thus from the light microscopy images, it can be suggested that both surfaces are suitable for the formation and deposition of collagen and the spread of the cells on their surfaces. However, the behaviour of the cells is different between the two surfaces. This is again might be related to the difference in the topography and chemistry of the sample surfaces.

Interestingly in Figure (7.7 b), it can be seen that the intensity of the collagen nodule staining on the un-abraded titanium part of the glass abraded sample is darker than that of the pure titanium. This might be due to the effect of the presence of the bioactive glass particles on the surface. This embedded glass showed a subsequent dissolution when immersed in Tris and SBF, as discussed previously in Chapter 6 section 6.5. This dissolution led to the release of multiple ions, such as, Ca^{2+}, Na^{+}, PO_4^{3-} and silicate in the media and these ions might have an effect on the cell behaviour. Many studies suggest that the ions which are released from the bioactive glass may alter different expression markers in the osteoblast cells, as well as modifying the osteoblasts function (Beck et al., 2000, Reffitt et al., 2003, Maeno et al., 2005).

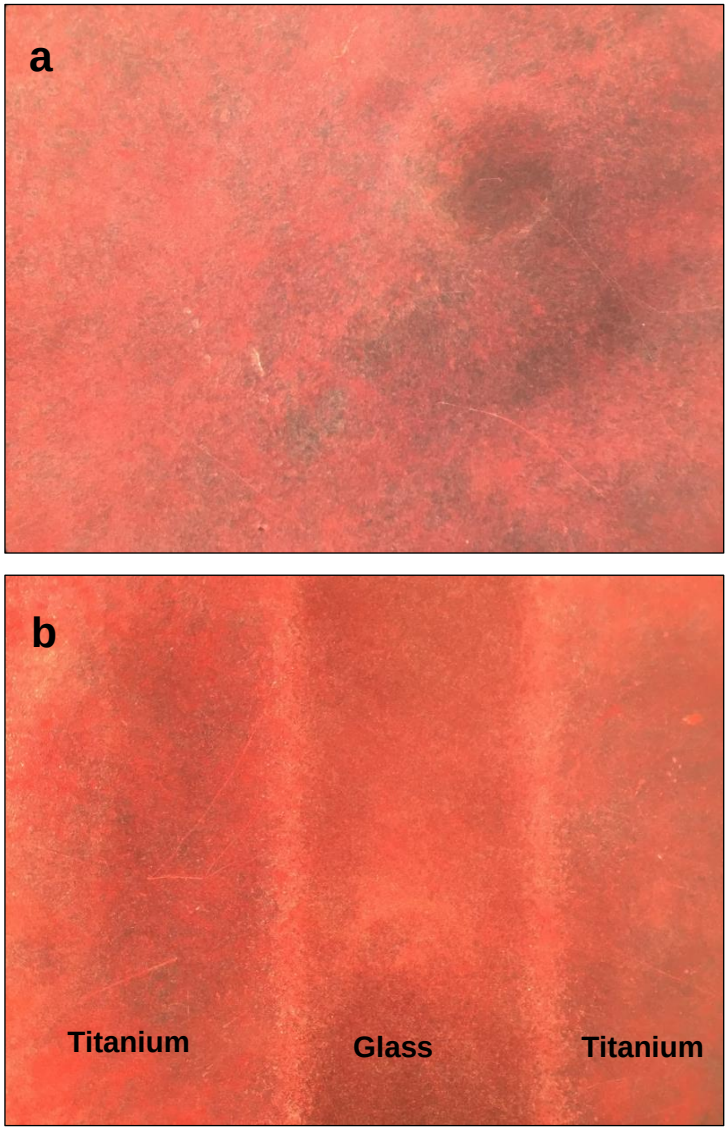

Figure 7.7: Light microscopy images showing the qualitative results of collagen type I nodule formation by using Sirius Red Stain on (a) smooth titanium surface (b) glass abraded surface after 28 days incubation. The collagen nodules are presented as connected beads across the abraded surface and as diffuse separated nodules on the pure titanium surface.

The quantification of Sirius red stain on both abraded and un-abraded titanium discs are shown in Figure (7.8). The results demonstrate an increase in the collagen content of MC3T3-E1 cells on the abraded discs with respect to the control pure titanium discs. These results are consistent with the light microscopy images, in

which the number of collagen beads appears more numerous on the abraded surface than the control un-abraded surface.

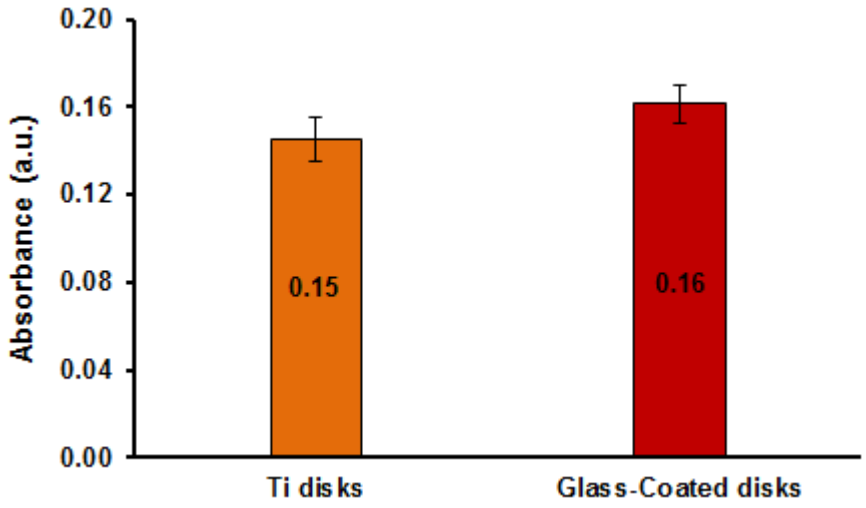

Figure 7.8: Quantitative results of Sirius Red Stain of MC3T3-E1 cells after 28 days incubation on smooth Ti discs and glass abraded discs. Each bar represents the mean of three experiments (each with 3 samples) and their standard deviations. Student *t-test* shows that there is no statistical significant difference between both groups *(P≥0.05)*.

For the mineralised nodule formation, the microscopy images of the glass abraded discs show the presence of small connected beads of mineralised nodules across the abraded line. The number of the bone-like nodules appear greater on the abraded line in comparison to that on the un-abraded part, as can be seen in Figure (7.9 b). The pure titanium disc, on the other hand, shows the presence of diffuse isolated mineralised nodules across the whole surface of the sample Figure (7. 9 a). The mineralised nodules are detected by the Alizarin red S stain and this stain is used for the identification of the calcium precipitation. Mineralised nodules act as nucleating agents which enriched with calcium and inorganic phosphate and it initiates the formation of the apatite (Wu et al., 1995).

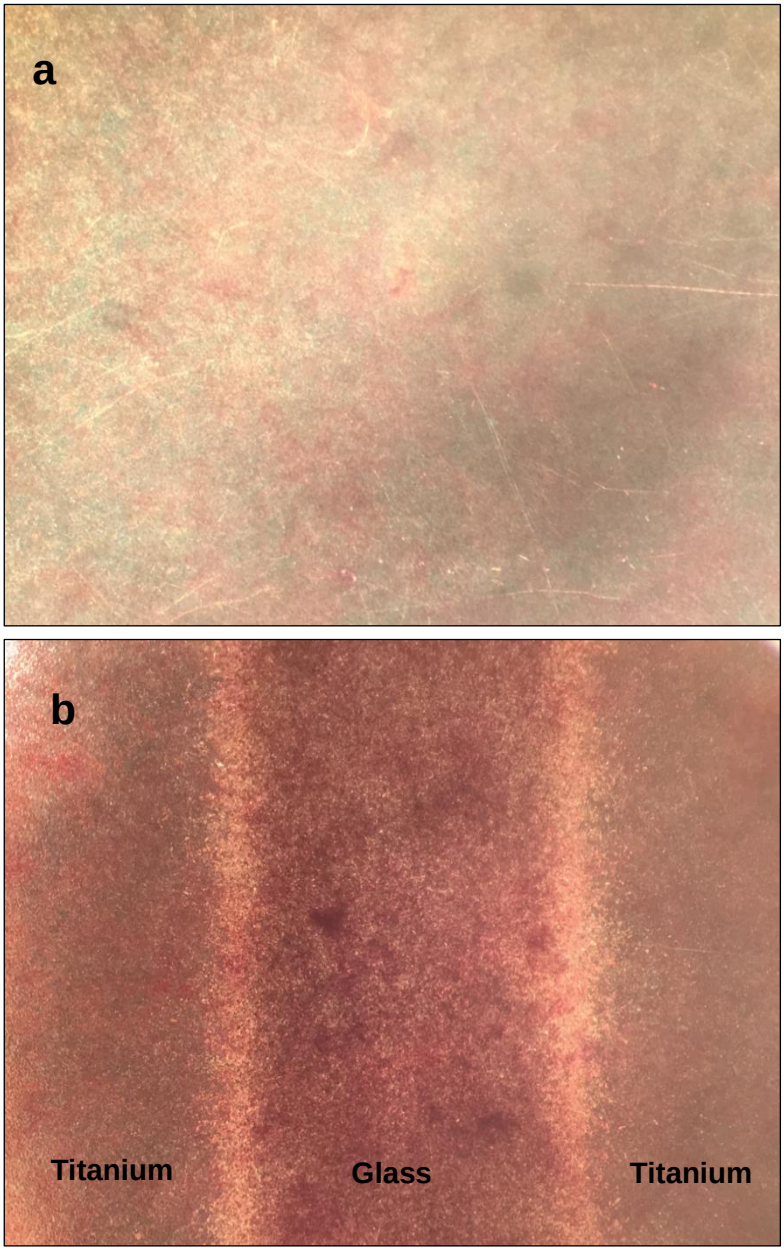

Figure 7.9: Light microscopy images showing the qualitative results of mineralised nodule formation by using Alizarin red S stain on (a) smooth titanium surface (b) glass abraded surface after 35 days incubation. The nodules are more numerous and connected on the glass surface than the smooth surface.

The quantitative analysis agrees with the visual observation and reveals that there is an insignificant difference in the amount of stain eluted and thus the level of calcium is presumably related to the number of nodules present between both surfaces. The nodules are more numerous on the abraded samples than the pure titanium discs Figure (7. 10).

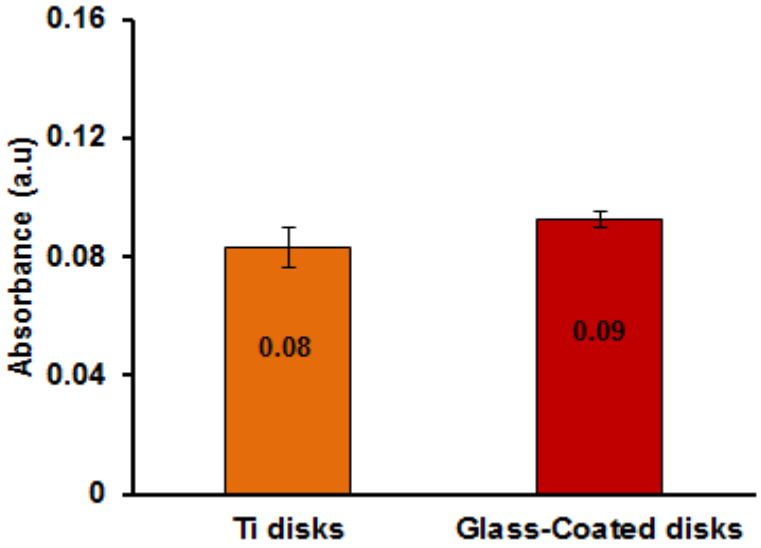

Figure 7.10: Quantitative results of Alizarin red S stain after 35 days incubation on smooth Ti discs and glass abraded discs. Each bar represents the mean of three experiments (each with 3 samples) and their standard deviations. Student *t-test* shows that there is no statistical significant difference between both groups *(P≥0.05)*.

These findings are consistent with the ALP and collagen type I results, where the nodules are more numerous on the glass abraded area than the pure titanium surface. Again, the bone nodules on the titanium surface of the abraded samples are relatively darker compared to that on the pure titanium surface. This feature was detected previously in the collagen type I results, as the density of the nodules on the former surface is higher than the un-abraded samples.

From the overall results, it can be seen that the coating of the titanium with the bioactive glass is advantageous in promoting the osteogenesis of the osteoblast

cells. Commercially pure titanium and its alloys are the material of choice in the fabrication of dental and orthopaedic implant. This is because of the good biocompatibility of this material *in vivo*. This material can form a direct bone-implant interface without the formation of a fibrous collagen layer, which is an important criterion in the implant stability and longevity (Klokkevold et al., 1997, Castellani et al., 1999). The modification of the pure titanium implant surface by its abrasion with bioactive glass was performed in order to create chemical and physical changes to the surface of the samples. These changes might improve the quality and the quantity of the bone-implant interface. Previous studies showed that these changes result in a significant effect on the biological response of the cultured cells and on the rate the cell attachments (Keller et al., 1989, Keller et al., 1990). The coating of the titanium implants with bioactive glasses results in a substantial improvement in the process of bone apposition on the implant surface and provides good bonding between the mineralised tissue and the abraded implant surfaces. This is due to the ability of the glass to dissolve in the body fluid and release the ions at the bone interface. These ions cause changes in the pH of the environment and result in an alkaline media. This environment stimulates the formation of HCA on the implant surface. This HCA layer has the affinity to bind to the collagen of the tissue and it facilitates the direct bonding to bone. As this material is chemically and structurally similar to bone tissue (Hench, 1991, Foppiano et al., 2004, Varanasi et al., 2006, O'Donnell et al., 2008, Jones, 2015). Additionally, the released ions Na^{+}, Ca^{2+}, PO_4^{3-} and silicate all induce the intracellular and extracellular responses, as these ions regulate the genes, which are responsible for stimulating the osteoblasts to secrete the bone matrix (Xynos et al., 2000, Jones, 2015). (Varanasi et al., 2009) reported that the Ca^{2+} and silicate which are released from the bioactive glass have a clear effect on the osteoblast cells behaviour. They found that the Ca^{2+} concentration between 8-20 ppm can increase the osteocalcin level of the cells and trigger the calcium receptors that cause a considerable response of the MC3T3-E1 cells.

Osteocalcin expression is increased with elevated Ca^{2+} levels in the conditioned media, and this can cause an increase in bone density (Maeno et al., 2005).

In addition to calcium, silicon also showed an effect on the osteogenic response of the osteoblasts cells. The low concentration of silicate increases the proliferation, collagen formation and osteocalcin expression (Gao et al., 2001, Reffitt et al., 2003, Varanasi et al., 2009). Therefore, the presence of Si ions in the glass structure could enhance the mineralisation process, which is consistent with the finding of the current study. Moreover, the designed glasses possess high concentration of phosphate in their compositions and this amount is essential in enhancing the bone mineralisation. The presence of high concentration of inorganic phosphate in the medium may increase the ALP activity of the cells together with increasing the collagen content. Additionally, this inorganic phosphate is responsible for the mineral deposition and this enhances the mineralisation and the calcification of the bone tissue (Beck, 2003). The presence of high phosphate in the glass composition is considered as a positive promoting factor in increasing the rate of apatite formation *in vitro*. The apatite layer is important in forming a chemical bond with the bone.

The formation of HAP layer on the surface of the glass material *in vivo* may promote the osseointegration process. This is due to the ability of the collagen fibres to adsorb and crosslink to the bone tissue surface (O'Donnell et al., 2008). However, in the current study, the designed glasses possess fluoride in their compositions and this gives the opportunity for the formation of the FAP. Many studies reported that FAP is more resistant to the acid dissolution and also shows good biocompatibility (LeGeros et al., 1988, Dhert et al., 1993, Okazaki et al., 1999). It is demonstrated previously in Chapter 6.4 that the concentration of fluoride in the abraded area is relatively small, and is significantly lower than that in the glass conditioned media. Therefore, the results of this part of the study provide positive and effective findings regarding the biological and osteogenic response of the MC3T3-E1 cells in vitro.

This is clear from the increase in the amount of the differentiation and the nodule formation markers. (Qu and Wei, 2006) found that the proliferation and differentiation of the SAOS-3 rat osteosarcoma on FAP discs is higher than that on the HAP discs and they suggested that it is related to the release of the F^- ion from the FAP, which causes high stimulation to the cells.

7.3 Summary:

Evaluating the mechanical and physical properties of the prepared materials is essential in the design of dental implants. However, the *in vitro* biological responses to the designed samples and their effect on the osteoblast cells are also necessary to be investigated prior to an *in vivo* study. In this study, the bioactivity of the designed glasses was investigated on the MC3T3-E1 cell line by measuring their DNA content and ALP activity. The glasses promote both proliferation and differentiation processes, however the enhancement effect is relatively small in comparison to the cells treated with the control α-MEM media.

The QMFA2 glass abraded discs were also investigated for their biocompatibility *in vitro* using the same cell line. The osteogenic response of the cells on these discs was tested and compared to that on the smooth un-abraded samples. The roughness of the implanted surface shows a clear effect on the cell morphology and the mineralisation process. The cells on the smooth titanium surface are flat in shape, while on the abraded surface they appear as spindle shaped cells with multiple microvilli. Moreover, the ALP activity, collagen type I and mineralised nodule formations of the cells are slightly higher on the abraded samples in comparison to the smooth pure titanium samples. However, this is not statistically significant.

Chapter 8
Conclusions and Future Work

8 Conclusions and Future Work

8.1 Conclusions

The sodium content in the glass composition is an effective factor in reducing both the hardness of the bioactive glass and the glass transition temperature. Both parameters are probably dependant on the strength of bonding in the glass network.

All three glasses show a good bioactivity *in vitro* as they form apatite within 3 h in Tris and within 24 h in SBF, which should ensure excellent osseointegration. However, the presence of proteins in the culture media slows the rate of glass degradation and decreases their ability to form apatite. The presence of high bicarbonate content in the immersion media in addition to the presence of small amount of fluoride in the glass composition results in the formation of a new type of apatite, which is a fluorocarbonated apatite, in which F^- substitutes along with CO_3^{2-} for a PO_4^{3-} in the B-site.

Regarding the grit blast process and the coating of titanium implants, the designed glass particles are coarse in nature with angular sharp edges. These features give rise to the abrasive nature of the glass particles and their embedding ability into the abraded titanium surface. The novel glasses are successfully modifying the surface of the titanium implant. The particles are abrasive enough to significantly increase the surface roughness of the titanium samples from Ra 0.1 µm to Ra 1.6 µm. The grit blast parameters, such as sample distance, velocity and air propellant pressure are all effective parameters in modifying the area covered by the bioactive glass and the amount of substrate removal. The spread pattern of the glass particles on the titanium surface is represented by the width of the abraded line. This pattern is highly controlled by changing the sample-nozzle distance and it is less affected by

changing the operating pressure parameter. However, the substrate velocity showed a medium effect on the spread pattern of the particles. The volume and depth of the abraded area are equally affected by all the operating parameters. The volume and depth of the abraded area decrease with increasing hardness of the glass, as more glass particles are embedded in the target area. However, the area coverage by the glass particles increases with increasing the hardness of the glass. Surface roughness is less affected by the glass hardness. Generally, high percentage of area coverage is shown with all the glasses and the range is from 52 to 62 %. From all these features, it can be concluded that the grit blast parameters together with the physical properties of the glass determine the coating process. The rough surface together with the good glass coverage is an attractive feature for good integrated implants. However the bond strength between the substrate surface and the coating material is a critical point, practically this criterion is difficult to measure. Therefore, in this study it was decided to measure the glass resistance to dissolution in a week acidic condition and determine this as a method of measuring the bond strength. The SEM-EDX analysis of the tested samples confirms the resistance of the glass to dissolution and the harder glass embeds more in the surface of the titanium. This is clear from the high concentrations of ions which were detected by the ICP-OES analysis. In addition to the bond strength, the *in vitro* bioactivity of the glass abraded discs was tested by the immersion of the abraded discs in Tris buffer and SBF. The formation of apatite on the surface of the discs was observed within 3 days of immersion and this is a positive sign of good bioactivity. The discs also show good bioactivity with the osteoblasts cells, as the abraded discs increase their differentiation and proliferation together with stimulating the collagen and nodules formation *in vitro*. Grit blasting with the chosen glasses appears to be a promising coating procedure for dental implants.

8.2 Suggestions for Future work

- The formation of fluorocarbonated apatite in SFα-MEM and the delay in apatite formation in 10% Sα-MEM suggests further studies: immersing the glasses in low concentration of serum containing α-MEM (2% and 5%) for various time periods and investigating the type of apatite formation, both qualitatively and quantitatively by XRD, FTIR, MAS-NMR and Neutron diffraction.
- The abrasive nature of the glass particles and the amount of particles embedded in the surface give the opportunity to investigate the effect of different particle size range (63-90 μm, 90-125 μm and 125-250 μm) on the surface roughness, the extent of glass embedding, the surface area coverage and the dimension of the abrasion.
- The formation of apatite on the titanium surface and its detection by EDX suggests the investigation of the surface chemistry of the un-abraded Ti discs and the glass abraded Ti discs by X-ray photoelectron spectroscopy (XPS) before and after immersion in Tris buffer and SBF for various time periods. This is to evaluate the sequential changes to the chemical structure of the surface.
- The composition of the glass has an effect on the amount of particles embedded in the abraded surface, as the glass of lower sodium content embedded more in the surface. This suggests the elemental evaluation of the released ions from the abraded samples prepared by all the parameters after their immersion in acetic acid for specific time period by using ICP-OES analysis and compare the outcome findings.

- It is apparent that the data from the glass abraded samples is diluted by the response of the cells on the un-abraded part of the discs; therefore, the effect of the whole abraded surface on the proliferation, differentiation and mineralisation, as well as on the gene expression is mandatory.
- It would be anticipated that such glass abraded metals would be implanted in the bone tissue to suppress peri-implantitis, it is necessary to investigate the antibacterial action of the glass coatings on the supra and sub-gingival pathogens.
- The good bioactivity of the glass coating and its promising results regarding osteoblast differentiation and mineralisation *in vitro* suggest the investigation of the effect of the glass coatings on the bone healing by histological analysis and on the strength of osseointegration by torque test *in vivo*.

9 References

AASETH, J., SHIMSHI, M., GABRILOVE, J. L. & BIRKETVEDT, G. S. 2004. Fluoride: a toxic or therapeutic agent in the treatment of osteoporosis? *The Journal of Trace Elements in Experimental Medicine,* 17**,** 83-92.

ABUHUSSEIN, H., PAGNI, G., REBAUDI, A. & WANG, H. L. 2010. The effect of thread pattern upon implant osseointegration. *Clinical oral implants research,* 21**,** 129-136.

AINA, V., MALAVASI, G., PLA, A. F., MUNARON, L. & MORTERRA, C. 2009. Zinc-containing bioactive glasses: surface reactivity and behaviour towards endothelial cells. *Acta Biomaterialia,* 5**,** 1211-1222.

AKAHORI, T., NIINOMI, M. & SUZUKI, A. 2002. Improvement in mechanical properties of dental cast Ti-6Al-7Nb by thermochemical processing. *Metallurgical and Materials Transactions A,* 33**,** 503-510.

AL-ANI, M. D. 2013. *GRIT BLASTING OF BIOACTIVE GLASS COATING ON TITANIUM.* Masters, Queen Mary, University of London.

AL-NOAMAN, A. 2012. *Novel bioactive glass coating for dental implant.*

AL-NOAMAN, A., RAWLINSON, S. C. & HILL, R. G. 2012a. The influence of CaF 2 content on the physical properties and apatite formation of bioactive glass coatings for dental implants. *Journal of Non-Crystalline Solids,* 358**,** 1850-1858.

AL-NOAMAN, A., RAWLINSON, S. C. & HILL, R. G. 2012b. The role of MgO on thermal properties, structure and bioactivity of bioactive glass coating for dental implants. *Journal of Non-Crystalline Solids,* 358**,** 3019-3027.

ALBREKTSSON, T., BRÅNEMARK, P.-I., HANSSON, H.-A. & LINDSTRÖM, J. 1981. Osseointegrated titanium implants: requirements for ensuring a long-lasting, direct bone-to-implant anchorage in man. *Acta Orthopaedica Scandinavica,* 52**,** 155-170.

ALBREKTSSON, T. & JOHANSSON, C. 2001. Osteoinduction, osteoconduction and osseointegration. *European Spine Journal,* 10**,** S96-S101.

ALBREKTSSON, T. & WENNERBERG, A. 2004. Oral implant surfaces: Part 1--review focusing on topographic and chemical properties of different surfaces and in vivo responses to them. *International Journal of Prosthodontics,* 17.

ALBREKTSSON, T., ZARB, G., WORTHINGTON, P. & ERIKSSON, A. 1986. The long-term efficacy of currently used dental implants: a review and proposed criteria of success. *Int J Oral Maxillofac Implants,* 1**,** 11-25.

ALBREKTSSON, T. & ZARB, G. A. 1993. Current interpretations of the osseointegrated response: clinical significance. *International Journal of Prosthodontics,* 6.

ALI, A. 2014. Short dental implants: an emerging concept in implant treatment.

ALLA, R. K., GINJUPALLI, K., UPADHYA, N., SHAMMAS, M., RAVI, R. K. & SEKHAR, R. 2011. Surface roughness of implants: a review. *Trends in Biomaterials and Artificial Organs,* 25**,** 112-118.

ALVIM-PEREIRA, F., MONTES, C. C., MIRA, M. T. & TREVILATTO, P. C. 2008. Genetic susceptibility to dental implant failure: a critical review. *International Journal of Oral & Maxillofacial Implants,* 23.

ANDERSSON, Ö. 1992. Glass transition temperature of glasses in the SiO2-Na2O-CaO-P2O5-Al2O3-B2O3 system. *Journal of Materials Science: Materials in Medicine,* 3**,** 326-328.

ANITUA, E., CARDA, C. & ANDIA, I. 2007. A novel drilling procedure and subsequent bone autograft preparation: a technical note. *International Journal of Oral and Maxillofacial Implants,* 22**,** 138.

ANSELME, K., BIGERELLE, M., NOEL, B., DUFRESNE, E., JUDAS, D., IOST, A. & HARDOUIN, P. 2000. Qualitative and quantitative study of human osteoblast adhesion on materials with various surface roughnesses. *Journal of Biomedical Materials Research Part A,* 49**,** 155-166.

APARICIO, C., GIL, F. J., FONSECA, C., BARBOSA, M. & PLANELL, J. A. 2003. Corrosion behaviour of commercially pure titanium shot blasted with different materials and sizes of shot particles for dental implant applications. *Biomaterials,* 24**,** 263-273.

ASHLEY, E. T., COVINGTON, L. L., BISHOP, B. G. & BREAULT, L. G. 2003. Ailing and failing endosseous dental implants: a literature review. *J Contemp Dent Pract,* 4**,** 35-50.

AYDıN, C., YıLMAZ, H. & BANKOĞLU, M. 2013. A single-tooth, two-piece zirconia implant located in the anterior maxilla: a clinical report. *The Journal of prosthetic dentistry,* 109**,** 70-74.

BAESSO, M., BENTO, A., DUARTE, A., NETO, A., MIRANDA, L., SAMPAIO, J., CATUNDA, T., GAMA, S. & GANDRA, F. 1999. Nd~ 2O~ 3 doped low silica calcium aluminosilicate glasses: Thermomechanical properties. *Journal of applied physics,* 85**,** 8112.

BAILEY, L. R. & PHILLIPS, R. W. 1950. Effect of certain abrasive materials on tooth enamel. *Journal of dental research,* 29**,** 740-748.

BALLO, A. M., OMAR, O., XIA, W. & PALMQUIST, A. 2011. Dental implant surfaces–physicochemical properties, biological performance, and trends. *Implant Dentistry-A Rapidly Evolving Practice.* InTech.

BANERJEE, A., UDDIN, M., PAOLINELIS, G. & WATSON, T. F. 2008. An investigation of the effect of powder reservoir volume on the consistency of alumina powder flow rates in dental air-abrasion devices. *journal of dentistry,* 36**,** 224-227.

BANERJEE, A. & WATSON, T. 2002. Air abrasion: its uses and abuses. *Dental update,* 29**,** 340-346.

BAQAIN, Z. H., MOQBEL, W. Y. & SAWAIR, F. A. 2012. Early dental implant failure: risk factors. *British Journal of Oral and Maxillofacial Surgery,* 50**,** 239-243.

BECK, G. R. 2003. Inorganic phosphate as a signaling molecule in osteoblast differentiation. *Journal of cellular biochemistry,* 90**,** 234-243.

BECK, G. R., ZERLER, B. & MORAN, E. 2000. Phosphate is a specific signal for induction of osteopontin gene expression. *Proceedings of the National Academy of Sciences,* 97**,** 8352-8357.

BEDI, R. S., BEVING, D. E., ZANELLO, L. P. & YAN, Y. 2009. Biocompatibility of corrosion-resistant zeolite coatings for titanium alloy biomedical implants. *Acta Biomaterialia,* 5**,** 3265-3271.

BERGLUNDH, T., ABRAHAMSSON, I., LANG, N. P. & LINDHE, J. 2003. De novo alveolar bone formation adjacent to endosseous implants. *Clinical oral implants research,* 14**,** 251-262.

BEUSELINCK, L., GOVERS, G., POESEN, J., DEGRAER, G. & FROYEN, L. 1998. Grain-size analysis by laser diffractometry: comparison with the sieve-pipette method. *Catena,* 32**,** 193-208.

BHARATI, S., SOUNDRAPANDIAN, C., BASU, D. & DATTA, S. 2009. Studies on a novel bioactive glass and composite coating with hydroxyapatite on titanium based alloys: Effect of γ-sterilization on coating. *Journal of the European Ceramic Society,* 29**,** 2527-2535.

BLACK, R. B. 1945. Technic for nonmechanical preparation of cavities and prophylaxis. *The Journal of the American Dental Association,* 32**,** 955-965.

BLACK, R. B. 1950. Airbrasive: some fundamentals. *The Journal of the American Dental Association,* 41**,** 701-710.

BLUMENTHAL, N. C. & COSMA, V. 1989. Inhibition of apatite formation by titanium and vanadium ions. *Journal of Biomedical Materials Research Part A,* 23**,** 13-22.

BODINE, R. L., YANASE, R. T. & BODINE, A. 1996. Forty years of experience with subperiosteal implant dentures in 41 edentulous patients. *The Journal of prosthetic dentistry,* 75**,** 33-44.

BOHNER, M. & LEMAITRE, J. 2009. Can bioactivity be tested in vitro with SBF solution? *Biomaterials,* 30**,** 2175-2179.

BOLELLI, G., CANNILLO, V., GADOW, R., KILLINGER, A., LUSVARGHI, L. & RAUCH, J. 2009. Microstructural and in vitro characterisation of high-velocity suspension flame sprayed (HVSFS) bioactive glass coatings. *Journal of the European Ceramic Society,* 29**,** 2249-2257.

BOSS, C. B. & FREDEEN, K. J. 1999. *Concepts, instrumentation and techniques in inductively coupled plasma optical emission spectrometry*, Perkin Elmer Norwalk.

BRAUER, D. S. 2015. Bioactive glasses—structure and properties. *Angewandte Chemie International Edition,* 54**,** 4160-4181.

BRAUER, D. S., KARPUKHINA, N., LAW, R. V. & HILL, R. G. 2009. Structure of fluoride-containing bioactive glasses. *Journal of Materials Chemistry,* 19**,** 5629-5636.

BRAUER, D. S., KARPUKHINA, N., O'DONNELL, M. D., LAW, R. V. & HILL, R. G. 2010. Fluoride-containing bioactive glasses: effect of glass design and structure on degradation, pH and apatite formation in simulated body fluid. *Acta Biomaterialia,* 6**,** 3275-3282.

BRAUER, D. S., KARPUKHINA, N., SEAH, D., LAW, R. V. & HILL, R. G. Fluoride-containing bioactive glasses. Advanced Materials Research, 2008. Trans Tech Publ, 297-302.

BRAY, G., FAUCI, A., BRAUNWALD, E., ISSELBACHER, K., WILSON, J., MARTIN, J. & KASPER, D. 1998. Harrison's principle of internal medicine.

BRUNETTE, D. M., TENGVALL, P., TEXTOR, M. & THOMSEN, P. 2012. *Titanium in medicine: material science, surface science, engineering, biological responses and medical applications*, Springer Science & Business Media.

BUSER, D., SCHENK, R., STEINEMANN, S., FIORELLINI, J., FOX, C. & STICH, H. 1991. Influence of surface characteristics on bone integration of titanium implants. A histomorphometric study in miniature pigs. *Journal of biomedical materials research,* 25**,** 889-902.

CARLSSON, L., RÖSTLUND, T., ALBREKTSSON, B., ALBREKTSSON, T. & BRÅNEMARK, P.-I. 1986. Osseointegration of titanium implants. *Acta Orthopaedica Scandinavica,* 57**,** 285-289.

CASTELLANI, R., DE RUIJTER, A., RENGGLI, H. & JANSEN, J. 1999. Response of rat bone marrow cells to differently roughened titanium discs. *Clinical Oral Implants Research,* 10**,** 369-378.

CAVALCANTE GOMES DE SOUZA CARVALHO, A., PEREIRA QUEIROZ, T., OKAMOTO, R., MARGONAR, R., RANGEL GARCIA, I. & MAGRO FILHO, O. 2011. Evaluation of bone heating, immediate bone cell viability, and wear of high-resistance drills after the creation of implant osteotomies in rabbit tibias. *International Journal of Oral & Maxillofacial Implants,* 26.

ÇEHRELI, M., ŞAHIN, S. & AKÇA, K. 2004. Role of mechanical environment and implant design on bone tissue differentiation: current knowledge and future contexts. *Journal of dentistry,* 32**,** 123-132.

CERRUTI, M., GREENSPAN, D. & POWERS, K. 2005. Effect of pH and ionic strength on the reactivity of Bioglass® 45S5. *Biomaterials,* 26**,** 1665-1674.

CHAKKALAKAL, D., MASHOOF, A., NOVAK, J., STRATES, B. & MCGUIRE, M. 1994. Mineralization and pH relationships in healing skeletal defects grafted with demineralized bone matrix. *Journal of Biomedical Materials Research Part A,* 28**,** 1439-1443.

CHAPPARD, D., AGUADO, E., HURÉ, G., GRIZON, F. & BASLE, M. F. 1999. The early remodeling phases around titanium implants: a histomorphometric assessment of bone quality in a 3-and 6-month study in sheep. *International Journal of Oral and Maxillofacial Implants,* 14**,** 189-196.

CHEANG, P. & KHOR, K. 1996. Addressing processing problems associated with plasma spraying of hydroxyapatite coatings. *Biomaterials,* 17**,** 537-544.

CHEN, Q., ZHU, C. & THOUAS, G. A. 2012. Progress and challenges in biomaterials used for bone tissue engineering: bioactive glasses and elastomeric composites. *Progress in Biomaterials,* 1**,** 2.

CHEN, Q. Z., THOMPSON, I. D. & BOCCACCINI, A. R. 2006. 45S5 Bioglass®-derived glass–ceramic scaffolds for bone tissue engineering. *Biomaterials,* 27**,** 2414-2425.

CHEN, X., CHEN, X., BRAUER, D. S., WILSON, R. M., HILL, R. G. & KARPUKHINA, N. 2014a. Bioactivity of sodium free fluoride containing glasses and glass-ceramics. *Materials,* 7**,** 5470-5487.

CHEN, X., CHEN, X., BRAUER, D. S., WILSON, R. M., HILL, R. G. & KARPUKHINA, N. 2014b. Novel alkali free bioactive fluorapatite glass ceramics. *Journal of Non-Crystalline Solids,* 402**,** 172-177.

CHERN LIN, J., LIU, M. & JU, C. 1994. Structure and properties of hydroxyapatite-bioactive glass composites plasma sprayed on Ti6Al4V. *Journal of Materials Science: Materials in Medicine,* 5**,** 279-283.

CHO, S.-A. & PARK, K.-T. 2003. The removal torque of titanium screw inserted in rabbit tibia treated by dual acid etching. *Biomaterials,* 24**,** 3611-3617.

CHRISSANTHOPOULOS, A., BOUROPOULOS, N. & YANNOPOULOS, S. 2008. Vibrational spectroscopic and computational studies of sol–gel derived CaO–MgO–SiO 2 binary and ternary bioactive glasses. *Vibrational Spectroscopy,* 48**,** 118-125.

CHRISTIE, J. K., PEDONE, A., MENZIANI, M. C. & TILOCCA, A. 2011. Fluorine environment in bioactive glasses: ab initio molecular dynamics simulations. *The Journal of Physical Chemistry B,* 115**,** 2038-2045.

CLUPPER, D. C., MECHOLSKY, J. J., LATORRE, G. P. & GREENSPAN, D. C. 2002. Bioactivity of tape cast and sintered bioactive glass-ceramic in simulated body fluid. *Biomaterials,* 23**,** 2599-2606.

COCCHI, M., DURANTE, C., LUSVARDI, G., MALAVASI, G. & MENABUE, L. 2012. Evaluation of the behaviour of fluorine-containing bioactive glasses: reactivity in a simulated body fluid solution assisted by multivariate data analysis. *Journal of Materials Science: Materials in Medicine,* 23**,** 639-648.

COELHO, P. G., GRANJEIRO, J. M., ROMANOS, G. E., SUZUKI, M., SILVA, N. R., CARDAROPOLI, G., THOMPSON, V. P. & LEMONS, J. E. 2009. Basic research methods and current trends of dental implant surfaces. *Journal of Biomedical Materials Research Part B: Applied Biomaterials,* 88**,** 579-596.

COOPER, L. F. 2000. A role for surface topography in creating and maintaining bone at titanium endosseous implants. *The Journal of prosthetic dentistry,* 84**,** 522-534.

COOPER, L. F., ZHOU, Y., TAKEBE, J., GUO, J., ABRON, A., HOLMÉN, A. & ELLINGSEN, J. E. 2006. Fluoride modification effects on osteoblast behavior and bone formation at TiO 2 grit-blasted cp titanium endosseous implants. *Biomaterials,* 27**,** 926-936.

COWIN, S. C. 1999. Bone poroelasticity. *Journal of biomechanics,* 32**,** 217-238.

DAVIES, J. 1996. In vitro modeling of the bone/implant interface. *The Anatomical Record,* 245**,** 426-445.

DAVIES, J. E. 2003. Understanding peri-implant endosseous healing. *Journal of dental education,* 67**,** 932-949.

DE AZA, P., DE AZA, A., PENA, P. & DE AZA, S. 2007. Bioactive glasses and glass-ceramics. *BOLETIN-SOCIEDAD ESPANOLA DE CERAMICA Y VIDRIO,* 46**,** 45.

DEE, K. C., PULEO, D. A. & BIZIOS, R. 2003. *An introduction to tissue-biomaterial interactions*, John Wiley & Sons.

DHERT, W., KLEIN, C., JANSEN, J., VAN DER VELDE, E., VRIESDE, R., ROZING, P. & DE GROOT, K. 1993. A histological and histomorphometrical investigation of fluorapatite, magnesiumwhitlockite, and hydroxylapatite plasma-sprayed coatings in goats. *Journal of Biomedical Materials Research Part A,* 27**,** 127-138.

DIBA, M., TAPIA, F., BOCCACCINI, A. R. & STROBEL, L. A. 2012. Magnesium-containing bioactive glasses for biomedical applications. *International Journal of Applied Glass Science,* 3**,** 221-253.

DIGIROLAMO, C. M., STOKES, D., COLTER, D., PHINNEY, D. G., CLASS, R. & PROCKOP, D. J. 1999. Propagation and senescence of human marrow stromal cells in culture: a simple colony-forming assay identifies samples with the greatest potential to propagate and differentiate. *British journal of haematology,* 107**,** 275-281.

DIMITRIOU, R. & BABIS, G. 2007. Biomaterial osseointegration enhancement with biophysical stimulation. *J Musculoskelet Neuronal Interact,* 7**,** 253-265.

DOBLARÉ, M., GARCıA, J. & GÓMEZ, M. 2004. Modelling bone tissue fracture and healing: a review. *Engineering Fracture Mechanics,* 71**,** 1809-1840.

DOYLE, W. M. 1992. Principles and applications of Fourier transform infrared (FTIR) process analysis. *Process control and quality,* 2**,** 11-41.

EBISAWA, Y., KOKUBO, T., OHURA, K. & YAMAMURO, T. 1990. Bioactivity of CaO· SiO 2-based glasses: in vitro evaluation. *Journal of materials science: Materials in Medicine,* 1**,** 239-244.

ECKERT, S. E., MERAW, S. J., WEAVER, A. L. & LOHSE, C. M. 2001. Early experience with Wide-Platform Mk II implants. Part I: Implant survival. Part II: Evaluation of risk factors involving implant survival. *International Journal of Oral & Maxillofacial Implants,* 16.

EHRENFEST, D. M. D., COELHO, P. G., KANG, B.-S., SUL, Y.-T. & ALBREKTSSON, T. 2010. Classification of osseointegrated implant surfaces: materials, chemistry and topography. *Trends in biotechnology,* 28**,** 198-206.

ELGAYAR, I., ALIEV, A., BOCCACCINI, A. & HILL, R. 2005. Structural analysis of bioactive glasses. *Journal of Non-Crystalline Solids,* 351**,** 173-183.

ELLINGSEN, J. E., JOHANSSON, C. B., WENNERBERG, A. & HOLMÉN, A. 2004. Improved retention and bone-to-implant contact with fluoride-modified titanium implants. *International Journal of Oral & Maxillofacial Implants,* 19.

ELLINGSEN, J. E., THOMSEN, P. & LYNGSTADAAS, S. P. 2006. Advances in dental implant materials and tissue regeneration. *Periodontology 2000,* 41**,** 136-156.

ERIKSSON, R. & ALBREKTSSON, T. 1984. The effect of heat on bone regeneration: an experimental study in the rabbit using the bone growth chamber. *Journal of Oral and Maxillofacial surgery,* 42**,** 705-711.

ESPOSITO, M., HIRSCH, J., LEKHOLM, U. & THOMSEN, P. 1998a. Biological factors contributing. *European journal of oral sciences,* 106**,** 527-551.

ESPOSITO, M., HIRSCH, J. M., LEKHOLM, U. & THOMSEN, P. 1998b. Biological factors contributing to failures of osseointegrated oral implants,(II). Etiopathogenesis. *European journal of oral sciences,* 106**,** 721-764.

FAROOQ, I., TYLKOWSKI, M., MÜLLER, S., JANICKI, T., BRAUER, D. S. & HILL, R. G. 2013. Influence of sodium content on the properties of bioactive glasses for use in air abrasion. *Biomedical Materials,* 8**,** 065008.

FEIGHAN, J. E., GOLDBERG, V. M., DAVY, D., PARR, J. A. & STEVENSON, S. 1995. The influence of surface-blasting on the incorporation of titanium-alloy implants in a rabbit intramedullary model. *JBJS,* 77**,** 1380-1395.

FILGUEIRAS, M. R., LA TORRE, G. & HENCH, L. L. 1993a. Solution effects on the surface reactions of a bioactive glass. *Journal of Biomedical Materials Research Part A,* 27**,** 445-453.

FILGUEIRAS, M. R. T., LA TORRE, G. & HENCH, L. L. 1993b. Solution effects on the surface reactions of three bioactive glass compositions. *Journal of biomedical materials research,* 27**,** 1485-1493.

FLEMMING, R., MURPHY, C. J., ABRAMS, G., GOODMAN, S. & NEALEY, P. 1999. Effects of synthetic micro-and nano-structured surfaces on cell behavior. *Biomaterials,* 20**,** 573-588.

FOPPIANO, S., MARSHALL, S. J., MARSHALL, G. W., SAIZ, E. & TOMSIA, A. P. 2004. The influence of novel bioactive glasses on in vitro osteoblast behavior. *Journal of Biomedical Materials Research Part A,* 71**,** 242-249.

FOPPIANO, S., MARSHALL, S. J., MARSHALL, G. W., SAIZ, E. & TOMSIA, A. P. 2007. Bioactive glass coatings affect the behavior of osteoblast-like cells. *Acta biomaterialia,* 3**,** 765-771.

FOWLER, B. 1974. Infrared studies of apatites. I. Vibrational assignments for calcium, strontium, and barium hydroxyapatites utilizing isotopic substitution. *Inorganic Chemistry,* 13**,** 194-207.

FRANCESCHI, R. T. & IYER, B. S. 1992. Relationship between collagen synthesis and expression of the osteoblast phenotype in MC3T3-E1 cells. *Journal of Bone and Mineral Research,* 7**,** 235-246.

FRANCESCHI, R. T., IYER, B. S. & CUI, Y. 1994. Effects of ascorbic acid on collagen matrix formation and osteoblast differentiation in murine MC3T3-E1 cells. *Journal of Bone and Mineral Research,* 9**,** 843-854.

FRANCHI, M., ORSINI, E., TRIRÉ, A., QUARANTA, M., MARTINI, D., PICCARI, G. G., RUGGERI, A. & OTTANI, V. 2004. Osteogenesis and morphology of the peri-implant bone facing dental implants. *The Scientific World Journal,* 4**,** 1083-1095.

FUJIBAYASHI, S., NEO, M., KIM, H.-M., KOKUBO, T. & NAKAMURA, T. 2003. A comparative study between in vivo bone ingrowth and in vitro apatite formation on Na 2 O–CaO–SiO 2 glasses. *Biomaterials,* 24**,** 1349-1356.

FULTZ, B. & HOWE, J. M. 2012. *Transmission electron microscopy and diffractometry of materials*, Springer Science & Business Media.

GAO, T., ARO, H. T., YLÄNEN, H. & VUORIO, E. 2001. Silica-based bioactive glasses modulate expression of bone morphogenetic protein-2 mRNA in Saos-2 osteoblasts in vitro. *Biomaterials,* 22**,** 1475-1483.

GAREFIS, P. N. 1978. Complete mandibular subperiosteal implants for edentulous mandibles. *The Journal of prosthetic dentistry,* 39**,** 670-677.

GASPAR, J., BORRECHO, G., OLIVEIRA, P., SALVADO, F. & MARTINS DOS SANTOS, J. 2013. Osteotomy at low-speed drilling without irrigation versus high-speed drilling with irrigation: an experimental study. *Acta Médica Portuguesa,* 26**,** 231-236.

GEBHARDT, F., SEUSS, S., TURHAN, M., HORNBERGER, H., VIRTANEN, S. & BOCCACCINI, A. R. 2012. Characterization of electrophoretic chitosan coatings on stainless steel. *Materials letters,* 66**,** 302-304.

GENTLEMAN, E., FREDHOLM, Y. C., JELL, G., LOTFIBAKHSHAIESH, N., O'DONNELL, M. D., HILL, R. G. & STEVENS, M. M. 2010. The effects of strontium-substituted bioactive glasses on osteoblasts and osteoclasts in vitro. *Biomaterials,* 31**,** 3949-3956.

GENTLEMAN, E., STEVENS, M. M., HILL, R. & BRAUER, D. S. 2013. Surface properties and ion release from fluoride-containing bioactive glasses promote osteoblast differentiation and mineralization in vitro. *Acta biomaterialia,* 9**,** 5771-5779.

GH, M. & LEHR, J. R. 1969. Crystal chemical investigation of natural apatites. *American Mineralogist,* 54**,** 1374-&.

GLIMCHER, M. J. 1986. The nature of the mineral component of bone and the mechanism of calcification. *Instructional course lectures,* 36**,** 49-69.

GOLUB, E., HARRISON, G., TAYLOR, A., CAMPER, S. & SHAPIRO, I. 1992. The role of alkaline phosphatase in cartilage mineralization. *Bone and mineral,* 17**,** 273-278.

GOMEZ-VEGA, J., SAIZ, E., TOMSIA, A., MARSHALL, G. & MARSHALL, S. 2000. Bioactive glass coatings with hydroxyapatite and Bioglass® particles on Ti-based implants. 1. Processing. *Biomaterials,* 21**,** 105-111.

GONZALEZ, J. & MIRZA-ROSCA, J. 1999. Study of the corrosion behavior of titanium and some of its alloys for biomedical and dental implant applications. *Journal of Electroanalytical Chemistry,* 471**,** 109-115.

GOTFREDSEN, K. & KARLSSON, U. 2001. A prospective 5-year study of fixed partial prostheses supported by implants with machined and TiO2-blasted surface. *Journal of Prosthodontics,* 10**,** 2-7.

GROESSNER-SCHREIBER, B. & TUAN, R. S. 1992. Enhanced extracellular matrix production and mineralization by osteoblasts cultured on titanium surfaces in vitro. *Journal of cell science,* 101**,** 209-217.

GRYNPAS, M. D. 1990. Fluoride effects on bone crystals. *Journal of Bone and Mineral Research,* 5**,** S169-S175.

GRYNPAS, M. D., CHACHRA, D. & LIMEBACK, H. 2000. The action of fluoride on bone. *The osteoporosis primer.* Cambridge University Press.

HABIBOVIC, P., BARRERE, F., BLITTERSWIJK, C. A., GROOT, K. & LAYROLLE, P. 2002. Biomimetic hydroxyapatite coating on metal implants. *Journal of the American Ceramic Society,* 85**,** 517-522.

HABIBOVIC, P., LI, J., VAN DER VALK, C. M., MEIJER, G., LAYROLLE, P., VAN BLITTERSWIJK, C. A. & DE GROOT, K. 2005. Biological performance of uncoated and octacalcium phosphate-coated Ti6Al4V. *Biomaterials,* 26**,** 23-36.

HADI, S., ASHFAQ, N., BEY, A. & KHAN, S. 2011. Biological factors responsible for failure of osseointegration in oral implants. *Biology and Medicine,* 3**,** 164-170.

HAKKI, S. S., BOZKURT, S. B., HAKKI, E. E., KORKUSUZ, P., PURALI, N., KOÇ, N., TIMUCIN, M., OZTURK, A. & KORKUSUZ, F. 2012. Osteogenic differentiation of MC3T3-E1 cells on different titanium surfaces. *Biomedical Materials,* 7**,** 045006.

HANSSON, S. 2000. Surface roughness parameters as predictors of anchorage strength in bone: a critical analysis. *Journal of Biomechanics,* 33**,** 1297-1303.

HARRISON, G., SHAPIRO, I. M. & GOLUB, E. E. 1995. The phosphatidylinositol-glycolipid anchor on alkaline phosphatase facilitates mineralization initiation in vitro. *Journal of Bone and Mineral Research,* 10**,** 568-573.

HAYASHI, M., NABESHIMA, N., FUKUYAMA, H. & NAGATA, K. 2002. Effect of fluorine on silicate network for CaO-CaF2-SiO2 and CaO-CaF2-SiO2-FeOx glasses. *ISIJ international,* 42**,** 352-358.

HAYASHI, M., WATANABE, T., NAKADA, H. & NAGATA, K. 2006. Effect of Na2O on crystallization of mould fluxes for continuous casting of steel. *ISIJ international,* 46**,** 1805-1809.

HEIJ, D. G. O., OPDEBEECK, H., STEENBERGHE, D. & QUIRYNEN, M. 2003. Age as compromising factor for implant insertion. *Periodontology 2000,* 33**,** 172-184.

HEITZ-MAYFIELD, L., SCHMID, B., WEIGEL, C., GERBER, S., BOSSHARDT, D., JÖNSSON, J. & LANG, N. 2004. Does excessive occlusal load affect osseointegration? An experimental study in the dog. *Clinical Oral Implants Research,* 15**,** 259-268.

HENCH, L. L. 1991. Bioceramics: from concept to clinic. *Journal of the american ceramic society,* 74**,** 1487-1510.

HENCH, L. L. & WILSON, J. 1993. *An introduction to bioceramics*, World scientific.

HENSTOCK, J., CANHAM, L. & ANDERSON, S. 2015. Silicon: the evolution of its use in biomaterials. *Acta biomaterialia,* 11**,** 17-26.

HERRMANN, I., LEKHOLM, U., HOLM, S. & KULTJE, C. 2005. Evaluation of patient and implant characteristics as potential prognostic factors for oral implant failures. *International Journal of Oral & Maxillofacial Implants,* 20.

HEUGHEBAERT, M., LEGEROS, R., GINESTE, M., GUILHEM, A. & BONEL, G. 1988. Physicochemical characterization of deposits associated with HA ceramics implanted in nonosseous sites. *Journal of biomedical materials research,* 22**,** 257-268.

HILL, D. 1998. Design engineering of biomaterials for medical devices. *Design Engineering of Biomaterials for Medical Devices, by David Hill, pp. 480. ISBN 0-471-96708-4. Wiley-VCH, October 1998.,* 1.

HILL, R. 1996. An alternative view of the degradation of bioglass. *Journal of Materials Science Letters,* 15**,** 1122-1125.

HILL, R. G. & BRAUER, D. S. 2011. Predicting the bioactivity of glasses using the network connectivity or split network models. *Journal of Non-Crystalline Solids,* 357**,** 3884-3887.

HILL, R. G., DA COSTA, N. & LAW, R. V. 2005. Characterization of a mould flux glass. *Journal of non-crystalline solids,* 351**,** 69-74.

HILL, R. G., GILLAM, D. G. & CHEN, X. 2015. The ability of a nano hydroxyapatite toothpaste and oral rinse containing fluoride to protect enamel during an acid challenge using 19 F solid state NMR spectroscopy. *Materials Letters,* 156**,** 69-71.

HIMMLOVA, L., DOSTÁLOVÁ, T. J., KÁCOVSKÝ, A. & KONVIČKOVÁ, S. 2004. Influence of implant length and diameter on stress distribution: a finite element analysis. *The Journal of prosthetic dentistry,* 91**,** 20-25.

HOFMANN, A. A., BLOEBAUM, R. D. & BACHUS, K. N. 1997. Progression of human bone ingrowth into porous-coated implants: Rate of bone ingrowth in humans. *Acta Orthopaedica Scandinavica,* 68**,** 161-166.

HÖLAND, W. 2012. Glass-Ceramics. *Bio-Glasses: An Introduction***,** 97-105.

HOLMGREN, E. P., SECKINGER, R. J., KILGREN, L. M. & MANTE, F. 1998. Evaluating parameters of osseointegrated dental implants using finite element analysis—a two-dimensional comparative study examining the effects of implant diameter, implant shape, and load direction. *Journal of Oral Implantology,* 24**,** 80-88.

HOPPE, A., GÜLDAL, N. S. & BOCCACCINI, A. R. 2011. A review of the biological response to ionic dissolution products from bioactive glasses and glass-ceramics. *Biomaterials,* 32**,** 2757-2774.

HORIGUCHI, S., YAMADA, T., INOKOSHI, S. & TAGAMI, J. 1998. Selective caries removal with air abrasion. *Operative dentistry,* 23**,** 236-243.

IHDE, S., KOPP, S., GUNDLACH, K. & KONSTANTINOVIĆ, V. 2009. Effects of radiation therapy on craniofacial and dental implants: a review of the literature. *Oral Surgery, Oral Medicine, Oral Pathology, Oral Radiology, and Endodontology,* 107**,** 56-65.

ILER, R. K. 1979. The chemistry of silica. Wiley, New York.

ISHIKAWA, K., MIYAMOTO, Y., NAGAYAMA, M. & ASAOKA, K. 1997. Blast coating method: new method of coating titanium surface with hydroxyapatite at room temperature. *Journal of Biomedical Materials Research Part A,* 38**,** 129-134.

ISIDOR, F. 1997. Histological evaluation of peri-implant bone at implants subjected to occlusal overload or plaque accumulation. *Clinical oral implants research,* 8**,** 1-9.

ISIDOR, F. 2006. Influence of forces on peri-implant bone. *Clinical Oral Implants Research,* 17**,** 8-18.

IVANOFF, C.-J., SENNERBY, L., JOHANSSON, C., RANGERT, B. & LEKHOLM, U. 1997. Influence of implant diameters on the integration of screw implants: an experimental study in rabbits. *International journal of oral and maxillofacial surgery,* 26**,** 141-148.

IYER, S., WEISS, C. & MEHTA, A. 1997. Effects of drill speed on heat production and the rate and quality of bone formation in dental implant osteotomies. Part I: Relationship between drill speed and heat production. *International Journal of Prosthodontics,* 10.

IZQUIERDO-BARBA, I., SALINAS, A. & VALLET-REGÍ, M. 1999. In vitro calcium phosphate layer formation on sol-gel glasses of the CaO-SiO 2 system. *Journal of biomedical materials research,* 47**,** 243-250.

JAFFIN, R. A. & BERMAN, C. L. 1991. The excessive loss of Branemark fixtures in type IV bone: a 5-year analysis. *Journal of periodontology,* 62**,** 2-4.

JALOTA, S., BHADURI, S. & TAS, A. 2006. Effect of carbonate content and buffer type on calcium phosphate formation in SBF solutions. *Journal of Materials Science: Materials in Medicine,* 17**,** 697-707.

JEONG, S.-J. & JEONG, M.-J. 2016. Effect of Thymosin β4 on the Differentiation and Mineralization of MC3T3-E1 Cell on a Titanium Surface. *Journal of nanoscience and nanotechnology,* 16**,** 1979-1983.

JOHNSSON, Å. A., SAWAII, T., JACOBSON, M., GRANSTRÖM, G. & TURESSON, I. 2000. A histomorphometric and biomechanical study of the effect of delayed titanium implant placement in irradiated rabbit bone. *Clinical implant dentistry and related research,* 2**,** 42-49.

JOKSTAD, A., BRAEGGER, U., BRUNSKI, J. B., CARR, A. B., NAERT, I. & WENNERBERG, A. 2003. Quality of dental implants. *International dental journal,* 53**,** 409-443.

JONES, J. R. 2015. Reprint of: Review of bioactive glass: From Hench to hybrids. *Acta biomaterialia,* 23**,** S53-S82.

JONES, J. R., SEPULVEDA, P. & HENCH, L. L. 2001. Dose-dependent behavior of bioactive glass dissolution. *Journal of biomedical materials research,* 58**,** 720-726.

JUNG, Y.-C., HAN, C.-H., LEE, I.-S. & KIM, H.-E. 2001. Effects of ion beam-assisted deposition of hydroxyapatite on the osseointegration of endosseous implants in rabbit tibiae. *International Journal of Oral and Maxillofacial Implants,* 16**,** 809-818.

JUNKER, R., DIMAKIS, A., THONEICK, M. & JANSEN, J. A. 2009. Effects of implant surface coatings and composition on bone integration: a systematic review. *Clinical oral implants research,* 20**,** 185-206.

KANIE, T., NAGATA, M. & BAN, S. 2004. Comparison of the mechanical properties of 2 prosthetic mini-implants. *Implant dentistry,* 13**,** 251-256.

KARLSSON, K. H., FRÖBERG, K. & RINGBOM, T. 1989. A structural approach to bone adhering of bioactive glasses. *Journal of Non-Crystalline Solids,* 112**,** 69-72.

KAYA, E., HOGG, R. & KUMAR, S. 2002. Particle shape modification in comminution. *KONA Powder and Particle Journal,* 20**,** 188-195.

KELLER, J. C., DOUGHERTY, W. J., GROTENDORST, G. R. & WIGHTMAN, J. P. 1989. In vitro cell attachment to characterized cp titanium surfaces. *The Journal of Adhesion,* 28**,** 115-133.

KELLER, J. C., DRAUGHN, R. A., WIGHTMAN, J. P., DOUGHERTY, W. J. & MELETIOU, S. D. 1990. Characterization of sterilized CP titanium implant surfaces. *International Journal of Oral & Maxillofacial Implants,* 5.

KHAN, M., WILLIAMS, R. & WILLIAMS, D. 1999. Conjoint corrosion and wear in titanium alloys. *Biomaterials,* 20**,** 765-772.

KIM, C. Y., CLARK, A. E. & HENCH, L. L. 1989. Early stages of calcium-phosphate layer formation in bioglasses. *Journal of non-crystalline solids,* 113**,** 195-202.

KIM, C. Y. & LEE, J. W. 2005. Surface bio-modification of titanium implants by an enamel process. *Journal of Ceramic Processing Research,* 6**,** 338.

KIM, H. M., KISHIMOTO, K., MIYAJI, F., KOKUBO, T., YAO, T., SUETSUGU, Y., TANAKA, J. & NAKAMURA, T. 1999. Composition and structure of the apatite formed on PET substrates in SBF modified with various ionic activity products. *Journal of biomedical materials research,* 46**,** 228-235.

KIM, H. M., MIYAZAKI, T., KOKUBO, T. & NAKAMURA, T. Revised simulated body fluid. Key Engineering Materials, 2001. Trans Tech Publ, 47-50.

KIM, S.-J., YOO, J., KIM, Y.-S. & SHIN, S.-W. 2010. Temperature change in pig rib bone during implant site preparation by low-speed drilling. *Journal of Applied Oral Science,* 18**,** 522-527.

KLEEREKOPER, M. & MENDLOVIC, D. B. 1993. Sodium fluoride therapy of postmenopausal osteoporosis. *Endocrine reviews,* 14**,** 312-323.

KLOKKEVOLD, P. R., NISHIMURA, R. D., ADACHI, M. & CAPUTO, A. 1997. Osseointegration enhanced by chemical etching of the titanium surface. A torque removal study in the rabbit. *Clinical oral implants research,* 8**,** 442-447.

KNIGHT, R. D., JONES, B. & FIELD, S. 2015. *college physics*, Pearson New York.

KOHAL, R.-J., PAPAVASILIOU, G., KAMPOSIORA, P., TRIPODAKIS, A. & STRUB, J. R. 2002. Three-Dimensional Computerized Stress Analysis of Commercially Pure Titanium and Yttrium--Partially Stabilized Zirconia Implants. *International Journal of Prosthodontics,* 15.

KOHAL, R. J., WENG, D., BÄCHLE, M. & STRUB, J. R. 2004. Loaded custom-made zirconia and titanium implants show similar osseointegration: an animal experiment. *Journal of Periodontology,* 75**,** 1262-1268.

KOKUBO, T., KUSHITANI, H., SAKKA, S., KITSUGI, T. & YAMAMURO, T. 1990. Solutions able to reproduce in vivo surface-structure changes in bioactive glass-ceramic A-W3. *Journal of biomedical materials research,* 24**,** 721-734.

KOKUBO, T. & TAKADAMA, H. 2006. How useful is SBF in predicting in vivo bone bioactivity? *Biomaterials,* 27**,** 2907-2915.

KOLLER, G., COOK, R. J., THOMPSON, I. D., WATSON, T. F. & DI SILVIO, L. 2007. Surface modification of titanium implants using bioactive glasses with air abrasion technologies. *Journal of Materials Science: Materials in Medicine,* 18**,** 2291-2296.

LACEFIELD, W. R. 1999. Materials characteristics of uncoated/ceramic-coated implant materials. *Advances in dental research,* 13**,** 21-26.

LAMBERT, P. M., MORRIS, H. F. & OCHI, S. 2000. The influence of smoking on 3-year clinical success of osseointegrated dental implants. *Annals of Periodontology,* 5**,** 79-89.

LAUSMAA, J. 2001. Mechanical, thermal, chemical and electrochemical surface treatment of titanium. *Titanium in medicine.* Springer.

LE GUÉHENNEC, L., SOUEIDAN, A., LAYROLLE, P. & AMOURIQ, Y. 2007. Surface treatments of titanium dental implants for rapid osseointegration. *Dental materials,* 23**,** 844-854.

LEGEROS, R., KIJOWSKA, R., JIA, W. & LEGEROS, J. 1988. Fluoride-cation interactions in the formation and stability of apatites. *Journal of fluorine chemistry,* 41**,** 53-64.

LI, P., NAKANISHI, K., KOKUBO, T. & DE GROOT, K. 1993. Induction and morphology of hydroxyapatite, precipitated from metastable simulated body fluids on sol-gel prepared silica. *Biomaterials,* 14**,** 963-968.

LI, P., OHTSUKI, C., KOKUBO, T., NAKANISHI, K., SOGA, N. & DE GROOT, K. 1994. The role of hydrated silica, titania, and alumina in inducing apatite on implants. *Journal of Biomedical Materials Research Part A,* 28**,** 7-15.

LI, R., CLARK, A. & HENCH, L. 1991. An investigation of bioactive glass powders by sol-gel processing. *Journal of Applied Biomaterials,* 2**,** 231-239.

LINDER, L. & HANSSON, H. 1983. Ultrastructural aspects of the interface between bone and cement in man. Report of three cases. *Bone & Joint Journal,* 65**,** 646-649.

LINDHE, J., KARRING, T. & LANG, N. P. 2003. *Clinical periodontology and implant dentistry*, Blackwell Munksgaard Copenhagen.

LIU, J., RAWLINSON, S. C., HILL, R. G. & FORTUNE, F. 2016. Fluoride incorporation in high phosphate containing bioactive glasses and in vitro osteogenic, angiogenic and antibacterial effects. *Dental Materials,* 32**,** e221-e237.

LOBEL, K. & HENCH, L. 1998. In vitro adsorption and activity of enzymes on reaction layers of bioactive glass substrates. *Journal of biomedical materials research,* 39**,** 575-579.

LOCCI, P., BECCHETTI, E., PUGLIESE, M., ROSSI, L., BELCASTRO, S., CALVITTI, M., PIETRARELLI, G. & STAFFOLANI, N. 1997. Phenotype expression of human bone cells cultured on implant substrates. *Cell biochemistry and function,* 15**,** 163-170.

LOCKYER, M., HOLLAND, D. & DUPREE, R. 1995. NMR investigation of the structure of some bioactive and related glasses. *Journal of non-crystalline solids,* 188**,** 207-219.

LOPEZ-ESTEBAN, S., SAIZ, E., FUJINO, S., OKU, T., SUGANUMA, K. & TOMSIA, A. P. 2003. Bioactive glass coatings for orthopedic metallic implants. *Journal of the European Ceramic Society,* 23**,** 2921-2930.

LORENZETTI, M., DAKISCHEW, O., TRINKAUS, K., SUSANNE LIPS, K., SCHNETTLER, R., KOBE, S. & NOVAK, S. 2015. Enhanced osteogenesis on titanium implants by UVB photofunctionalization of hydrothermally grown TiO2 coatings. *Journal of biomaterials applications,* 30**,** 71-84.

LOVERIDGE, N. 1999. Bone: more than a stick. *Journal of animal science,* 77**,** 190.

LU, X. & LENG, Y. 2005. Theoretical analysis of calcium phosphate precipitation in simulated body fluid. *Biomaterials,* 26**,** 1097-1108.

LUSVARDI, G., MALAVASI, G., CORTADA, M., MENABUE, L., MENZIANI, M., PEDONE, A. & SEGRE, U. 2008. Elucidation of the structural role of fluorine in potentially bioactive glasses by experimental and computational investigation. *The Journal of Physical Chemistry B,* 112**,** 12730-12739.

LUSVARDI, G., MALAVASI, G., MENABUE, L., AINA, V. & MORTERRA, C. 2009. Fluoride-containing bioactive glasses: surface reactivity in simulated body fluids solutions. *Acta Biomaterialia,* 5**,** 3548-3562.

MAÇON, A. L., KIM, T. B., VALLIANT, E. M., GOETSCHIUS, K., BROW, R. K., DAY, D. E., HOPPE, A., BOCCACCINI, A. R., KIM, I. Y. & OHTSUKI, C. 2015. A unified in vitro evaluation for apatite-forming ability of bioactive glasses and their variants. *Journal of Materials Science: Materials in Medicine,* 26**,** 1-10.

MAENO, S., NIKI, Y., MATSUMOTO, H., MORIOKA, H., YATABE, T., FUNAYAMA, A., TOYAMA, Y., TAGUCHI, T. & TANAKA, J. 2005. The effect of calcium ion concentration on osteoblast viability, proliferation and differentiation in monolayer and 3D culture. *Biomaterials,* 26**,** 4847-4855.

MAHMOOD, A., MNEIMNE, M., ZOU, L. F., HILL, R. G. & GILLAM, D. G. 2014. Abrasive wear of enamel by bioactive glass-based toothpastes. *American journal of dentistry,* 27**,** 263-267.

MAMI, M., OUDADESSE, H. & DOEBEZ-SRIDI, R. 2008. Synthesis and in-vitro characterization of melt derived 47S CaO–P2O5–SiO2–Na2O bioactive glass. *Ceram− Silik,* 52**,** 121-9.

MANERO, J., SALSENCH, J., NOGUERAS, J., APARICIO, C., PADRÓS, A., BALCELLS, M., GIL, F. & PLANELL, J. 2002. Growth of bioactive surfaces on dental implants. *Implant dentistry,* 11**,** 170-175.

MANJUBALA, I., SIVAKUMAR, M. & NIKKATH, S. N. 2001. Synthesis and characterisation of hydroxy/fluoroapatite solid solution. *Journal of materials science,* 36**,** 5481-5486.

MARTIN, T. J., NG, K. W. & NICHOLSON, G. C. 1988. 1 Cell biology of bone. *Bailliere's Clinical endocrinology and metabolism,* 2**,** 1-29.

MASON, H. E., MCCUBBIN, F. M., SMIRNOV, A. & PHILLIPS, B. L. 2009. Solid-state NMR and IR spectroscopic investigation of the role of structural water and F in carbonate-rich fluorapatite. *American Mineralogist,* 94**,** 507-516.

MASSIOT, D., FAYON, F., MONTOUILLOUT, V., PELLERIN, N., HIET, J., ROILAND, C., FLORIAN, P., COUTURES, J.-P., CORMIER, L. & NEUVILLE, D. R. 2008. Structure and dynamics of oxide melts and glasses: A view from multinuclear and high temperature NMR. *Journal of Non-Crystalline Solids,* 354**,** 249-254.

MATUSOVITS, D. 2009. *Investigation of the Osseointegration of Dental Implants and Different Biomaterials Used in Guided Tissue Regeneration.* szte.

MAURER, A., MERRITT, K. & BROWN, S. 1994. Cellular uptake of titanium and vanadium from addition of salts or fretting corrosion in vitro. *Journal of Biomedical Materials Research Part A,* 28**,** 241-246.

MCMILLAN, P. 1979. Glass-ceramics 2nd ed. *Non-Metallic Solids*.

MEYER, U., JOOS, U., MYTHILI, J., STAMM, T., HOHOFF, A., FILLIES, T., STRATMANN, U. & WIESMANN, H. 2004. Ultrastructural characterization of the implant/bone interface of immediately loaded dental implants. *Biomaterials,* 25**,** 1959-1967.

MILLER, A. & PARKER, S. 1984. Collagen: the organic matrix of bone [and discussion]. *Philosophical Transactions of the Royal Society of London B: Biological Sciences,* 304**,** 455-477.

MILLER, J. M. 1996. Fluorine-19 magic-angle spinning NMR. *Progress in Nuclear Magnetic Resonance Spectroscopy,* 28**,** 255-281.

MILLY, H., AUSTIN, R., THOMPSON, I. & BANERJEE, A. 2014. In vitro effect of air-abrasion operating parameters on dynamic cutting characteristics of alumina and bio-active glass powders. *Operative dentistry,* 39**,** 81-89.

MIOLA, M., VERNÉ, E., CIRALDO, F. E., CORDERO-ARIAS, L. & BOCCACCINI, A. R. 2015. Electrophoretic deposition of chitosan/45S5 bioactive glass composite coatings doped with Zn and Sr. *Frontiers in bioengineering and biotechnology,* 3.

MISCH, C. E. 2007. *Contemporary implant dentistry*, Elsevier Health Sciences.

MNEIMNE, M., HILL, R. G., BUSHBY, A. J. & BRAUER, D. S. 2011. High phosphate content significantly increases apatite formation of fluoride-containing bioactive glasses. *Acta Biomaterialia,* 7**,** 1827-1834.

MOORE, G. L. 2012. *Introduction to inductively coupled plasma atomic emission spectrometry*, Elsevier.

MORITZ, N., VEDEL, E., YLÄNEN, H., JOKINEN, M., HUPA, M. & YLI-URPO, A. 2004. Characterisation of bioactive glass coatings on titanium substrates produced using a CO 2 laser. *Journal of Materials Science: Materials in Medicine,* 15**,** 787-794.

MOUNT, G. 2009. Minimal intervention dentistry: Cavity classification & preparation. *Journal of Minimum Intervention in Dentistry,* 2**,** 150-163.

MOY, P. K., MEDINA, D., SHETTY, V. & AGHALOO, T. L. 2005. Dental implant failure rates and associated risk factors. *International Journal of Oral & Maxillofacial Implants,* 20.

MÜELLER, W. D., GROSS, U., FRITZ, T., VOIGT, C., FISCHER, P., BERGER, G., ROGASCHEWSKI, S. & LANGE, K. P. 2003. Evaluation of the interface between bone and titanium surfaces being blasted by aluminium oxide or bioceramic particles. *Clinical Oral Implants Research,* 14**,** 349-356.

MÜLLER, L. & MÜLLER, F. A. 2006. Preparation of SBF with different content and its influence on the composition of biomimetic apatites. *Acta Biomaterialia,* 2**,** 181-189.

MUSTAFA, K., LOPEZ, B. S., HULTENBY, K., WENNERBERG, A. & ARVIDSON, K. 1998. Attachment and proliferation of human oral fibroblasts to titanium surfaces blasted with TiO2 particles. A scanning electron microscopic and histomorphometric analysis. *Clinical oral implants research,* 9**,** 195-207.

NAERT, I., KOUTSIKAKIS, G., DUYCK, J., QUIRYNEN, M., JACOBS, R. & VAN STEENBERGHE, D. 2002. Biologic outcome of implant-supported restorations in the treatment of partial edentulism. *Clinical oral implants research,* 13**,** 381-389.

NIKČEVIĆ, I., JOKANOVIĆ, V., MITRIĆ, M., NEDIĆ, Z., MAKOVEC, D. & USKOKOVIĆ, D. 2004. Mechanochemical synthesis of nanostructured fluorapatite/fluorhydroxyapatite and carbonated fluorapatite/fluorhydroxyapatite. *Journal of Solid State Chemistry,* 177**,** 2565-2574.

O'DONNELL, M. & HILL, R. 2010. Influence of strontium and the importance of glass chemistry and structure when designing bioactive glasses for bone regeneration. *Acta Biomaterialia,* 6**,** 2382-2385.

O'DONNELL, M., WATTS, S., HILL, R. & LAW, R. 2009. The effect of phosphate content on the bioactivity of soda-lime-phosphosilicate glasses. *Journal of Materials Science: Materials in Medicine,* 20**,** 1611-1618.

O'DONNELL, M., WATTS, S., LAW, R. & HILL, R. 2008. Effect of P 2 O 5 content in two series of soda lime phosphosilicate glasses on structure and properties–Part II: Physical properties. *Journal of Non-Crystalline Solids,* 354**,** 3561-3566.

O'DONNELL, M. D. 2011. Predicting bioactive glass properties from the molecular chemical composition: Glass transition temperature. *Acta biomaterialia,* 7**,** 2264-2269.

OF PROSTHODONTICS, A. B., OF PROSTHODONTISTS, A. C., SOCIETY, A. E., SOCIETY, A. P., SOCIETY, A. P., CONFERENCE, C. O. B. P., OF PROSTHODONTICS, G. N. Y. A., SOCIETY, I. P., ACADEMY, J. P. & OF PROSTHODONTICS, K. A. 1999. The Glossary of Prosthodontic Terms Seventh Edition (GPT-7). *The Journal of Prosthetic Dentistry,* 81**,** 48-110.

OGURO, A., KAWASE, T. & ORIKASA, M. 2003. NaF induces early differentiation of murine bone marrow cells along the granulocytic pathway but not the monocytic or preosteoclastic pathway in vitro. *In Vitro Cellular & Developmental Biology-Animal,* 39**,** 243-248.

ÖHRNEL, L.-O., BRÅNEMARK, R., NYMAN, J., NILSSO, P. & THOMSEN, P. 1997. Effects of irradiation on the biomechanics of osseointegration: an experimental in vivo study in rats. *Scandinavian journal of plastic and reconstructive surgery and hand surgery,* 31**,** 281-293.

OKAZAKI, M., MIAKE, Y., TOHDA, H., YANAGISAWA, T., MATSUMOTO, T. & TAKAHASHI, J. 1999. Functionally graded fluoridated apatites. *Biomaterials,* 20**,** 1421-1426.

OKAZAKI, Y. & GOTOH, E. 2005. Comparison of metal release from various metallic biomaterials in vitro. *Biomaterials,* 26**,** 11-21.

OLATE, S., LYRIO, M. C. N., DE MORAES, M., MAZZONETTO, R. & MOREIRA, R. W. F. 2010. Influence of diameter and length of implant on early dental implant failure. *Journal of Oral and Maxillofacial Surgery,* 68**,** 414-419.

OLDANI, C., DOMINGUEZ, A. & ELI, T. 2012. *Titanium as a Biomaterial for Implants*, Citeseer.

OLIVEIRA, J., CORREIA, R. & FERNANDES, M. 2002. Effects of Si speciation on the in vitro bioactivity of glasses. *Biomaterials,* 23**,** 371-379.

OLMEDO, D. G., TASAT, D. R., DUFFÓ, G., GUGLIELMOTTI, M. B. & CABRINI, R. L. 2009. The issue of corrosion in dental implants: a review. *Acta Odontol Latinoam,* 22**,** 3-9.

PAOLINELIS, G., BANERJEE, A. & WATSON, T. 2008. An in vitro investigation of the effect and retention of bioactive glass air-abrasive on sound and carious dentine. *Journal of dentistry,* 36**,** 214-218.

PAOLINELIS, G., BANERJEE, A. & WATSON, T. 2009. An in-vitro investigation of the effects of variable operating parameters on alumina air-abrasion cutting characteristics. *Operative dentistry,* 34**,** 87-92.

PARK, J. B. & BRONZINO, J. D. 2002. *Biomaterials: principles and applications*, crc press.

PARK, J. Y. & DAVIES, J. E. 2000. Red blood cell and platelet interactions with titanium implant surfaces. *Clinical oral implants research,* 11**,** 530-539.

PAUL, A. 1989. *Chemistry of glasses*, Springer Science & Business Media.

PAZO, A., SAIZ, E. & TOMSIA, A. 1998. Silicate glass coatings on Ti-based implants. *Acta Materialia,* 46**,** 2551-2558.

PEDONE, A., CHARPENTIER, T. & MENZIANI, M. C. 2012. The structure of fluoride-containing bioactive glasses: new insights from first-principles calculations and solid state NMR spectroscopy. *Journal of Materials Chemistry,* 22**,** 12599-12608.

PEITL FILHO, O., LATORRE, G. P. & HENCH, L. 1996. Effect of crystallization on apatite-layer formation of bioactive glass 45%. *J Biomed Mater Res,* 30**,** 509-514.

PEREIRA, M., CLARK, A. & HENCH, L. 1994. Calcium phosphate formation on sol-gel-derived bioactive glasses in vitro. *Journal of Biomedical Materials Research Part A,* 28**,** 693-698.

PERUCHI, C., SANTOS-PINTO, L., SANTOS-PINTO, A. & BARBOSA E SILVA, E. 2002. Evaluation of cutting patterns produced in primary teeth by an air-abrasion system. *Quintessence international,* 33.

PIATTELLI, M., SCARANO, A., PAOLANTONIO, M., IEZZI, G., PETRONE, G. & PIATTELLI, A. 2002. Bone response to machined and resorbable blast material titanium implants: an experimental study in rabbits. *Journal of Oral Implantology,* 28**,** 2-8.

PIVODOVA, V., FRANKOVA, J. & ULRICHOVA, J. 2011. Osteoblast and gingival fibroblast markers in dental implant studies. *Biomedical Papers,* 155**,** 109-116.

PORTER, J. A. & VON FRAUNHOFER, J. A. 2004. Success or failure of dental implants? A literature review with treatment considerations. *General dentistry,* 53**,** 423-32; quiz 433, 446.

POURBAIX, M. 1984. Electrochemical corrosion of metallic biomaterials. *Biomaterials,* 5**,** 122-134.

PULEO, D. & NANCI, A. 1999. Understanding and controlling the bone–implant interface. *Biomaterials,* 20**,** 2311-2321.

PYE, A., LOCKHART, D., DAWSON, M., MURRAY, C. & SMITH, A. 2009. A review of dental implants and infection. *Journal of Hospital infection,* 72**,** 104-110.

QU, H. & WEI, M. 2006. The effect of fluoride contents in fluoridated hydroxyapatite on osteoblast behavior. *Acta biomaterialia,* 2**,** 113-119.

QUARLES, L. D., YOHAY, D. A., LEVER, L. W., CATON, R. & WENSTRUP, R. J. 1992. Distinct proliferative and differentiated stages of murine MC3T3-E1 cells in culture: an in vitro model of osteoblast development. *Journal of Bone and Mineral Research,* 7**,** 683-692.

RADIN, S. & DUCHEYNE, P. 1993. The effect of calcium phosphate ceramic composition and structure on in vitro behavior. II. Precipitation. *Journal of Biomedical Materials Research Part A,* 27**,** 35-45.

RADIN, S., DUCHEYNE, P. & CHEN, L. The Effect of Serum Proteins on the Kinetics of Reactions to Form Biologically Equivalent Apatite on Bioactive Glasses and Ceramics. ANNUAL MEETING-SOCIETY FOR BIOMATERIALS IN CONJUNCTION WITH THE INTERNATIONAL BIOMATERIALS SYMPOSIUM, 1994. SOCIETY FOR BIOMATERIALS, 37-37.

RADIN, S., DUCHEYNE, P., ROTHMAN, B. & CONTI, A. 1997. The effect of in vitro modeling conditions on the surface reactions of bioactive glass. *Journal of biomedical materials research,* 37**,** 363-375.

RAHAMAN, M. N., DAY, D. E., BAL, B. S., FU, Q., JUNG, S. B., BONEWALD, L. F. & TOMSIA, A. P. 2011. Bioactive glass in tissue engineering. *Acta biomaterialia,* 7**,** 2355-2373.

RAJENDRAN, V., BEGUM, A. N., AZOOZ, M. & EL BATAL, F. 2002. Microstructural dependence on relevant physical–mechanical properties on SiO 2–Na 2 O–CaO–P 2 O 5 biological glasses. *Biomaterials,* 23**,** 4263-4275.

RÁMILA, A. & VALLET-REGı, M. 2001. Static and dynamic in vitro study of a sol–gel glass bioactivity. *Biomaterials,* 22**,** 2301-2306.

RASMUSSON, L., ROOS, J. & BYSTEDT, H. 2005. A 10-Year Follow-Up Study of Titanium Dioxide–Blasted Implants. *Clinical implant dentistry and related research,* 7**,** 36-42.

RAWLINGS, R. D. 1993. Bioactive glasses and glass-ceramics. *Clinical materials,* 14**,** 155-179.

RAY, N. 1974. Composition—property relationships in inorganic oxide glasses. *Journal of Non-Crystalline Solids,* 15**,** 423-434.

REFFITT, D., OGSTON, N., JUGDAOHSINGH, R., CHEUNG, H., EVANS, B. A. J., THOMPSON, R., POWELL, J. & HAMPSON, G. 2003. Orthosilicic acid stimulates collagen type 1 synthesis and osteoblastic differentiation in human osteoblast-like cells in vitro. *Bone,* 32**,** 127-135.

REIGNER, P., LASAGA, A., BERNER, R., HAN, O. & ZILM, K. 1994. Mechanism of CO (Super 2-) 3 substitution in carbonate-fluorapatite; evidence from FTIR spectroscopy. *Am Mineral,* 79**,** 809-18.

RICH, C. & ENSINCK, J. 1961. Effect of sodium fluoride on calcium metabolism of human beings. *Nature,* 191**,** 184-185.

ROHANOVÁ, D., BOCCACCINI, A. R., HORKAVCOVÁ, D., BOZDĚCHOVÁ, P., BEZDIČKA, P. & ČASTORÁLOVÁ, M. 2014. Is non-buffered DMEM solution a suitable medium for in vitro bioactivity tests? *Journal of Materials Chemistry B,* 2**,** 5068-5076.

ROMANOS, G. E., TOH, C. G., SIAR, C. H., WICHT, H., YACOOB, H. & NENTWIG, G.-H. 2003. Bone-implant interface around titanium implants under different loading conditions: a histomorphometrical analysis in the Macaca fascicularis monkey. *Journal of periodontology,* 74**,** 1483-1490.

RØNOLD, H. J. & ELLINGSEN, J. E. 2002. Effect of micro-roughness produced by TiO 2 blasting—tensile testing of bone attachment by using coin-shaped implants. *Biomaterials,* 23**,** 4211-4219.

ŞAHIN, S., CEHRELI, M. C. & YALÇıN, E. 2002. The influence of functional forces on the biomechanics of implant-supported prostheses—a review. *Journal of dentistry,* 30**,** 271-282.

SAIZ, E., GOLDMAN, M., GOMEZ-VEGA, J. M., TOMSIA, A. P., MARSHALL, G. W. & MARSHALL, S. J. 2002. In vitro behavior of silicate glass coatings on Ti6Al4V. *Biomaterials,* 23**,** 3749-3756.

SAKAE, T., HOSHINO, K., FUJIMORI, Y., KOZAWA, Y. & LEGEROS, R. Z. In vitro interactions of bone marrow cells with carbonate and fluoride containing apatites. Key Engineering Materials, 2001. Trans Tech Publ, 347-350.

SALONEN, M. A., OIKARINEN, K., VIRTANEN, K. & PERNU, H. 1993. Failures in the osseointegration of endosseous implants. *International Journal of Oral and Maxillofacial Implants,* 8**,** 92-92.

SAUER, G. & WUTHIER, R. 1988. Fourier transform infrared characterization of mineral phases formed during induction of mineralization by collagenase-released matrix vesicles in vitro. *Journal of Biological Chemistry,* 263**,** 13718-13724.

SCHMIDT, C., KASPAR, D., SARKAR, M. R., CLAES, L. E. & IGNATIUS, A. A. 2002. A scanning electron microscopy study of human osteoblast morphology on five orthopedic metals. *Journal of biomedical materials research,* 63**,** 252-261.

SCHROEDER, A., BELSER, U. & WILLIAMS, R. C. 1996. *Oral implantology: basics, ITI hollow cylinder system*, G. Thieme.

SENNERBY, L., GOTTLOW, J. & ANDNEIL MEREDITH, F. E. 2008. Histological and Biomechanical Aspects of Surface Topography and Geometry of Neoss Implants. A Study in Rabbits. *Appl Osseointegration Res,* 6**,** 18-22.

SEPULVEDA, P., JONES, J. & HENCH, L. 2002. In vitro dissolution of melt-derived 45S5 and sol-gel derived 58S bioactive glasses. *Journal of Biomedical Materials Research Part A,* 61**,** 301-311.

SERINO, G. & STRÖM, C. 2009. Peri-implantitis in partially edentulous patients: association with inadequate plaque control. *Clinical Oral Implants Research,* 20**,** 169-174.

SHAH, F. A., BRAUER, D. S., DESAI, N., HILL, R. G. & HING, K. A. 2014. Fluoride-containing bioactive glasses and Bioglass® 45S5 form apatite in low pH cell culture medium. *Materials Letters,* 119**,** 96-99.

SHELBY, J. E. 2005. *Introduction to glass science and technology*, Royal Society of Chemistry.

SHEN, Y., LIU, W., WEN, C., PAN, H., WANG, T., DARVELL, B. W., LU, W. W. & HUANG, W. 2012. Bone regeneration: importance of local pH—strontium-doped borosilicate scaffold. *Journal of Materials Chemistry,* 22**,** 8662-8670.

SIESLER, H. W. & HOLLAND-MORITZ, K. 1980. *Infrared and Raman spectroscopy of polymers*, M. Dekker.

SILVER, I. A., DEAS, J. & ERECIŃSKA, M. 2001. Interactions of bioactive glasses with osteoblasts in vitro: effects of 45S5 Bioglass®, and 58S and 77S bioactive glasses on metabolism, intracellular ion concentrations and cell viability. *Biomaterials,* 22**,** 175-185.

SITTIG, C., TEXTOR, M., SPENCER, N., WIELAND, M. & VALLOTTON, P. 1999. Surface characterization. *Journal of Materials Science: Materials in Medicine,* 10**,** 35-46.

SNAUWAERT, K., DUYCK, J., VAN STEENBERGHE, D., QUIRYNEN, M. & NAERT, I. 2000. Time dependent failure rate and marginal bone loss of implant supported prostheses: a 15-year follow-up study. *Clinical oral investigations,* 4**,** 13-20.

SØBALLE, K. 1993. Hydroxyapatite ceramic coating for bone implant fixation: mechanical and histological studies in dogs. *Acta Orthopaedica Scandinavica,* 64**,** 1-58.

SOLA, A., BELLUCCI, D., CANNILLO, V. & CATTINI, A. 2011. Bioactive glass coatings: a review. *Surface Engineering,* 27**,** 560-572.

STANFORD, C. 2008. Surface modifications of dental implants. *Australian dental journal,* 53.

STEBBINS, J. F. & ZENG, Q. 2000. Cation ordering at fluoride sites in silicate glasses: a high-resolution 19 F NMR study. *Journal of Non-Crystalline Solids,* 262**,** 1-5.

STELLINGSMA, C., VISSINK, A., MEIJER, H., KUIPER, C. & RAGHOEBAR, G. 2004. Implantology and the severely resorbed edentulous mandible. *Critical Reviews in Oral Biology & Medicine,* 15**,** 240-248.

STOOR, P., SÖDERLING, E. & SALONEN, J. I. 1998. Antibacterial effects of a bioactive glass paste on oral microorganisms. *Acta Odontologica Scandinavica,* 56**,** 161-165.

SUDO, H., KODAMA, H.-A., AMAGAI, Y., YAMAMOTO, S. & KASAI, S. 1983. In vitro differentiation and calcification in a new clonal osteogenic cell line derived from newborn mouse calvaria. *The Journal of cell biology,* 96**,** 191-198.

SUN, L., BERNDT, C. C., GROSS, K. A. & KUCUK, A. 2001. Material fundamentals and clinical performance of plasma-sprayed hydroxyapatite coatings: a review. *Journal of biomedical materials research,* 58**,** 570-592.

SYKARAS, N., IACOPINO, A. M., MARKER, V. A., TRIPLETT, R. G. & WOODY, R. D. 2000. Implant materials, designs, and surface topographies: their effect on osseointegration. A literature review. *International Journal of Oral & Maxillofacial Implants,* 15.

TESTORI, T., WISEMAN, L., WOOLFE, S. & PORTER, S. S. 2001. A prospective multicenter clinical study of the Osseotite implant: four-year interim report. *International Journal of Oral & Maxillofacial Implants,* 16.

THOMAS, K. A. & COOK, S. D. 1985. An evaluation of variables influencing implant fixation by direct bone apposition. *Journal of Biomedical Materials Research Part A,* 19**,** 875-901.

THUY, T. T., NAKAGAKI, H., KATO, K., HUNG, P. A., INUKAI, J., TSUBOI, S., NAKAGAKI, H., HIROSE, M. N., IGARASHI, S. & ROBINSON, C. 2008. Effect of strontium in combination with fluoride on enamel remineralisation in vitro. *archives of oral biology,* 53**,** 1017-1022.

TILOCCA, A. & CORMACK, A. N. 2007. Structural effects of phosphorus inclusion in bioactive silicate glasses. *The Journal of Physical Chemistry B,* 111**,** 14256-14264.

TRUHLAR, R. S., ORENSTEIN, I. H., MORRIS, H. F. & OCHI, S. 1997. Distribution of bone quality in patients receiving endosseous dental implants. *Journal of Oral and Maxillofacial Surgery,* 55**,** 38-45.

TURKYILMAZ, I. & MCGLUMPHY, E. A. 2008. Influence of bone density on implant stability parameters and implant success: a retrospective clinical study. *BMC Oral Health,* 8**,** 32.

UDOMLERTPREECHA, S., PAVASANT, P. & LOHWONGWATANA, B. 2014. Surface Modification of Titanium Alloys Using Alumina Particles Blasting for Biomedical Applications. *Advanced Materials Research,* 983.

VARANASI, V., SAIZ, E., LOOMER, P., ANCHETA, B., URITANI, N., HO, S., TOMSIA, A., MARSHALL, S. & MARSHALL, G. 2009. Enhanced osteocalcin expression by osteoblast-like cells (MC3T3-E1) exposed to bioactive coating glass (SiO 2–CaO–P 2 O 5–MgO–K 2 O–Na 2 O system) ions. *Acta biomaterialia,* 5**,** 3536-3547.

VARANASI, V. G., VALLORTIGARA, T., LOOMER, P., SAIZ, E., TOMSIA, A., MARSHALL, S. & MARSHALL, G. Improving biomaterials from a cellular point of view. MRS Proceedings, 2006. Cambridge Univ Press, 0925-BB03-02.

VASANKARI, K., LIPPOLASSILA,NRHI, T.O. 2011. Surface Modification of Titanium by Sandblasting With Bioactive Glass Particles. *IADR* IADR General Session.

VESTERGAARD, P., JORGENSEN, N., SCHWARZ, P. & MOSEKILDE, L. 2008. Effects of treatment with fluoride on bone mineral density and fracture risk-a meta-analysis. *Osteoporosis international,* 19**,** 257-268.

VON RECUM, A. F. 1998. *Handbook of biomaterials evaluation: scientific, technical and clinical testing of implant materials*, CRC Press.

WALLACE, K., HILL, R., PEMBROKE, J., BROWN, C. & HATTON, P. 1999. Influence of sodium oxide content on bioactive glass properties. *Journal of Materials Science: Materials in Medicine,* 10**,** 697-701.

WANG, D., CHRISTENSEN, K., CHAWLA, K., XIAO, G., KREBSBACH, P. H. & FRANCESCHI, R. T. 1999. Isolation and characterization of MC3T3-E1 preosteoblast subclones with distinct in vitro and in vivo differentiation/mineralization potential. *Journal of Bone and Mineral Research,* 14**,** 893-903.

WANG, G., LI, J., LV, K., ZHANG, W., DING, X., YANG, G., LIU, X. & JIANG, X. 2016. Surface thermal oxidation on titanium implants to enhance osteogenic activity and in vivo osseointegration. *Scientific reports,* 6.

WANG, Q., HU, B., FAYON, F., TRÉBOSC, J., LEGEIN, C., LAFON, O., DENG, F. & AMOUREUX, J.-P. 2009. Double-quantum 19 F–19 F dipolar recoupling at ultra-fast magic angle spinning NMR: application to the assignment of 19F NMR spectra of inorganic fluorides. *Physical Chemistry Chemical Physics,* 11**,** 10391-10395.

WATSON, T., PILECKI, P., COOK, R., AZZOPARDI, A., PAOLINELIS, G., BANERJEE, A., THOMPSON, I. & BOYDE, A. 2008. Operative dentistry and the abuse of dental hard tissues: confocal microscopical imaging of cutting. *Operative dentistry,* 33**,** 215-224.

WEINER, S., ARAD, T. & TRAUB, W. 1991. Crystal organization in rat bone lamellae. *FEBS letters,* 285**,** 49-54.

WENNERBERG, A. & ALBREKTSSON, T. 2009. Effects of titanium surface topography on bone integration: a systematic review. *Clinical oral implants research,* 20**,** 172-184.

WENNERBERG, A., ALBREKTSSON, T., JOHANSSON, C. & ANDERSSON, B. 1996. Experimental study of turned and grit-blasted screw-shaped implants with special emphasis on effects of blasting material and surface topography. *Biomaterials,* 17**,** 15-22.

WENNERBERG, A., HALLGREN, C., JOHANSSON, C. & DANELLI, S. 1998. A histomorphometric evaluation of screw-shaped implants each prepared with two surface roughnesses. *Clinical oral implants research,* 9**,** 11-19.

WHITE, J. M. & EAKLE, W. S. 2000. Rationale and treatment approach in minimally invasive dentistry. *The Journal of the American Dental Association,* 131**,** 13S-19S.

WILLIAMS, D. F. 1999. *The Williams dictionary of biomaterials*, Liverpool University Press.

WILLIAMS, D. F. 2008. On the mechanisms of biocompatibility. *Biomaterials,* 29**,** 2941-2953.

WINKLER, S., MORRIS, H. F. & OCHI, S. 2000. Implant survival to 36 months as related to length and diameter. *Annals of Periodontology,* 5**,** 22-31.

WU, L. N., ISHIKAWA, Y., SAUER, G. R., GENGE, B. R., MWALE, F., MISHIMA, H. & WUTHIER, R. E. 1995. Morphological and biochemical characterization of mineralizing primary cultures of avian growth plate chondrocytes: evidence for cellular processing of Ca2+ and Pi prior to matrix mineralization. *Journal of cellular biochemistry,* 57**,** 218-237.

XYNOS, I. D., EDGAR, A. J., BUTTERY, L. D., HENCH, L. L. & POLAK, J. M. 2000. Ionic products of bioactive glass dissolution increase proliferation of human osteoblasts and induce insulin-like growth factor II mRNA expression and protein synthesis. *Biochemical and biophysical research communications,* 276**,** 461-465.

XYNOS, I. D., EDGAR, A. J., BUTTERY, L. D., HENCH, L. L. & POLAK, J. M. 2001. Gene-expression profiling of human osteoblasts following treatment with the ionic products of Bioglass® 45S5 dissolution. *Journal of Biomedical Materials Research Part A,* 55**,** 151-157.

YENIYOL, S., JIMBO, R., MARIN, C., TOVAR, N., JANAL, M. N. & COELHO, P. G. 2013. The effect of drilling speed on early bone healing to oral implants. *Oral surgery, oral medicine, oral pathology and oral radiology,* 116**,** 550-555.

YESINOWSKI, J. P. & MOBLEY, M. J. 1983. Fluorine-19 MAS-NMR of fluoridated hydroxyapatite surfaces. *Journal of the American Chemical Society,* 105**,** 6191-6193.

YI, H., BALAN, E., GERVAIS, C., SEGALEN, L., FAYON, F., ROCHE, D., PERSON, A., MORIN, G., GUILLAUMET, M. & BLANCHARD, M. 2013. Letter. A carbonate-fluoride defect model for carbonate-rich fluorapatite. *American Mineralogist,* 98**,** 1066-1069.

YLÄNEN, H. 2011. *Bioactive glasses: materials, properties and applications*, Elsevier.

YOON, K., GOLUB, E. & RODAN, G. A. 1989. Alkaline phosphatase cDNA transfected cells promote calcium and phosphate deposition. *Connective tissue research,* 22**,** 643-651.

YORUC, A., GÜLAY, O. & SENER, B. 2007. Examination of the properties of Ti-6Al-4V based plates after oral and maxillofacial application. *Journal of optoelectronics and advanced materials,* 9**,** 2627-2633.

ZAMBONIN, G., LOSITO, I., TRIFFITT, J. T. & ZAMBONIN, C. G. 2000. Detection of collagen synthesis by human osteoblasts on a tricalcium phosphate hydroxyapatite: An X-ray photoelectron spectroscopy investigation. *Journal of Biomedical Materials Research Part A,* 49**,** 120-126.

ZARB, G. A., HOBKIRK, J., ECKERT, S. & JACOB, R. 2013. *Prosthodontic treatment for edentulous patients: complete dentures and implant-supported prostheses*, Elsevier Health Sciences.

ZECHNER, W., TANGL, S., FÜRST, G., TEPPER, G., THAMS, U., MAILATH, G. & WATZEK, G. 2003. Osseous healing characteristics of three different implant types. *Clinical oral implants research,* 14**,** 150-157.

ZHANG, S. 2011. *Biological and Biomedical Coatings Handbook: Applications*, CRC Press.

ZITZMANN, N. U. & BERGLUNDH, T. 2008. Definition and prevalence of peri-implant diseases. *Journal of clinical periodontology,* 35**,** 286-291.

10 Appendices

Appendix 1 Statistical Analysis

10.1 Glass hardness statistics

Multiple Comparisons (Tukey HSD test)	*P value*
QMFA1 vs QMFA2	0.001
QMFA1 vs QMFA3	0.000
QMFA2 vs QMFA3	0.000

10.2 PFR statistics

1. Multiple comparisons (Tukey HSD test) of PFR between the prepared glasses at three air pressures and between air pressures of the same glass composition.

Comparison	PFR *P value* 2 bar	PFR *P value* 3 bar	PFR *P value* 4 bar	PFR *P value* QMFA1	PFR *P value* QMFA2	PFR *P value* QMFA3
QMFA1 vs QMFA2	0.000	0.000	0.000	----------	----------	---------
QMFA1 vs QMFA3	0.000	0.000	0.000	----------	----------	----------
QMFA2 vs QMFA3	0.421	0.104	0.000	----------	----------	----------
2 bar vs 3 bar	----------	----------	----------	0.275	0.978	0.174
2 bar vs 4 bar	----------	----------	----------	0.010	0.987	0.100
3 bar vs 4 bar	----------	----------	----------	0.231	0.999	0.951

2. Multiple comparisons (Tukey HSD test) of the abraded line width between the glasses abraded disc compositions at three distances and between the distances at each glass composition.

Comparison	Width *P value* D 1mm	Width *P value* D 3 mm	Width *P value* D 5 mm	Width *P value* QMFA1	Width *P value* QMFA2	Width *P value* QMFA3
QMFA1 vs QMFA2	0.000	0.000	0.000	----------	----------	---------
QMFA1 vs QMFA3	0.000	0.000	0.000	----------	----------	----------
QMFA2 vs QMFA3	0.871	0.000	0.710	----------	----------	----------
1 mm vs 3 mm	----------	----------	----------	0.000	0.000	0.000
1 mm vs 5 mm	----------	----------	----------	0.000	0.000	0.000
3 mm vs 5 mm	----------	----------	----------	0.000	0.000	0.000

10.3 WLP statistics

1. Multiple comparisons (Tukey HSD test) of the abraded line depth between the glasses abraded disc compositions at three distances and between the distances at each glass composition.

Comparison	Depth *P value* D 1mm	Depth *P value* D 3 mm	Depth *P value* D 5 mm	Depth *P value* QMFA1	Depth *P value* QMFA2	Depth *P value* QMFA3
QMFA1 vs QMFA2	0.000	0.000	0.619	----------	----------	---------
QMFA1 vs QMFA3	0.000	0.000	0.000	----------	----------	----------
QMFA2 vs QMFA3	0.042	0.000	0.000	----------	----------	----------
1 mm vs 3 mm	----------	----------	----------	0.550	0.660	0.000
1 mm vs 5 mm	----------	----------	----------	0.000	0.115	0.000
3 mm vs 5 mm	----------	----------	----------	0.000	0.557	0.900

2. Multiple comparisons (Tukey HSD test) of the abraded line volume between the glasses abraded disc compositions at three different distances and between the distances at each glass composition.

Comparison	Volume *P value* D 1mm	Volume *P value* D 3 mm	Volume *P value* D 5 mm	Volume *P value* QMFA1	Volume *P value* QMFA2	Volume *P value* QMFA3
QMFA1 vs QMFA2	0.485	0.370	0.276	----------	----------	---------
QMFA1 vs QMFA3	0.000	0.000	0.000	----------	----------	----------
QMFA2 vs QMFA3	0.000	0.000	0.025	----------	----------	----------
1 mm vs 3 mm	----------	----------	----------	0.004	0.141	0.000
1 mm vs 5 mm	----------	----------	----------	0.000	0.000	0.000
3 mm vs 5 mm	----------	----------	----------	0.000	0.034	0.009

3. Multiple comparisons (Tukey HSD test) of the abraded line width between the glasses abraded disc compositions at three sample velocities and between the velocities at each glass composition.

Comparison	Width *P value* 0.25mm/sec	Width *P value* 0. 5mm/sec	Width *P value* 1mm/sec	Width *P value* QMFA1	Width *P value* QMFA2	Width *P value* QMFA3
QMFA1 vs QMFA2	0.853	0.359	0.000	----------	----------	---------
QMFA1 vs QMFA3	0.000	0.000	0.000	----------	----------	----------
QMFA2 vs QMFA3	0.000	0.000	0.000	----------	----------	----------
0.25 vs 0.5 mm/sec	----------	----------	----------	0.000	0.000	0.000
0.25 vs 1 mm/sec	----------	----------	----------	0.000	0.000	0.000
0.5 vs 1 mm/sec	----------	----------	----------	0.000	0.000	0.005

4. Multiple comparisons (Tukey HSD test) of the abraded line depth between the glasses abraded disc compositions at three sample velocities and between the velocities at each glass composition.

Comparison	Depth *P value* 0.25mm/sec	Depth *P value* 0. 5mm/sec	Depth *P value* 1mm/sec	Depth *P value* QMFA1	Depth *P value* QMFA2	Depth *P value* QMFA3
QMFA1 vs QMFA2	0.899	0.000	0.639	----------	----------	---------
QMFA1 vs QMFA3	0.000	0.000	0.462	----------	----------	----------
QMFA2 vs QMFA3	0.000	0.000	0.955	----------	----------	----------
0.25 vs 0.5 mm/sec	----------	----------	----------	0.000	0.000	0.000
0.25 vs 1 mm/sec	----------	----------	----------	0.000	0.000	0.000
0.5 vs 1 mm/sec	----------	----------	----------	0.000	0.000	0.000

5. Multiple comparisons (Tukey HSD test) of the abraded line volume between the glasses abraded disc compositions at three sample velocities and between the velocities at each glass composition.

Comparison	Volume *P value* 0.25mm/sec	Volume *P value* 0. 5mm/sec	Volume *P value* 1mm/sec	Volume *P value* QMFA1	Volume *P value* QMFA2	Volume *P value* QMFA3
QMFA1 vs QMFA2	0.050	0.050	0.444	----------	----------	---------
QMFA1 vs QMFA3	0.000	0.000	0.019	----------	----------	----------
QMFA2 vs QMFA3	0.000	0.000	0.269	----------	----------	----------
0.25 vs 0.5 mm/sec	----------	----------	----------	0.000	0.000	0.000
0.25 vs 1 mm/sec	----------	----------	----------	0.000	0.000	0.000
0.5 vs 1 mm/sec	----------	----------	----------	0.000	0.001	0.000

6. Multiple comparisons (Tukey HSD test) of the abraded line width between the glasses abraded disc compositions at three different pressures and between the pressures at each glass composition.

Comparison	Width *P value* 2 bar	Width *P value* 3 bar	Width *P value* 4 bar	Width *P value* QMFA1	Width *P value* QMFA2	Width *P value* QMFA3
QMFA1 vs QMFA2	0.000	0.000	0.982	----------	----------	---------
QMFA1 vs QMFA3	0.023	0.232	0.001	----------	----------	----------
QMFA2 vs QMFA3	0.042	0.034	0.002	----------	----------	----------
2 bar vs 3 bar	----------	----------	----------	0.973	0.915	0.767
2 bar vs 4 bar	----------	----------	----------	0.000	0.005	0.000
3 bar vs 4 bar	----------	----------	----------	0.000	0.002	0.000

7. Multiple comparisons (Tukey HSD test) of the abraded line depth between the glasses abraded disc compositions at three different pressures and between the pressures at each glass composition.

Comparison	Depth *P value* 2 bar	Depth *P value* 3 bar	Depth *P value* 4 bar	Depth *P value* QMFA1	Depth *P value* QMFA2	Depth *P value* QMFA3
QMFA1 vs QMFA2	0.000	0.000	0.258	----------	----------	---------
QMFA1 vs QMFA3	0.000	0.000	0.022	----------	----------	----------
QMFA2 vs QMFA3	0.000	0.000	0.448	----------	----------	----------
2 bar vs 3 bar	----------	----------	----------	0.000	0.000	0.000
2 bar vs 4 bar	----------	----------	----------	0.000	0.000	0.000
3 bar vs 4 bar	----------	----------	----------	0.000	0.000	0.000

8. Multiple comparisons (Tukey HSD test) of the abraded line volume between the glasses abraded disc compositions at three different pressures and between the pressures at each glass composition.

Comparison	Volume *P value* 2 bar	Volume *P value* 3 bar	Volume *P value* 4 bar	Volume *P value* QMFA1	Volume *P value* QMFA2	Volume *P value* QMFA3
QMFA1 vs QMFA2	0.000	0.000	0.002	----------	----------	---------
QMFA1 vs QMFA3	0.000	0.000	0.000	----------	----------	----------
QMFA2 vs QMFA3	0.000	0.000	0.133	----------	----------	----------
2 bar vs 3 bar	----------	----------	----------	0.000	0.000	0.000
2 bar vs 4 bar	----------	----------	----------	0.000	0.000	0.000
3 bar vs 4 bar	----------	----------	----------	0.000	0.000	0.000

9. Multiple comparisons (Tukey HSD test) of the surface roughness between the glasses abraded disc compositions at three different distances and between the distances at each glass composition.

Comparison	Ra *P value* D 1mm	Ra *P value* D 3 mm	Ra *P value* D 5 mm	Ra *P value* QMFA1	Ra *P value* QMFA2	Ra *P value* QMFA3
QMFA1 vs QMFA2	0.689	0.642	1.000	----------	----------	---------
QMFA1 vs QMFA3	1.000	0.893	0.905	----------	----------	----------
QMFA2 vs QMFA3	0.689	0.893	0.905	----------	----------	----------
1 mm vs 3 mm	----------	----------	----------	0.000	0.000	0.000
1 mm vs 5 mm	----------	----------	----------	0.000	0.000	0.000
3 mm vs 5 mm	----------	----------	----------	0.372	0.899	0.468

10. Multiple comparisons (Tukey HSD test) of the surface roughness between the glasses abraded disc compositions at three sample velocities and between the velocities at each glass composition.

Comparison	Ra *P value* 0.25mm/sec	Ra *P value* 0. 5mm/sec	Ra *P value* 1mm/sec	Ra *P value* QMFA1	Ra *P value* QMFA2	Ra *P value* QMFA3
QMFA1 vs QMFA2	0.416	0.0488	0.932	----------	----------	---------
QMFA1 vs QMFA3	0.416	0.289	0.757	----------	----------	----------
QMFA2 vs QMFA3	1.000	0.921	0.932	----------	----------	----------
0.25 vs 0.5 mm/sec	----------	----------	----------	0.832	0.511	0.652
0.25 vs 1 mm/sec	----------	----------	----------	0.215	0.008	0.005
0.5 vs 1 mm/sec	----------	----------	----------	0.490	0.087	0.037

11. Multiple comparisons (Tukey HSD test) of the surface roughness between the glasses abraded disc compositions at three different pressures and between the pressures at each glass composition.

Comparison	Volume *P value* 2 bar	Volume *P value* 3 bar	Volume *P value* 4 bar	Volume *P value* QMFA1	Volume *P value* QMFA2	Volume *P value* QMFA3
QMFA1 vs QMFA2	1.000	0.952	0.809	----------	----------	---------
QMFA1 vs QMFA3	0.929	0.470	0.809	----------	----------	----------
QMFA2 vs QMFA3	0.929	0.315	1.000	----------	----------	----------
2 bar vs 3 bar	----------	----------	----------	0.735	0.946	0.340
2 bar vs 4 bar	----------	----------	----------	0.000	0.000	0.000
3 bar vs 4 bar	----------	----------	----------	0.000	0.000	0.012

10.4 Surface coverage statistics

1. Multiple comparisons (Tukey HSD test) of the area percentage coverage between the glasses abraded disc compositions at three different distances and between the distances at each glass composition.

Comparison	Ra *P value* D 1mm	Ra *P value* D 3 mm	Ra *P value* D 5 mm	Ra *P value* QMFA1	Ra *P value* QMFA2	Ra *P value* QMFA3
QMFA1 vs QMFA2	0.007	0.122	0.872	----------	----------	---------
QMFA1 vs QMFA3	0.000	0.000	0.000	----------	----------	----------
QMFA2 vs QMFA3	0.000	0.000	0.000	----------	----------	----------
1 mm vs 3 mm	----------	----------	----------	0.063	0.737	0.000
1 mm vs 5 mm	----------	----------	----------	0.000	0.003	0.000
3 mm vs 5 mm	----------	----------	----------	0.000	0.023	0.000

2. Multiple comparisons (Tukey HSD test) of the area percentage coverage between the glasses abraded disc compositions at three sample velocities and between the velocities at each glass composition.

Comparison	Ra *P value* 0.25mm/sec	Ra *P value* 0. 5mm/sec	Ra *P value* 1mm/sec	Ra *P value* QMFA1	Ra *P value* QMFA2	Ra *P value* QMFA3
QMFA1 vs QMFA2	0.000	0.375	0.465	----------	----------	---------
QMFA1 vs QMFA3	0.000	0.000	0.000	----------	----------	----------
QMFA2 vs QMFA3	0.539	0.000	0.000	----------	----------	----------
0.25 vs 0.5 mm/sec	----------	----------	----------	0.000	0.000	0.146
0.25 vs 1 mm/sec	----------	----------	----------	0.000	0.000	0.848
0.5 vs 1 mm/sec	----------	----------	----------	0.092	0.048	0.046

3. Multiple comparisons (Tukey HSD test) of the area percentage coverage between the glasses abraded disc compositions at three different pressures and between the pressures at each glass composition.

Comparison	Volume *P value* 2 bar	Volume *P value* 3 bar	Volume *P value* 4 bar	Volume *P value* QMFA1	Volume *P value* QMFA2	Volume *P value* QMFA3
QMFA1 vs QMFA2	0.000	0.000	0.002	----------	----------	---------
QMFA1 vs QMFA3	0.000	0.000	0.022	----------	----------	----------
QMFA2 vs QMFA3	0.000	0.000	0.133	----------	----------	----------
2 bar vs 3 bar	----------	----------	----------	0.592	0.021	0.000
2 bar vs 4 bar	----------	----------	----------	0.461	0.051	0.000
3 bar vs 4 bar	----------	----------	----------	0.975	0.942	0.003